UNIVERSIDAD DE CHILE
FACULTAD DE CIENCIAS
ESCUELA DE POSTGRADO

ANALISIS TEORICO DE REACCIONES QUIMICAS EN LA REPRESENTACION $\{\mu, \eta, E\}$

MARIA SOLEDAD GUTIERREZ OLIVA

SANTIAGO–CHILE

2004

UNIVERSIDAD DE CHILE
FACULTAD DE CIENCIAS
ESCUELA DE POSTGRADO

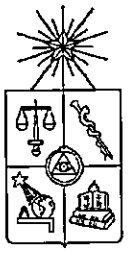

ANALISIS TEORICO DE REACCIONES QUIMICAS EN LA REPRESENTACION $\{\mu, \eta, E\}$

por

María Soledad Gutiérrez Oliva

Tesis Entregada a la
Universidad de Chile
en cumplimiento parcial de los requisitos
para optar al grado de
Doctor en Ciencias con Mención en Química
SEPTIEMBRE 2004

Director de Tesis: Dr. Alejandro Toro Labbé

UNIVERSIDAD DE CHILE
FACULTAD DE CIENCIAS

INFORME DE APROBACION
TESIS DE DOCTORADO

Se informa a la Escuela de Postgrado de la Facultad de Ciencias, que la Tesis de Doctorado presentada por la Candidata:

MARIA SOLEDAD GUTIERREZ OLIVA

ha sido aprobada por la comisión de evaluación de la Tesis como requisito para optar al grado de Doctor en Ciencias con Mención en Química, en el examen de defensa de Tesis rendido el día 22 de Septiembre de 2004.

Director de Tesis:
Dr. Alejandro Toro Labbé

Comisión Evaluadora de Tesis:
Dr. Ricardo Letelier D.

Dr. Arie Aizman R.

Dr. Raúl Morales S.

Dr. Margarita Prendez B.

Dr. Octavio Vásquez A.

A mi Madre

Tabla de Contenidos

Indice de Tablas

Indice de Figuras

Resumen

En este trabajo de tesis se establece que los mecanismos, junto con aspectos termodinámicos y cinéticos de una reacción química, pueden ser caracterizados a través del análisis de propiedades electrónicas globales y locales en complemento a la caracterización energética. En particular, se muestra que el potencial químico (μ) y la dureza (η) son complementarios a la energía (E) y en muchos casos estas propiedades están analíticamente conectadas definiendo la representación $\{\mu, \eta, E\}$ en la cual una reacción química se caracteriza a través de algunos parámetros específicos (propiedades de activación, posición del estado de transición, energía de la reacción, etc.). El marco conceptual que permite conectar diferentes propiedades se define por un conjunto de principios y ecuaciones de reactividad, tales como el postulado de *Hammond*, el Principio de Máxima Dureza y la ecuación de *Marcus*.

En este contexto, el estudio de diferentes sistemas y reacciones indica que los conceptos clásicos que hemos incorporado junto con descriptores de la reactividad derivados de la Teoría de Funcionales de la Densidad (*TFD*) constituyen una herramienta poderosa de análisis para caracterizar reacciones químicas. Ejemplos representativos de reacciones de rotación interna, de transferencia protónica y de formación de agregados moleculares confirman la validez del modelo propuesto en este trabajo de Tesis.

Abstract

In this work we point out that the mechanisms, the thermodynamic and kinetics aspects of chemical reactions can be characterized through the analysis of global and local electronic properties that complement the energy characterization. In particular it is shown that global properties such as chemical potential (μ) and hardness (η) are complementary to the energy (E) and, in many cases these properties are analytically related thus giving rise to the so called $\{\mu, \eta, E\}$ representation in which a chemical reaction is characterized through few specific parameters (activation properties, position of transition state, reaction energy etc.). The conceptual frame that links different properties is defined by few reactivity principles and equations such as the *Hammond* postulate, the Principle of Maximum Hardness and the *Marcus* equation.

Within this framework, the study of different kinds of chemical reaction indicate that the classical concepts of reactivity that have been incorporated in connection with Density Functional Theory (DFT) descriptors are adequate and powerful tools for characterizing chemical reactions. Illustrative examples of representative systems undergoing internal rotations, proton transfer and formation of molecular aggregates reactions confirm the validity of the overall model proposed in this work.

Agradecimientos

Agradezco a las siguientes personas e instituciones que han contribuido a la realización de mis estudios de Doctorado.

- Mi más sincero y profundo agradëcimiento al Dr. Alejandro Toro–Labbé, por contribuir en mi formación científica y en especial por su constante apoyo aún en los momentos más difíciles.
- A los miembros de la comisión examinadora de esta Tesis por sus comentarios y sugerencias en el desarrollo de ésta: Dr. Ricardo Letelier (Presidente), Dr. Arie Aizman, Dr. Raúl Morales, Dr. Margarita Prendez y Dr. Octavio Vásquez.
- A la Comisión Nacional de Investigación Científica y Tecnológica (CONICYT) por una beca de Doctorado.
- Al Fondo Nacional de Desarrollo Científico y Tecnológico (FONDECYT) por financiamiento a través de los proyectos N°s 2010139, 1990543 y 1020534.
- Al proyecto Cátedra Presidencial (1998), otorgada al Dr. Alejandro Toro–Labbé.
- Al departamento de Química de la Facultad de Ciencias de la Universidad de Chile.
- A la Facultad de Química de la Pontificia Universidad Católica de Chile.
- A mi hijo Fernando, a mi hermana Lina y a mi sobrino Patricio.

- Finalmente, agradezco a mis compañeros de esta etapa y en especial a Pablo por su amistad e infinitas discusiones científicas inmensamente motivadoras.

Capítulo 1

Introducción

1.1 Aspectos Históricos

En los últimos años la Química Computacional se ha transformado en un complemento necesario de estudios experimentales y en una herramienta que ha abierto la posibilidad de estudiar sistemas pequeños, macromoléculas de interés farmacológico, estructuras cristalinas inorgánicas y materiales de interés por sus diversas aplicaciones tecnológicas. Los métodos computacionales descansan en modelos teóricos que permiten racionalizar las características estructurales y electrónicas de átomos, fragmentos, moléculas aisladas y moléculas en interacción.

El esfuerzo realizado por investigadores en Química Teórica Computacional ha sido reconocido mundialmente a través de varios premios Nobel otorgados a investigadores del área. La Real Academia de Ciencias de Suecia otorgó el premio Nobel de Química de 1998 a :

- John A. Pople (1925–2004) (*Universidad de Northwestern, Evanston, Illinois, EUA*), por su contribución al desarrollo de métodos computacionales en Química Cuántica y

- Walter Kohn (1923–)(*Universidad de California, Santa Bárbara, California, EUA*), por su contribución al desarrollo de la Teoría de Funcionales de la Densidad.

Pople, advirtió que la utilidad de los métodos computacionales para la investigación científica estaba condicionada por la capacidad de producir una gran cantidad de información y entonces desarrolló algoritmos para extraer de la función de onda datos útiles para la comprensión del comportamiento de átomos y moléculas. A partir del conocimiento de una geometría de equilibrio correspondiente a un punto mínimo en una superficie de energía del sistema, se desarrollaron métodos elaborados para la determinación precisa de puntos de mínimo. La química cuántica se vuelve así una herramienta capaz de entregar información confiable sobre la geometría molecular. Luego se desarrollaron algoritmos que permitieron localizar y caracterizar estructuras de transición en transformaciones químicas. En los años 1970, Pople y *col.* desarrollaron el programa computacional *Gaussian*, ampliamente usado para calcular propiedades moleculares, dando resultados en buena concordancia cualitativa y cuantitativa con los datos experimentales.

En general, Pople y *col.* desarrollaron programas computacionales introduciendo correcciones necesarias, como por ejemplo, para obtener superficies de potencial calculadas con errores mínimos, obteniéndose así soluciones que posibilitan la utilización de la química cuántica para estudiar reacciones químicas. En conjunto con el formalismo de la mecánica estadística, así como con los resultados obtenidos con programas de química cuántica, se pudo establecer datos confiables para la termoquímica, inclusive en situaciones donde no existe el acceso a trabajos experimentales.

Una alternativa simple para la ecuación de *Schrödinger* fue propuesta por Thomas y Fermi en 1927, conocida como la aproximación de Thomas–Fermi. En esta aproximación, en lugar de usar la función de onda del sistema, se considera su densidad electrónica $\rho(\vec{r})$. Una simplificación drástica y admirable: una ecuación para un sistema de N-partículas con $3N$ coordenadas independientes es reducida por la aproximación de Thomas–Fermi a un problema de sólo tres dimensiones, las coordenadas

de un punto en el espacio. La energía total del sistema es escrita como un funcional de $\rho(\vec{r})$, o sea, $E[\rho(\vec{r})]$. Metodologías originadas de esta aproximación, no tuvieron mucho impacto para justificar cambios en el camino trazado para la resolución de la ecuación de *Schrödinger* directamente.

Sin embargo, este panorama cambió a partir de la contribución de Walter Kohn. En 1964, Hohenberg y Kohn demostraron un teorema importante: la densidad electrónica exacta del estado fundamental de una molécula determina de manera unívoca todas las propiedades del estado fundamental de esa molécula. En un trabajo posterior, Kohn y Sham deducen las ecuaciones necesarias para que la densidad electrónica $\rho(\vec{r})$ sea calculada utilizando procedimientos basados en el método variacional. Esta teoría, basada en la densidad electrónica, recibe el nombre de Teoría de Funcionales de la Densidad (*TFD*). Sin embargo, la viabilidad de la *TFD* depende del conocimiento del funcional que expresa la energía total E del sistema, es decir, $E[\rho(\vec{r})]$. Desde el inicio de su proposición, la *TFD* ha sido aplicada para estudiar sistemas multielectrónicos con énfasis en la estructura electrónica de sólidos y ha sido implementada en programas computacionales de química cuántica, entre estos *Gaussian*. Estas nuevas facilidades computacionales, apoyadas por una fundamentación teórica consistente, ha incentivado la utilización de la *TFD* en la investigación de propiedades electrónicas de sistemas químicos poliatómicos, incluyendo el estudio de sitios activos en enzimas, reacciones en superficies, propiedades electrónicas de sólidos, polímeros, etc.

Una rama de la *TFD* que ha sido desarrollada desde finales de los años 1970 por Robert G. Parr y *col.* [1], conocida como la *TFD conceptual*, conecta parámetros que formalmente se derivan de la *TFD* con propiedades conocidas en el ámbito de la reactividad química. La *TFD* conceptual constituye la base teórica de este trabajo de Tesis.

1.2 Algunos Principios de Reactividad Química

En el análisis de reacciones químicas, el conocimiento de la estructura y propiedades de reactivos, productos y especialmente de estados de transición permite avanzar hacia la identificación de las interacciones específicas que producen el cambio químico, es decir, caracterizar mecanismos de reacción. La comprensión de mecanismos y cambios energéticos de las reacciones químicas es un tema central de investigación en química básica. Se han realizado varios intentos para proporcionar una justificación teórica de la preferencia para un camino de reacción sobre otro y la formación de solamente algunos productos seleccionados entre las varias opciones posibles [2,3].

En el año 1963, basado en observaciones experimentales, Pearson propuso el principio *HSAB* (*Hard Soft Acid Base*) que establece que la interacción *duro* − *duro* y *blando* − *blando* es más favorable, tanto desde un punto de vista termodinámico como cinético. El principio *HSAB* ha encontrado una amplia utilidad para establecer reglas empíricas de combinación y predecir la formación de productos de una reacción química [4,5].

El principio *HSAB* está estrechamente relacionado con el principio de la teoría de estructura electrónica molecular propuesto por Pearson y denominado Principio de Máxima Dureza (*PMD*) [6,7], que establece que *las moléculas en sus estados de equilibrio tienden a ser tan duras como sea posible* [6–11].

Chattaraj y *col.* propusieron el Principio de Mínima Polarizabilidad (PMP) [12], el cual establece que *la dirección natural de evolución de cualquier sistema es hacia un estado de mínima polarizabilidad.* En general, las condiciones de mínima polarizabilidad dada por el PMP y máxima dureza dada por el *PMD*, complementan el criterio de mínima energía para la estabilidad molecular y son criterios usados como guía en la caracterización de los sistemas que estudiamos.

1.3 Objetivos e Hipótesis de la Tesis

Esta Tesis tiene como objetivo general, proponer un modelo teórico unificado que permita caracterizar simultáneamente los aspectos energéticos, cinéticos y mecanísticos involucrados en una reacción química, los descriptores de reactividad química potencial químico (μ), dureza molecular (η) y energía (E) son las variables fundamentales de dicho modelo.

Objetivos Específicos.

1. Establecer relaciones analíticas entre energía y propiedades electrónicas.
2. Caracterizar los mecanismos de reacción e identificar interacciones específicas que caracterizan a los reactivos, productos y estados de transición.
3. Caracterizar el origen físico de las barreras de energía en términos de la naturaleza de las interacciones involucradas.
4. Proponer y validar esquemas de aditividad para el potencial químico y la dureza molecular con el objeto de determinar el rol de átomos y/o fragmentos en la formación de especies químicas.

Para llevar a finalidad estos objetivos, se estudiaron diferentes tipos de reacciones químicas como reacciones de rotación interna, de transferencia protónica y de formación de agregados moleculares, las que involucraron el estudio de una gran variedad de sistemas moleculares.

Hipótesis. Esta Tesis se basa en las siguientes hipótesis:

1. Los índices teóricos que se derivan de la energía y de la densidad electrónica dentro de la estructura de la *TFD*, son adecuados para caracterizar los diferentes tipos de reacciones estudiadas en esta Tesis.
2. El uso de la aproximación de diferencia finita para determinar μ, η y la función de *Fukui* produce resultados confiables de estas propiedades.

3. La ecuación de *Marcus* y las propiedades que de ella se derivan ($\Delta E^{\neq}$, $\Delta E_{o}^{\neq}$, β) permiten caracterizar y racionalizar los estados de transición en los diferentes tipos de reacciones estudiadas en esta Tesis.

4. La fuerza asociada a la reacción química, junto con el análisis de propiedades locales, permite identificar interacciones específicas que definen los mecanismos que operan en diferentes regiones de la coordenada de reacción.

1.4 Metodología

La optimización completa de geometrías, para todas las especies consideradas en esta Tesis, fue realizada a nivel de teoría *RHF* (*Restricted Hartree-Fock*), usando la base de orbitales 6-311G** (*RHF/6-311G***), y de Teoría de Funcionales de la Densidad, *TFD*, usando el funcional de intercambio y correlación B3LYP (B3LYP/6-311G**), todos los cálculos se realizaron usando el programa *Gaussian94/98/03* [13–15]. La optimización de los fragmentos radicalarios se realizó a nivel de teoría *UHF* (*Unrestricted Hartree-Fock*). Además, se realizaron cálculos de frecuencia sobre las especies de referencia y los estados de transición para su completa caracterización. El potencial químico electrónico y la dureza molecular fueron calculados aplicando las ecuaciones (2.21) y (2.23), respectivamente (ver Capítulo 2), con ϵ_H y ϵ_L obtenidos a partir de cálculos *RHF/UHF* de las especies totalmente optimizadas.

En particular, todos los perfiles de energía y propiedades electrónicas para los procesos de isomerización rotacional (Capítulo 3) se obtuvieron realizando cálculos cada 10° a lo largo del ángulo de torsión en un intervalo de 0° a 180°; además se realizaron cálculos a nivel de teoría de Perturbaciones *MP2* (Møller–Plesset de segundo orden); ésta última metodología fue usada con el objeto de estudiar el efecto de la correlación electrónica sobre los perfiles de las propiedades globales y locales. Por otra parte, todos los perfiles de energía y propiedades electrónicas para los procesos de transferencia protónica (ver Artículo **B4** y **B7** en Anexo B), se obtuvieron a través de cálculos de puntos sencillos de las estructuras optimizadas indicadas por el procedimiento *IRC* (*Intrinsic Reaction Coordinate*).

Esta Tesis está organizada de la siguiente manera. En el Capítulo 2 se revisan las bases teóricas para el cálculo de propiedades que caracterizan los conceptos de reactividad y selectividad. Además, se presentan expresiones analíticas para estimar barreras de activación y caracterizar estados de transición.

En el Capítulo 3, se estudian reacciones de rotación interna. Los procesos de isomerización rotacional son caracterizados básicamente en términos del análisis de los perfiles de descriptores de reactividad y su relación con la energía potencial torsional.

En el Capítulo 4, se presenta el uso del principio de igualación de la electronegatividad para estimar propiedades globales de 14 sistemas moleculares. Además, se propone un nuevo esquema de aditividad para obtener propiedades electrónicas de moléculas y agregados moleculares a partir de las respectivas propiedades de los fragmentos aislados.

En el Capítulo 5, se presentan las Conclusiones Generales y más relevantes de este trabajo de Tesis y en el Anexo B se adjuntan los siete artículos generados como parte de esta Tesis.

Capítulo 2

Base y Desarrollos Teóricos

Resumen

En este Capítulo, se describen brevemente las bases teóricas de la Teoría de Funcionales de la Densidad, las cuales permiten determinar la estructura electrónica y energía de sistemas moleculares. Uno de los grandes éxitos de esta teoría, es que ha generado descriptores para analizar procesos químicos, en particular el potencial químico (μ) y la dureza molecular (η), que son propiedades relevantes en relación a la reactividad de un sistema puesto que están directamente relacionadas con las energías de los orbitales frontera $HOMO$ y $LUMO$, ε_H y ε_L, respectivamente.

2.1 Teoría de Funcionales de la Densidad

En el análisis de reacciones químicas, el conocimiento de la estructura y propiedades de reactivos, productos y especialmente de estados de transición permite avanzar hacia la identificación de las interacciones específicas que producen el cambio químico, es decir, caracterizar mecanismos de reacción. En este contexto, como se mencionó en el Capítulo 1, uno de los objetivos de esta Tesis, ha sido validar y establecer modelos de análisis de reacciones químicas y de la reactividad intrínseca de las especies involucradas, sobre la base de conceptos provenientes de la Teoría de Funcionales de la Densidad los cuales se definen en las próximas secciones.

2.1.1 Descriptores de Reactividad Química

Una rama de la *TFD* que ha sido desarrollada desde finales de los años 1970 por R. G. Parr y *col.* [1], conocida como la *TFD conceptual*, conecta parámetros que formalmente se derivan de la *TFD* con propiedades conocidas en el ámbito de la reactividad química. En particular, la relación potencial químico–electronegatividad proporciona una base formal para conceptos químicos que hasta ahora habían sido definidos sobre bases puramente empíricas [16–18].

La *TFD* ha influido fuertemente en la evolución de la Química Cuántica durante los últimos veinte años, proporcionando la base para el desarrollo de estrategias computacionales para obtener información sobre la energía, estructura y propiedades de átomos y moléculas a mucho menor costo que las tradicionales técnicas *ab-initio* para la determinación de la función de onda. Basada en los teoremas de *Hohenberg y Kohn* [16, 19], la *TFD* establece que existe una relación biunívoca entre el potencial externo, $v(\vec{r})$, y la densidad del estado fundamental $\rho(\vec{r})$ lo que conduce a la ecuación fundamental de *Euler-Lagrange*, que es la ecuación fundamental en *TFD*.

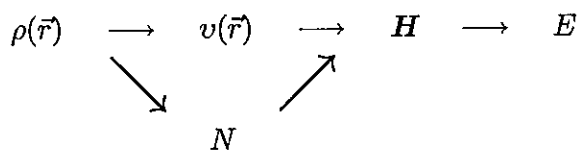

Esquema 1: Interdependencia de las variables básicas en el teorema de *Hohenberg y Kohn.*

En el *Esquema 1*, se muestra la interdependencia de las variables básicas del teorema de *Hohenberg y Kohn* y, dado que $\rho(\vec{r})$ determina el número total de electrones (N) del sistema y el potencial externo $\upsilon(\vec{r})$, según el primer teorema de *Hohenberg y Kohn*, se concluye que $\rho(\vec{r})$ determina el hamiltoniano H y la función de onda del estado fundamental y por extensión, todas las propiedades observables del estado fundamental. Entonces la energía del estado fundamental de un sistema electrónico es un funcional único de su densidad electrónica [19–22]:

$$E = E[\rho(\vec{r})] \tag{2.1}$$

Las ecuaciones básicas de la *TFD* se obtienen por medio de la minimización de la energía como un funcional de la densidad electrónica, $E[\rho(\vec{r})]$:

$$\delta\left[E - \mu\left(\int \rho(\vec{r})\, d\vec{r}\right)\right] = 0, \tag{2.2}$$

bajo la condición de que la densidad integre al número total de electrones N

$$\int \rho(\vec{r})\, d\vec{r} = N. \tag{2.3}$$

En la ecuación (2.2), μ es un multiplicador indeterminado de *Lagrange* [16], asociado a la condición de normalización dada por la ecuación (2.3). Este multiplicador de *Lagrange* es el potencial químico electrónico [1, 16]. El principio variacional conduce

a la ecuación de *Euler-Lagrange*:

$$\mu = v(\vec{r}) + \frac{\delta F_{HK}[\rho(\vec{r})]}{\delta \rho(\vec{r})}, \tag{2.4}$$

que es la ecuación fundamental de la *TFD*, donde $v(\vec{r})$ es el potencial externo, y $F_{HK}[\rho(\vec{r})]$ es el funcional universal de *Hohenberg* y *Kohn* que contiene el funcional de la energía cinética electrónica, $T[\rho]$, y el funcional de interacción electrón-electrón, $V_{ee}[\rho]$, ($F_{HK}[\rho] = T[\rho] + V_{ee}[\rho]$) [17,19,20]. La ecuación (2.4), nos entrega una fórmula para minimizar la energía y determinar así, la densidad del estado fundamental. Diferenciando la ecuación (2.4) se obtiene [19–22]:

$$E[\rho(\vec{r})] = \int \rho(\vec{r}) v(\vec{r})\, d\vec{r} + F_{HK}[\rho(\vec{r})]. \tag{2.5}$$

Para dar un significado físico de μ e introducir otros conceptos, es necesario considerar el cambio de energía, dE, de un sistema atómico o molecular cuando pasa de un estado fundamental a otro. Puesto que, según los teoremas de *Hohenberg* y *Kohn* [19] la densidad electrónica está determinada por el potencial externo $v(\vec{r})$ y N, entonces, la energía se escribe como un funcional que depende del número de electrones y del potencial externo $E[\rho(\vec{r})] \equiv E[N, v(\vec{r})]$, entonces :

$$dE = \int \left(\frac{\partial E}{\partial N}\right)_{v(\vec{r})} dN + \int \left(\frac{\delta E}{\delta v(\vec{r})}\right)_{N} \delta v(\vec{r})\, d\vec{r}. \tag{2.6}$$

Similarmente, la energía se puede escribir como un funcional de la densidad electrónica y del potencial externo, $E = E[\rho(\vec{r}), v(\vec{r})]$, entonces:

$$dE = \int \left(\frac{\partial E}{\partial \rho(\vec{r})}\right)_{v(\vec{r})} \delta\rho(\vec{r})\, d\vec{r} + \int \left(\frac{\delta E}{\delta v(\vec{r})}\right)_{\rho(\vec{r})} \delta v(\vec{r})\, d\vec{r}. \tag{2.7}$$

Se debe mencionar que la ecuación (2.7) es solamente aproximada, porque se asume que $\rho(\vec{r})$ y $v(\vec{r})$ son independientes, mientras que los teoremas de *Hohenberg* y *Kohn* demostraron que $v(\vec{r})$ determina completamente la densidad del estado fundamental, $\rho(\vec{r})$.

De la ecuación fundamental de la *TFD* (ecuación (2.4)) junto a la ecuación (2.5), se tiene que :

$$\left(\frac{\delta E}{\delta \rho(\vec{r})}\right)_{v(\vec{r})} = \mu, \tag{2.8}$$

y diferenciando la ecuación (2.3), obtenemos:

$$dN = \int \partial \rho(\vec{r}) d\vec{r}. \tag{2.9}$$

Sustituyendo las ecuaciones (2.8) y (2.9) en la ecuación (2.7) se llega a :

$$dE = \mu dN + \int \left(\frac{\delta E}{\delta v(\vec{r})}\right)_{\rho(\vec{r})} \delta v(\vec{r}) d\vec{r}. \tag{2.10}$$

La comparación de la ecuación (2.10) con la ecuación (2.6) nos lleva a una nueva definición para μ:

$$\left(\frac{\delta E}{\delta \rho(\vec{r})}\right)_{v(\vec{r})} = \left(\frac{\partial E}{\partial N}\right)_{v(\vec{r})} = \mu. \tag{2.11}$$

Esta última ecuación nos dice que $\mu \equiv \mu[N, v(\vec{r})]$ es la derivada de la energía con respecto al número total de electrones, nos indica cómo cambia la energía al variar el número de electrones, y de ahí que recibe el nombre de potencial químico, dado que esta definición es análoga a la del potencial químico en termodinámica clásica. Además, μ ha sido identificado con el negativo de la electronegatividad ($\mu = -\chi$), lo que permite establecer relaciones formales entre la *TFD* y la química estructural clásica.

Físicamente, el potencial químico es una propiedad global que *caracteriza la tendencia de escape de los electrones desde el sistema en equilibrio.* Debido a que μ es una función de N y un funcional de $v(\vec{r})$, $\mu \equiv \mu[N, v(\vec{r})]$, tenemos:

$$d\mu = \left(\frac{\partial \mu}{\partial N}\right)_{v(\vec{r})} dN + \int \left(\frac{\delta \mu}{\delta v(\vec{r})}\right)_N \delta v(\vec{r})\, d\vec{r}, \tag{2.12}$$

esta ecuación nos indica cómo varía el potencial químico frente a un cambio en el número de electrones y en el potencial externo. Definiendo η como la dureza química y $f(\vec{r})$ como la función de *Fukui*, propiedad local del sistema que mide la reactividad de diferentes sitios dentro de la molécula, podemos escribir:

$$d\mu = \eta dN + \int f(\vec{r}) \delta v(\vec{r})\, d\vec{r}, \tag{2.13}$$

donde

$$\eta = \left(\frac{\partial^2 E}{\partial N^2}\right)_{v(\vec{r})} = \left(\frac{\partial \mu}{\partial N}\right)_{v(\vec{r})} \quad y \quad f(\vec{r}) = \left[\frac{\delta \mu}{\delta v(\vec{r})}\right]_N = \left(\frac{\partial \rho(\vec{r})}{\partial N}\right)_{v(\vec{r})}, \tag{2.14}$$

η es una propiedad global, introducida por Parr y Pearson [5] en 1983, la cuál entrega por primera vez una definición precisa para la dureza, un concepto vagamente definido hasta entonces, pero ampliamente usado por Pearson [6] en los años de 1960 para la racionalización de las reacciones ácido-base. La dureza química puede ser vista como la *resistencia* de un sistema a transferir carga y depende de N y $v(\vec{r})$. Esta propiedad juega un papel importante en la determinación de la estabilidad y reactividad de un sistema químico [16, 23], a través del Principio de Máxima Dureza [6, 24], el cual establece que *una mayor estabilidad está asociada a una dureza máxima.*

Por otra parte, la blandura, S, es una propiedad global definida simplemente como el inverso de la dureza:

$$S = \frac{1}{\eta} = \left(\frac{\partial N}{\partial \mu}\right)_{v(\vec{r})} \tag{2.15}$$

Como la dureza es un funcional que depende del número de electrones y del potencial externo, $\eta \equiv \eta[N, v(\vec{r})]$, se puede escribir la siguiente expresión:

$$d\eta = \gamma dN + \int h(\vec{r}) dv(\vec{r}) d\vec{r}, \tag{2.16}$$

con

$$\gamma = \left(\frac{\partial \eta}{\partial N}\right)_{v(\vec{r})} \quad y \quad h(\vec{r}) = \left[\frac{\delta \eta}{\delta v(\vec{r})}\right]_N = \left(\frac{\partial f(\vec{r})}{\partial N}\right)_{v(\vec{r})}, \tag{2.17}$$

donde γ es una propiedad global que mide el cambio en la dureza debido a la variación del número de electrones y $h(\vec{r})$ es una propiedad local que mide la fluctuación de la dureza química debido al cambio en el potencial externo; a través de la relación de *Maxwell* puede ser vista como la respuesta de la función de *Fukui* al variar el número total de electrones.

Asumiendo la diferenciabilidad (funcional) de E con respecto a N y $v(\vec{r})$, surgen una serie de funciones de respuesta, como se muestra en el *Esquema 2.* En este *Esquema* se presentan las derivadas de orden superior de la energía, junto con la identificación o definición de la correspondiente función de respuesta. Aparecen dos tipos de cantidades en las derivadas de primer orden: una cantidad global, χ, la cual es una característica de todo el sistema y una cantidad local, $\rho(\vec{r})$, valor que cambia dependiendo de $\vec{r}$, es decir, cambia punto a punto. En las segundas derivadas, aparece un kernel, $\chi(\vec{r}, \vec{r}')$, que representa la respuesta de una cantidad local en un punto $\vec{r}$, cuando se perturba el sistema en un punto $\vec{r}'$. En resumen, las cantidades globales aparecen hacia el lado izquierdo, con derivadas superiores de la electronegatividad o dureza con respecto al número de electrones y las cantidades locales, hacia la derecha.

$$E[N, v(\vec{r})]$$

$$\frac{\partial}{\partial N} \swarrow \qquad \searrow \frac{\delta}{\delta v(\vec{r})}$$

$$\left(\frac{\partial E}{\partial N}\right)_{v(\vec{r})} = \mu = -\chi \qquad \left(\frac{\delta E}{\delta v(\vec{r})}\right)_{N} = \rho(\vec{r})$$

$$\swarrow \quad \searrow \qquad \swarrow \quad \searrow$$

$$\left(\frac{\partial^2 E}{\partial N^2}\right)_{v(\vec{r})} = \eta \quad \left(\frac{\partial^2 E}{\partial N \partial v(\vec{r})}\right) = f(\vec{r}) \qquad \left(\frac{\delta^2 E}{\delta v(\vec{r}) \delta v(\vec{r}')}\right)_{N} = \chi(\vec{r}, \vec{r}').$$

Esquema 2: Derivadas superiores de la energía. En este *esquema*, las derivadas que se indican por flechas hacia la izquierda son derivadas parciales de la energía con respecto al número de electrones, mientras que las derivadas que se indican hacia la derecha son derivadas parciales de la energía con respecto al potencial, $v(\vec{r})$.

2.1.2 Cálculo de Descriptores Globales

2.1.2.1 Electronegatividad y Potencial Químico Electrónico

La electronegatividad es una idea antigua, originalmente introducida por Pauling en 1932; *describe la capacidad de un átomo o molécula de atraer electrones.* Unos años más tarde, Mulliken propuso una definición práctica de electronegatividad, *el promedio aritmético del potencial de ionización (PI) y la afinidad electrónica (AE)*:

$$\chi = \frac{PI + AE}{2} \tag{2.18}$$

Resultó interesante que Iczkowski y *col.* [25], señalaran que la definición de Mulliken (ecuación (2.18)) es la aproximación de diferencia finita para una derivada parcial de la energía *versus* el número de electrones. Esta expresión se puede obtener en

forma natural dentro de la estructura de la *TFD*, a través de la identificación de la electronegatividad, χ, con el negativo del potencial químico [26]:

$$\chi = -\mu = -\left(\frac{\partial E}{\partial N}\right)_{v(\vec{r})}, \tag{2.19}$$

donde E es la energía electrónica, N el número de electrones y $v(\vec{r})$ el potencial externo en el cual se mueven los electrones.

La identificación del multiplicador de *Lagrange* μ en la ecuación (2.2) con el negativo de la electronegatividad, ofrece una vía para calcular valores de electronegatividad para átomos, grupos funcionales, clusters y moléculas.

En aplicaciones numéricas μ se calcula a partir de la aproximación de diferencia finita:

$$\mu \simeq -\frac{1}{2}(PI + AE), \tag{2.20}$$

donde PI y AE son el primer potencial de ionización y la afinidad electrónica de la molécula neutra. En cálculos basados en la teoría de Orbitales Moleculares, con el uso del teorema de *Koopmans* [27], PI y AE pueden aproximarse numéricamente por el negativo de las energías de los orbitales frontera *HOMO (High Occupied Molecular Orbital)* y *LUMO (Lowest Unoccupied Molecular Orbital)*, ε_H y ε_L, respectivamente, entonces:

$$\mu \simeq \frac{1}{2}(\varepsilon_L + \varepsilon_H) \tag{2.21}$$

Las ecuaciones (2.20) y (2.21) han sido profusamente usadas en la determinación de potenciales químicos; son las únicas definiciones operacionales que permiten cuantificar esta propiedad con resultados generalmente satisfactorios.

2.1.2.2 Dureza Global y Blandura

Como en el caso de μ, en aplicaciones numéricas η se calcula a partir de la aproximación de diferencia finita:

$$\eta \simeq -\frac{1}{2}(PI - AE); \tag{2.22}$$

si además se hace uso del teorema de *Koopmans* [27] η puede aproximarse numéricamente en términos de las energías de los orbitales frontera [5, 7, 26]:

$$\eta \simeq \frac{1}{2}(\varepsilon_L - \varepsilon_H). \tag{2.23}$$

Estas ecuaciones permiten determinar la dureza molecular directamente a partir de datos experimentales de PI y AE o directamente de cálculos basados en la Teoría de Orbitales Moleculares.

Por otra parte, la blandura (S) se define como el inverso de la dureza ($S = 1/\eta$), propiedad que da cuenta de la reactividad global del sistema. En muchos casos es ventajoso trabajar con S en vez de η debido a su característica de aditividad $S = \sum_k S_k$.

En resumen, uno de los grandes éxitos de la *TFD* es que ha generado descriptores para analizar procesos químicos, propiedades relevantes en relación a la reactividad de un sistema puesto que están directamente relacionadas con las energías de los orbitales frontera, y de esta forma se establece un vinculo con la teoría de *Fukui* de reactividad química basada en la caracterización de los orbitales frontera.

2.2 Otros Descriptores de Reactividad Química

2.2.1 Potencial Electrostático Molecular

El potencial electrostático molecular, $V(\vec{r})$, ha sido reconocido como una medida efectiva de análisis e interpretación de la conducta reactiva molecular, particularmente en interacciones no-covalentes [28,29]. El potencial electrostático que es creado en un punto $\vec{\mathbf{r}}$ por los electrones y núcleos de una molécula, está dado por:

$$V(\vec{r}) = \sum_A \frac{Z_A}{|R_A - \vec{r}|} - \int \frac{\rho(\vec{r'})d\vec{r'}}{|\vec{r'} - \vec{r}|} \tag{2.24}$$

donde Z_A es la carga sobre el núcleo A localizado en R_A y $\rho(\vec{r'})$ es la densidad electrónica molecular. $V(\vec{r})$ es un observable físico, el cual puede ser determinado experimentalmente por técnicas de difracción [29–31]. El signo de $V(\vec{r})$ en cualquier región del espacio depende de la contribución dominante, ya sea positiva del núcleo o negativa de los electrones. Los valores más negativos son generalmente asociados con pares solitarios de átomos electronegativos, mientras que los valores más positivos son asociados a hidrógenos enlazados a tales átomos (ver Artículo **B7** en Anexo B).

2.2.2 Energía de Ionización Local Promedio

Otra propiedad interesante es la energía de ionización local promedio, $\bar{I}(\vec{r})$, definida como [32]:

$$\bar{I}(\vec{r}) = \sum_i \frac{\rho_i(\vec{r})|\varepsilon_i|}{\rho(\vec{r})} \tag{2.25}$$

donde $\rho_i(\vec{r})$ y ε_i son la densidad electrónica y la energía del *i–ésimo* orbital atómico o molecular ocupado, respectivamente. Haciendo uso del teorema de *Koopmans* [27], el cual otorga la justificación para tratar a ε_i como el potencial de ionización electrónico, se interpreta $\bar{I}(\vec{r})$ como la energía promedio requerida para remover un electrón de

cualquier punto $\vec{r}$ de un átomo o molécula. $\bar{I}(\vec{r})$ es un descriptor que ha sido exitosamente usado en predecir la activación y el efecto de los sustituyentes en el benceno [28], sitios reactivos en varias moléculas orgánicas, incluyendo bases de nucleósidos [33,34]. En particular, en un reciente trabajo que hemos realizado [35] (ver Artículo **B7** en Anexo B), este descriptor ha sido usado con éxito, junto con otros índices de reactividad, en el análisis del mecanismo involucrado en las reacciones de transferencia protónica intramolecular.

En general, estos descriptores de reactividad global y los principios de estructura electrónica asociados han sido muy útiles en la comprensión de la reactividad química, formando una base conceptual de cualquier teoría de reactividad.

2.3 Modelo Teórico para Rotaciones Internas

Los procesos químicos pueden ser caracterizados a través de perfiles que ilustran el camino en el cual las propiedades de los sistemas que reaccionan cambian en función de la coordenada de reacción (**CR**). Estas propiedades pueden ser globales (energía, potencial químico, dureza, polarizabilidad, etc.) o locales (poblaciones electrónicas, funciones de *Fukui*, etc.). Dentro de la aproximación de *Born-Oppenheimer* [36], la **CR** representa la reorganización nuclear que tiene lugar a medida que la reacción avanza, es decir, la variación de las longitudes y ángulos de enlaces durante la reacción química, por lo tanto, la **CR** es una coordenada multidimensional. En muchos casos la coordenada de reacción puede ser una variable conformacional la cual conecta dos conformaciones que pueden ser vistas como reactantes y productos de una reacción química, desafortunadamente, en muchos procesos químicos la **CR** es muy difícil de visualizar. En esta Tesis, nos interesamos por reacciones elementales dentro de la estructura de la teoría del estado de transición en la cual los reactantes (**R**) cambian a productos (**P**) pasando por un estado de transición (**TS**), quedando conectados estos tres estados por una dada **CR**.

El entendimiento de la reactividad química nos permite predecir los mecanismos de la reacción y determinar cómo la energía de activación depende de las propiedades específicas de los reactantes y productos. En este contexto, la identificación de estas propiedades y la caracterización de los estados de transición pueden llegar a ser especialmente importantes. Para el primer propósito, la *TFD* es adecuada para describir la reorganización electrónica que tiene lugar durante una reacción química a través de las definiciones de las propiedades de reactividad. Por otra parte, para caracterizar los estados de transición existe un conjunto de interesantes herramientas conceptuales que proporcionan ideas complementarias sobre su estructura y propiedades. Estos elementos conceptuales son: **(a)** el postulado de *Hammond* (PH) [37] que interrelaciona la posición de la estructura de transición con la exotermicidad de la reacción, el PH establece que *si el **TS** es cercano en energía a un complejo estable dado adyacente, entonces puede además ser similar en estructura al mismo complejo*; **(b)** el postulado de *Leffler* [38] que sugiere una interpretación mecanística del llamado coeficiente de

Brønsted (β), el cual es una medida de la localización del **TS** a lo largo de la **CR**; esto define β como un índice de similaridad que puede ser interpretado como el grado de semejanza del **TS** con respecto al producto; **(c)** la ecuación de *Marcus* (EM) [39] que es una expresión simple para la energía de activación en términos de la energía de la reacción y de propiedades estructurales de reactantes y productos y **(d)** el Principio de Máxima Dureza (PMD) que *establece que los sistemas moleculares en equilibrio tienden a estados de máxima dureza* [6, 7]. Como corolario del PMD se espera que el **TS** presente un mínimo valor de dureza. Aunque estos principios no son ampliamente aplicables ellos proveen una estructura conceptual para racionalizar estados de transición y ayudan a caracterizar los mecanismos de una reacción.

Un proceso de isomerización rotacional puede ser visto como el resultado de la redistribución de la densidad electrónica de la molécula manteniendo el número total de electrones constante. Ahora bien, la modelización de estos procesos presenta gran importancia en campos que van desde la bioquímica hasta la ingeniería de materiales moleculares. La determinación de estabilidades relativas, identificación de mecanismos de reacción e interacciones específicas y la evaluación de barreras de potencial entre varias conformaciones, son factores de relevancia de investigaciones que tienen como objetivo la obtención de propiedades biológicas, químicas y físicas. En este contexto, un objetivo de este trabajo de Tesis, ha sido la proposición de formas analíticas parametrizadas que conduzcan al análisis simplificado del proceso de rotación interna y que permitan determinar características físicas de estados de transición involucrados en el proceso de rotación interna.

2.3.1 Coordenada de Reacción

Dentro de la teoría del estado de transición se asume que una reacción se lleva a cabo desde un mínimo de energía a otro vía una coordenada de reacción, pasando por un máximo intermediario (**R**$\rightarrow$ **TS** $\rightarrow$ **P**). Esta representación clásica se muestra en la *Figura 2.1(a)*, la cual está caracterizada por un perfil de energía potencial donde, los puntos estacionarios están conectados a través de la **CR**. Por otra parte, es útil y

siempre posible expresar la **CR** en términos de una coordenada de reacción reducida (**CRR**), definida en el intervalo [0,1], que mide el progreso de la reacción desde reactantes hacia productos. En la *Figura 2.1(b)*, se muestra un esquema del mismo perfil de energía, pero ahora a lo largo de una nueva coordenada reducida. Es importante hacer notar que la nueva representación entrega una correcta y directa caracterización de la posición y de la energía del estado de transición, el proceso químico queda especificado de una forma simple y esquemática y sin perder información relevante.

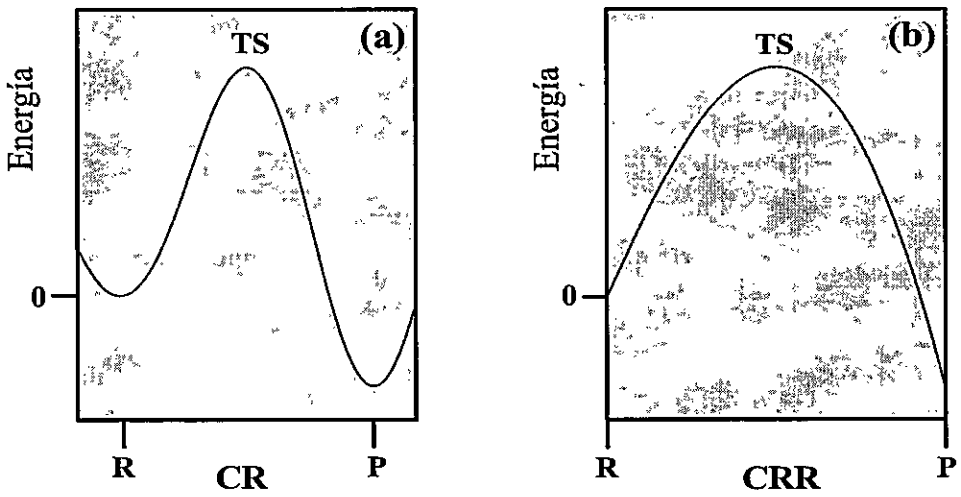

Figura 2.1: *Representación del perfil genérico de energía potencial para una situación de doble-pozo* ***(a)*** *a lo largo de la coordenada de la reacción* ***(CR)*** *y* ***(b)*** *de la coordenada de reacción reducida* ***(CRR)****.*

En el Capítulo 3, consideraremos reacciones químicas del tipo que se muestra en la *Figura 2.1*, la cual es una representación general de la energía potencial para una situación de *doble-pozo* de potencial (*Figura 2.1(a)*), donde el reactante (**R**) se transforma en producto (**P**) pasando por un estado de transición (**TS**). Además, se considerarán reacciones químicas del tipo que se muestra en la *Figura 2.2*, la cual es una representación general de la energía potencial para una situación de *doble-barrera* de potencial (*Figura 2.2(a)*), donde el estado inicial **i** cambia a un estado final **f** pasando por un intermediario estable.

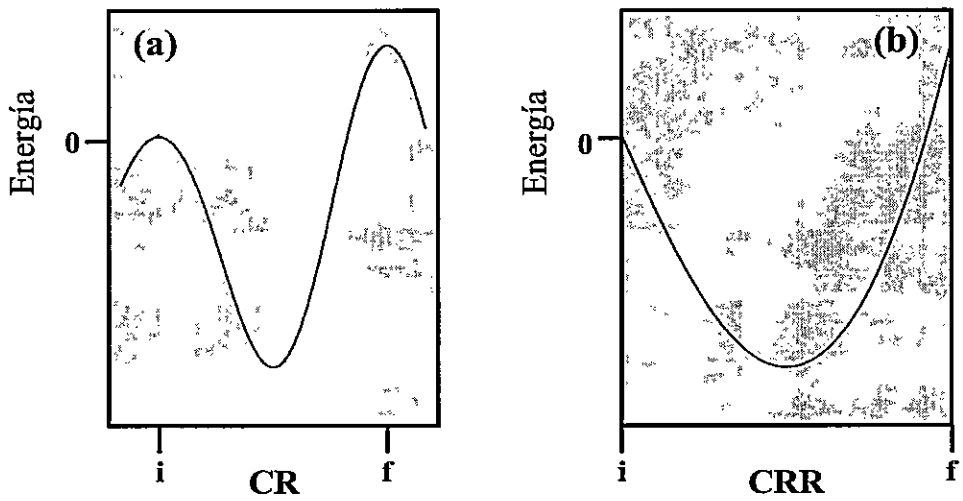

Figura 2.2: *Representación del perfil genérico de energía potencial para una situación de doble–barrera* ***(a)*** *a lo largo de la coordenada de reacción* ***(CR)*** *y* ***(b)*** *de la coordenada de reacción reducida* ***(CRR).***

Los resultados que se presentan en el Capítulo 3, muestran perfiles del tipo que se muestran en las *Figuras 2.1* y *2.2*; los estados involucrados están conectados por una coordenada de reacción α, la cual es el ángulo de torsión (ver *Figura 2.4*) definido con respecto al enlace central y medido desde el **R** ($\alpha = 0°$) a **P** ($\alpha = 180°$). De aquí en adelante, **R** define la conformación *trans* y **P** la conformación *cis*. Además, si consideramos a la conformación *trans* como el origen de la energía, el potencial modelo que usamos para describir la rotación interna de las moléculas de interés es [40–42]:

$$E(\alpha) = \frac{1}{4}K_E(1 - \cos^2\alpha) + \frac{1}{2}\Delta E°(1 - \cos\alpha), \tag{2.26}$$

donde K_E es un parámetro asociado con las conformaciones de referencia (K_E es negativo en procesos de doble barrera [41]) y $\Delta E° = (E(180°) - E(0°))$ es la energía de la reacción entre los isómeros *trans* y *cis*.

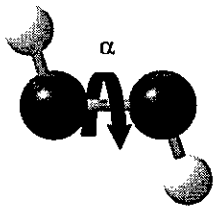

Figura 2.3: *Representación general del proceso de isomerización rotacional, donde α es el ángulo de torsión.*

Además, la coordenada de reacción reducida ω, que define la *función conformacional*, está relacionada con el ángulo de torsión a través de $\omega = (1 - \cos\alpha)/2$, nótese que ω varía desde 0 (*trans*) a 1 (*cis*). La funcional que define la energía potencial, en la nueva representación ω está dada por [41–44]:

$$E[\omega] = K_E f[\omega] + \omega\Delta E^\circ, \tag{2.27}$$

donde $f[\omega] = \omega(1-\omega)$, obtenida al reemplazar la definición de ω en la ecuación (2.26).

Puesto que μ y η son propiedades globales del sistema, su evolución a lo largo de ω puede ser representada a través de la misma forma analítica usada para $E[\omega]$, entonces:

$$\mu[\omega] = \mu[0] + K_\mu f[\omega] + \omega\Delta\mu^\circ, \tag{2.28}$$

$$\eta[\omega] = \eta[0] + K_\eta f[\omega] + \omega\Delta\eta^\circ. \tag{2.29}$$

Los parámetros $\Delta\mu^\circ, K_\mu$ y $\Delta\eta^\circ, K_\eta$ tienen el mismo significado que $\Delta E^\circ, K_E$ tienen para $E[\omega]$. Hacemos notar que $\mu[\omega]$ y $\eta[\omega]$ son relativos para $\mu[0]$ y $\eta[0]$, para simplificar debemos usar la siguiente ecuación $\Delta\mu[\omega] = \mu[\omega] - \mu[0]$ y $\Delta\eta[\omega] = \eta[\omega] - \eta[0]$. Es posible determinar los valores numéricos de los parámetros de las ecuaciones (2.27), (2.28) y (2.29), a partir de cálculos en la vecindad de los confórmeros de referencia [43, 44].

2.3.2 Relaciones entre μ, η y E

Es claro que, a partir de las ecuaciones anteriores, E, μ y η están conectadas a través de $f[\omega]$, entonces al combinar las ecuaciones (2.27), (2.28) y (2.29) se obtiene:

$$E_\eta[\omega] = \omega\Delta E^\circ + Q_\eta\left(\Delta\mu[\omega] - \omega\Delta\mu^\circ\right), \tag{2.30}$$

$$E_\mu[\omega] = \omega\Delta E^\circ + Q_\mu\left(\Delta\eta[\omega] - \omega\Delta\eta^\circ\right), \tag{2.31}$$

y

$$\Delta\mu[\omega] = \omega\Delta\mu^\circ + Q\left(\Delta\eta[\omega] - \omega\Delta\eta^\circ\right). \tag{2.32}$$

Los nuevos parámetros $\{Q_\eta, Q_\mu, Q\}$ están relacionadas con los antiguos ($\{K_E, K_\mu, K_\eta\}$) a través de $Q_\eta = K_E/K_\mu$ and $Q_\mu = K_E/K_\eta$, y se obtiene $Q = Q_\mu/Q_\eta$, estos nuevos parámetros están relacionados con la redistribución de carga electrónica durante el proceso de rotación interna.

A partir de las ecuaciones anteriores es posible obtener una expresión global para la evolución simultánea de las tres propiedades a lo largo de una coordenada de reacción, tal que combinando las ecuaciones (2.30) y (2.31) se obtiene:

$$\begin{aligned} E[\omega] &\equiv \frac{1}{2}\left(E_\eta[\omega] + E_\mu[\omega]\right) \\ &= \omega\Delta E^\circ + \frac{1}{2}Q_\eta(\Delta\mu[\omega] - \omega\Delta\mu^\circ) + \frac{1}{2}Q_\mu(\Delta\eta[\omega] - \omega\Delta\eta^\circ). \end{aligned} \tag{2.33}$$

Nótese que esta última ecuación combina aspectos energéticos, como el potencial torsional, con aspectos mecanísticos, que están incluidos en las propiedades μ y η de los procesos. Es interesante mencionar que esta ecuación es homogénea con la introducida por Parr y Pearson que describe la energía de un átomo en una molécula

con un flujo de electrones, desde o hacia el átomo, manteniendo el potencial externo constante $v(\vec{r})$ [5]. Una decripción más detallada de este desarrollo teórico que hemos realizado, se encuentra en el Artículo **B1** del Anexo B.

2.3.3 Caracterización de Puntos Críticos

En esta sección se presentan expresiones analíticas, que hemos desarrollado en este trabajo de Tesis, las cuales caracterizan al punto crítico presente en un perfil entre las conformaciones de referencia *trans* y *cis*. Este punto crítico, puede estar asociado a un estado de transición para un perfil que presenta *doble–pozo de potencial* (ver *Figura 2.1*) o a una conformación estable *gauche* para un perfil de *doble–barrera de potencial* (ver *Figura 2.2*). La posición del punto crítico se determina diferenciando la ecuación (2.26), tal que $(dE/d\alpha)_{\alpha=\alpha_0} = 0$, ($\alpha_0$ es la posición de la conformación *gauche* o del **TS**). En la representación ω del potencial torsional definimos $\beta = (1-\cos\alpha_0)/2$ como la posición del punto crítico. Estas cantidades pueden ser definidas en términos de parámetros de energía potencial, como:

$$\left(\frac{dE}{d\alpha}\right)_{\alpha=\alpha_0} = 0 \Rightarrow \cos(\alpha_\circ) = -\frac{\Delta E^\circ}{K_E} \Rightarrow \beta = \frac{1}{2} + \frac{\Delta E^\circ}{2K_E}. \tag{2.34}$$

Al introducir $cos(\alpha_\circ)$ en la ecuación (2.26) o β en la ecuación (2.27), obtenemos la siguiente expresión para la energía del punto crítico:

$$\Delta E^{\neq} \equiv \pm E[\beta] = \pm\left(\frac{1}{4}K_E + \frac{1}{2}\Delta E^\circ + \frac{(\Delta E^\circ)^2}{4K_E}\right), \tag{2.35}$$

donde el signo positivo se aplica a reacciones de *doble–pozo* y el signo negativo se aplica a reacciones de *doble–barrera*. En el primer caso $\Delta E^{\neq}$ representa una barrera de energía mientras en el segundo caso corresponde a una energía de estabilización. Al evaluar la ecuación (2.35) con $\omega = \beta$ obtenemos una expresión alternativa para $\Delta E^{\neq}$, ahora en términos del potencial químico y la dureza evaluados en $\omega = \beta$ ($\Delta\mu^{\neq} = \Delta\mu[\beta]$ y $\Delta\eta^{\neq} = \Delta\eta[\beta]$).

$$\Delta E^{\neq} = \pm \left(\beta \Delta E^{\circ} + \frac{1}{2} Q_{\eta} (\Delta \mu^{\neq} - \beta \Delta \mu^{\circ}) + \frac{1}{2} Q_{\mu} (\Delta \eta^{\neq} - \beta \Delta \eta^{\circ}) \right). \tag{2.36}$$

Es interesante observar que esta ecuación otorga nuevas interpretaciones acerca de la naturaleza de la energías de activación o de estabilización y ciertamente ayuda a obtener nuevas señales sobre los mecanismos de reacción. Se ha encontrado en diferentes tipos de reacciones que μ y η pasan por o muy cerca de un extremo en β lo que asegura que la ecuación (2.35) produzca valores fiables de barreras de potencial o energías de estabilización a partir del conocimiento de las propiedades electrónicas globales μ y η.

Por lo tanto, el punto crítico se caracteriza en términos de su posición en la coordenada de reacción y de la energía, del potencial químico y de la dureza molecular. Junto a estas propiedades, es interesante considerar la constante de fuerza torsional, la cual, a partir de un modelo de potencial armónico como $E(\alpha)$, se define a partir de la segunda derivada de la ecuación (2.26):

$$\frac{d^2 E}{d\alpha^2} = \frac{1}{2} K_E (2\cos^2 \alpha - 1) + \frac{1}{2} \Delta E^{\circ} \cos \alpha, \tag{2.37}$$

Evaluando la posición del isómero estable (α_0), pero introduciendo de inmediato el parámetro β, obtenemos la constante de fuerza torsional asociada a la conformación de mínima energía:

$$k(\beta) \equiv \left(\frac{d^2 E}{d\alpha^2} \right)_{\alpha = \alpha_0} = \frac{1}{2} (K_E + \Delta E^{\circ}) - (4K_E + \Delta E^{\circ}) \beta + 4K_E \beta^2. \tag{2.38}$$

Debido a que todos los parámetros involucrados en la ecuación anterior son conocidos, los valores numéricos de $k(\beta)$ se pueden determinar directamente. Usando β, dado en la ecuación (2.34), obtenemos:

$$k(\beta) = \frac{1}{2}\left(\frac{(\Delta E^{\circ})^2}{K_E} - K_E\right). \tag{2.39}$$

Es interesante analizar la constante de fuerza torsional no sólo paramétricamente, sino también como una función de β y eventualmente se puede maximizar con respecto a este parámetro. Diferenciando la ecuación (2.38) con respecto a β, obtenemos:

$$\frac{dk(\beta)}{d\beta} = -\left(4K_E + \Delta E^{\circ}\right) + 8K_E\beta. \tag{2.40}$$

La condición que maximiza $k(\beta)$ es:

$$\left(\frac{dk(\beta)}{d\beta}\right)_{\beta=\beta_0} = 0 \Rightarrow \beta_0 = \frac{1}{2} + \frac{\Delta E^{\circ}}{8K_E}, \tag{2.41}$$

y la posición del máximo de $k(\beta)$ no coincide con el valor determinado a partir del potencial torsional (ecuación (2.34)). Entonces β_0 puede ser escrita como:

$$\beta_0 = \beta - \frac{3\Delta E^{\circ}}{8K_E}, \tag{2.42}$$

donde es aparente que las desviaciones a partir de β pueden ocurrir dependiendo de los valores relativos de ΔE° y K_E.

La evaluación de la ecuación (2.38) en β_0 conduce a k_{max} :

$$k_{max} = k - \frac{9(\Delta E^{\circ})^2}{16K_E}, \tag{2.43}$$

Nótese que aunque β_0 y k_{max} no presentan un significado físico preciso, las ecuaciones (2.42) y (2.43) se pueden usar para ayudar a caracterizar tendencias cualitativas observadas en las moléculas bajo estudio (ver Artículo **B3** del Anexo B). Físicamente, la constante se asocia con la rigidez y fuerza de un enlace, y además está usualmente relacionada con la población electrónica de tal enlace, este punto es discutido en el Capítulo 3.

2.4 Mecanismos de Reacción

2.4.1 Fuerza Química

El concepto de mecanismo de una reacción química está relacionado con la idea de estructura molecular y cualquier proceso reactivo puede ser representado por desplazamientos nucleares del sistema molecular cuando va desde reactantes a productos. Estos desplazamientos están relacionados con las fuerzas que actúan sobre el sistema para transformar reactantes en productos y se asume que dependen sólo de la posición a lo largo de la coordenada de reacción (ω). Entonces, definimos la fuerza de *Hellmann–Feynman* [45] de una reacción química como [35, 44, 46]:

$$F(\omega) = -\frac{dE(\omega)}{d\omega}, \tag{2.44}$$

y suponiendo que $E(\omega)$ (ecuación (2.27)) pueda ser expresada en términos de una coordenada de reacción reducida definida en el intervalo [0,1] como [44]:

$$E[\omega] = K_E f[\omega] + \omega \Delta E^\circ, \tag{2.45}$$

entonces:

$$F(\omega) = -(K_E + \Delta E^\circ) + (2K_E)\omega. \tag{2.46}$$

En la *Figura 2.4*, se ilustra el comportamiento cualitativo de la fuerza a lo largo de ω para reacciones con diferentes contribuciones termodinámicas. Entonces, para tener una adecuada descripción de toda la reacción química, es necesario distinguir los diferentes procesos que tienen lugar a lo largo de la coordenada de reacción.

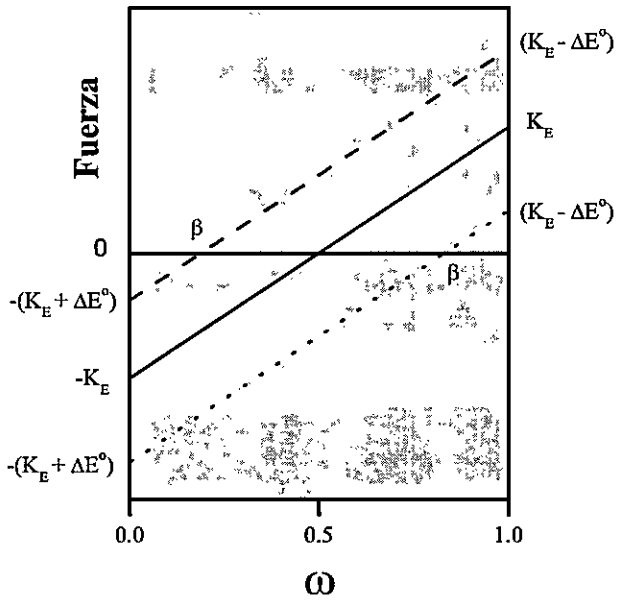

Figura 2.4: *Perfil cualitativo de la fuerza de la reacción química a lo largo de la coordenada de reacción. La línea de referencia (sólida) representa una reacción isoenergética. La línea superior (segmentada) e inferior (punteada), representan reacciones exoenergéticas y endoenergéticas, respectivamente.*

Dentro de la región de reactantes un proceso de activación tiene lugar, mientras que en la región de productos tiene lugar un proceso de relajación; el trabajo asociado con estos procesos se define como:

$$W_{act} = \int_0^{\beta} F(\omega)d\omega = \Delta E^{\ddagger} \tag{2.47}$$

y

$$W_{rel} = \int_{\beta}^{1} F(\omega)d\omega = \Delta E^{\circ} - E^{\ddagger}. \tag{2.48}$$

Las reacciones isoenergéticas (representadas por la línea sólida en la *Figura 2.4*), presentan el estado de transición en $\beta = \omega = 1/2$, donde el trabajo de activación es

igual al trabajo de relajación. Por lo tanto, la cantidad de energía requerida para la activación llega a ser igual a la cantidad de energía liberada durante la relajación. Por otra parte, las reacciones exoenergéticas (representadas por la línea superior segmentada en la *Figura 2.4*), son caracterizadas por un estado de transición temprano ($\beta < 1/2$) y el trabajo de activación es menor que el trabajo de relajación. Finalmente, una reacción endoenergética (representada por la línea inferior de puntos en la *Figura 2.4*), está caracterizada a través de $\beta > 1/2$ y el trabajo de activación es mayor que el trabajo de relajación.

En la *Figura 2.5*, se ilustran los perfiles cualitativos de la energía y de la fuerza, en función de una coordenada de reacción general ξ, para una dada reacción. Este tipo de perfiles son analizados simultáneamente para racionalizar los mecanismos involucrados en una reacción química [35]. En particular, en el Artículo **B7** del Anexo B, se estudia el mecanismo involucrado en dos procesos de transferencia protónica. En la *Figura 2.5*, los puntos críticos en el perfil de fuerza (*Figura 2.5(b)*) corresponden a los puntos de inflexión en el perfil de energía (ξ_o, ξ_1). El análisis del perfil de fuerza permite ampliar el concepto de regiones mencionado anteriormente, se puede definir la región de reactantes ($-\infty \leq \xi \leq \xi_o$), asociada a un proceso de activación, la región de productos ($\xi_1 \leq \xi \leq \infty$) asociada a un proceso de relajación y la región del estado de transición ($\xi_o < \xi < \omega_1$), donde los procesos de activación y relajación coexisten.

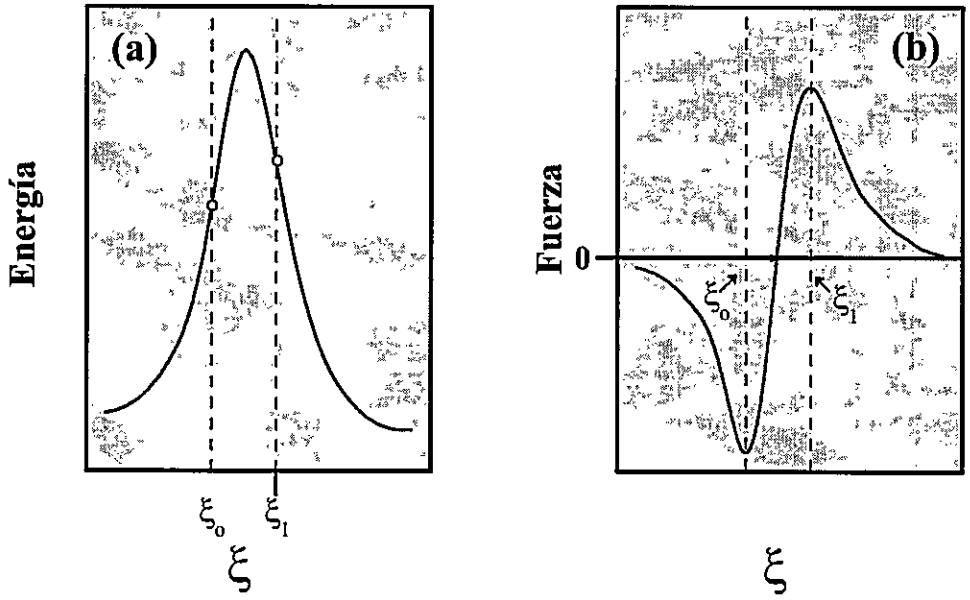

Figura 2.5: *Perfiles cualitativos de la energía (a) y de la fuerza química (b), en función de una coordenada de reacción reducida, ξ, para una dada reacción química. Los puntos críticos en el perfil de fuerza (ξ_o, ξ_1), corresponden a los puntos de inflexión en el perfil de energía.*

2.5 Química de Fragmentos

Uno de los objetivos más ambicionados que se propone cualquier modelo de análisis de reacciones químicas es la posibilidad de establecer esquemas de transferibilidad y aditividad de propiedades locales en el contexto de la predicción de propiedades de moléculas a partir del conocimiento de las propiedades de las especies constituyentes aisladas [46–48], esta idea es particularmente interesante en el estudio de reacciones de formación.

La energía asociada a la formación de una molécula o complejo molecular a partir de n_f fragmentos constituyentes no enlazados, viene dada por:

$$\Delta E_{n_f} = E - E^{\circ}_{n_f} \tag{2.49}$$

donde E es la energía de la molécula o del complejo molecular resultante optimizado y $E^{\circ}_{n_f} = \sum_x^{n_f} E_x$, con E_x la energía del fragmento x debidamente optimizado. En nuestro caso la energía de los complejos moleculares será estimada a partir de la - energía de dos o cuatro fragmentos, con energías E°_2 y E°_4, respectivamente.

Por otra parte, el principio de igualación de la electronegatividad propuesto por *Sanderson*, que define la electronegatividad molecular como *el promedio geométrico de las electronegatividades de los átomos o fragmentos aislados*, permite estimar directamente potenciales químicos y durezas moleculares a partir de [12,46]:

$$\mu^{\circ}_{n_f} = -\left(\prod_x |\mu^{\circ}_x|\right)^{\frac{1}{n_f}}, \tag{2.50}$$

donde el producto es tomado sobre los n_f fragmentos constituyentes y μ°_x se refiere al potencial químico del fragmento aislado x.

La dureza obtenida diferenciando $\mu^{\circ}_{n_f}$ con respecto a N, conduce a [46–48]:

$$\eta^{\circ}_{n_f} = \left(\frac{d\mu^{\circ}_{n_f}}{dN}\right)_{v(\vec{r})} = \frac{\mu^{\circ}_{n_f}}{n_f}\sum_{x}^{n_f}\frac{\eta^{\circ}_{x}}{\mu^{\circ}_{x}}. \tag{2.51}$$

donde η°_{x} es la dureza del fragmento x. La diferencia entre los valores aproximados ($\mu^{\circ}_{n_f}$ y $\eta^{\circ}_{n_f}$) y los valores de referencia determinados a partir de cálculos *ab-initio*, puede ser atribuida a la relajación de la densidad electrónica después del enlazamiento. La cuantificación de esta diferencia puede ayudar en el entendimiento del reordenamiento de la densidad electrónica cuando ocurre la reacción.

La derivada de la dureza con respecto a N a potencial externo constante, ha sido definida previamente [49] como γ y ha sido numéricamente estimada sólo en átomos e iones atómicos. Como es de esperar en la mayoría de los casos γ presenta valores más pequeños que μ y η [49]. Dentro del esquema de *Sanderson*, hemos obtenido a partir de la ecuación (2.51) la siguiente expresión [47]:

$$\gamma^{\circ}_{n_f} = \left(\frac{\partial\eta^{\circ}_{n_f}}{\partial N}\right)_{v(\vec{r})} = \frac{(\eta^{\circ}_{n_f})^2}{\mu^{\circ}_{n_f}} - \frac{\mu^{\circ}_{n_f}}{n_f}\sum_{x}^{n_f}\left(\frac{\eta^{\circ}_{x}}{\mu^{\circ}_{x}}\right)^2 + \frac{\mu^{\circ}_{n_f}}{n_f}\sum_{x}^{n_f}\frac{\gamma^{\circ}_{x}}{\mu^{\circ}_{x}}, \tag{2.52}$$

que permite estimar γ, usando potenciales químicos y durezas atómicas (o de fragmentos). El tercer término de la ecuación (2.52) contiene la propiedad γ de los fragmentos, γ°_{x}, que será obtenida a través de una expresión empírica en términos de las energías de los orbitales frontera de los fragmentos involucrados, como se verá en el Cápítulo 4.

Dentro de los resultados más relevantes relacionados con las reacciones de formación de agregados moleculares (Capítulo 4), se encuentra la formulación de un nuevo esquema de aditividad para el potencial químico y la dureza molecular, esquema alternativo al propuesto por *Sanderson* [47]. Estos resultados, que se muestran en el Capítulo 4, fueron confrontados exitosamente con los obtenidos a través del esquema de *Sanderson* y otros esquemas de aditividad de propiedades electrónicas.

Capítulo 3

Reacciones de Rotación Interna

Resumen

En este Capítulo, se muestra el estudio de varios procesos de rotación interna desde la perspectiva de la evolución simultánea de los perfiles de energía, potencial químico y dureza molecular. El interés de este estudio se centra en la caracterización y racionalización simultánea de los aspectos energéticos y mecanísticos durante el progreso de una reacción química. Dentro de los resultados más relevantes que se muestran está la caracterización de diferentes mecanismos de isomerización a través de la identificación de interacciones locales específicas y la clasificación de las correspondientes barreras de energía en términos de interacciones a través del enlace y del espacio.

3.1 Introducción

En este Capítulo, se muestra el estudio de los procesos de isomerización rotacional mediante el análisis de perfiles de energía, potencial químico y dureza molecular. En este contexto, nuestro trabajo contribuye a la racionalización y comprensión de los aspectos energéticos y mecanísticos involucrados en reacciones de isomerización rotacional.

En este Capítulo, se presentan resultados para los procesos de rotación interna de diferentes tipos de reacciones de isomerización: **(a)** peróxido de hidrógeno (HOOH), tioperóxido de hidrógeno (HOSH) y persúlfuro de hidrógeno (HSSH), resultados que permiten caracterizar los mecanismos de isomerización desde la conformación más estable *gauche* pasando por barreras en las conformaciones *trans* y *cis*. Estas son reacciones que hemos denominado de *doble–barrera* (ver *Figura 2.2*, Capítulo 2). Se identifican interacciones específicas y clasifican las correspondientes barreras de energía de acuerdo a interacciones a través del enlace y/o del espacio; **(b)** ácidos nitroso (HONO) y ditionitroso (HSNS), reacciones de *doble–pozo* (ver *Figura 2.1*, Capítulo 2), donde se discuten los perfiles de los índices de reactividad para la rotación interna a través de principios de reactividad química; y **(c)** cloruro de oxalilo (ClOC-COCl), reacción cuyo perfil de energía presenta un mínimo y un máximo. En este caso los resultados permiten explorar las interacciones intramoleculares específicas que son el origen de la estabilización de las conformaciones de interés.

3.2 Resultados y Discusión

3.2.1 Rotación Interna de HOOH, HSOH y HSSH

En esta sección presentamos el proceso de rotación interna en peróxido de hidrógeno (HOOH) y derivados azufrados, tioperóxido (HSOH) y persúlfuro (HSSH) y se muestran los resultados del estudio de la evolución simultánea a lo largo de la coordenada de reacción de E, μ y η. Nótese nuevamente que se trata de procesos torsionales que

presentan un pozo de potencial en la conformación *gauche* y dos barreras de energía en *trans* y *cis*. Esto nos lleva a estudiar, en un sistema simple, dos posibles caminos de isomerización que están asociados a diferentes mecanismos debido a interacciones locales específicas. Como se mencionó en el Capítulo 1, dentro de los objetivos específicos de esta Tesis está la caracterización de los mecanismos de reacción y la naturaleza de las barreras de potencial.

Existe bastante información experimental sobre HOOH [50–52] y HSSH [37, 53–55]. La unidad **OO** aparece en muchas moléculas interesantes y reacciones atmosféricas que involucran radicales; moléculas que contienen enlaces **SS** sirven como prototipo para las uniones **SS** en proteínas, otorgando un punto de partida para entender la estructura de muchos sistemas. Por otra parte, el tioperóxido de hidrógeno es una molécula que se cree participa como intermediario en reacciones atmosféricas que conducen al consumo de ozono y en varios procesos asociados con la oxidación atmosférica de sulfuros, uno de los procesos químicos que conducen a la lluvia ácida [56–59]. Desde un punto de vista teórico, estas moléculas han sido estudiadas extensamente, en especial HOOH [42,60–62] y HSSH [40,41,63,64]; HSOH ha sido menos estudiada aunque existen algunos trabajos en donde se han estudiado la estructura molecular y la termoquímica a partir de sus radicales [48, 65–67]. Todas estas moléculas poseen dos conformaciones planares, los isómeros *trans* y *cis*, los cuales presentan mayor energía que la conformación estable *gauche*.

3.2.1.1 Caracterización del Isómero Estable

Los parámetros geométricos optimizados al nivel de cálculo ya mencionado (ver Capítulo 1) para la conformación estable *gauche*, están dados en la *Tabla 3.1*. Las longitudes de enlace de HSOH son muy similares a las de HOOH y HSSH; nótese que la distancia **S-O** es intermedia entre las distancias **O-O** y **S-S**. Es interesante notar que la configuración estable *gauche* en HOOH es más cercana al isómero *trans* que en las moléculas que contienen azufre.

Tabla 3.1: *Parámetros estructurales (longitudes de enlace (r), ángulos (<) y momentos dipolares ($\vec{\mu}$) de las conformaciones* gauche *de los peróxidos de hidrógeno, calculados a través de cálculos ab-initio 6-311G**. α_0 es la posición del isómero* gauche. *r está en Å, < en grados y $\vec{\mu}$ en Debye.*

Parámetro	HOOH	HSOH	HSSH
$r(OH)$	0.942	0.942	
$r(SH)$		1.333	1.331
$r(OO)$	1.386		
$r(SO)$		1.652	
$r(SS)$			2.078
$< HOO$	102.7		
$< HOS$		109.1	
$< HSO$		98.7	
$< HSS$			98.6
α_0	63.7	88.4	90.2
$\vec{\mu}$	1.911	1.992	1.573

La *Figura 3.1* indica que los perfiles de energía de HSOH y HSSH son similares pero difieren significativamente del perfil de HOOH. Esto indica la posibilidad de distinguir estos sistemas en términos de sus interacciones locales específicas.

En la *Tabla 3.2*, se presentan las barreras de activación junto con las propiedades más relevantes de la conformación *gauche* y los parámetros necesarios para definir los perfiles de E, μ y η a lo largo de la coordenada de reacción. La conformación estable *gauche* se encontró en $\beta = 0.279$, 0.486 y 0.502 para HOOH, HSOH y HSSH, respectivamente, con barreras *cis* más altas en energía que las barreras *trans* ($\Delta E^{\neq} =$ 0.87 *kcal/mol*, 4.62 *kcal/mol* y 5.65 *kcal/mol*, para HOOH, HSOH y HSSH, respectivamente). Las barreras *trans* experimentales están disponibles para HOOH y HSSH: éstas son de 1.10 *kcal/mol* [52] y 5.82 *kcal/mol* [53], respectivamente, valores que están en muy buen acuerdo con nuestros cálculos. Es importante destacar que la barrera *trans* de HSOH se encontró dentro de los límites definidos por las correspondientes barreras de HOOH y HSSH.

Tabla 3.2: *Propiedades de activación y parámetros que definen los perfiles de energía, potencial químico y dureza de HOOH, HSOH y HSSH. La energía está en kcal/mol; μ y η están en eV.*

Parámetro	HOOH	HSOH	HSSH
$\Delta E^{\neq}_{trans}$	0.87	4.62	5.65
$\Delta E^{\neq}_{cis}$	8.65	6.83	7.90
ΔE°	7.78	2.21	2.25
β	0.279	0.486	0.502
$E(\beta)$	-0.87	-4.62	-5.65
$\mu(\beta)$	-4.24	-3.58	-4.17
$\eta(\beta)$	8.56	6.62	6.35
K_E	-15.03	-22.68	-26.92
K_μ	-1.41	-0.55	-2.02
K_η	2.00	1.48	3.01
Q_μ	-0.33	-0.67	-0.39
Q_η	0.46	1.78	0.58
Q	-0.71	-0.37	-0.67

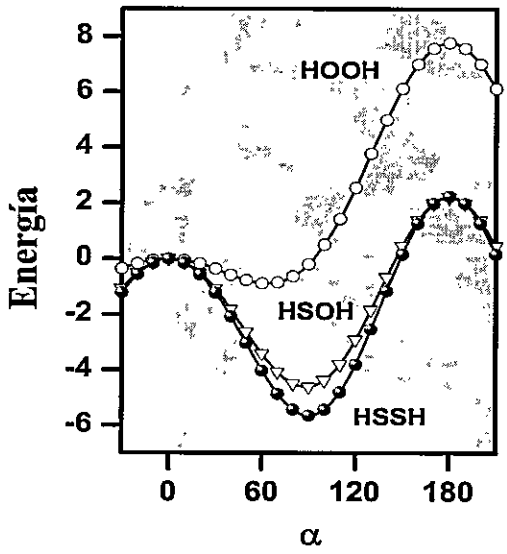

Figura 3.1: *Perfil a lo largo del ángulo torsional α de HOOH, HSOH, HSSH. La energía está en kcal/mol, α está en grados.*

Usando los valores optimizados de $\Delta E^{\neq}$ y ΔE° en la ecuación (2.35), hemos determinado los parámetros K_E de las tres moléculas. Estos son K_E(HOOH) = -15.03 *kcal/mol*, K_E(HSOH) = -22.68 *kcal/mol* y K_E(HSSH) = -26.92 *kcal/mol*. Debemos mencionar que el uso de β y ΔE° en la ecuación (2.34) para obtener todos los K_E conduce a resultados poco fiables debido a la inestabilidad numérica que aparece para valores de β muy cercanos a 0.50, como es el caso para HSOH y HSSH. Sin embargo, hemos usado la ecuación (2.34) para chequear la consistencia del modelo de potencial: los valores numéricos de todos los K_E son usados para obtener una estimación independiente de β y hemos obtenido 0.241 para HOOH; 0.451 y 0.458 para HSOH y HSSH, respectivamente, valores que son muy cercanos a los optimizados. La diferencia en β supone un cambio pequeño de alrededor de 5° en el ángulo torsional y puede ser usado para estimar la exactitud de nuestros resultados. La consistencia se ha alcanzado dentro de un margen razonable de error en β y por lo tanto, los resultados a partir del modelo son considerados fiables.

Conociendo ahora los valores de todos los K_E , es posible tener una mejor caracterización de los isómeros estables *gauche*, calculando la constante de fuerza torsional a través de la ecuación (2.39) y obtenemos k(HOOH) = 0.0382 $mdyn$Å$/rad^2$,k(HSOH) = 0.0781 $mdyn$Å$/rad^2$ y k(HSSH) = 0.0929 $mdyn$Å$/rad^2$. Nuevamente notamos que la constante de fuerza de HSOH se encuentra dentro de los límites de los valores de HOOH y HSSH, aunque es más cercana a k(HSSH) como se esperaba a partir del análisis de los perfiles de energía.

Los valores de k muestran que HSSH es torsionalmente la molécula más rígida, seguida de HSOH, HOOH presenta un movimiento vibracional de gran amplitud alrededor del ángulo de equilibrio α_0. Es necesario mencionar que sólo en esta última molécula, existe una desviación significativa de β_0 (ecuación (2.42)) con respecto a β, encontrando un valor de $\beta_0 = 0.435$ comparado con $\beta = 0.279$. Esta diferencia se debe al alto valor de $\Delta E°$. En las otras dos moléculas la diferencia entre β y β_0 no es relevante. Observamos que un máximo valor de la población electrónica del enlace central en HOOH es muy cercana a β_0.

3.2.1.2 Perfiles de μ y η

En las *Figuras 3.2(a)* y *3.2(b)* se presentan los perfiles del potencial químico y de dureza. A partir de los valores optimizados de $\mu[\beta]$ y $\eta[\beta]$ hemos determinado los parámetros K_μ y K_η de las ecuaciones (2.28) y (2.29), valores que se muestran en la *Tabla 3.2* junto con K_E y Q. Es así, como los perfiles analíticos de E, μ y η son totalmente definidos a través del conocimiento de los parámetros involucrados. Nótese que en la *Figura 3.2(a)* los perfiles de μ de HOOH y HSSH son cualitativamente similares: en ambos casos μ decae en forma drástica a partir de la conformación *trans* y estas dos moléculas presentan una variación mayor del potencial químico a lo largo de α. Nótese que el valor mínimo de μ se encuentra alrededor de $\alpha = 90°$ y en HOOH se desvía significativamente del mínimo de energía que se muestra en la *Figura 3.1.* En HSOH, μ permanece casi constante a lo largo de la coordenada de reacción. En la *Figura 3.2(b)* se presentan las tres moléculas con una máxima dureza cerca de $\alpha = 90°$.

En general, se sabe que μ y η presentan puntos críticos cercanos a la posición donde el perfil de energía presenta un punto crítico, este es el caso para HSOH y HSSH, pero como ya mencionamos, HOOH presenta un desplazamiento entre la posición del mínimo de energía y los puntos críticos de μ y η.

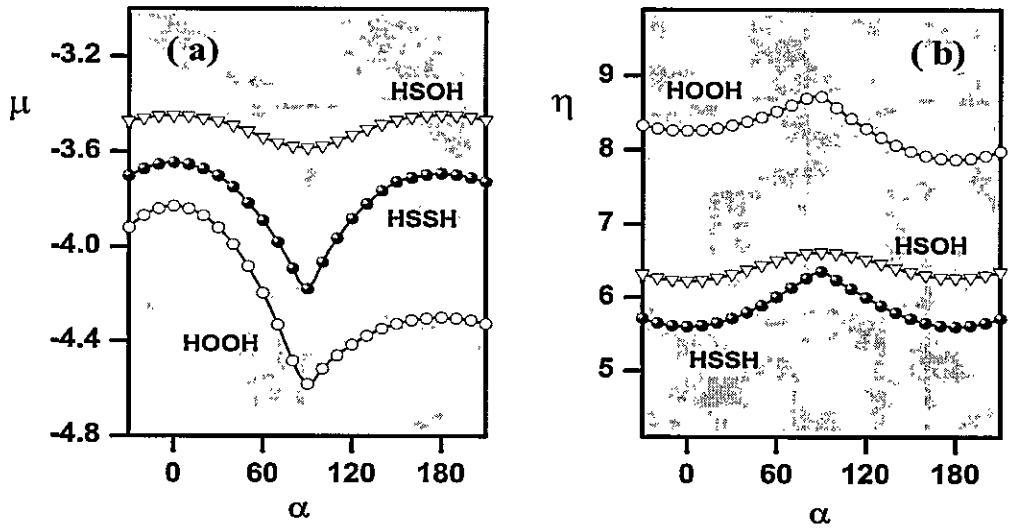

Figura 3.2: *Perfil a lo largo del ángulo torsional α de (a) potencial químico y (b) dureza molecular para HOOH, HSOH, HSSH. μ y η están en eV.*

En la molécula de peróxido de hidrógeno, los puntos críticos para μ y η se encontraron en $\beta = 0.45$, muy cercano a β_0, la posición para el valor máximo de la constante de fuerza torsional. Esto indica que las interacciones locales específicas que aseguran la estabilidad de la conformación *gauche* no son el origen de la máxima dureza, probablemente debido al hecho de que el potencial químico no permanece constante a lo largo de la coordenada de reacción, como lo requiere el *PMD*.

3.2.1.3 El Principio de Máxima Dureza

En la *Figura 3.3* se presentan simultáneamente los perfiles de potencial torsional y de la dureza molecular para los tres sistemas, se observa que en los tres casos el mínimo de energía está asociado con la máxima dureza, mientras que los máximos

en energía están asociados con mínimos de dureza. Entonces, el *PMD* se satisface y la condición de máxima dureza complementa el criterio de mínima energía para la estabilidad molecular.

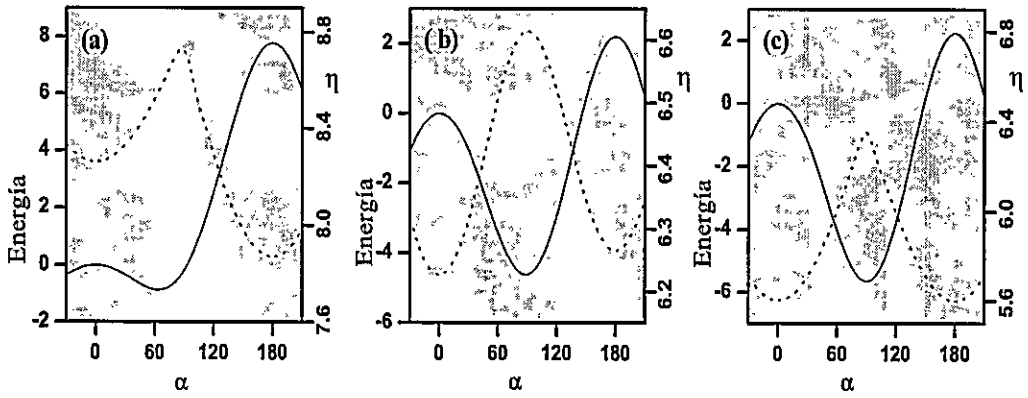

Figura 3.3: *Perfiles de energía y dureza molecular (- - -), a lo largo del ángulo torsional α para (a) HOOH, (b) HSOH y (c) HSSH. La energía está en kcal/mol, η en eV y α está en grados.*

Sin embargo, se ha mostrado que el *PMD* no es el producto de una simple relación opuesta entre energía y dureza; por ejemplo, los perfiles de dureza y energía pueden presentar puntos críticos que no coinciden entre sí, produciendo una particular conducta en la representación $\{\eta, E\}$. En el presente caso, un análisis de los perfiles de E y η muestran que globalmente estas propiedades presentan una tendencia opuesta, aunque presentan discrepancias que pueden ser debido a otros efectos o al hecho de que el *PMD* fue planteado bajo las condiciones de potencial químico y externo constantes [24, 68].

3.2.1.4 Mecanismos de Isomerización

Con el objeto de avanzar en el entendimiento del mecanismo torsional, es necesario caracterizar cuantitativamente la densidad de carga. Sin embargo, aunque no hay una vía rigurosa para esto, el análisis de la población electrónica se puede

usar para este propósito. Entonces, analizamos la evolución a lo largo de ω de la población electrónica de *Mulliken* localizada sobre las regiones del enlace. La población electrónica total de enlace ρ_{bond} está dada por la suma de las poblaciones electrónicas localizadas sobre las regiones de enlace de la molécula:

$$\rho_{bond}(\omega) = \rho_{XH}(\omega) + \rho_{XY}(\omega) + \rho_{YH}(\omega), \tag{3.1}$$

con X, Y= O, S. La *Figura 3.4(a)* muestra la evolución de ρ_{bond} y la *Figura 3.4(b)* muestra la variación de la población del enlace central ρ_{xy}. En HOOH y HSOH ρ_{bond} disminuye monotónicamente a partir del isómero *trans* ($\omega = 0.0$) hacia el isómero *cis* ($\omega = 1.0$), mientras que en HSSH presenta una conducta parabólica con un máximo valor en el isómero *gauche*. Por otra parte, en las tres moléculas, la población del enlace central ρ_{xy} muestra una conducta parabólica con un máximo valor en la región del isómero *gauche*. En conexión con las constantes de fuerza torsional, las que varían según k(HSSH) > k(HSOH) > k(HOOH), esperaríamos el mismo orden para ρ_{xy}, sin embargo y como resultado opuesto, hemos encontrado a lo largo de la coordenada de reacción que $\rho_{SO} > \rho_{SS} > \rho_{OO}$. Estos resultados indican que las conformaciones estables no están determinadas sólo por un fuerte solapamiento, sino que también, por interacciones específicas a través del espacio y las constantes de fuerza asociadas pueden ser caracterizadas a través del teorema electrostático de $Hellman-Feynman$ [42,45]. Este es el caso para el peróxido de hidrógeno, donde ρ_{OO} presenta un valor máximo pero no en el mínimo de energía sino que alrededor de β_0, donde la constante de fuerza torsional y la dureza presentan valores máximos.

La *Figura 3.4(a)* muestra que el isómero estable de HOOH y HSOH no está asociado con un valor extremo de ρ_{bond}, lo cual indica que los dos mecanismos para la isomerización, los caminos *trans* y *cis* son diferentes, debido a que ellos están acompañados de un aumento y disminución de los valores de ρ_{bond}, respectivamente. Como se indica por las flechas de trayectoria. Es por esta razón, que hemos caracterizado cualitativamente el mecanismo *trans* principalmente con interacciones a través del enlace

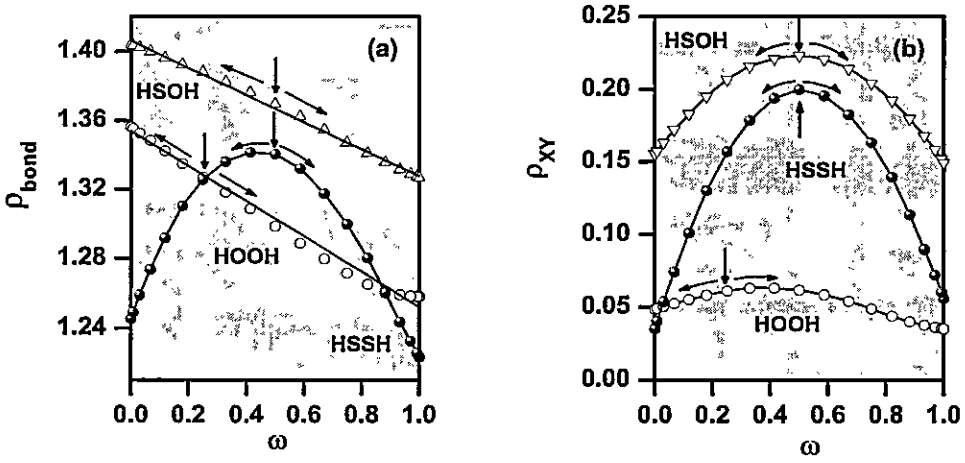

Figura 3.4: *Perfiles para HOOH, HSOH y HSSH a lo largo de la coordenada de reacción ω de* ***(a)*** *la población electrónica de enlace total (ρ_{bond}) y* ***(b)*** *la población del enlace central (ρ_{xy}). Las flechas verticales indican la posición de la conformación estable. Las flechas de trayectoria $\leftarrow$ y $\rightarrow$ indican el camino hacia el isómero* trans *y hacia el isómero* cis*, respectivamente.*

(aumento de ρ_{bond}), mientras que el mecanismo *cis* puede ser asociado con interacciones electrostáticas a través del espacio (disminución de ρ_{bond}). El caso de HSSH es diferente, ya que cualquier desviación desde la estructura de equilibrio, involucra una disminución en ρ_{bond} y ρ_{SS}. Este último resultado indica que los cambios locales concentrados en los centros atómicos están aumentando. En los términos anteriormente mencionados, concluimos que en HSSH, ambos mecanismos de reacción son caracterizados principalmente a través de interacciones electrostáticas a través del espacio.

3.2.1.5 Naturaleza de las Barreras en la Rotación Interna

Debido a que no hay cambios en el número total de electrones durante la rotación interna, cualquier cambio en ρ_{bond} puede estar acompañado por un cambio opuesto en las cargas atómicas. El cambio en las cargas atómicas locales a lo largo de la coordenada de reacción, se puede reflejar en el cambio de una propiedad global como el momento dipolar. En la *Figura 3.5*, se presenta la evolución de esta propiedad a lo

largo de ω. El análisis simultáneo de la población electrónica de enlace y el momento dipolar ayudan a entender la naturaleza de las dos barreras de potencial involucradas en el proceso de isomerización rotacional.

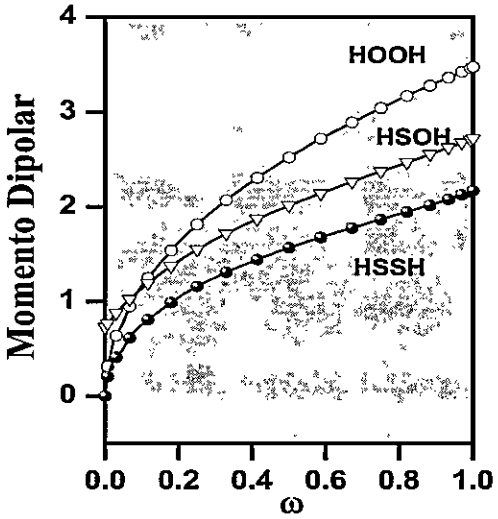

Figura 3.5: *Momento dipolar para HOOH, HSOH y HSSH a lo largo de la coordenada de reacción ω. El momento dipolar está en Debye.*

En el peróxido y tioperóxido de hidrógeno, la barrera *trans* se puede ser racionalizar en términos de un aumento de ρ_{bond} y una disminución en el momento dipolar y, por esta razón, esta barrera se debe principalmente a interacciones a través del enlace. Por otra parte, la barrera *cis* presenta una conducta opuesta, la cual está asociada con una disminución de ρ_{bond} y un aumento del momento dipolar, lo que conduce a una barrera debida principalmente a interacciones a través del espacio.

En HSSH ambos pasos torsionales están acompañados por una disminución de los valores de ρ_{bond} y ρ_{SS} y un aumento en el momento dipolar está indicando que la barrera *cis* está asociada con interacciones a través de espacio. No es posible clasificar con certeza la naturaleza de la barrera *trans*; creemos que ésta debe ser el resultado de un balance de interacciones a través del enlace y del espacio.

3.2.2 Rotación Interna de HONO y HSNS

En esta sección presentamos los resultados más relevantes para la reacción de isomerización *trans* $\Leftrightarrow$ *cis* de ácido nitroso (HONO) y su análogo azufrado (HSNS), el cual se ilustra en la *Figura 3.6.* La importancia de estos sistemas radica en que ambos compuestos contienen la unidad S(O)-N, que permite caracterizar enlaces S(O)-N presentes en compuestos inorgánicos de interés [69].

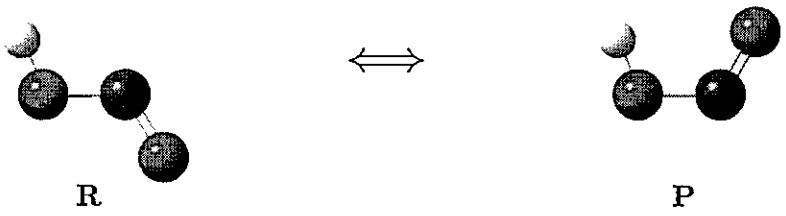

Figura 3.6: *Representación del equilibrio conformacional en la reacción de isomerización rotacional de las moléculas HXNX, (X= O, S).*

3.2.2.1 Propiedades Globales: E, μ y η

En la *Figura 3.7* se muestran los perfiles de E, μ y η estudiados a lo largo del ángulo de torsión definido como el ángulo dihedro HXNX. Los resultados que se discuten son los más relevantes evitando un análisis similar al efectuado para los derivados del peróxido de hidrógeno que mostramos en la sección anterior. La isomerización rotacional para HONO y HSNS presenta perfiles con *doble–pozo* de potencial a diferencia de los perfiles de *doble–barrera* presentados para el peróxido de hidrógeno y sus derivados azufrados.

La *Figura 3.7* ilustra la validez del Principio de Máxima Dureza en estos sistemas rotacionales. El mínimo en la energía está asociado con un máximo en la dureza, mientras que el **TS** está asociado con un mínimo de dureza.

En la *Tabla 3.3* se muestran a nivel HF/6-311G** y B3LYP/6-311G**, los resultados

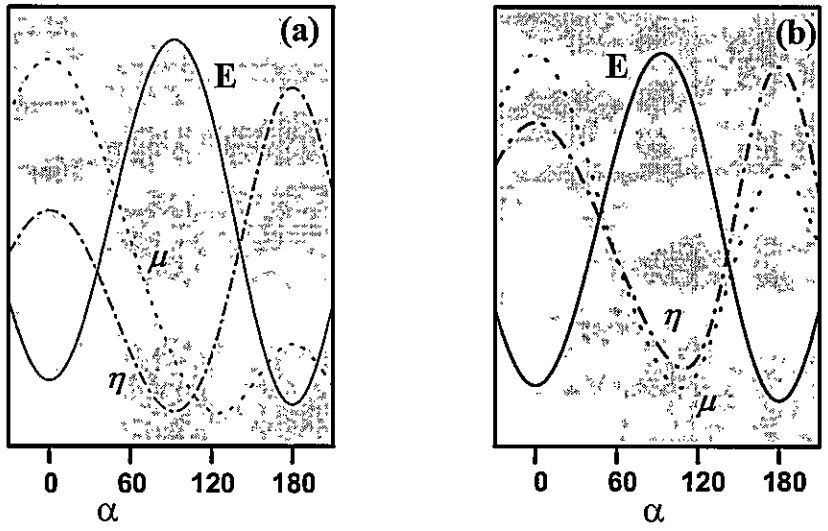

Figura 3.7: *Perfiles cualitativos de propiedades de reactividad global a lo largo de la coordenada torsional de* ***(a)*** *HONO y* ***(b)*** *HSNS. Los valores numéricos representativos para estas propiedades están dados en la Tabla 3.3.*

para la energía (ΔE° y $\Delta E^{\neq}$), el potencial químico ($\Delta\mu^{\circ}$ y $\Delta\mu^{\neq}$) y la dureza molecular ($\Delta\eta^{\circ}$ y $\Delta\eta^{\neq}$), también se incluye en esta *Tabla* el coeficiente de *Brønsted* β, el cual indica si el **TS** es cercano a reactante o producto.

Es interesante hacer notar, a partir de los valores de la *Tabla 3.3*, que a los dos niveles de teoría (Hartree-Fock y Teoría de Funcionales de la Densidad), las barreras torsionales de HONO y HSNS son muy similares; en ambos cálculos HSNS presenta

Tabla 3.3: *Propiedades de activación de la reacción de isomerización de HONO y HSNS. Todos los valores están en kcal/mol.*

HONO	ΔE^{o}	$\Delta E^{\neq}$	$\Delta\mu^{o}$	$\Delta\mu^{\neq}$	$\Delta\eta^{o}$	$\Delta\eta^{\neq}$	β
HF	-0.8082	11.0611	-7.3424	-7.8428	3.3876	-5.5852	0.4912
DFT	-0.2391	13.0051	-5.5230	-10.2296	2.5113	-6.2125	0.4977
HSNS							
HF	-0.6200	12.8728	-2.3706	-6.4638	0.7010	-2.6358	0.4941
DFT	-1.1201	15.3884	-1.9463	-12.1113	1.1277	-3.5767	0.4912

un valor levemente mayor de $\Delta E^{\neq}$ que HONO. Esto puede estar indicando que HSNS presenta un efecto hiperconjugativo en las unidades SNS lo que aumenta la energía requerida para la rotación interna.

Es importante señalar que en el Articulo **B5** (*Molecular Physics*, 101 **(2003)** 2841-2853) del Anexo B, se incluye el análisis exhaustivo del cambio que experimenta un conjunto de propiedades globales y locales durante la rotación interna de HONO y HSNS.

3.2.3 Rotación Interna de ClOC-COCl

En esta sección presentamos el estudio del proceso de rotación interna alrededor del enlace **C-C** del cloruro de oxalilo (ClOC-COCl). La motivación para este estudio proviene de la aparente contradicción entre resultados experimentales [66, 70–74] y teóricos [75–79], sobre la existencia de un confórmero *gauche* que aparece entre los isómeros de referencia *trans* y *cis*. El isómero *trans* fue identificado como un isómero estable a través de estudios espectroscópicos y de rayos X mientras que un isómero *gauche* fue caracterizado a través de experimentos de difracción de electrones. Estos estudios muestran que el isómero *gauche* es menos estable que el *trans* por alrededor de 1.4 *kcal/mol* [73, 74]. Los resultados a partir de espectros *Raman* presentan consistencia y predicen una diferencia de energía entre los dos confórmeros de 0.9 *kcal/mol* en favor de la forma *trans* [71, 72, 80]. Por otra parte hay coincidencias en que el isómero *cis* en un máximo de energía. En este contexto el perfil energético que presenta la torsión en el cloruro de oxalilo no se puede asimilar a los perfiles analizados en las secciones anteriores.

El estudio teórico de la rotación interna en el cloruro de oxalilo ha presentado dificultades tanto a nivel *Hartree–Fock* como *post Hartree-Fock*, en particular para caracterizar inequívocamente el isómero *gauche*. Un gran número de cálculos, usando una variedad de bases, fueron realizados por diferentes autores [75–79] y como resultado, muchos de estos cálculos fallaron en predecir la conformación estable *gauche*.

El estudio teórico que realizamos se apoya en la *TFD*, que ha sido usada satisfactoriamente en varios estudios teóricos de sistemas que contienen átomos de oxígeno y cloro [81, 82].

Primero es importante mencionar que la comparación favorable de geometrías de los isómeros *trans*, *gauche* y *cis* nos lleva a validar los métodos de cálculo usados. La comparación entre los datos experimentales [73, 74] y los teóricos de los parámetros geométricos de estas tres estructuras, son mostrados en la *Figura 3.8*, notamos que la comparación es satisfactoria.

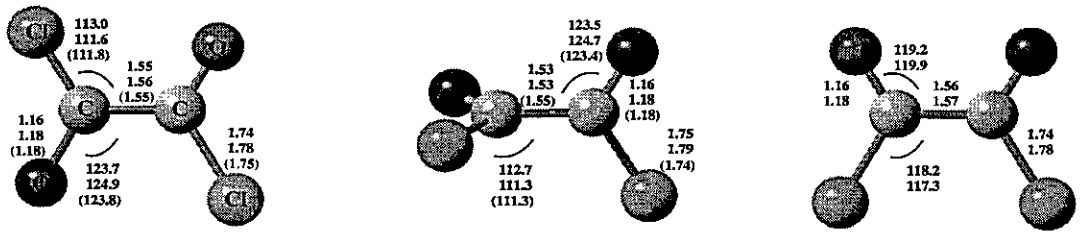

trans (α=0°) **gauche (α~90°)** **cis (α=180°)**

Figura 3.8: *Parámetros estructurales de los isómeros principales, a lo largo del ángulo de torsión, determinados a nivel HF/6-311G** (valor superior) y B3LYP/6-311G**. Los valores experimentales están dados entre paréntesis. Las distancias de enlace están en Å; ángulos de enlace están en grados.*

3.2.3.1 Potencial Torsional

En la *Figura 3.9* se muestra el potencial torsional determinado a través de la metodología HF y *TFD*. El análisis de nuestros resultados muestra que la molécula, en su estado fundamental, es plana, presentando una configuración *trans* y un isómero *gauche* que aparece entre el isómero *trans* y *cis*. Las curvas HF y *TFD* en la *Figura 3.9* presentan la misma tendencia cualitativa y en ambos métodos, el isómero *cis* corresponde al estado de transición con barrera de energía de 2.5 *kcal/mol* a nivel *TFD* y 4.0 *kcal/mol* a nivel HF. Ambas curvas presentan un *"hombro"* alrededor de $\alpha = 90°$, el isómero *gauche* aparece en nuestros cálculos como una conformación intermediaria metaestable, energéticamente sobre el isómero *trans* por 1.0-2.0 *kcal/mol*. Como resultado relevante, los cálculos dados por *TFD* otorgan una mejor caracterización que HF para del isómero *gauche*. La evidencia energética de la existencia del isómero *gauche* será verificada, a través del análisis de las diferentes propiedades globales.

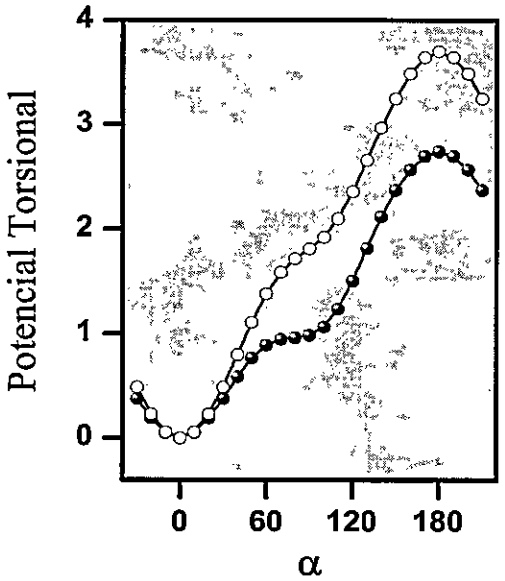

Figura 3.9: *Potencial torsional (en* kcal/mol*) a nivel HF/6-311G** (∘ – ∘) y B3LYP/-6-311G** (• – •) para la rotación interna del cloruro de oxalilo a lo largo del ángulo de torsión α (en grados).*

3.2.3.2 Potencial Químico y Dureza Molecular

La *Figura 3.10* muestra los perfiles de μ y η, calculados a partir de la definición dada por Parr y Pearson [5], a lo largo del ángulo torsional α. Se encontró que los perfiles a nivel HF y *TFD* son similares, en ambos casos la conformación *gauche* presenta un máximo en el potencial químico y la dureza y un mínimo en los isómeros *trans* y *cis*.

La *Figura 3.10(a)* indica un máximo de dureza en la región de la conformación *gauche*, lo que basado en el *PMD* agrega elementos para confirmar la existencia del isómero *gauche*. La *Figura 3.10(b)* muestra que a nivel HF y *TFD*, el potencial químico presenta una variación a lo largo del ángulo torsional, μ presenta un mínimo en las conformaciones planares *trans* y *cis* y un máximo en el isómero *gauche*. Los cambios en el potencial químico indican que la densidad electrónica sufre un reordenamiento, la variación de μ durante la rotación interna puede ser explicada en términos de la transferencia electrónica a partir de las conformaciones con valores altos de μ, en este

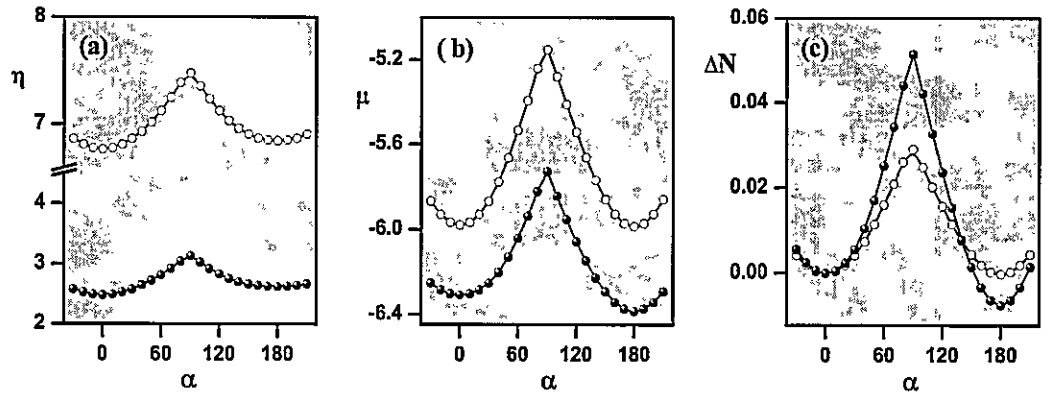

Figura 3.10: *Perfiles a nivel HF/6-311G** y (o – –o) B3LYP/6-311G** (• – –•) de* ***(a)*** *dureza molecular,* ***(b)*** *potencial químico y* ***(c)*** *transferencia de carga intramolecular. Los valores de μ y η están en eV.*

caso el flujo electrónico ocurre desde la conformación *gauche* hacia las conformaciones planares. Además, la cantidad de flujo de carga, ΔN, a lo largo de la rotación interna puede ser estimada a través de la fórmula para la transferencia de carga intermolecular [5,26], cuando vamos desde una conformación de referencia α_1 a α:

$$\Delta N(\alpha) = \frac{1}{2}\frac{[\mu(\alpha) - \mu(\alpha_1)]}{[\eta(\alpha) + \eta(\alpha_1)]}. \tag{3.2}$$

Esta expresión muestra que cuando el sistema se aleja de su conformación de equilibrio, el flujo electrónico está dado por cambios en el potencial químico, al mismo tiempo que la dureza actúa como una resistencia a éste [83].

Los perfiles de ΔN, a nivel HF y *TFD*, se calculan usando la conformación *trans* como referencia ($\alpha_1 = 0^o$) y se muestran en la *Figura 3.10(c)*, el máximo observado en la conformación *gauche* está confirmando el flujo establecido a través del análisis de la población electrónica y del momento dipolar.

3.2.3.3 Análisis de la Población Electrónica

Una caracterización cuantitativa de la densidad de carga está dada por el análisis de la evolución a lo largo de α, de la población electrónica de *Mulliken* localizada sobre las regiones de enlace [84] y de la valencia molecular [85,86], (ver Anexo **A**).

Las figuras *3.11(a) y (b)* muestran los perfiles a lo largo de α de las poblaciones electrónicas $\rho_b(\alpha)$ y ρ_{cc}, respectivamente. Ambas poblaciones presentan mínimos en las conformaciones *trans* y *cis* y un máximo en la *gauche*. Esto indica que ambas conformaciones planares, *trans* y *cis*, no están determinadas sólo por el recubrimiento, sino que también por interacciones específicas a través del espacio. El máximo en la conformación *gauche* indica que esta conformación es principalmente estabilizada por interacciones a través del enlace.

Los resultados discutidos anteriormente se confirman debido a la forma que presenta en la *Figura 3.11(c)* la valencia molecular a lo largo de α. El perfil de V_M presenta un máximo en la conformación *gauche*, confirmando que este isómero está favorecido por interacciones a través del enlace.

Es posible identificar, al menos cualitativamente, la naturaleza de las barreras de potencial en la conformación *cis*. Cuando vamos desde el isómero *gauche* hacia el *cis*, ρ_b, ρ_{cc} y V_M disminuyen, mientras que la población electrónica total permanece constante, hay entonces un reordenamiento de la población electrónica de enlace que favorece la localización de la población electrónica sobre centros atómicos específicos, esto conduce a un importante cambio en el momento dipolar (ver *Figura 3.12*), el aumento hacia el isómero *cis* y la disminución hacia el isómero *trans*. La barrera de energía en la conformación *cis* parece ser del tipo a través del espacio, en otras palabras, la barrera de la conformación *cis* para la rotación interna se debe principalmente a interacciones electrostáticas entre cargas locales centradas en los átomos de oxígeno y cloro.

Por otra parte, la concentración de carga observada en la región del enlace del isómero

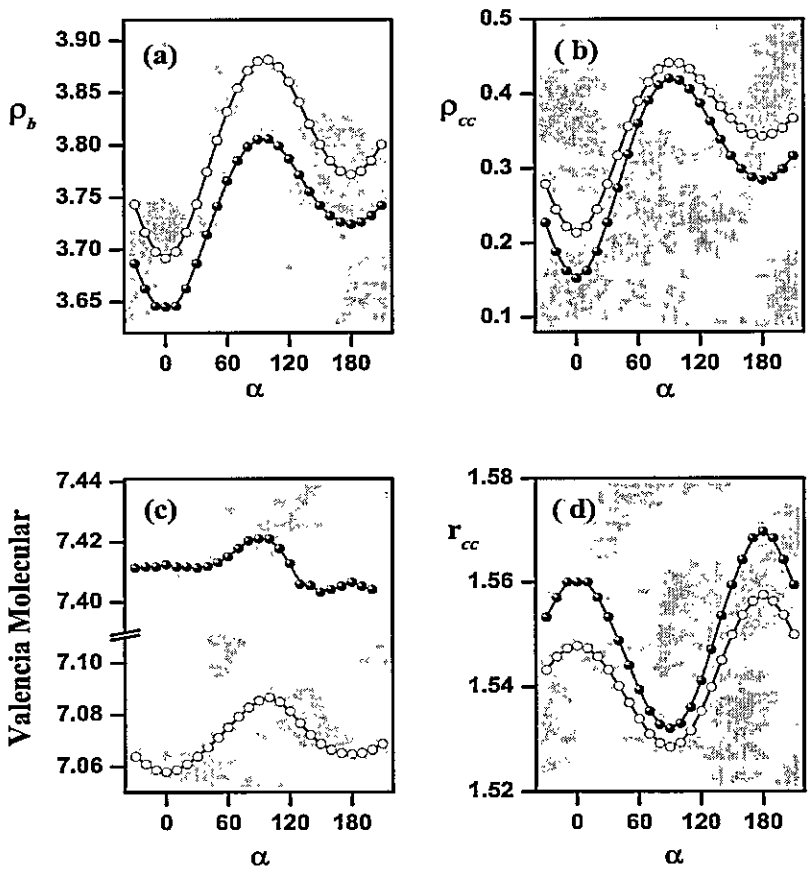

Figura 3.11: *Perfiles torsionales a nivel HF/6-311G** (o — o) y B3LYP/6-311G** (• — •) de* ***(a)*** *población de enlace total,* ***(b)*** *población del enlace central* ***CC,*** ***(c)*** *valencia molecular y* ***(d)*** *distancia del enlace* ***CC*** *a lo largo del ángulo de torsión α.*

gauche está acompañada por un acortamiento de la distancia del enlace central C-C, *Figura 3.11(d)*, siendo este resultado consistente con las conductas descritas anteriormente por las poblaciones y valencia.

3.2.3.4 Momento Dipolar

La discusión anterior sugiere que la energía relativa de los tres confórmeros a lo largo de α se puede racionalizar en términos de interacciones electrostáticas a través de espacio y del enlace y, por lo tanto es pertinente analizar la evolución del momento

dipolar (MD) a lo largo de la coordenada de reacción, esperando que esta propiedad de cuenta, de forma cualitativa, de las interacciones electrostáticas a través del espacio. La *Figura 3.12* muestra que el MD aumenta monotónicamente a partir de la conformación estable *trans* y llegando a una máximo en el isómero inestable *cis*. Un valor máximo del MD junto con mínimos de ρ_b, ρ_{cc} y V_m en el isómero *cis*, confirman que la barrera es principalmente debida a interacciones a través del espacio.

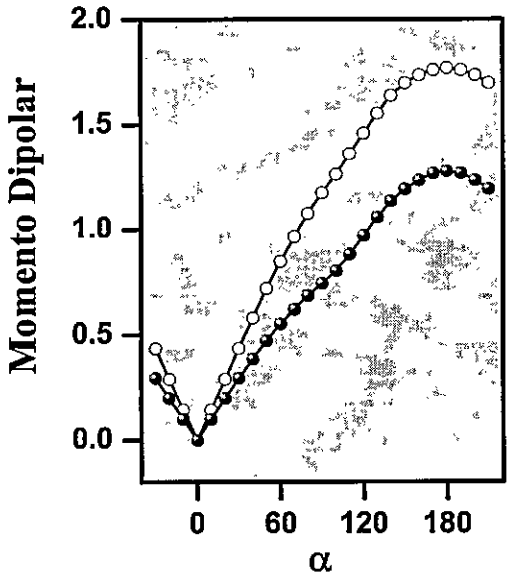

Figura 3.12: *Perfiles del momento dipolar (en Debye) a nivel HF/6-311G** (o − o) y B3LYP/6-311G** (• − •) a lo largo del ángulo de torsión α (en grados).*

3.3 Conclusiones

1. El estudio de la evolución simultánea de propiedades globales como E, μ y η, permitió caracterizar los procesos de rotación interna en HXYH (X, Y = O, S).

2. Junto con el análisis de índices de reactividad global, $\{\mu, \eta, E\}$, para estudiar los procesos de isomerización rotacional, es necesario incorporar el estudio de poblaciones electrónicas de enlace y momento dipolar para identificar las interacciones específicas que caracterizan los mecanismos de reacción.

3. Las barreras de potencial que están presentes en el proceso torsional de HXYH (X, Y = O, S), son debidas principalmente a interacciones a través del enlace en HOOH y HSOH y debidas a un balance de interacciones a través del enlace y del espacio en HSSH.

4. El *PMD* se verifica cualitativamente para los sistemas HOOH, HSOH, HSSH, HONO y HSNS.

5. Los cálculos a nivel HF y *TFD* del potencial torsional para el cloruro de oxalilo muestran la existencia de un isómero planar estable *trans* y un isómero *cis* que corresponde al estado de transición para este proceso torsional.

6. Los cálculos a nivel HF y *TFD*, de la rotación interna del cloruro de oxalilo, indican la existencia de un isómero *gauche*, el cual es caracterizado a través de los perfiles de energía, dureza y propiedades locales. El máximo en la población electrónica asociada al isómero *gauche* indica que está especialmente estabilizado por interacciones a través del enlace.

7. Los resultados de la rotación interna del cloruro de oxalilo, a partir, de los perfiles de energía, poblaciones electrónicas y momento dipolar indican que la estabilidad del isómero *trans* se debe a un balance entre interacciones a través del espacio y del enlace, en cambio la barrera de potencial para la conformación *cis* se debe principalmente a interacciones a través del espacio.

Capítulo 4

Reacciones de Formación

Resumen

En este Capítulo se usa el principio de igualación de la electronegatividad para derivar expresiones para la dureza molecular y su derivada $\gamma = \left(\frac{\partial \eta}{\partial N}\right)_{v(\vec{r})}$. Estas expresiones permiten estimar las propiedades electrónicas de catorce moléculas y complejos bimoleculares enlazados por puentes de hidrógeno (cuatro moléculas del tipo HCX-YH y diez complejos bimoleculares cíclicos del tipo HCXYH:::HCXYH, (X,Y =O,S)). Más allá de la determinación de propiedades electrónicas, se muestra que este esquema puede ser usado como un método para racionalizar reacciones químicas cuando el número de electrones N y el potencial externo $v(\vec{r})$ varían.

Además, el desarrollo teórico que se ha seguido permite proponer un nuevo esquema de aditividad para obtener propiedades electrónicas de moléculas y agregados moleculares a partir de las respectivas propiedades de los fragmentos aislados. Los resultados están en excelente acuerdo con los determinados por medio del esquema de *Sanderson.*

4.1 Introducción

Una reacción de formación es el resultado de la combinación de los fragmentos constituyentes. El sistema resultante, una molécula o un complejo molecular, presenta propiedades que en muchos casos pueden ser racionalizadas en términos de las propiedades de los fragmentos constituyentes aislados. En este Capítulo se estudian esquemas de aditividad para determinar propiedades electrónicas globales de moléculas y agregados moleculares con la idea de determinar el rol de átomos y/o fragmentos en la formación de especies químicas e investigar si estos esquemas de aditividad se pueden usar para discutir el reordenamiento de la densidad electrónica mediante el proceso de formación. En este contexto, exploramos como las propiedades electrónicas se pueden relacionar con las energías de enlace involucradas en los procesos de formación de moléculas y complejos moleculares.

Para relacionar la electronegatividad molecular (χ) a la de átomos o fragmentos aislados que constituyen la molécula, *Sanderson* propuso el principio de igualación que define la electronegatividad molecular como *el promedio geométrico de las electronegatividades de los átomos o fragmentos constituyentes* [23, 87]. A partir de este promedio geométrico para μ, fue posible obtener expresiones para η y γ, que son las derivadas de μ con respecto al número total de electrones N.

Se estudió la formación de cuatro moléculas, HCO-OH, HCO-SH, HCS-OH y HCS-SH a partir de los sistemas radicalarios HCO, HCS, OH y SH. Además se estudiaron diez complejos bimoleculares cíclicos del tipo HCXYH:::HCXYH enlazados por dos puentes de hidrógeno, formados por combinación de las especies HCX-YH (X,Y = O,S) anteriormente formadas. Todas las especies estudiadas se muestran en la *Figura 4.1.*

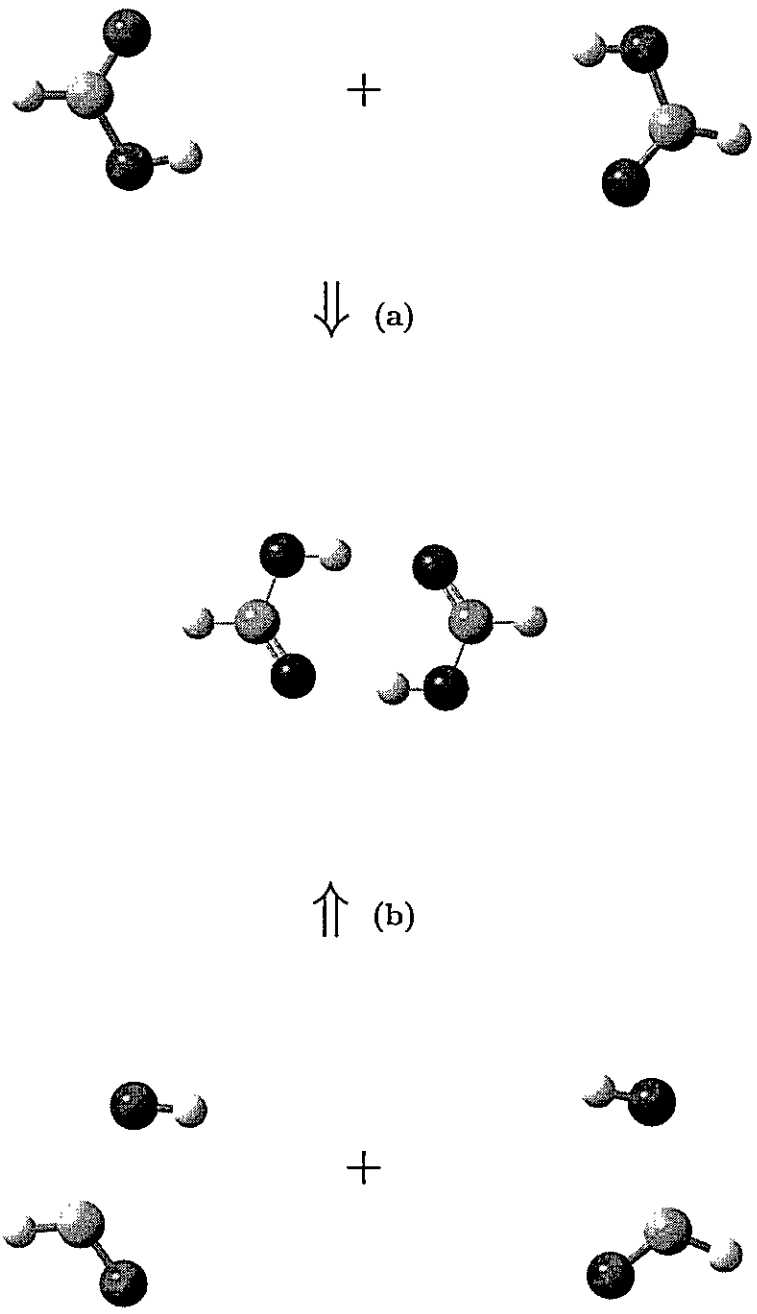

Figura 4.1: Esquema del proceso de formación de agregados bimoleculares del tipo HCX–YH$\cdots$HCX–YH (X,Y= O,S) a partir de **(a)** 2 fragmentos moleculares del tipo HCX–YH (X,Y= O,S), y **(b)** 4 fragmentos radicalarios del tipo HCX(Y) y HY(X) (X,Y= O,S).

Tabla 4.1: *Valores de energía, potencial químico y dureza molecular para las estructuras optimizadas de fragmentos radicalarios determinados a través de cálculos ab initio* UHF/6-311G**. *Todos los valores están en ua.*

Fragmento	E	μ	η
CHO	-113.2802	-0.1327	0.2450
OH	-75.4107	-0.1906	0.3153
CHS	-435.9153	-0.1492	0.1852
SH	-398.0929	-0.1907	0.1864

4.2 Resultados y Discusión

En la *Tabla 4.1* se muestran los valores de referencia de la energía, potencial químico y dureza molecular para las especies radicales aisladas HCX y XH (X = O, S). La formación de las moléculas HCO-OH (**M1**), HCS-OH (**M2**), HCO-SH (**M3**) y HCS-SH (**M4**) a partir de los dos radicales constituyentes involucra un cambio en la energía y propiedades electrónicas, básicamente debido a la formación de un enlace covalente del tipo $C-X$ (X = O, S). Entonces, al comparar μ_2° y η_2° con los valores de referencia μ y η, obtendremos como resultado, una estimación del efecto del potencial de enlazamiento sobre estas propiedades electrónicas específicas.

Entre muchas estructuras bimoleculares posibles, consideramos sólo los complejos cíclicos que están estabilizados a través de dos enlaces de hidrógeno [47]. La combinación de unidades monoméricas de los ácidos fórmico (HCO-OH), tiona-fórmico (HCS-OH), tiol-fórmico (HCO-SH) y ditio-fórmico (HCS-SH) conduce a diez complejos bimoleculares cíclicos **C1–C10** (ver *Figura 4.1* y *Tabla 4.2*). Para construir estos complejos, hemos considerado dos aproximaciones: **(a)** la formación a partir de dos moléculas neutras ($n_f = 2$) donde los valores optimizados *ab-initio* de E, μ y η de cada molécula ($HCX-YH, (X, Y = O, S)$) se usan para producir E_2°, μ_2° y η_2°; la diferencia $\Delta E_2 = E - E_2^\circ$ permite cuantificar la energía de los enlaces de hidrógeno; **(b)** la formación a partir de cuatro fragmentos radicales aislados ($n_f = 4$). Esta última aproximación conduce a E_4°, μ_4° y η_4°; se espera que la diferencia $\Delta E_4 = E - E_4^\circ$ sea proporcional a la energía de los enlaces de hidrógeno más dos enlaces covalentes formados en cada molécula que constituye el complejo.

4.2.1 Estimación de Energías de Enlace C-X (X= O, S)

En la *Tabla 4.2* se entregan los valores de $E^{\circ}_{n_f}$ junto con las energías ΔE_2 y ΔE_4. Los valores de ΔE_{n_f} son todos negativos, es decir, la formación de las moléculas (**M1**–**M4**) y de los complejos bimoleculares (**C1**–**C10**) son procesos termodinámicamente favorables. La característica más importante que aparece en la energía de formación de **M1** y **M2**, es que los valores de ΔE_2 pueden ser identificados con la energía de un enlace simple $C-O$, el valor promedio determinado a partir de la *Tabla 4.2* es $<\Delta E_2>_{co} \approx 0.12$ *ua*, mientras que el valor experimental es 0.13 *ua* [88], lo que indica un buen acuerdo. En la formación de **M3** y **M4**, ΔE_2 es principalmente atribuido a la formación de un enlace simple $C-S$ para el cual la energía de enlace experimental promedio es de 0.10 *ua*, nuestro valor estimado es $<\Delta E_2>_{cs} \approx 0.08$ *ua* indicando nuevamente un acuerdo satisfactorio. Aunque los valores numéricos difieren en alguna medida, nuestros resultados muestran que el enlace $C-O$ está correctamente estimado, siendo más fuerte que el enlace $C-S$ por alrededor de 0.04 *ua*, lo que está en buen acuerdo con los datos experimentales [88]. $<\Delta E_2>_{co}$ y $<\Delta E_2>_{cs}$ al menos cualitativamente, permiten racionalizar la formación de los complejos bimoleculares, como se verá en los párrafos siguientes.

Cuando los complejos se forman a partir de cuatro fragmentos aislados ($n_f = 4$), las energías de reacción están relacionadas con las energías de los enlaces que se están formando en cada complejo. En la *Tabla 4.2*, se muestra que en los sistemas **C1**, **C2** y **C3** los valores de ΔE_4 van desde -0.28 *ua* (**C1**) a -0.25 *ua* (**C3**); correspondiendo estos valores a la contribución aproximada de los dos enlaces $C-O$ que se están formando ($\Delta E_4 \approx 2 <\Delta E_2>_{co}$). En los sistemas **C4**–**C7**, encontramos que el valor promedio de ΔE_4 es -0.21 *ua* que se asocia con la contribución energética debido a la formación de un enlace $C-O$ y un enlace $C-S$, ($\Delta E_4 \approx <\Delta E_2>_{co} + <\Delta E_2>_{cs}$). En los sistemas **C8**–**C10**, encontramos que $\Delta E_4 \approx -0.16$ *ua*, valor que corresponde a la contribución energética debido a la formación de dos enlaces $C-S$ ($\Delta E_4 \approx 2 <\Delta E_2>_{cs}$).

Tabla 4.2: *Energías totales y de reacción en procesos de formación de sistemas moleculares a nivel RHF/6-311G**. Todos los valores están en ua.*

Sistema		$-E$	$-E_2^\circ$	$-E_4^\circ$	$-\Delta E_2$	$-\Delta E_4$
HCOOH	**(M1)**	188.8205	188.6910		0.1295	
HCSOH	**(M2)**	511.4454	511.3260		0.1194	
HCOSH	**(M3)**	511.4493	511.3731		0.0762	
HCSSH	**(M4)**	834.0867	834.0082		0.0785	
HCOOH···HCOOH	**(C1)**	377.6641	377.6410	377.3819	0.0231	0.2822
HCOOH···HCSOH	**(C2)**	700.2840	700.2659	700.0170	0.0181	0.2670
HCSOH···HCSOH	**(C3)**	1022.9027	1022.8908	1022.6520	0.0119	0.2507
HCOOH···HCOSH	**(C4)**	700.2847	700.2698	700.0641	0.0149	0.2206
HCOOH···HCSSH	**(C5)**	1022.9176	1022.9072	1022.6992	0.0104	0.2184
HCOSH···HCSOH	**(C6)**	1022.9068	1022.8947	1022.6992	0.0121	0.2076
HCSSH···HCSOH	**(C7)**	1345.5389	1345.5320	1345.3342	0.0069	0.2047
HCOSH···HCOSH	**(C8)**	1022.9076	1022.8987	1022.7463	0.0089	0.1613
HCSSH···HCOSH	**(C9)**	1345.5425	1345.5360	1345.3813	0.0065	0.1612
HCSSH···HCSSH	**(C10)**	1668.1770	1668.1733	1668.0164	0.0037	0.1606

4.2.2 Energías de Enlace de Hidrógeno: H··· X (X= O, S)

Es importante mencionar que los valores de $-\Delta E_2$ para **C1-C10** (*Tabla 4.2*) siguen una tendencia cualitativa correcta y son comparables satisfactoriamente con otras estimaciones teóricas [89,90]. Respecto de la comparación con datos experimentales, hacemos notar que nuestros valores de energías de enlace de hidrógeno están en buen acuerdo con valores experimentales disponibles en literatura. Por ejemplo, el valor experimental de $\Delta E_2 = -0.0233$ *ua* para **C1** [91] se compara satisfactoriamente con nuestro valor de $\Delta E_2 = -0.0231$ *ua* (*Tabla 4.2*) y la energía de un enlace de hidrógeno en **C10** fue estimada experimentalmente en 0.0016 *ua* [92], valor muy cercano a la mitad de nuestro valor de ΔE_2 dado en la *Tabla 4.2* ($\Delta E_2/2 = 0.0019$ *ua*), donde el factor $\frac{1}{2}$ es introducido para una comparación apropiada, ya que **C10** presenta dos enlaces de hidrógeno. Este último resultado muestra que las energías de enlace de hidrógeno para la serie de sistemas que hemos estudiado y presentado en este Capítulo, pueden ser racionalizadas en términos de la suma de las energías de enlace de hidrógeno individuales presentes en el complejo.

Para explorar esta idea, usamos la energía de formación a partir de dos fragmentos (ΔE_2) para los dímeros **C1** y **C10**, los cuales presentan sólo enlaces del tipo $H\cdots O$ y $H\cdots S$, como valores de referencia: $E(H\cdots O) = \Delta E_2(\mathbf{C1})/2 = -0.0116$ *ua* y $E(H\cdots S) = \Delta E_2(\mathbf{C10})/2 = -0.0019$ *ua*. Usando estos valores, aproximamos los valores de ΔE_2 para los ocho complejos restantes como $\Delta E_2^{(a)} = \sum_X E(H\cdots X)$, que representa la suma de las energías de los enlaces de hidrógeno presentes en el sistema. Estos resultados están incluidos en la *Tabla 4.3*. Hacemos notar que esta estimación de $\Delta E_2^{(a)}$ presenta errores considerables que están sobre el 70% (**C3**). Además, esta cruda estimación de las energías de enlace de hidrógeno a partir de los sistemas de referencia **C1** y **C10** no es lo bastante exacta para entregar una adecuada descripción de los valores de ΔE_2 para los otros complejos. Queda en evidencia que para cuantificar la energía de un enlace de hidrógeno se requiere además, caracterizar el entorno químico donde se encuentra dicho enlace.

Una mejor aproximación para ΔE_2 se obtiene al considerar explícitamente el efecto que puede tener el heteroátomo vecino; de esta forma definimos la energía del fragmento $X-H\cdots Y$ (X, Y = O, S). Para esto, usamos como referencia cuatro dímeros (**C1, C3, C8** y **C10**) que presentan los fragmentos requeridos: $E(O-H\cdots O) = \Delta E_2(\mathbf{C1})/2 = -0.0116$ *ua*; $E(O-H\cdots S) = \Delta E_2(\mathbf{C3})/2 = -0.0060$ *ua*; $E(S-H\cdots O) = \Delta E_2(\mathbf{C8})/2 = -0.0045$ *ua* y $E(S-H\cdots S) = \Delta E_2(\mathbf{C10})/2 = -0.0019$ *ua*. Cabe hacer notar que un átomo de azufre adyacente al enlace de hidrógeno, hace a éste último más débil en comparación a un átomo de oxígeno adyacente. Entonces, a partir de esta aproximación definimos $\Delta E_2^{(b)} = \sum_{X,Y} E(X-H\cdots Y)$, los resultados se muestran en la *Tabla 4.3* y son comparados con ΔE_2 y $\Delta E_2^{(a)}$. Ahora podemos apreciar que las desviaciones con respecto a los valores calculados de ΔE_2 (valores de referencia) son muy pequeñas. La desviación estándar de $\Delta E_2^{(b)}$ con respecto de ΔE_2 es $\sigma = 0.0045$, lo que indica que el efecto del heteroátomo adyacente al enlace de hidrógeno es muy importante al momento de caracterizar las energías de enlace de hidrógeno en diferente entorno químico. En resumen, con esta aproximación estimamos la energía del enlace $H\cdots O$ en 0.0080 ± 0.0036 *ua* y la del enlace $H\cdots S$

Tabla 4.3: *Energías de enlaces de hidrógeno de complejos bimoleculares* ($\Delta E_2 = E - E_2^\circ$; $\Delta E_2^{(a)} = \sum_X E(H\cdots X)$; $\Delta E_2^{(b)} = \sum_{X,Y} E(X-H\cdots Y)$). *Todos los valores están en ua.*

Sistema	N	$-\Delta E_2$	$-\Delta E_2^{(a)}$	$-\Delta E_2^{(b)}$
C1	48	0.0231		
C2	56	0.0181	0.0134	0.0175
C3	64	0.0119	0.0037	
C4	56	0.0149	0.0231	0.0160
C5	64	0.0104	0.0134	0.0104
C6	64	0.0121	0.0134	0.0134
C7	72	0.0069	0.0134	0.0078
C8	64	0.0089	0.0231	
C9	72	0.0065	0.0134	0.0063
C10	80	0.0037		

en 0.0039 ± 0.0021 *ua*; el enlace $H\cdots O$ es por lo tanto, dos veces más fuerte que el enlace $H\cdots S$, como lo demuestran datos experimentales.

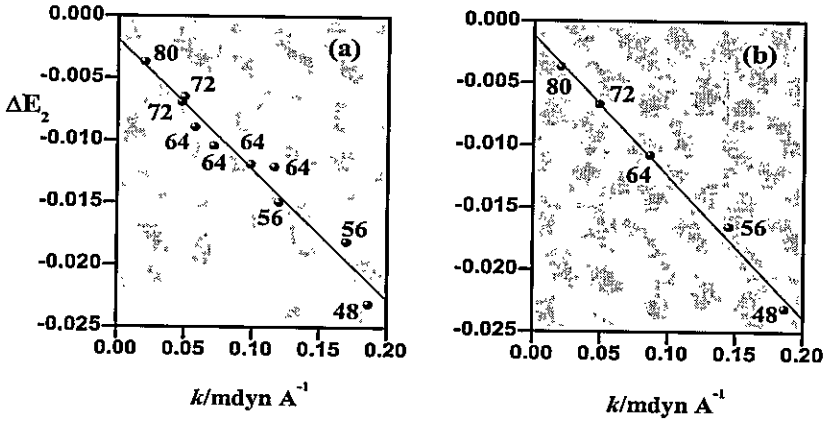

Figura 4.2: *Correlación entre energías de enlaces de hidrógeno y constantes de fuerza de complejos bimoleculares identificados a través de su número de electrones* ***(a)****. Valores promedios de* ΔE_2 *y* k *en sistemas que presentan igual número de electrones* ***(b)****.*

4.2.3 Constantes de Fuerza y Energías de Enlace de Hidrógeno

Hemos visto que cuando la energía de sistemas bimoleculares se estima usando $n_f = 2$, la cantidad $\Delta E_2 = E - E_2^\circ$ entrega una estimación de las energías de enlace de

hidrógeno y mientras mayor sea el valor de ΔE_2 más fuerte se espera que sea el par de enlaces de hidrógeno que se forma. En la *Tabla 4.3* se muestra que la energía de enlace disminuye con el número de electrones N del sistema y que los enlaces $O\cdots H$ son más fuertes que los enlaces $S\cdots H$. La fuerza de un enlace químico es usualmente representada por su constante de fuerza; en nuestro caso, esperamos que ΔE_2 este relacionada con las constantes de fuerza k asociadas con el par de enlaces de hidrógeno de los complejos. Valores de las constantes de fuerza han sido determinados a través de cálculos *ab-initio* de frecuencias, sobre las estructuras optimizadas de los complejos, la *Figura 4.2(a)*, muestra una buena correlación lineal ($r = 0.980$) entre ΔE_2 y k para los diez complejos identificados por su número total de electrones. Debido a que existen dos complejos con 56 electrones (**C2** y **C4**), cuatro con 64 electrones (**C3**, **C5**, **C6** y **C8**) y dos con 72 electrones (**C7** y **C9**), en estos casos tomamos el promedio de los valores de ΔE_2 y los graficamos *versus* k, lo que mejora la correlación ($r = 0.996$). Además, es importante destacar que las constantes de fuerza determinadas a través de cálculos *ab-initio* son consistentes con los resultados energéticos, es decir, el enlace de hidrógeno más fuerte está asociado con el mayor valor en $|\Delta E_2|$.

4.2.4 Potencial Químico

La ecuación (2.50) ha sido usada para obtener el potencial químico dentro del esquema de *Sanderson*. En el caso de las moléculas **M1**–**M4**, para obtener μ_2° se requieren los datos *ab initio* (μ_x° y η_x°) de las especies radicalarias ($x = CHO, OH, CHS$ y SH), los cuales se entregan en la *Tabla 4.1*. Los efectos de la relajación y de la redistribución de la densidad electrónica sobre el potencial químico debido a la formación de enlaces covalentes y de hidrógeno pueden ser cuantitativamente caracterizados por los valores numéricos de $\mu_{n_f}^\circ$, tomando como referencia el potencial químico calculado; los valores numéricos se presentan en la *Tabla 4.4*. Hacemos notar que las desviaciones de $\mu_{n_f}^\circ$ con respecto al valor *ab initio* (valor de referencia) son razonablemente pequeñas; sin embargo en la mayoría de los casos, μ_2° se aproxima mucho mejor al valor de referencia que como lo hace μ_4°. El potencial químico al igual que la energía, depende del número de fragmentos usados.

Tabla 4.4: *Potencial químico de moléculas (**M1–M4**) y complejos bimoleculares (**C1–C10**). μ fue obtenido mediante cálculos RHF/6-311G** y los valores de $\mu^{\circ}_{n_f}$ fueron estimados mediante la ecuación (2.50). Todos los valores están en ua.*

Sistema	μ	μ°_2	μ°_4
M1	-0.1554	-0.1590	
M2	-0.1402	-0.1686	
M3	-0.1391	-0.1591	
M4	-0.1532	-0.1687	
C1	-0.1503	-0.1554	-0.1590
C2	-0.1411	-0.1476	-0.1638
C3	-0.1462	-0.1402	-0.1686
C4	-0.1402	-0.1470	-0.1590
C5	-0.1601	-0.1543	-0.1638
C6	-0.1320	-0.1397	-0.1638
C7	-0.1604	-0.1466	-0.1687
C8	-0.1331	-0.1391	-0.1591
C9	-0.1511	-0.1460	-0.1638
C10	-0.1576	-0.1532	-0.1687

Cuando dos fragmentos se ponen en contacto, los electrones fluyen desde el fragmento que tiene el mayor potencial químico hacia el que tiene el menor μ; la cantidad de carga que fluye es proporcional a la diferencia en los potenciales químicos de los fragmentos [5, 16, 26]. Una estimación cualitativa de la transferencia de carga (ΔN) que está involucrada en los procesos de formación de una reacción de dos fragmentos se puede determinar a través de la siguiente expresión:

$$\Delta N = \frac{1}{2}\frac{(\mu_x - \mu_y)}{(\eta_x + \eta_y)}, \tag{4.1}$$

donde x e y representan los diferentes fragmentos usados en la formación del producto a estudiar. Los valores de ΔN están dados en la *Tabla 4.5*, donde es interesante hacer notar que las reacciones involucradas en la formación de enlaces covalentes van acompañadas de valores positivos altos de ΔN, mientras que en la formación de complejos bimoleculares, encontramos valores pequeños de ΔN.

Tabla 4.5: *Valores de transferencia de carga (ΔN) en la formación de sistemas moleculares y complejos bimoleculares.*

Sistema	ΔN	δN_2	δN_4
M1	0.0516	0.0036	
M2	0.0414	0.0284	
M3	0.0672	0.0200	
M4	0.0558	0.0155	
C1	0.0	0.0051	0.0087
C2	-0.0142	0.0065	0.0227
C3	0.00	-0.0060	0.0224
C4	-0.0142	0.0068	0.0188
C5	-0.0021	-0.0058	0.0037
C6	0.0011	0.0077	0.0318
C7	-0.0155	-0.0138	0.0083
C8	0.0	0.0060	0.0260
C9	-0.0153	-0.0051	0.0127
C10	0.0	-0.0044	0.011

De acuerdo con la ecuación (4.1), la cantidad de carga que no está relajada (δN_{n_f}) en los procesos de formación a partir de los fragmentos rígidos, es proporcional a $\Delta\mu_{n_f} = (\mu - \mu^{\circ}_{n_f})$. Además, definimos $\delta N_{n_f} \equiv \Delta\mu_{n_f}$ cuyos valores aparecen en la *Tabla 4.5*. Es interesante hacer notar que, para complejos bimoleculares, la formación a partir de cuatro fragmentos en muchos casos implica valores altos de este índice con respecto a la formación a partir de dos fragmentos, lo que implica que el reordenamiento de la densidad electrónica aumenta de manera significativa con el número de fragmentos.

4.2.5 Dureza Molecular

Dentro del esquema de *Sanderson*, hemos determinado la dureza molecular η°_2 y η°_4 usando la ecuación (2.51); estos resultados se muestran en la *Tabla 4.6* y se pueden comparar con los valores de referencia *ab-initio* (η), también incluídos en la *Tabla*.

Es interesante hacer notar que la dureza se puede aproximar correctamente usando

Tabla 4.6: *Dureza molecular de moléculas (M1–M4) y complejos bimoleculares (C1–C10). η fue obtenida mediante cálculos RHF/6-311G** y los valores de $\eta^{\circ}_{n_f}$ fueron estimados mediante la ecuación (2.51). Todos los valores están en ua.*

Sistema	η	η°_2	η°_4
M1	0.3138	0.2783	
M2	0.2206	0.2441	
M3	0.2608	0.2246	
M4	0.1996	0.1872	
C1	0.3204	0.3138	0.2783
C2	0.2251	0.2652	0.2619
C3	0.2169	0.2206	0.2441
C4	0.2609	0.2863	0.2515
C5	0.2021	0.2563	0.2342
C6	0.2215	0.2408	0.2342
C7	0.1966	0.2108	0.2157
C8	0.2607	0.2608	0.2246
C9	0.2000	0.2319	0.2065
C10	0.1965	0.1996	0.1871

ya sea η°_2 o η°_4, dependiendo del sistema específico; la dureza parece ser menos dependiente del número de fragmentos que el potencial químico. En este contexto, un atributo interesante que presenta η es su estabilidad en términos de n_f. La consistencia encontrada entre η°_2 o η°_4 indica que la ecuación (2.51) es una expresión viable para estimar la dureza molecular.

4.2.5.1 Comparación de Esquemas de Aditividad para η

Existen pocas vías para estimar η a partir de valores de fragmentos, entre las más relevantes están: *(a)* el esquema de aditividad propuesto por Ghosh y *col.* [93], el cual expresa la dureza del agregado molecular como el recíproco de la blandura del sistema ($S = 1/\eta$), calculado como el promedio de las blanduras de los fragmentos constituyentes del sistema:

$$\frac{1}{\eta^{G}_{n_f}} = \frac{1}{n_f}\sum_{i}^{n}\frac{1}{\eta_i}, \tag{4.2}$$

Tabla 4.7: *Comparación de valores de dureza obtenidos a través de diferentes esquemas. η es el valor ab-initio de referencia. Las ecuaciones (4.2) y (4.3) son usadas con dos fragmentos. Todos los valores están en ua.*

Sistema	η	η_2° Ec. (2.51)	η^G Ec. (4.2)	η^D Ec. (4.3)
M1	0.3138	0.2783	0.2757	0.2779
M2	0.2206	0.2441	0.2333	0.2417
M3	0.2608	0.2246	0.2117	0.2137
M4	0.1996	0.1872	0.1858	0.1858
C1	0.3204	0.3138	0.3138	0.3138
C2	0.2251	0.2652	0.2591	0.2631
C3	0.2169	0.2206	0.2206	0.2206
C4	0.2609	0.2863	0.2849	0.2861
C5	0.2021	0.2563	0.2440	0.2503
C6	0.2215	0.2408	0.2390	0.2399
C7	0.1966	0.2108	0.2096	0.2098
C8	0.2607	0.2608	0.2608	0.2608
C9	0.2000	0.2319	0.2261	0.2282
C10	0.1965	0.1996	0.1996	0.1996

Los valores dados por este esquema se encuentran en la cuarta columna de la *Tabla 4.7*; *(b)* el esquema de aditividad de Datta y *col.* [94], el cual expresa la dureza del agregado molecular como el promedio geométrico de las durezas respectivas de los fragmentos constituyentes y cuya expresión viene dada por:

$$\eta_{n_f}^D = (\prod_i^{n_f} \eta_i)^{1/n_f}, \tag{4.3}$$

donde n en ambos esquemas representa el número de fragmentos constituyentes del agregado molecular.

En la *Tabla 4.7* se comparan los valores numéricos de η, calculados usando la ecuación (2.51), con los valores determinados usando los esquemas antes mencionados y con $n_f = 2$. Hacemos notar que la comparación es muy satisfactoria, solamente existen algunas desviaciones entre los valores obtenidos a través de los diferentes métodos

mencionados. Estos resultados confirman nuestra observación respecto de que la dureza, es una propiedad numéricamente estable. Este atributo en combinación con el principio de máxima dureza, el cual establece que *los sistemas moleculares en el equilibrio tienden a estados de mayor dureza* sugieren que para sistemas en los cuales la energía es difícil de obtener, el conocimiento de η puede abrir vías para obtener información energética [44,95].

En un trabajo reciente, Sengupta y Toro-Labbé [96], compararon exhaustivamente estos esquemas para determinar la dureza molecular, a partir de dos fragmentos, para ello consideraron 46 sistemas moleculares. Los resultados indicaron que la ecuación (2.51) produce valores numéricos que son muy comparables a los resultados determinados a partir de otros esquemas.

4.2.6 Relación entre Energía y Dureza Molecular

Se han hecho algunos esfuerzos para relacionar las propiedades electrónicas con la energía de la reacción [43, 44, 95, 97, 98]. Pearson, propuso un método empírico para ordenar los ácidos y las bases de Lewis en términos de sus durezas y sitios de reacción [6,97]. Más recientemente, *Gázquez* [98] propuso una expresión para la energía de enlace en términos del potencial químico, la dureza y la función de *Fukui* condensada de las especies aisladas. La conexión entre energía y dureza a través del *PMD* nos llevó a investigar la relación entre las energías de formación ΔE_2 y ΔE_4 de los complejos bimoleculares y las correspondientes durezas η_2° y η_4°, determinadas usando la ecuación (2.51). Los gráficos *a* y *b* de la *Figura 4.3* muestran una buena correlación lineal entre ΔE_{n_f} y $\eta_{n_f}^\circ$ para los complejos identificados por su número total de electrones. Esta correlación se mejora al usar el valor promedio de las propiedades de los complejos isoelectrónicos ($N = 56, 64$ y 72), como se muestra en las figuras *4.3(c)* y *4.3(d)*. Como enuncia el *PMD*, el complejo más estable es el más duro.

Es interesante hacer notar que el análisis de las figuras *4.2* y *4.3*, sugieren que la dureza y las constantes de fuerza del enlace de hidrógeno están relacionadas. En la *Figura 4.4* se muestra una buena relación lineal entre estas propiedades. Mientras

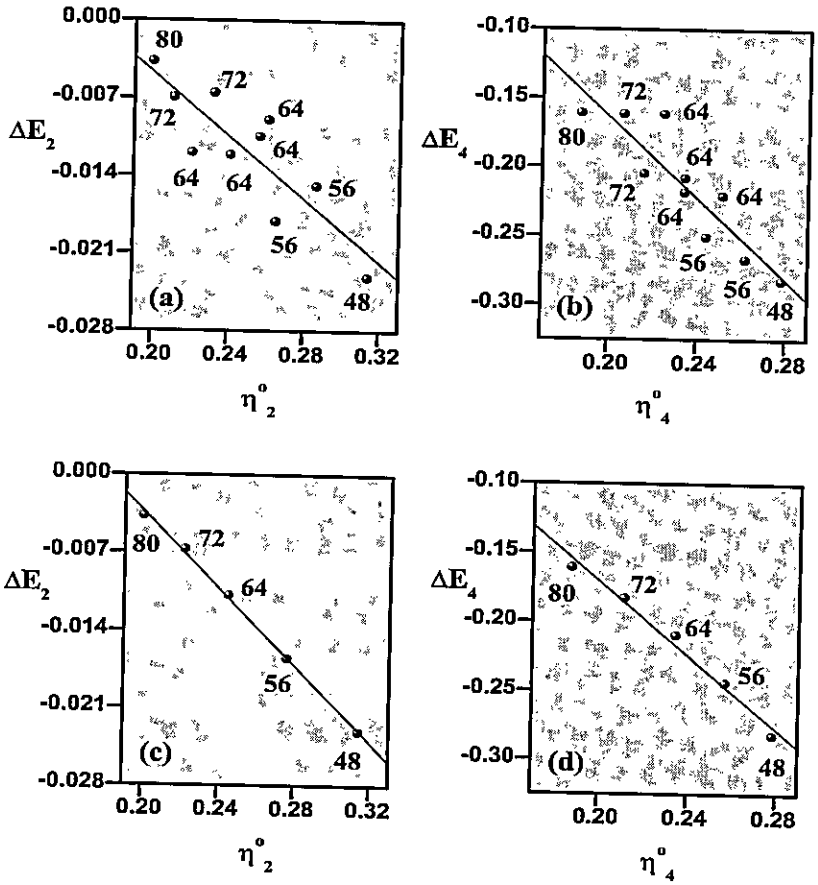

Figura 4.3: *Correlación entre energía de enlace y dureza del producto determinada a partir de la aproximación de Sanderson considerando (a) $n_f = 2$ y (b) $n_f = 4$. (c) y (d) representan los valores promedio de (a) y (b) respectivamente, en sistemas que presentan igual número de electrones.*

más fuerte es el enlace que se forma, más duro es el complejo. Este resultado confirma la proporcionalidad entre durezas y constantes de fuerza observada por otros autores [99].

4.2.7 Función de *Fukui* de la Reacción

Formalmente el potencial químico es una función de N y un funcional del potencial externo $v(\vec{r})$ y se escribe como $\mu \equiv \mu[N, v(\vec{r})]$, entonces diferenciamos la ecuación (2.50) con respecto a $v(\vec{r})$, definiendo la cantidad $F^{\circ}_{n_f}$:

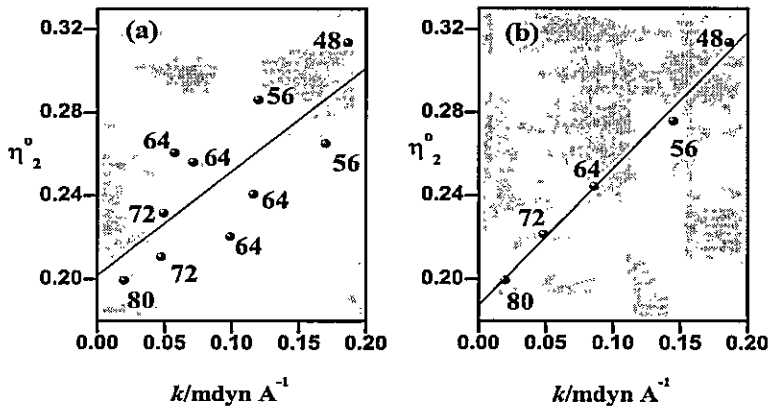

Figura 4.4: *(a) Correlación entre dureza y constantes de fuerza del enlace de hidrógeno de los complejos bimoleculares. (b) Considera los valores promedios para los sistemas que tienen igual número de electrones*

$$F^\circ_{n_f} \equiv \left(\frac{\partial \mu^\circ_{n_f}}{\partial v}\right)_N \approx \frac{\mu^\circ_{n_f}}{n_f} \sum_x^{n_f} \left(\frac{f^\circ_x}{\mu^\circ_x}\right) \tag{4.4}$$

Debido a que la definición formal de $F^\circ_{n_f}$ es análoga a la función de *Fukui* usada para cuantificar la reactividad de un sitio específico sobre una molécula es que llamamos a esta cantidad *Función de Fukui de la Reacción (FFR)*. A partir de la ecuación (4.4), hacemos notar que $F^\circ_{n_f}$ es una propiedad global que contiene las reactividades de los fragmentos a través de las funciones de *Fukui* $f^\circ_x = (\partial \mu^\circ_x / \partial v)_N$. Sin embargo, como $F^\circ_{n_f}$ es una propiedad global asociada a la formación de una especie química, las funciones de *Fukui* individuales no tienen la interpretación usual de índice de reactividad, más bien juegan el rol de función de peso para el inverso del potencial químico del fragmento x. En este contexto, hacemos uso de la aproximación de densidad local y tomamos $f^\circ_x = \frac{N_x}{N}$, donde N_x es el número de electrones del fragmento x y N es el número total de electrones del sistema que se forma.

$$F^\circ_{n_f} = \frac{\mu^\circ_{n_f}}{n_f} \frac{1}{N} \sum_x^{n_f} \left(\frac{N_x}{\mu^\circ_x}\right) \tag{4.5}$$

Entonces hemos determinado valores numéricos de *FFR* [47]. Los valores de f°_x fueron

aproximados como N_x/N, con N_x definido como el número de electrones del fragmento x y N el número total de electrones del sistema compuesto, tal que, $\sum_x N_x = N$. En la *Figura 4.5(a)* se muestra que *FFR* está linealmente relacionada con la energía de la reacción, indicando esto que *FFR* es una medida de la exotermicidad de la reacción: el menor valor de ΔE_2 corresponde al más alto valor en *FFR*. Por otra parte, es claro que todo este procedimiento basado en el esquema de *Sanderson* es una poderosa herramienta par caracterizar las reacciones químicas cuando N y v varían.

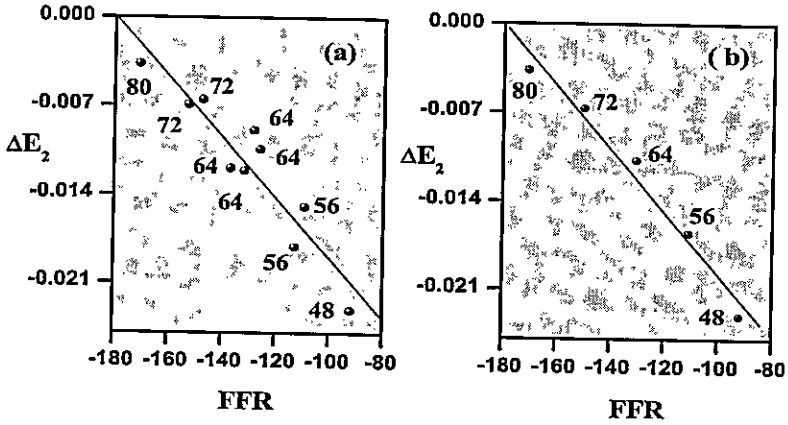

Figura 4.5: *Caracterización de la Función de Fukui de la Reacción (FFR) en función de* ***(a)*** *la energía de la reacción y* ***(b)*** *del valor promedio para los sistemas que tienen igual número de electrones. Todos los valores están en ua.*

4.2.8 Derivada de la Dureza: $\gamma = \left(\frac{\partial \eta}{\partial N}\right)_{v(\vec{r})}$

La dureza es reconocida como una importante propiedad para caracterizar procesos químicos, entonces es necesario conocer cómo cambia esta propiedad con el número de electrones y el potencial externo. La cantidad γ mide el cambio de la dureza con el número de electrones. Hemos usado la ecuación (2.52) para estimar valores numéricos de esta propiedad. Primero, hacemos notar que al evaluar el tercer término de esta ecuación, necesitamos los valores de γ_x° de los fragmentos aislados. los cuales fueron estimados a partir de la siguiente fórmula aproximada, propuesta por Fuentealba y Parr [49]:

$$\gamma_x^\circ \approx \left[\frac{\epsilon_L}{\epsilon_L - 3\epsilon_H}\right]_x^\circ \eta_x^\circ \tag{4.6}$$

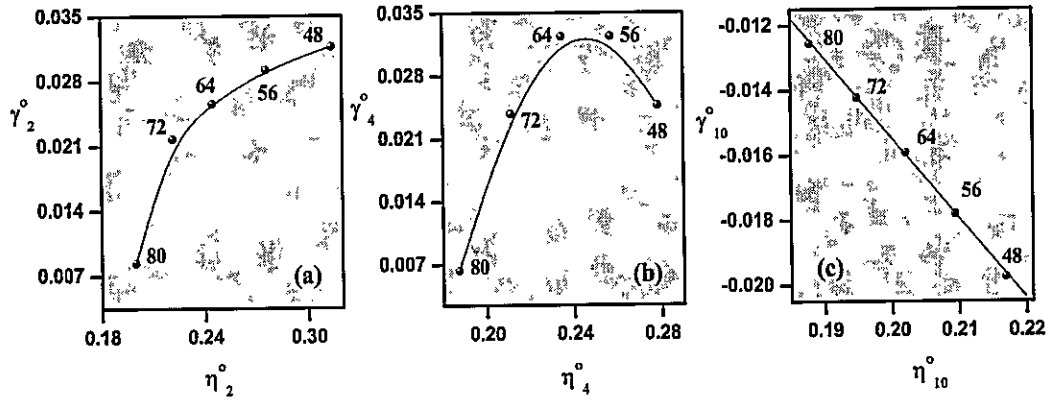

Figura 4.6: *Relación entre $\eta_{n_f}^\circ$ y $\gamma_{n_f}^\circ$ de los sistemas enlazados por hidrógeno, ordenados en términos de su número total de electrones:* ***(a)*** *$n_f = 2$,* ***(b)*** *$n_f = 4$ y* ***(c)*** *$n_f = 10$ (a partir de datos atómicos tomados de referencia [48]). Todos los valores están en ua.*

Hacemos notar, que los valores de γ_2° y γ_4°, dados en la *Tabla 4.8*, son positivos y pequeños. La ecuación (2.52) muestra una dependencia compleja de γ con respecto de η, la cual está lejos de presentar la linealidad indicada en la ecuación (4.6). La validez de esta última ecuación y su consistencia con el esquema de *Sanderson* ha sido probada tomando los valores de $\eta_{n_f}^\circ$ y $\gamma_{n_f}^\circ$ $(n_f = 2, 4)$, calculados a partir de las ecuaciones (2.51) y (2.52), respectivamente, para así comprobar la posible relación lineal entre estas dos propiedades. Como resultado, se muestra en la *Figura 4.6(a)* y *4.6(b)* que no hay tal dependencia lineal entre γ y η. Sin embargo, cuando se usan los datos atómicos de Fuentealba y Parr para construir las propiedades de los complejos bimoleculares, esto es, obtener η_{10}° y γ_{10}° a partir de los 10 átomos constituyentes, encontramos valores negativos de γ y una conducta lineal con η, como se muestra en la *Figura 4.6(c)*. Es necesario hacer notar, que para los complejos bimoleculares que presentan la misma composición atómica, sus valores de η_{10}° y γ_{10}° son los mismos. Se muestra en la *Figura 4.6(c)* los sistemas ordenados en términos de su número total

Tabla 4.8: *Valores de $\gamma^{\circ}_{n_f}$ ($n_f = 2$ y 4) determinados mediante la ecuación (2.52). Todos los valores están en ua.*

Sistema	γ°_2	γ°_4
M1	0.0247	
M2	0.0214	
M3	0.0431	
M4	0.0062	
C1	0.0317	0.0247
C2	0.0303	0.0269
C3	0.0153	0.0214
C4	0.0281	0.0380
C5	0.0398	0.0326
C6	0.0231	0.0326
C7	0.0148	0.0187
C8	0.0240	0.0431
C9	0.0288	0.0289
C10	0.0084	0.0064

de electrones.

4.2.9 Nuevo Esquema de Aditividad para μ y η

En esta sección, proponemos un nuevo esquema de aditividad para el potencial químico y la dureza, el cual está basado en un análisis dimensional de la ecuación (4.4), que muestra que es posible definir el inverso del potencial químico [47]:

$$\frac{1}{\mu'_{n_f}} \approx \sum_{x}^{n_f} \left(\frac{f^{\circ}_x}{\mu^{\circ}_x} \right) \tag{4.7}$$

La determinación del potencial químico de un sistema compuesto, a partir de las propiedades de los fragmentos aislados, a través de la ecuación (4.7) produce resultados que están en muy buen acuerdo con los determinados usando la ecuación (2.50). Esto se puede verificar en la *Figura 4.7*, donde se muestra la comparación de ambas aproximaciones para estimar el potencial químico de los diez complejos bimoleculares

usando $n_f = 2$. Más aún, hemos verificado que en todos los casos estudiados aquí, μ'_{n_f} otorga una mejor aproximación a los valores *ab-initio* de referencia que $\mu^\circ_{n_f}$, los cuales se determinaron a partir de la ecuación (2.50); esto fue verificado para $n_f = 2, 4$ y 10. Estos resultados muestran que la ecuación (4.7) representa una alternativa valida a la formulación original de *Sanderson*. Resulta interesante hacer notar que esta nueva expresión, contiene las poblaciones electrónicas de los fragmentos aislados, la cual es una cantidad local, junto con el potencial químico, una propiedad global del fragmento.

En este nuevo esquema la dureza viene dada por:

$$\eta'_{n_f} = \left(\frac{\partial \mu'_{n_f}}{\partial N}\right)_{v(\vec{r})} = (\mu'_{n_f})^2 \sum_x^{n_f} \frac{1}{(\mu^\circ_x)^2}[f^\circ_x \eta^\circ_x - h^\circ_x \mu^\circ_x], \tag{4.8}$$

donde h°_x es una medida de la fluctuación de la dureza química debido a la variación en el potencial externo. De forma alternativa, a través de la relación de *Maxwell*, h°_x puede ser entendida como la respuesta de la función de *Fukui* con la variación del número total de electrones:

$$h^\circ_x = \left(\frac{\delta \eta^\circ_x}{\delta v}\right)_N = \left(\frac{\partial f^\circ_x}{\partial N}\right)_{v(\vec{r})} \tag{4.9}$$

En conclusión, estas nuevas ecuaciones para el potencial químico y la dureza molecular, las cuales contienen propiedades globales y locales, determinan un nuevo método para caracterizar los conceptos de reactividad y selectividad en una perspectiva unificada.

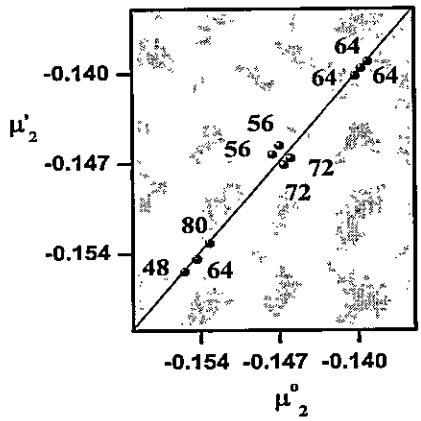

Figura 4.7: *Comparación del potencial químico determinado a través de las ecuaciones (2.50) y (4.7). Todos los valores están en ua.*

4.3 Conclusiones

1. Se usó el principio de *Sanderson* para estimar la primera, segunda y tercera derivada de la energía con respecto al número total de electrones. Los resultados para $\mu^{\circ}_{n_f}$ $\eta^{\circ}_{n_f}$ muestran que en todos los casos tratados aquí, el promedio geométrico del potencial químico es adecuado para determinar derivadas de orden superior.

2. Se mostró que el esquema de *Sanderson* es muy útil no sólo para determinar propiedades electrónicas, sino que también para racionalizar reacciones químicas cuando N y v varían.

3. Se encontró que el Principio de Máxima Dureza y Mínima Polarizabilidad son válidos para racionalizar la formación de moléculas y complejos bimoleculares.

Capítulo 5

Conclusiones Generales

1. Las propiedades que se obtienen de la *TFD conceptual* aplicadas al análisis de reacciones químicas, ha permitido identificar interacciones específicas que producen los cambios químicos, es decir, son propiedades que permiten caracterizar mecanismos de reacción.

2. En general, se encontró que el Principio de Máxima Dureza es valido para racionalizar los procesos de isomerización rotacional y de formación de moléculas y complejos bimoleculares.

3. Junto con el uso de índices de reactividad global, $\{\mu, \eta, \mathrm{E}\}$, es necesario aplicar descriptores de reactividad local con el objetivo de identificar la interacciones específicas que caracterizan los mecanismos de reacción.

4. La extensión del principio de igualación del potencial químico de *Sanderson* que hemos mostrado en este trabajo indica que puede ser usado como un método para racionalizar reacciones químicas cuando el número de electrones N y el potencial externo $v(\vec{r})$ varían.

5. Se propuso un nuevo esquema para obtener propiedades moleculares a partir de los fragmentos aislados con resultados muy satisfactorios, la validación de esquemas de aditividad nos lleva a caracterizar propiedades globales y determinar el rol de átomos y/o fragmentos en la formación de especies químicas.

Referencias

[1] R.G. Parr and W. Yang. *Annu. Rev. Phys. Chem.*, 46:701, **1995**.

[2] S. Nath, A.B. Sannigrahi, and P.K. Chattaraj. *J. Mol. Struct. (THEOCHEM)*, 309:65, **1994**.

[3] S. Gutiérrez-Oliva, P. Jaque, and A. Toro-Labbé. *Reviews of Modern Quantum Chemistry: A Celebration of The Contributions of Robert G. Parr*, page 966. World Scientific, K.D. Sen Editor, London, U.K., **2002**.

[4] P.K. Chattaraj, H. Lee, and R.G. Parr. *J. Am. Chem. Soc.*, 113:1855, **1991**.

[5] R.G. Parr and R.G. Pearson. *J. Am. Chem. Soc.*, 105:7512, **1983**.

[6] R.G. Pearson. *Chemical Hardness: Applications from Molecules to Solids.* Wiley-VCH, New York, **1997**.

[7] R.G. Pearson. *J. Chem. Educ.*, 64:561, **1987**.

[8] R.G. Pearson. *J. Am. Chem. Soc.*, 107:6801, **1985**.

[9] R.G. Pearson. *Acc. Chem. Res.*, 26:250, **1993**.

[10] R.G. Pearson. *Science*, 151:172, **1993**.

[11] R.G. Pearson. *J. Am. Chem. Soc.*, 85:3533, **1963**.

[12] P.K. Chattaraj and S. Sengupta. *J. Phys. Chem. A*, 100:16126, **1996**.

[13] J.M. Frisch, G.W. Trucks, and H.B. Schlegel *et al. Gaussian94.* Gaussian Inc., Pittsburgh, PA, **1995**.

[14] J.M. Frisch, G.W. Trucks, and H.B. Schlegel *et al. Gaussian98.* Revision A9. Gaussian Inc., Pittsburgh, PA, **1998**.

[15] J.M. Frisch, G.W. Trucks, and H.B. Schlegel *et al. Gaussian03.* Revision B04. Gaussian Inc., Pittsburgh, PA, **2003**.

[16] R.G. Parr and W. Yang. *Density Functional Theory of Atoms and Molecules.* Oxford University Press, New York, **1989**.

[17] P. Geerlings, F. De Proft, and W. Langenaeker. *Chem. Rev.*, 103:1793, **2003**.

[18] H. Chermette. *J. Comput. Chem.*, 20:129, **1999.**

[19] P. Hohenberg and W. Kohn. *Phys. Rev. B*, 136:864, **1964.**

[20] W. Kohn and L.J. Sham. *Phys. Rev. A*, 140:1133, **1965.**

[21] T.K. Ghanty and S.K. Ghosh. *J Am. Chem. Soc.*, 116:8801, **1994.**

[22] F. De Proft and P. Geerlings. *J. Chem. Phys.*, 106:3270, **1997.**

[23] R.T. Sanderson. *Science*, 121:207, **1955.**

[24] R.G. Parr and P.K. Chattaraj. *J. Am. Chem. Soc*, 113:1854, **1991.**

[25] R.P. Iczkowski and J.L. Margrave. *J. Am. Chem. Soc.*, 83:3547, **1961.**

[26] R.G. Parr, R.A. Donnelly, M. Levy, and W.E. Palke. *J. Chem. Phys.*, 68:3801, **1978.**

[27] T.A. Koopmans. *Physica*, 1:104, **1933.**

[28] P. Politzer, F. Abu-Awwad, and J. S. Murray. *Int. J. of Quantum Chem.*, 69:607, **1998.**

[29] P. Politzer and D. G. Truhlar. *Chemical Applications of Atomic and Molecular Electrostatic Potentials.* Plenum Press, New York, **1981.**

[30] G. Naray-Szabo and G. G. Ferenczy. *Chem. Rev.*, 95, **1995.**

[31] D. Feil. *Molecular Electrostatic Potentials: Concepts and Applications.* Elsevier, Amsterdam, **1996.**

[32] J. S. Murray P. Sjoberg, T. Brick, and P. Politzer. *Can. J. Chem.*, 68, **1990.**

[33] J. S. Murray, Z. Peralta-Inga, P. Politzer, K. Ekanayake, and P. LeBreton. *Int. J. of Quantum Chem.*, 83:245, **2001.**

[34] P. Politzer, J. S. Murray, and M. C. Concha. *Int. J. of Quantum Chem.*, 88:19, **2002.**

[35] A. Toro-Labbé, S. Gutiérrez-Oliva, M. Concha, Jane S. Murray, and P. Politzer. *J. Chem. Phys.*, 121:4570, **2004.**

[36] M. Born and J.R. Oppenheimer. *Ann. Phys. (Leipzig)*, 84:457, **1927.**

[37] G.S. Hammond. *J. Am. Chem. Soc.*, 77:334, **1955.**

[38] J.E. Leffler. *Science*, 117:340, **1953.**

[39] R.A. Marcus. *Ann. Rev. Phys. Chem.*, 15:155, **1964.**

[40] C. Cardenas-Lailhacar and A. Toro-Labbé. *Theoret. Chem. Acta*, 76:411, **1990.**

[41] G.I. Cardenas-Jirón, J. Lahsen, and A. Toro-Labbé. *J. Phys. Chem.*, 99:5325, **1995.**

[42] G.I. Cardenas-Jirón and A. Toro-Labbé. *J. Phys. Chem.*, 99:12730, **1995.**

[43] G.I. Cardenas-Jirón, S. Gutiérrez-Oliva, J. Melin, and A. Toro-Labbé. *J. Phys. Chem. A*, 101:4621, **1997.**

[44] A. Toro-Labbé. *J. Phys. Chem. A*, 103:4398, **1999.**

[45] R.P. Feynman. *Phys. Rev.*, 56:340, **1939.**

[46] P. Jaque and A. Toro-Labbé. *J. Phys. Chem. A*, 104:995, **2000.**

[47] S. Gutiérrez-Oliva, P. Jaque, and A. Toro-Labbé. *J. Phys. Chem. A*, 104:8955, **2000.**

[48] G.I. Cardenas-Jirón and A. Toro-Labbé. *J. Mol. Struct.:THEOCHEM*, 390:79, **1997.**

[49] P. Fuentealba and R.G. Parr. *J. Chem. Phys.*, 94:5559, **1991.**

[50] P.R. Fleming, M. Li, and T.R. Rizzo. *J. Chem. Phys.*, 95:865, **1991** .

[51] X. Luo, P.R. Fleming, and T.R. Rizzo. *J. Chem. Phys.*, 96:5659, **1992** .

[52] R.H. Hunt, R.A. Leacock, C.W. Peters, and K.T. Hecht. *J. Chem. Phys.*, 42:1931, **1965** .

[53] G. Pelz, K.M.T. Yamada, and G. Winnewisser. *J. Mol. Spectrosc.*, 159:507, **1993** .

[54] E. Herbst and G. Winnewisser. *Chem. Phys. Lett.*, 155:572, **1989** .

[55] E. Herbst, G. Winnewisser, K.M.T. Yamada, D.J. DeFrees, and A.D. McLean. *J. Chem. Phys.*, 91:5905, **1989** .

[56] N. Balucani, L. Beneventi, P. Casavecchia, D. Stranges, and G.G. Volpi. *J. Chem. Phys.*, 94:8611, **1991** .

[57] N. Balucani, P. Casavecchia, D. Stranges, and G.G. Volpi. *Chem. Phys. Lett.*, 211:469, **1993** .

[58] R.R. Smardzewski and M.C. Lin. *J. Chem. Phys.*, 66:3197, **1997** .

[59] M. Iraqi and H. Schwarz. *Chem. Phys. Lett.*, 221:359, **1994** .

[60] D. Christen, H.G. Mack, and H. Oberhammer. *Tetrahedron*, 44:7363, **1988** .

[61] J.A. Dorado and J. Molina. *J. Phys. Chem.*, 98:7819, **1994** .

[62] D.R. Alleres, D.L. Cooper, T.P. Cunningham, J. Gerratt, P.B. Karadakov, and M. Raimondi. *J. Chem. Soc.*, 91:3357, **1995** .

[63] T.-K. Ha and W. Cencek. *Chem. Phys. Lett.*, 182:519, **1991** .

[64] R. Cimiraglia, J. Tomasi, and R. Cammi. *Chem. Phys.*, 136:399, **1989** .

[65] G.I. Cardenas-Jirón, J.R. Letelier, and A. Toro-Labbé. *J. Phys. Chem. A*, 102:7864, **1998.**

[66] S.S. Xantheas and Jr. Dunning. *J. Phys. Chem.*, 97:18, **1993** .

[67] R.A.J. O'Hair, C.H. Depuy, and V.M. Bierbaum. *J. Phys. Chem.*, 97:7955, **1993** .

[68] P.K. Chattaraj, G.H. Lee, and R.G. Parr. *Chem. Phys Lett.*, 237:171, **1995**.

[69] P.K. Chattaraj, S. Gutiérrez-Oliva, P. Jaque, and A. Toro-Labbé. *Mol. Phys.*, 101:2841, **2003**.

[70] K.G. Kidd and G.W. King. *J. Mol. Spectrosc.*, 16:411, **1968**.

[71] J.R. Durig and S.E. Hannum. *J. Chem. Phys.*, 52:6089, **1970** .

[72] J.R. Durig, J.F. Davis, and A. Wang. *J. Mol. Struct.*, 375:67, **1996** .

[73] K. Hagen and K. Hedberg. *J. Am. Chem. Soc.*, 95:1003, **1973** .

[74] D.D. Danielson, L. Hedberg, K. Hedberg, K. Hagen, and M. Traetteberg. *J. Phys. Chem.*, 99:9374, **1995** .

[75] J. Tyrrel. *J. Am. Chem. Soc.*, 98:5456, **1976** .

[76] Ch.W. Bock and A. Toro-Labbé. *J. Mol. Struct. (THEOCHEM)*, 232:239, **1991**.

[77] D.M. Hassett, K. Hedberg, and C.J. Marsden. *J. Phys. Chem.*, 97:4670, **1993** .

[78] P. Senet. *J. Chem. Phys.*, 107:2516, **1997**.

[79] G. Chung and Y. Kwon. *J. Mol. Struct. (THEOCHEM)*, 496:199, **2000** .

[80] J.F. Davis, A. Wang, and J.R. Durig. *J. Mol. Struct.*, 293:27, **1993** .

[81] B.S. Jursic. *J. Chem. Phys.*, 106:2555, **1997** .

[82] F.A. Bulat and A. Toro-Labbé. *Chem. Phys. Lett.*, 354:508, **2002**.

[83] S. Gutiérrez-Oliva and A. Toro-Labbé. *Chem. Phys. Lett.*, 383:435, **2004**.

[84] S. Gutiérrez-Oliva, J.R. Letelier, and A. Toro-Labbé. *Mol. Phys.*, 96:61, **1999**.

[85] P.K. Chattaraj, S. Nath, and A.B. Sannigrahi. *Chem. Phys Lett.*, 212:223, **1993**.

[86] P.K. Chattaraj, P. Pérez, J. Zevallos, and A. Toro-Labbé. *J. Phys. Chem. A*, 105:4272, **2001**.

[87] R.T. Sanderson. *Chemical Bond and Bond Energy.* Academic Press, New York, 2nd edition, **1976**.

[88] R.S. Berry, S.A. Rice, and J. Ross. *Physical Chemistry.* John Wiley and Sons, New York, **1980**.

[89] Y. Kim. *J. Am. Chem. Soc.*, 118:1522, **1996**.

[90] J.H. Lim, E.K. Lee, and Y. Kim. *J. Phys. Chem. A*, 101:2233, **1997**.

[91] A. Winkler and P. Hess. *J. Am. Chem. Soc.*, 116:9233, **1994** .

[92] G. Allen and R.O. Colclough. *J. Chem. Soc.*, 3:3912, **1957** .

[93] W. Yang, C. Lee, and S.K. Ghosh. *J. Phys. Chem.*, 89:5412, **1985.**

[94] D. Datta. *J. Phys. Chem.*, 90:4216, **1986.**

[95] M.J. Aguirre, G.I. Cardenas-Jirón, A. Toro-Labbé, and J.H. Zagal. *J. Mol. Struct.:THEOCHEM*, 493:219, **1999.**

[96] S. Sengupta and A. Toro-Labbé. *J. Phys. Chem. A*, 106:4443, **2002.**

[97] R.G. Pearson. *J. Am. Chem. Soc.*, 110:7684, **1988.**

[98] J.L. Gázquez. *J. Phys. Chem.*, 101:9464, **1997.**

[99] S. Arulmozhiraja and P. Kolandaibel. *Mol. Phys.*, 92:353, **1997** .

[100] R.G. Parr, L. von Szentpaly, and S. Liu. *J. Am. Chem. Soc.*, 121:1922, **1999.**

[101] R.G. Parr and W. Yang. *J. Am. Chem. Soc.*, 106:4049, **1984.**

[102] W. Yang and R.G. Parr. *Proc. Natl. Acad. Sci. USA*, 82:6723, **1985.**

[103] W. Yang and W.J. Mortier. *J. Am. Chem. Soc.*, 108:5708, **1986.**

[104] R. Contreras, P. Fuentealba, M. Galván, and P. Pérez. *Chem. Phys. Lett.*, 304:405, **1999.**

[105] Y. Li and J.N.S. Evans. *J. Am. Chem. Soc.*, 117:7756, **1995.**

[106] A.B. Sannigrahi. *Adv. Quantum Chem.*, 23:302, **1992.**

Anexos

Anexo A

Otros Conceptos Basados en la *TFD*

A.1 Indice de Electrofilia

Otro índice de reactividad global [100] recientemente propuesto es el índice de electrofília (ω),

$$\omega = \frac{\mu^2}{2\eta}, \tag{A.1}$$

que permite caracterizar la estabilización del sistema, al saturarse de carga proveniente de un medio con mayor potencial químico, en términos de μ y η.

A.2 Función de *Fukui* y Blandura Local

La función de *Fukui* electrónica, $f(\vec{r})$, fue introducida por Parr y Yang [101] como una generalización del concepto de orbitales frontera de *Fukui*. Los descriptores de reactividad local como la función de *Fukui*, $f(\vec{r})$, y la blandura local, $s(\vec{r})$ [102], son necesarios para explicar la selectividad de sitio en una molécula. La función de *Fukui* está definida como:

$$f(\vec{r}) = \left(\frac{\delta\mu}{\delta v(\vec{r})}\right)_N = \left(\frac{\partial\rho(\vec{r})}{\partial N}\right)_{v(\vec{r})} = \left(\frac{\partial^2 E}{\partial N \partial v(\vec{r})}\right). \tag{A.2}$$

Dentro de la aproximación de *core* rígido (o ausencia de relajación orbital) este descriptor correspondería a la densidad de los orbitales moleculares de frontera, permitiendo hacer un puente entre la teoría de orbitales de frontera desarrollada por *Fukui* y la *TFD*. Debido a la discontinuidad propia de la derivada $\left(\frac{\partial\rho(\vec{r})}{\partial N}\right)_{v(\vec{r})}$, tres diferentes tipos de funciones de *Fukui* pueden ser definidas:

$$\begin{aligned} f^+(\vec{r}) &= \left(\tfrac{\partial\rho(\vec{r})}{\partial N}\right)^+_{v(\vec{r})} \approx [\rho_{N+1}(\vec{r}) - \rho_N(\vec{r})] \approx \rho_{LUMO}(\vec{r}), \\ f^-(\vec{r}) &= \left(\tfrac{\partial\rho(\vec{r})}{\partial N}\right)^-_{v(\vec{r})} \approx [\rho_N(\vec{r}) - \rho_{N-1}(\vec{r})] \approx \rho_{HOMO}(\vec{r}), \\ f^o(\vec{r}) &= \tfrac{1}{2}[f^+(\vec{r}) + f^-(\vec{r})] \approx \tfrac{1}{2}[\rho_{LUMO}(\vec{r}) + \rho_{HOMO}(\vec{r})], \end{aligned} \tag{A.3}$$

donde, $f^+(\vec{r})$ mide la reactividad hacia un ataque nucleofílico; $f^-(\vec{r})$ mide la reactividad hacia un ataque electrofílico y $f^o(\vec{r})$ mide la reactividad hacia un ataque radicalario. La conexión con la teoría de orbitales frontera es clara en la ecuaciones anteriores. Dentro de la aproximación de *core* rígido, el máximo valor de la función de *Fukui* en un sitio dado, al ser preferido por un reactivo, ocasionaría un gran cambio en el potencial químico como lo indica la ecuación (A.2). Las cantidades anteriores pueden ser condensadas para un átomo k en una molécula, en términos de la población electrónica sobre el átomo [103]:

$$\begin{aligned} f_k^+ &= [q_k(N+1) - q_k(N)], \\ f_k^- &= [q_k(N) - q_k(N-1)], \\ f_k^o &= \tfrac{1}{2}[q_k(N+1) - q_k(N-1)]. \end{aligned} \tag{A.4}$$

En particular, la condensación puede realizarse considerando sólo las contribuciones de los orbitales frontera sobre un átomo dado, esto conduce a [104]:

$$\begin{aligned} f_k^+ &= q_k^L, \\ f_k^- &= q_k^H, \\ f_k^o &= \tfrac{1}{2}[f_k^+ + f_k^-], \end{aligned} \tag{A.5}$$

donde q_k^L y q_k^H, son las poblaciones electrónicas sobre el átomo k asociadas a los orbitales frontera *LUMO* y *HOMO*, respectivamente. Por otra parte, la blandura local se define como [102]:

$$s(\vec{r}) = f(\vec{r})S \tag{A.6}$$

donde S es la blandura global. De acuerdo a esta definición se obtienen diferentes tipos de blandura local al igual que para la función de *Fukui*, a partir de este descriptor local es posible establecer una versión local del principio HSAB [105].

A.3 Valencia Molecular

La valencia molecular, V_M, se define como:

$$V_M = \frac{1}{2}\sum_k V_k, \tag{A.7}$$

y corresponde a una medida de los enlaces covalentes dentro de la molécula; una molécula descrita por enlaces covalentes o levemente polares en su conformación de mínima energía se espera que presente un valor máximo de V_M. En esta última ecuación, V_k corresponde a la valencia atómica, la cual esta definida como:

$$V_k = \sum_{\ell \neq k} \left[\sum_{a \in k} \sum_{b \in \ell} D_{ab} D_{ba} \right], \tag{A.8}$$

donde D_{ab} son elementos de la matriz de orden de enlace [106]. V_k es entonces una medida del número de enlaces covalentes del átomo k dentro de la molécula y V_M corresponde a una medida de los enlaces covalentes dentro de la molécula, una molécula descrita por enlaces covalentes o levemente polares en su conformación de mínima energía se espera que presente un valor máximo de V_M.

Anexo B

Publicaciones generadas como parte de esta Tesis

Relations between Potential Energy, Electronic Chemical Potential, and Hardness Profiles

Gloria I. Cárdenas-Jirón, Soledad Gutiérrez-Oliva, Junia Melin, and Alejandro Toro-Labbé*

Centro de Mecánica Cuántica Aplicada, Departamento de Química, Facultad de Ciencias, Universidad de Chile, Casilla 653, Santiago, Chile

Received: November 20, 1996; In Final Form: February 20, 1997[⊗]

In recent papers we defined a theoretical frame aimed at characterizing the hardness and potential energy profiles along a reduced reaction coordinate (ω) varying from 0 to 1. In this paper we generalize that model to propose a global procedure that allows one to consider simultaneously the evolution of the potential energy (V) in connection with that of the electronic chemical potential (μ) and the molecular hardness (η). Important results have been obtained: (a) the potential energy profile can be expressed in terms of the μ and η profiles through an equation which is analogous to that used by Parr and Pearson to demonstrate the HSAB principle; (b) the chemical potential along ω is in turn written in terms of the hardness profile, an equation which is analogous to that proposed by the same authors to quantify the electron tranfer induced by a chemical potential gradient; and (c) useful expressions for the activation properties have been derived. As an illustration we study the *trans* ⇌ *cis* isomerization of diimide, a reaction that may occur through either an internal rotation or an inversion mechanism. The most relevant result concerning the chemical system is that for both mechanisms the principle of maximum hardness holds even though the electronic chemical potential strongly varies along the reaction coordinates. Our analysis suggests that if a system is constrained to chose among different reaction paths connecting two stable states, it will prefer the one presenting a minimum chemical potential.

1. Introduction

Density functional theory (DFT), a theory based upon the ground state electronic density distribution of atoms and molecules, has provided the theoretical basis for concepts like electronic chemical potential (μ) and molecular hardness (η).[1−6] The electronic chemical potential characterizes the escaping tendency of electrons from the equilibrium system, whereas molecular hardness can be seen as a resistance to charge transfer. Both μ and η are global properties of the system.

It has been recently shown that the hardness profile along a reaction coordinate is quite useful to study the progress of chemical reactions.[7] In this context, the relation between hardness and energy profiles appears to be especially important for characterizing transition states.[8,9] The hardness profile passes through a minimum near or at the transition state for different types of reactions, although some symmetric stretching modes of deformation do not always correspond to extremum values of hardness at the equilibrium conformation.[7−10] In connection with this, the principle of maximum hardness (PMH) asserts that molecular systems at equilibrium tend to states of high hardness;[4] transition states should therefore present a minimum value of hardness. It follows that the combination of the PMH with the Hammond postulate[11] constitutes a quite powerful tool for a qualitative characterization of transition states.[9] Parr and Chattaraj[12] showed that the PMH holds under the constraints that the external potential and the electronic chemical potential must remain constant upon distorsion of the molecular structure. However, the PMH seems to be valid even under less restrictive conditions than the ones stated above. Relaxation of the constraints seems to be permissible, and in particular, it has been found that the electronic chemical potential is not always constant along a reaction coordinate.[9,13−15]

As far as the electronic chemical potential is concerned, most studies have been performed within the frame of the constraints of the PMH; they have been confined to evaluate μ under small distorsions of the molecular structure with the result that it remains reasonably constant.[13−15] However, few molecules presenting torsional isomerization reactions show a non-negligible variation of μ along a reaction coordinate.[7,9] It is thus of interest to study the variation of this property in connection with the potential energy and hardness profiles. To do so we propose in this paper a theoretical framework that provides analytic expressions for the evolution of these global properties along a reaction coordinate and allows direct connections among them.

Due to the above commented fact that most studies on the variation of the electronic chemical potential concluded that it remains constant upon distorsions of the molecule, validating in this way the PMH, we choose to illustrate our model relating energetic and electronic properties with the study of two different isomerization mechanisms in a system where the energy barriers separating two stable states are sufficiently high to expect strong variations of the chemical potential and hardness. A challenging process for our purposes is the *trans* ⇌ *cis* isomerization reaction of diimide (HN=NH) which can occur through internal rotation about the double bond or through inversion at one nitrogen atom. Diimide (or diazene) is a short lived species that has been identified as one of the decomposition products of the hydrazoic acid and hydrazine reaction.[16] It is usually employed in the selective reduction of nonpolar bonds and as ligands in transition metal complexes. Although N_2H_2 cannot be isolated under ordinary conditions, its infrared spectrum has been studied by many authors.[17−20] From a theoretical viewpoint, diimide has also been studied by many authors, and the most relevant conclusion that concerns this paper is that the barriers associated with the different isomerization mechanisms have been found to be about 46−60 kcal/

[⊗] Abstract published in *Advance ACS Abstracts*, May 15, 1997.

S1089-5639(96)03870-4 CCC: $14.00

mol,[21-26] high enough to expect a strong variation of the electronic properties along the different reaction pathways.

2. Theory

Energy, Chemical Potential, and Hardness Profiles. We start by defining a reduced reaction coordinate ω, which can be related to the actual reaction coordinate through a scaling procedure under the condition that it varies from 0 (initial state) to 1 (final state) with $\omega = 0.50$ at midway between the reference states. These are characterized by the extremum values of ω, in the present case the *trans* and *cis* conformations that correspond to $\omega = 0$ and $\omega = 1$, respectively. The reduced coordinate can therefore be viewed as a measure of the reaction progress going from reactants ($\omega = 0$) to products ($\omega = 1$), passing through a transition state.

The potential energy representing a *trans* ⇌ *cis* isomerization process, following the rotation or inversion pathways, is given by[8,9]

$$V(\omega) = K_V f(\omega) + \omega\Delta V^0 \tag{1}$$

where $K_V = (k_t + k_c)$ with k_t and k_c the torsional force constants associated with the reference conformations (for the inversion mechanism they will correspond to bending force constants) and $\Delta V^0 = (V(1) - V(0))$ is the energy difference between those conformations. In eq 1, $f(\omega)$ is a function which must be symmetric about $\omega = {}^1/_2$ where it is maximal. Many conveniently normalized functions qualify with this requirement; they all must have the same behavior about $\omega = {}^1/_2$, and therefore they only may differ in their wings. Due to its thermodynamic implicancies, an appealing function that satisfies the above requirement is $f(\omega) = -[\omega \ln \omega + (1 - \omega)\ln(1 - \omega)]$; however, the function $f(\omega) = \omega(1 - \omega)$, that came out from a Fourier expansion of the torsional potential, has been used in our previous papers[8,9] and will be used here to rationalize the *ab initio* results of the internal rotation and inversion of diimide.

Since the electronic chemical potential and molecular hardness are global properties of the system, they can be written in terms of the same analytic form used for the potential energy in eq 1. Therefore we have

$$\mu(\omega) = K_\mu f(\omega) + \omega\Delta\mu^0 \tag{2}$$

and

$$\eta(\omega) = K_\eta f(\omega) + \omega\Delta\eta^0 \tag{3}$$

In eqs 2 and 3 the parameters $\Delta\mu^0$, $K_\mu = (\mu_t + \mu_c)$ and $\Delta\eta^0$, $K_\eta = (\eta_t + \eta_c)$, respectively, have the same meaning that ΔV^0, K_V, has for $V(\omega)$. The parameters of eqs 1−3 will be determined following a prescription given in our previous works[8,9] and briefly reviewed in section 3.

The $\{\mu,V\}$ Representation. The above equations show that $V(\omega)$, $\mu(\omega)$, and $\eta(\omega)$ are connected through the function $f(\omega)$. Using eq 2 to express $f(\omega)$ in terms of the electronic chemical potential allows one to define with eq 1 a potential energy $V_\eta(\omega)$, where the index is indicating that it formally considers the hardness as being constant

$$V_\eta(\omega) = \omega\Delta V^0 + Q_\eta(\mu(\omega) - \omega\Delta\mu^0) \tag{4}$$

where $Q_\eta = K_V/K_\mu$. In Figure 1a we show a schematic view of the progress of a chemical reaction in the $\{\mu,V\}$ space; the arrows are indicating the sense of the reaction (from *trans* to *cis* passing through the transition state). The parameter Q_η appearing in eq 4 can be independently determined by drawing

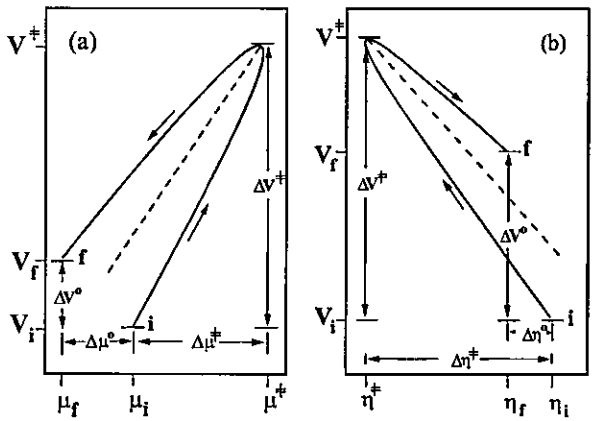

Figure 1. Schematic view of the 2D representations of the evolution of a chemical reaction in the $\{\mu,V\}$ and $\{\eta,V\}$ spaces. The arrows indicate the sense of the reaction going from the initial state (i) to the final state (f) and passing through the transition state.

a straight line intersecting the parabolic function, a straight line that is rigorously obtained through the rectilinear diameters law (RDL) usually invoked to determine critical constants in thermodynamics.[8] It can be noticed that for reactions presenting small values of ΔV^0 and $\Delta\mu^0$ the parabolic form of Figure 1a reduces to a straight line with slope Q_η.

The $\{\eta,V\}$ Representation. When the electronic chemical potential remains constant along ω, it is interesting to express $V(\omega)$ in terms of $\eta(\omega)$. This allows to connect concepts like the PMH and the Hammond postulate.[9] Following the same procedure we used to obtain $V_\eta(\omega)$, the combination of eqs 1 and 3 leads to definition of $V_\mu(\omega)$

$$V_\mu(\omega) = \omega\Delta V^0 + Q_\mu(\eta(\omega) - \omega\Delta\eta^0) \tag{5}$$

with $Q_\mu = K_V/K_\eta$. Equation 5 was discussed in our previous papers with the result that Q_μ should be negative in attention to the PMH.[8,9] In Figure 1b is displayed the progress of the chemical reaction in the $\{\eta,V\}$ space. Isomerization processes going from one stable conformation to another stable conformation lead to a clockwise *trans* → transition state → *cis* path in the $\{\eta,V\}$ diagram, as indicated by the arrows in Figure 1b. As in the precedent case, the straight line with slope Q_μ that bisects the parabola is obtained using the RDL.

It should be noted that the $\{\mu,V\}$ and $\{\eta,V\}$ diagrams show that a necessary condition for consistency between $V(\omega)$, as defined in eq 1, $V_\eta(\omega)$, and $V_\mu(\omega)$ is that $V_\eta(\omega) = V_\mu(\omega) = V(\omega)$ for all ω. In particular, the energy barrier separating two stable conformations can be derived from any of the equations defining the potential energy function.

The $\{\eta,\mu\}$ Representation. From the fundamental DFT it has been shown that at equilibrium systems attain a given chemical potential, which can be written in terms of the properties of isolated reactants.[4,5,27] For a A + B → AB type of reaction, Parr and Pearson showed that the number of electrons (ΔN) tranferred between A and B is given by:[2]

$$\Delta N = \frac{(\mu_B - \mu_A)}{(\eta_B + \eta_A)} \tag{6}$$

This equation states that the difference in chemical potential drives the electron transfer, whereas the sum of the individual hardnesses inhibits it.[4,5,27] Our model that considers reactants and products as different chemical species trapped on local potential wells leads to the following expression for the

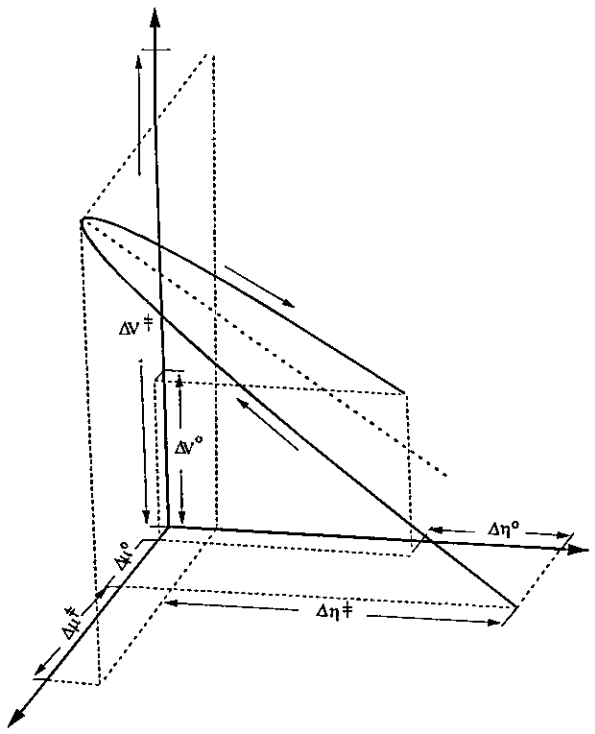

Figure 2. Schematic view of the 3D representation of the evolution of the potential energy in the $\{\mu,\eta,V\}$ space.

electronic chemical potential in terms of the molecular hardness

$$\mu(\omega) = \omega\Delta\mu^0 + Q(\eta(\omega) - \omega\Delta\eta^0) \tag{7}$$

with $Q = Q_\mu/Q_\eta$, given by

$$Q = \frac{\mu(\omega) - \omega\Delta\mu^0}{\eta(\omega) - \omega\Delta\eta^0} \tag{8}$$

The minus signs appearing in eq 8 are due to the fact that we are dealing with relative values of μ and η. Since all values are relative to those of the *trans* conformations, negative values of $\eta(\omega)$ are allowed, and so eq 8 is well-defined in the range $0 < \omega < 1$. On the other hand, we have checked the behavior of Q along ω and found that it is constant with singularities at $\omega = 0$ and $\omega = 1$ because μ and η are defined with respect to their values at $\omega = 0$. It is interesting to compare, at least qualitatively, eqs 6 and 8. It follows that Q might be related to some charge redistributed among the atoms in the molecule during the chemical reaction, and the hardness appears to be acting as a resistance to that redistribution.

The $\{\mu,\eta,V\}$ Representation. When both μ and η vary with ω it is then possible to obtain an alternative and more general expression for the potential energy. We take the arithmetic average of eqs 4 and 5 to obtain

$$V(\omega) \equiv {}^1/_2(V_\eta(\omega) + V_\mu(\omega)) = \omega\Delta V^0 + {}^1/_2Q_\eta(\mu(\omega) - \omega\Delta\mu^0) + {}^1/_2Q_\mu(\eta(\omega) - \omega\Delta\eta^0) \tag{9}$$

Figure 2 shows how the reaction progress looks like in the $\{\mu,\eta,V\}$ space. As in the previous diagrams, the parabolic form can be rationalized with the help of the 3D RDL, and it reduces to a 3D straight line in the case of symmetric reactions.

It is interesting to note that eq 9 is analogous to

$$E = E^0 + \Delta N\,\mu + {}^1/_2(\Delta N)^2\,\eta + \ldots \tag{10}$$

which, according to Parr and Pearson,[2] is the energy of an atom in a molecule with electrons flowing from or to that atom and keeping the external potential (v) constant. Changes in N and v lead to a more general expression for the energy that includes the Fukui function and allows discussion of energy in terms of frontier orbital theories of chemical reactivity.[5,27] Again, the term to term comparison of eqs 9 and 10 suggests that Q_η and Q_μ are related in some way to the change of the electronic charge (ΔN) when going from reactants to products.

Another evidence pointing at the sense that eq 9 correctly contains the μ and η dependence of the energy is that it is very similar to

$$\Delta E = \Delta E^0 + {}^1/_2a\Delta\mu^0 + {}^1/_2b\Delta\eta^0 \tag{11}$$

which we have derived in the context of the thermochemistry of formation of hydrogen thioperoxide (HSOH) from its radical and ionic fragments.[28]

The above characterization of a chemical reaction presents the advantage of giving simultaneous information about the change of energy and electronic properties along the reaction coordinate. In fact, since the change in electronic properties is related to the reaction mechanism, eq 9 is connecting the energetic and mechanistic aspects of a chemical reaction. Our approach appears to be complementary to other approaches aimed at following the course of chemical reactions. For example, in the frame of the time-dependent DFT, Chattaraj and Nath have studied the electronegativity (the negative of the chemical potential) and hardness dynamics in chemical reactions,[29,30] obtaining important insights that help characterize the temporal evolution of electronic properties. An interesting extension of this work would be to study the behavior of eq 9 under the temporal evolution of V, μ, and η.

A Thermodynamic-like Approach. Equation 9 suggests that it should be possible to build up a thermodynamic-like approach connecting the three properties we are studying here. Let us write the potential energy in the $\{\mu,\eta,V\}$ space considering the electronic chemical potential and the molecular hardness as independent variables. The differential expression of $V(\mu,\eta)$ is

$$dV = \left(\frac{\partial V}{\partial \mu}\right)_\eta d\mu + \left(\frac{\partial V}{\partial \eta}\right)_\mu d\eta \tag{12}$$

where we took $dV = (V(\omega) - \omega\Delta V^0)$. The slopes appearing in the above equation are obtained from eqs 4 and 5

$$\left(\frac{\partial V}{\partial \mu}\right)_\eta \equiv \frac{1}{2}\left(\frac{dV_\eta}{d\mu}\right) = \frac{1}{2}\frac{(V_\eta(\omega) - \omega\Delta V^0)}{(\mu(\omega) - \omega\Delta\mu^\circ)} = \frac{1}{2}Q_\eta \tag{13}$$

and

$$\left(\frac{\partial V}{\partial \eta}\right)_\mu \equiv \frac{1}{2}\left(\frac{dV_\mu}{d\eta}\right) = \frac{1}{2}\frac{(V_\mu(\omega) - \omega\Delta V^0)}{(\eta(\omega) - \omega\Delta\eta^\circ)} = \frac{1}{2}Q_\mu \tag{14}$$

Equation 12 can now be rewritten as

$$dV = {}^1/_2Q_\eta\,d\mu + {}^1/_2Q_\mu\,d\eta \tag{15}$$

Assuming now that Q_η and Q_μ are variables and the pairs $\{Q_\eta,\mu\}$ and $\{Q_\mu,\eta\}$ are conjugated to one another, appropiate Legendre

transformations lead to

$$U(\omega) = \omega\Delta U^0 - {}^1/_2(\mu(\omega) - \omega\Delta\mu^0)\,\mathrm{d}Q_\eta - \frac{1}{2}(\eta(\omega) - \omega\Delta\eta^0)\,\mathrm{d}Q_\mu \quad (16)$$

where after the transformation the energy U is defined as $U=V - (Q_\eta\mu + Q_\mu\eta)/2$. Therefore, if the parameters Q_η and Q_μ are allowed to vary, then we obtain an equation that is homogeneous to eq 10, the Parr and Pearson expression used to explain a formation process of a molecule from the isolated atoms.[2]

Activation Properties. To determine the position of the transition state associated with the potential $V(\omega)$ we make use of the function $f(\omega) = (1 - \omega)\omega$ in eq 1 such that $(\mathrm{d}V/\mathrm{d}\omega)_{\omega=\beta} = 0$, thus obtaining the position β in terms of the potential energy parameters:

$$\beta = \frac{1}{2} + \frac{\Delta V^0}{2K_V} \quad (17)$$

This equation is in fact a quantitative formulation of the Hammond postulate: if $\Delta V^0 > 0$ then $\beta > {}^1/_2$ and the transition state is closer to products, whereas if $\Delta V^0 < 0$ then $\beta < {}^1/_2$ and the transition state is closer to reactants.[11] Putting β in eq 1 yields to the following expression for the activation energy:

$$\Delta V^\ddagger \equiv V(\beta) = \frac{1}{4}K_V + \frac{1}{2}\Delta V^0 + \frac{(\Delta V^0)^2}{4K_V} \quad (18)$$

Note that this equation is similar to the one derived by Marcus in his theory of electron tranfer in solution.[31] The parameter β is known as the Brønsted coefficient, and physically it represents a measure of the degree of resemblance of the transition state with respect to the product. The Brønsted coefficient is often used to quantify the empirical concepts of *reactant-like* ($0 \le \beta \le {}^1/_2$) and *product-like* (${}^1/_2 \le \beta \le 1$) transition state.[8,9,32-34] By evaluating eq 9 in $\omega = \beta$ we obtain an alternative expression for the activation energy, now in terms of the activation chemical potential ($\Delta\mu^\ddagger \equiv \mu(\beta)$) and the activation hardness ($\Delta\eta^\ddagger \equiv \eta(\beta)$):

$$\Delta V^\ddagger = \beta\Delta V^0 + {}^1/_2\,Q_\eta(\Delta\mu^\ddagger - \beta\Delta\mu^0) + {}^1/_2\,Q_\mu(\Delta\eta^\ddagger - \beta\Delta\eta^0) \quad (19)$$

This equation connecting the three activation properties might provide new interpretations of the nature of activation energies, and certainly it may help to give new insights about reaction mechanisms. It has been found in different types of reactions that μ and η pass through an extrema at β or very near to it;[8-10] this ensures that eq 19 produces reliable values of potential barriers from the knowledge of activation electronic properties.

The activation chemical potential is obtained by evaluating eq 4 at $\omega = \beta$, thus obtaining:

$$\Delta\mu^\ddagger = \beta\Delta\mu^0 + \frac{1}{Q_\eta}(\Delta V^\ddagger - \beta\Delta V^0) \quad (20)$$

The electronic chemical potential is expected to be smaller than the total energy; it then follows that $|Q_\eta| \ge 1$ to have $\Delta\mu^\ddagger \le \Delta V^\ddagger$.

On the other hand, the activation hardness is obtained from eq 5:

$$\Delta\eta^\ddagger = \beta\Delta\eta^0 + \frac{1}{Q_\mu}(\Delta V^\ddagger - \beta\Delta V^0) \quad (21)$$

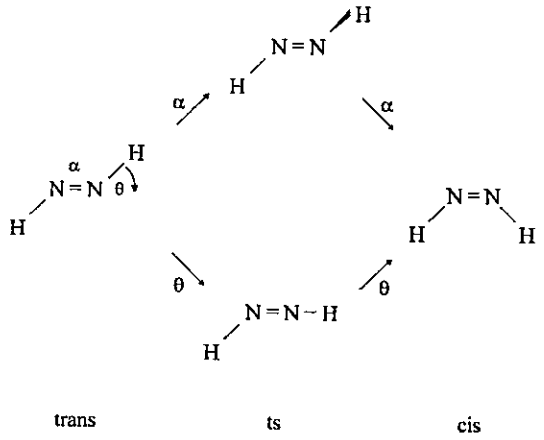

Figure 3. Rotation and inversion mechanisms for the isomerization of diimide.

It is proportional and opposite (Q_μ is negative) to the activation energy. The above equation was derived in slightly different terms in our previous papers and was used with success in the determination of activation hardnesses for rotational isomerization processes.[8,9] It is important to mention that Zhou and Parr also found proportionality between $\Delta\eta^\ddagger$ and $\Delta V^\ddagger$ in electrophilic aromatic substitution processes.[35] Finally, we note that alternative expressions for the electronic activation properties in terms of the potential parameters K_V and ΔV^0 can be obtained by using in the above equations the definition of β and $\Delta V^\ddagger$ (eqs 17 and 18, respectively).

3. Calculations

The above described model relating the profiles of the potential energy, electronic chemical potential, and molecular hardness is now used to rationalize *ab initio* calculations of the *trans* ⇌ *cis* isomerization of the HN=NH molecule, isomerization that can occur through a rotation or an inversion mechanism, as shown in Figure 3. Both are important mechanisms in chemistry, and their study constitutes a challenge to test our model in different reaction pathways where the electronic chemical potential is expected to change strongly along the reaction coordinates. The isomerization of diimide has been widely studied, and high-level calculations estimating barrier heights and structural properties are currently available.[25,26] It has been established that since the inversion mechanism leads to a closed shell transition state whereas the internal rotation yields to a biradical transition state, sophisticated calculations going beyond the self-consistent field (SCF) energy are necessary to have a common theoretical method allowing proper comparisons among these structures.[25,26] However, since the aim of this paper is mainly methodological ,we will concentrate our analysis to $\mu(\omega)$ and $\eta(\omega)$ in terms of their relationships with $V(\omega)$ and all properties will be calculated in the frame of the Hartree−Fock SCF theory, without paying further attention to the accuracy of the numerical values obtained. Therefore, our numerical results should be taken on a qualitative basis, they will be used to illustrate the theoretical procedure depicted in section 2, keeping in mind that for quatitative purposes they may need further improvements.

The Reaction Coordinates. We start by defining the reduced reaction coordinate for the different reaction mechanisms. The coordinate ω is related to the torsional (dihedral) angle α through[8,9] $\omega(\alpha) = (1 - \cos\alpha)/2$ with ω varying from 0 ($\alpha = 0$) to 1 ($\alpha = \pi$), extrema that indicate the *trans* and *cis* reference conformations, respectively. On the other hand, the inversion mechanism is represented by moving a hydrogen in the NNH

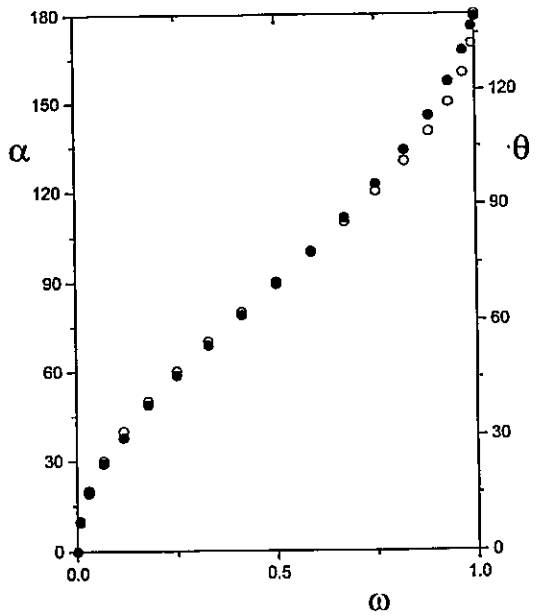

Figure 4. Representation of the rotation (α, open circles) and inversion (θ, filled circles) coordinates (in degrees) in terms of the reduced coordinate ω.

plane; this generates a trajectory defined by the angle θ, as shown in Figure 3. The angle θ goes from 0 (*trans*, $\omega = 0$) to 139.29° (*cis*, $\omega = 1$) and passes through $\theta = 69.65°$ where $\omega = 0.50$. These three values were used to determine $\omega(\theta) = 0.7044 - 0.5255 \cos\theta - 0.1789 \cos^2\theta$. In Figure 4 we display the evolution of the torsional and inversion coordinates along the reduced variable ω.

Parameters Defining $V(\omega)$, $\mu(\omega)$ and $\eta(\omega)$. The parameters involved in eqs 1−3 were determined following the prescription given in our previous works.[8,9] It asserts that two energy points at the vicinity of the reference conformations are needed to estimate the curvature of the assumed harmonic potential wells in which the reference conformations are trapped. For the internal rotation we have performed calculations at $\omega = 0$ and $\omega = 0.0076$ (α = 0° and 10°, respectively), leading to determination of k_t, μ_t and η_t. Calculations at $\omega = 0.9924$ and $\omega = 1$ (α = 170° and 180°, respectively) led to k_c, μ_c, and η_c.[8,9] In the case of the inversion mechanism, calculations at $\omega = 0$ and $\omega = 0.0105$ ($\theta = 0°$ and 10°, respectively) led to k_t, μ_t, and η_t and calculations at $\omega = 0.9715$ and $\omega = 1$ (θ = 129.29° and 139.29°, respectively) led to k_c, μ_c and η_c. For a more detailed discussion about the procedure we use to numerically obtain the input parameters needed to define $V(\omega)$, $\mu(\omega)$ and $\eta(\omega)$, the reader is referred to our previous papers.[32−34] In Table 1 are quoted the input parameters necessary to obtain the profiles of these properties along the reaction paths.

Method of Calculation. We have performed calculations at the Hartree−Fock (HF) SCF level with a standard 6-31G** basis set and with full geometry optimization at the points mentioned in the preceding paragraph. The calculations were performed through the Spartan package.[36] A recent theoretical study of the diimide isomerization showed that when the isomerization path does not involve breaking and forming bonds, HF and post-HF calculations lead to quite similar results concerning geometric parameters and barrier heights.[37] Our results concerning the optimized geometrical parameters of the structures considered in this work are in good agreement with the available experimental data and theoretical results at different levels of calculation.

TABLE 1: Input Data and Activation Properties for the Internal Rotation and Inversion of Diimide[a]

input data	rotation	inversion
k_t	78.4445	168.3952
k_c	60.8893	166.8302
$K_V = (k_t + k_c)$	139.3338	335.2254
ΔV^0	6.8166	6.8166
μ_t	20.1673	312.0726
μ_c	51.8500	338.1055
$K_\mu = (\mu_t + \mu_c)$	72.0173	650.1781
$\Delta\mu^0$	−3.6741	-3.6741
η_t	−79.0007	−205.3633
η_c	−107.1526	−259.4150
$K_\eta = (\eta_t + \eta_c)$	−186.1533	−464.7783
$\Delta\eta^0$	0.6137	0.6137
$Q_\eta = K_V/K_\mu$	1.9347	0.5156
$Q_\mu = K_V/K_\eta$	−0.7485	−0.7213
$Q = Q_\mu/Q_\eta$	−0.3869	−1.3990
output data	**rotation**	**inversion**
β	0.5245	0.5102
$\Delta V^\ddagger$	38.3251	87.2493
$\Delta\mu^\ddagger$	16.0344	160.6024
$\Delta\eta^\ddagger$	−46.1044	−115.8331

[a] The input parameters are given in kcal/mol · rad², and the energies are in kcal/mol.

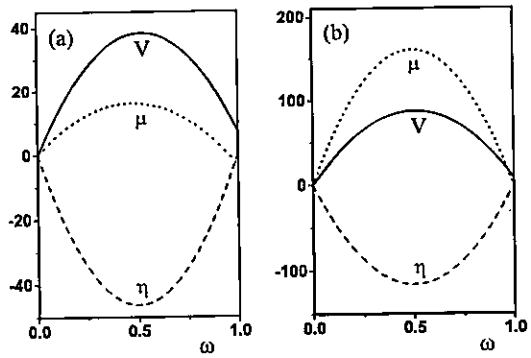

Figure 5. Potential energy, electronic chemical potential, and hardness profiles for the isomerization reaction of diimide following the rotation (a) and inversion (b) mechanisms.

The reference values of electronic chemical potential and molecular hardness were obtained from HF calculations through the operational formulas which come out from the finite-difference approximation.[5] I and A correspond to the first ionization potential and electron affinity of the molecule and were determined through a ΔSCF procedure. Calculations on ions were performed using the unrestricted Hartree−Fock procedure on the already optimized neutral molecular structure.

4. Results and Discussion

Energy, Chemical Potential, and Hardness Profiles. In Figure 5 we display the curves of potential energy, chemical potential, and hardness along ω for the rotation and inversion mechanisms. We note that for both mechanisms, the potential energy and electronic chemical potential profiles exhibit the same trend with maximum values at the transition state. Opposite to this is the behavior of the hardness, indicating that the PMH is verified for the two isomerization paths. It should be noted that since all values are relative to those of the *trans* conformation, $\eta(\omega)$ may be negative.

The potential barrier associated with the inversion mechanism is higher than the one associated with the internal rotation, indicating that rotation should be the preferred mechanism for isomerization. For the internal rotation, the electronic chemical

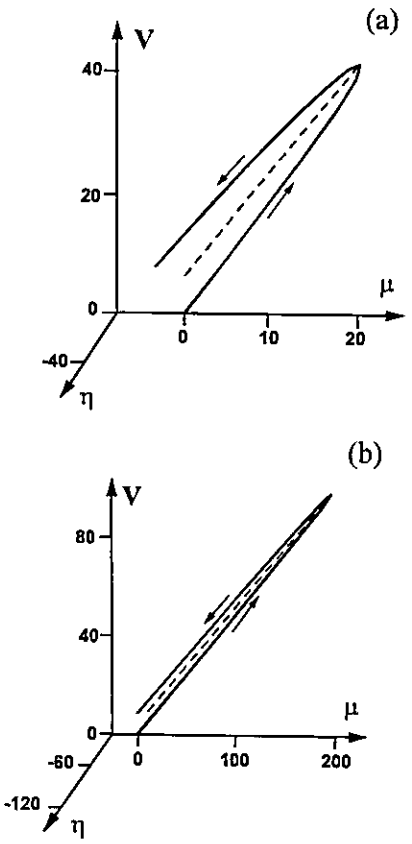

Figure 6. 3D representations of the evolution of the isomerization reaction in the $\{\mu,\eta,V\}$ space following the rotation (a) and inversion (b) mechanisms.

potential along ω is lower than the potential energy, presenting intermediate values between the potential energy and the molecular hardness. This situation is not reproduced for the inversion mechanism, where the μ values are higher than the potential energy values. In both cases the hardness profile behaves similarly although in the inversion mechanism it attains a deeper minimum at the transition state.

A chemical process is driven by μ when this property follows a minimum chemical potential path which, in the present case, corresponds to the rotation mechanism. In this case a delicate balance between potential energy and hardness seems to be present: the chemical potential profile is intermediate between the η and V profiles. In contrast to this, the inversion mechanism presents a chemical potential profile which is even higher than energy profile due to an anomalous value of the parameter Q_η (0.5156) that should be higher than one (see Table 1).

3D Representation of the Isomerization Process. In Figure 6 are displayed the 3D representations of the different isomerization mechanisms studied in this paper. We note that the rotation mechanism is represented by an open parabola, whereas the parabola representing the inversion mechanism is closer to a straight line. It is interesting to mention that projections of the 3D straight lines of Figure 6 onto the $\{\mu,V\}$, $\{\eta,V\}$, and $\{\mu,\eta\}$ planes leads to three 2D straight lines defined through their slopes Q_η, Q_μ, and Q, respectively. These are quasi orthogonal to each other and may be orthogonalized through classical methods. This confirms the assumption we made in performing Legendre transformations on eq 9 that Q_η and Q_μ are conjugated variables of μ and η, respectively. This may be an important result and merits further attention since it suggests that it should be possible to perform mathematical transformations to express the energy and electronic properties in some $\{Q_\eta,Q_\mu\}$ space. In particular, if orthogonality is verified, then the parabolic forms obtained in the $\{\mu,\eta,V\}$ space suggest that in the $\{Q_\eta,Q_\mu\}$ space we should be able to write $Q_\mu \approx CQ_\eta^2$ and therefore the correspondence between the parameters appearing in eqs 9 and 10, $Q_\eta \leftrightarrow \Delta N$ and $Q_\mu \leftrightarrow \Delta N^2$, seem to be correct, at least qualitatively. Moreover, by defining the origin of the coordinate system at the transition state, it should be possible to determine rules to make the system decide among different reaction paths in terms of the numerical values of Q_η and Q_μ.

On the other hand, in all the representations of the potential energy, electronic chemical potential, and hardness profiles, the inversion mechanism exhibits close linear dependences, which are the characteristic feature of symmetric situations. In this mechanism, the symmetry plane of the molecule is conserved along the reaction coordinate, whereas torsion about the central bond breaks down all symmetry elements of the molecule. This observation may be used to confirm the fact that a reaction path that keeps a symmetry element along it might not necessarily be the preferred direction that follows the system. Such a symmetry element might be considered as unstable, in the sense pointed out by Pearson and Palke.[13]

Activation Properties. In Table 1 are displayed the activation properties we have obtained through eqs 17–21. Note that for the two mechanisms we are studying in this paper the parameter β is showing that transition states are closer to the product than to the reactants, a result that verifies the Hammond postulate ($\Delta V^0 > 0$). On the other hand, relatively good agreement of the value for the rotation barrier, predicted through eq 18, is anticipated on the basis of comparisons with the available literature data at the HF level. For the rotation about the N=N central bond, a value of 38.3 kcal/mol is anticipated which is in good agreement with 37.2 kcal/mol obtained by Cimiraglia *et al.*[25] In contrast to this, for the inversion mechanism, eq 18 predicts a value of 87.2 kcal/mol that is too high when compared to the available literature data.[25,26,37]

Barrier heights at higher levels of calculation have been recently reported by Cimiraglia *et al.*[26] These authors used different polarized basis sets going beyond Hartree–Fock by means of complete active space–self-consistent field (CAS-SCF) and CIPSI techniques to perform quantitative comparisons of the energy and structures of the different transition states involved in the isomerization mechanisms of diimide. They suggest that both mechanisms are quite competitive. Our estimations for the barrier heights associated with the different reaction mechanisms and the criterium that a reaction must follow a minimum chemical potential path lead us to conclude that rotation would be the preferred mechanism.

Our $\Delta V^\ddagger$ values allow one to conclude that while the parameter K_V for the rotational mechanism seems to be quite well-estimated, leading to a reasonably good barrier for internal rotation, the corresponding parameter for the inversion mechanism seems to be overestimated, thus producing a too large barrier to inversion. To quantify the error we have in our calculation of this parameter for inversion, we use the $\Delta V^\ddagger$ and ΔV^0 values reported by Cimiraglia *et al.* (51.7 kcal/mol and 3.15 kcal/mol, respectively) obtained at the CAS-SCF level[26] to solve the second-order equation in K_V that can be derived from eq 18. As a result, we obtain $K_V = 243.6$ kcal/mol · rad^2 that compared with our original estimation of 335.2 kcal/mol · rad^2 leads to an error of about 27%. Similar effects are expected in our estimation of the remaining parameters associated with the inversion. It is therefore clear that more sophisticated wave

functions will improve quantitatively and qualitatively our results, especially those concerning the inversion mechanism.

5. Summary and Concluding Remarks

In this paper we have proposed a theoretical model aimed at considering simultaneously the evolution of the potential energy, electronic chemical potential, and molecular hardness along a reaction coordinate. The model proposed was used in the study of the *trans* ⇌ *cis* isomerization reaction of diimide following two different pathways: internal rotation about the double bond or inversion at one nitrogen atom. In both mechanisms the principle of maximum hardness holds even though the electronic chemical potential changes strongly during the chemical reaction.

The analysis presented in this paper suggests that the chemical potential responds to a delicate balance between the potential energy and hardness. In some cases this may lead to a constant chemical potential along the reaction coordinate, although variations are permissible in the range $\eta(\omega) \leq \mu(\omega) \leq V(\omega)$. Our results show that internal rotation is the preferred mechanism for isomerization because it presents the lowest energy barrier and the minimum chemical potential path.

The parameters Q_η, Q_μ, and Q have been qualitatively related to some charge redistributed among the atoms in the molecule during the isomerization process. However, open questions remain. They concern the exact identification of these charges and their eventual use as quantitative indexes to make the system decide among different reactive channels. Since for the isomerization reactions we have studied in this paper only intramolecular charge transfer may occur, it may be redistributed in specific regions of the molecular topology, and therefore the analysis of condensed charges along the reaction coordinate certainly will help identify these parameters. Concerning their use as reactivity indexes, we believe that convenient transformations putting the transition state at the origin of a new coordinate system, the $\{Q_\eta,Q_\mu\}$ space, will allow determination of empirical relations between these parameters, giving insights about this point.

Acknowledgment. The authors are thankful for the financial support from FONDECYT through projects numbered 2950029/95 and 1961021.

References and Notes

(1) Parr, R. G.; Yang, W. *Annu. Rev. Phys. Chem.* **1995**, *46*, 701.
(2) Parr, R. G.; Pearson, R. G. *J. Am. Chem. Soc.* **1983**, *105*, 7512.
(3) Pearson, R. G. *J. Am. Chem. Soc.* **1985**, *107*, 6801.
(4) Pearson, R. G. *J. Chem. Educ.* **1987**, *64*, 561.
(5) Parr, R. G.; Yang, W. *Density Functional Theory of Atoms and Molecules*; Oxford University Press: New York, 1989.
(6) Dreizler, R. M.; Gross, E. K. V. *Density Functional Theory*; Springer: Berlin, 1990.
(7) Chattaraj, P. K.; Nath, S.; Sannigrahi, A. B. *J. Phys. Chem.* **1994**, *98*, 9143.
(8) Cárdenas-Jirón, G. I.; Lahsen, J.; Toro-Labbé, A. *J. Phys. Chem.* **1995**, *99*, 5325.
(9) Cárdenas-Jirón, G. I.; Toro-Labbé, A. *J. Phys. Chem.* **1995**, *99*, 12730.
(10) Chattaraj, P. K.; Nath, S.; Sannigrahi, A. B. *Chem. Phys. Lett.* **1993**, *212*, 223.
(11) Hammond, G. S. *J. Am. Chem. Soc.* **1955**, *77*, 334.
(12) Parr, R. G.; Chattaraj, P. K. *J. Am. Chem. Soc.* **1991**, *113*, 1854. Chattaraj, P. K.; Liu, G. H.; Parr, R. G. *Chem. Phys. Lett.* **1995**, *237*, 171.
(13) Pearson, R. G.; Palke, W. E. *J. Phys. Chem.* **1992**, *96*, 3283.
(14) Gázquez, J. L.; Martínez, A.; Méndez, F. *J. Phys. Chem.* **1993**, *97*, 4059.
(15) Nath, S.; Sannigrahi, A. B.; Chattaraj, P. K. *J. Mol. Struct. (THEOCHEM)* **1994**, *309*, 65.
(16) Willis, C.; Back, R. A. *Can. J. Chem.* **1973**, *51*, 3605.
(17) Blau, E. J.; Hochheimer, B. F. *J. Chem. Phys.* **1964**, *41*, 1174.
(18) Rosengren, K.; Pimentel, G. C. *J. Chem. Phys.* **1965**, *43*, 507.
(19) Trombetti, A. *Can. J. Phys.* **1968**, *46*, 1005.
(20) Bondybey, V. E.; Nibler, J. W. *J. Chem. Phys.* **1973**, *58*, 2125.
(21) Winter, N. W.; Pitzer, R. M. *J. Chem. Phys.* **1975**, *62*, 1269.
(22) Spears, L. G., Jr.; Hutchinson, J. S. *J. Chem. Phys.* **1988**, *88*, 240.
(23) Spears, L. G., Jr.; Hutchinson, J. S. *J. Chem. Phys.* **1988**, 88, 250.
(24) Coxon, J. M.; McDonald, D. Q. *Tetrahedron Lett.* **1992**, *33*, 3673.
(25) Cimiraglia, R.; Hofmann, H. J. *Chem. Phys. Lett.* **1994**, *217*, 430.
(26) Angeli, C.; Cimiraglia, R.; Hofmann, H. J. *Chem. Phys. Lett.* **1996**, *259*, 276.
(27) Kohn, W.; Becke, A. D.; Parr, R. G. *J. Phys. Chem.* **1996**, *100*, 12974 and references therein.
(28) Cárdenas-Jirón, G. I.; Toro-Labbé A. *J. Mol. Struct. (THEOCHEM)*, **1997**, *390*, 79.
(29) Chattaraj, P. K.; Nath, S. *Int. J. Quantum Chem.* **1994**, *49*, 705.
(30) Chattaraj, P. K.; Nath, S. *Chem. Phys. Lett.* **1994**, *217*, 342.
(31) Marcus, R. A. *Annu. Rev. Phys. Chem.* **1964**, *15*, 155.
(32) Cárdenas-Jirón, G. I.; Toro-Labbé, A.; Bock, Ch. W.; Maruani, J. In *Structure and Dynamics of Non-Rigid Molecular* Systems; Smeyers, Y. G., Ed.; Kluwer Academic: Dordrecht, 1995; pp 97−120, and references therein.
(33) Cárdenas-Jirón, G. I.; Cárdenas-Lailhacar, C.; Toro-Labbé, A. *J. Mol. Struct. (THEOCHEM)*, **1990**, *210*, 279.
(34) Cárdenas-Lailhacar, C.; Toro-Labbé, A. *Theor. Chim. Acta* **1990**, *76*, 411.
(35) Zhou, Z.; Parr, R. G. *J. Am. Chem. Soc.* **1990**, *112*, 5720.
(36) Spartan version 4.1; Wavefunction Inc.: 18401 Von Karman Ave., #370, Irvine, CA 92715.
(37) Jursic, B. S. *Chem. Phys. Lett.* **1996**, *261*, 13.

MOLECULAR PHYSICS, 1999, VOL. 96, NO. 1, 61–70

Energy, chemical potential and hardness profiles for the rotational isomerization of HOOH, HSOH and HSSH

SOLEDAD GUTIÉRREZ-OLIVA[1], JORGE RICARDO LETELIER[2] and ALEJANDRO TORO-LABBÉ[1]

[1] Departamento de Química Física, Facultad de Química, Pontificia Universidad Católica de Chile, Casilla 306, Correo 22, Santiago, Chile

[2] Departamento de Química, FCFM, Universidad de Chile, Casilla 2777, Santiago, Chile

(*Received 8 May 1998; revised version accepted 7 July 1998*)

A theoretical study is reported of the mechanisms for internal rotation of hydrogen peroxide (HOOH), hydrogen thioperoxide (HSOH) and hydrogen persulphide (HSSH). Calculations at the *ab initio* HF//6-311G** and MP2//6-311G** levels show that these are *gauche* molecules presenting double-barrier torsional potentials. Important results have been obtained: two different isomerization mechanisms (*trans* and *cis*) have been characterized in terms of specific local interactions; the corresponding energy barriers have been classified according to through bond and through space interactions; and the principle of maximum hardness is qualitatively verified in all three molecules.

1. Introduction

In this paper we are concerned with the internal rotation process in hydrogen peroxide (HOOH), thioperoxide (HSOH) and persulphide (HSSH), and are studying the simultaneous evolution along the reaction coordinate of the potential energy v, the electronic chemical potential μ and the molecular hardness η. Along the torsional angle these molecules present the interesting feature of having a single well with two energy barriers. This allows one to study, in a single system, the isomerization paths that are associated with different mechanisms which, in turn, are due to specific local interactions. Our goal is to obtain insights into the reaction mechanisms and the nature of the potential barriers.

A rotational isomerization reaction can be seen as resulting from redistribution of electron density among atoms in a molecule, even though the total number of electrons is conserved along the reaction coordinate. Density functional theory (DFT) is well suited to describing such electronic reorganization processes, especially to providing the theoretical basis for concepts like μ, that characterizes the escaping tendency of electrons from the equilibrium system, and η, that can be seen as a resistance to charge transfer [1–6]. Both are global properties of the system and are implicated in the reactivity of molecular systems. The study of their profiles along a reaction coordinate has been shown to be useful to rationalize different aspects within the progress of chemical reactions [7–10]. One major focus of attention in DFT is the principle of maximum hardness (PMH) that asserts that molecular systems at equilibrium tend to states of high hardness [4, 11–13], and therefore transition states should present a minimum value of η. There are many examples showing that the PMH complements the minimum energy criterion for stability [11, 12]. Furthermore there is evidence indicating that the PMH holds, at least qualitatively, under less severe conditions [9, 10, 14–17] than those stated originally as proof of the principle [18]. The PMH is an important issue that will be discussed in the present work.

We have proposed [8–10] a theoretical model to relate electronic properties such as μ and η with the potential energy v. In the framework of that model we shall analyse the profiles of these global properties along the reaction coordinate and, with the aim of identifying the specific local interactions that might explain the nature of the *trans* and *cis* torsional mechanisms, we will extend our study to the evolution of local electronic densities. We expect that, in contributing to the knowledge of dihydride molecules, our procedure will be useful in rationalizing simultaneously energetic and mechanistic aspects of a chemical reaction.

There is plenty of experimental information about HOOH [19–21] and HSSH [22–24]. The OO unit appears in many interesting molecules and atmospheric reactions involving radicals, molecules containing SS bonds serve as prototypes for the SS linkages in proteins and provide a starting point for understanding the struc-

0026–8976/99 $12·00

ture of many systems. On the other hand, hydrogen thioperoxide is a molecule that is thought to participate as an intermediate in atmospheric reactions leading to depletion of ozone and in various processes associated with the atmospheric oxidation of sulphides, one of the chemical processes that leads to acid rain [25–27]. From a theoretical viewpoint these molecules have been studied extensively, especially HOOH [9, 28–30] and HSSH [8, 31–33]. Again HSOH has been less studied theoretically although a few papers aimed at studying the molecular structure and the thermochemistry from its radicals have been published recently [17, 34–36]. All three molecules possess two planar conformers, the *trans* and *cis* isomers, which are higher in energy than the *gauche* stable conformation.

2. Theoretical background

2.1. *General definitions*

The reaction coordinate is the torsional angle α defined with respect to the central bond and measured from *trans* ($\alpha = 0$) to the *cis* ($\alpha = \pi$) conformations. Considering the *trans* conformation as the origin of the energy, the model potential that we use to describe the internal rotation of dihydride molecules is [8–10]

$$v(\alpha) = \tfrac{1}{4}K_V(1-\cos^2\alpha) + \tfrac{1}{2}\Delta v^\circ(1-\cos\alpha), \qquad (1)$$

where K_V is a parameter associated with the reference conformations (for molecules presenting a single well with two energy barriers K_V is negative [8, 9]) and $\Delta v^\circ = (v(\pi) - v(0))$ is the energy difference between the *trans* and *cis* isomers.

It is useful to define a reduced reaction coordinate ω measuring the reaction progress when going from reactants to products, it is called conformational function and is related to the torsional angle through $\omega = (1-\cos\alpha)/2$, note that ω varies from zero (*trans*) to one (*cis*). The functional defining the potential energy, in the new ω representation is therefore given by [8–10]

$$v[\omega] = K_V f[\omega] + \omega\Delta v^\circ, \qquad (2)$$

where $f[\omega] = \omega(1-\omega)$, obtained by replacing the definition of ω in equation (1).

Formal definitions of μ and η were given by Parr and Pearson [2] and a three-point finite difference approximation led them to the following working formulae of these quantities [5]:

$$\mu = -\tfrac{1}{2}(\mathrm{IP} + \mathrm{EA}); \qquad \eta = \tfrac{1}{2}(\mathrm{IP} - \mathrm{EA}). \qquad (3)$$

IP and EA are the first vertical ionization potential and electron affinity of the neutral molecule, respectively. Koopmans theorem ($\mathrm{IP} \approx -\varepsilon_H$ and $\mathrm{EA} \approx -\varepsilon_L$) allows one to write μ and η in terms of the energy of frontier HOMO (ε_H) and LUMO (ε_L) molecular orbitals:

$$\mu = \tfrac{1}{2}(\varepsilon_L + \varepsilon_H); \qquad \eta = \tfrac{1}{2}(\varepsilon_L - \varepsilon_H). \qquad (4)$$

Determination of μ and η from quantum chemistry involves different kinds of calculation: a ΔSCF procedure should be used when applying equation (3) whereas only RHF calculations are needed when using equation (4). Reliability and stability of numerical results obtained through different methodologies have been analysed and published elsewhere [17, 37–39]. Now, since μ and η are global properties of the system, their evolution along ω can be expressed through the same analytical form as used for $v[\omega]$ in equation (2). Therefore we have for the chemical potential:

$$\mu[\omega] = \mu[0] + K_\mu f[\omega] + \omega\Delta\mu^\circ; \qquad (5)$$

and similarly for the molecular hardness we have

$$\eta[\omega] = \eta[0] + K\rho_\eta f[\omega] + \omega\Delta\eta^\circ. \qquad (6)$$

The parameters $(\Delta\mu^\circ, K_\mu)$ and $(\Delta\eta^\circ, K_\eta)$ have the same meaning that $(\Delta v^\circ, K_V)$ have for $v[\omega]$. Note that $\mu[\omega]$ and $\eta[\omega]$ are relative to $\mu[0]$ and $\eta[0]$; for simplicity we shall use in the following few equations $\Delta\mu[\omega] = \mu[\omega] - \mu[0]$ and $\Delta\eta[\omega] = \eta[\omega] - \eta[0]$. It is possible to determine the numerical values of the parameters of equations (1), (5) and (6) from a few calculations in the vicinity of the reference conformations, and this can be done following a prescription we gave previously [8–10]. However, since the accuracy of the resulting functions is not crucial to this work, we shall determine the parameters defining the profiles of v, μ and η from the optimized activation properties that we shall define in section 2.3.

2.2. *Relations between μ, η and V*

It is clear from the above equations that v, μ and η are connected through $f[\omega]$, and combining equations (2), (5) and (6) we obtain

$$v_\eta[\omega] = \omega\Delta v^\circ + \varrho_\eta(\Delta\mu[\omega] - \omega\Delta\mu^\circ), \qquad (7)$$

$$v_\mu[\omega] = \omega\Delta v^\circ + \varrho_\mu(\Delta\eta[\omega] - \omega\Delta\eta^\circ), \qquad (8)$$

and

$$\Delta\mu[\omega] = \omega\Delta\mu^\circ + \varrho(\Delta\eta[\omega] - \omega\Delta\eta^\circ). \qquad (9)$$

The new parameters $\{\varrho_\eta, \varrho_\mu, \varrho\}$ are related to the old ones $(\{K_V, K_\mu, K_\eta\})$ through $\varrho_\eta = K_V/K_\mu$ and $\varrho_\mu = K_V/K_\eta$, in addition $\varrho = \varrho_\mu/\varrho_\eta$. It has been shown that these new parameters are related to the electronic charge redistributed during the internal rotation process [10]. From the above equations it is possible to obtain a global expression accounting for the simultaneous evolution of the three properties along a reac-

tion coordinate, so that combining equations (7) and (8) yields

$$\nu[\omega] \equiv \tfrac{1}{2}(\nu_\eta[\omega] + \nu_\mu[\omega]) = \omega\Delta\nu^\circ + \tfrac{1}{2}Q_\eta(\Delta\mu[\omega] - \omega\Delta\mu^\circ) + \tfrac{1}{2}Q_\mu(\Delta\eta[\omega] - \omega\Delta\eta^\circ). \quad (10)$$

Note that equation (10) combines energetic aspects, like the torsional potential, with mechanistics aspects, that are included in the electronic properties μ and η of a dynamic process. It is interesting to mention that this equation is homogeneous with that introduced by Parr and Pearson to demonstrate the HSAB principle [12].

2.3. *Characterization of the stable conformation*

The position of the stable isomer can be determined by differentiating equation (1) such that $(d\nu/d\alpha)_{\alpha=\alpha_0} = 0$, α_0 is the position of the *gauche* conformation. In the ω representation of the torsional potential we define $\beta = (1 - \cos\alpha_0)/2$ as the position of the *gauche* isomer. These quantities can be defined in terms of the potential energy parameters as

$$\left(\frac{d\nu}{d\alpha}\right)_{\alpha=\alpha_0} = 0 \Rightarrow \cos\alpha_0 = -\frac{\Delta\nu^\circ}{K_V} \Rightarrow \beta = \tfrac{1}{2} + \frac{\Delta\nu^\circ}{2K_V}. \quad (11)$$

Putting $\cos\alpha_0$ in equation (1) or β in equation (2) yields to the following expression for the energy of the *gauche* isomer (the negative of it corresponds to the *trans* potential barrier $(\Delta\nu^{\neq}_{trans})$):

$$\Delta\nu^{\neq}_{trans} \equiv -\nu[\beta] = -\left(\tfrac{1}{4}K_V + \tfrac{1}{2}\Delta\nu^\circ + \frac{(\Delta\nu^\circ)^2}{4K_V}\right). \quad (12)$$

By evaluating equation (10) with $\omega = \beta$ we obtain an alternative expression for the *trans* activation energy, now in terms of the activation chemical potential $(\Delta\mu^{\neq} \equiv \Delta\mu[\beta])$ and the activation hardness $(\Delta\eta^{\neq} \equiv \Delta\eta[\beta])$:

$$\Delta\nu^{\neq}_{trans} = -(\beta\Delta\nu^\circ + \tfrac{1}{2}Q_\eta(\Delta\mu^{\neq} - \beta\Delta\mu^\circ) + \tfrac{1}{2}Q_\mu(\Delta\eta^{\neq} - \beta\Delta\eta^\circ)). \quad (13)$$

This equation connecting the three activation properties might provide new interpretations of the nature of activation energies, and certainly may help to give new insights about reaction mechanisms. It has been found in different types of reaction that μ and η pass through extrema at β or very near to it [8–10]; this ensures that equation (13) produces reliable values of potential barriers from a knowledge of activation electronic properties.

Therefore the *gauche* stable conformation is characterized in terms of its position in the reaction coordinate, and properties like energy, chemical potential and hardness. In addition to these properties it is interesting to consider the torsional force constant, which from a harmonic potential model as $\nu(\alpha)$ is defined from the second derivative of equation (1):

$$\frac{d^2\nu}{d\alpha^2} = \tfrac{1}{2}K_V(2\cos^2\alpha - 1) + \tfrac{1}{2}\Delta\nu^\circ\cos\alpha \quad (14)$$

Evaluating at the position of the stable isomer (α_0) but introducing instead the parameter β, we obtain the torsional force constant associated to the minimum energy conformation:

$$k(\beta) \equiv \left(\frac{d^2\nu}{d\alpha^2}\right)_{\alpha=\alpha_0} = \tfrac{1}{2}(K_V + \Delta\nu^\circ) - (4K_V + \Delta\nu^\circ)\beta + 4K_V\beta^2. \quad (15)$$

Since all the parameters involved in the above equation are known, numerical values of k can be determined directly. Using β as given by equation (11) we obtain:

$$k = \frac{1}{2}\left(\frac{(\Delta\nu^\circ)^2}{K_V} - K_V\right). \quad (16)$$

Equation (16) has been used to obtain the numerical values of torsional force constants quoted in the next section.

It is interesting to see the torsional force constant not only parametrically but as a function of β, and eventually it may be maximized with respect to this parameter. Differentiating equation (15) with respect to β leads to

$$\frac{dk}{d\beta} = -(4K_V + \Delta\nu^\circ) + 8K_V\beta. \quad (17)$$

The condition that maximizes k is

$$\left(\frac{dk}{d\beta}\right)_{\beta=\beta_0} = 0 \Rightarrow \beta_0 = \frac{1}{2} + \frac{\Delta\nu^\circ}{8K_V}, \quad (18)$$

and the position of the maximum of k does not coincide with the value determined from the torsional potential (equation (11)). Then β_0 can be written as

$$\beta_0 = \beta - \frac{3\Delta\nu^\circ}{8K_V}, \quad (19)$$

where it is apparent that deviations from β may occur depending on the relative values of $\Delta\nu^\circ$ and K_V.

Evaluation of equation (15) at β_0 leads to k_{max}:

$$k_{max} = k - \frac{9(\Delta\nu^\circ)^2}{16K_V}. \quad (20)$$

Note that although β_0 and k_{max} do not present any precise meaning, they will be used to help characterize qualitative trends observed in the molecules under investigation (section 3.1). Physically, the force constant is associated with rigidity and strength of a bond, and

therefore usually it is related to the electronic population of that bond. This point will be discussed in the next section.

3. Results and discussion

Since RHF theory has been shown to lead to adequate descriptions of μ and η [17, 37–39], the profiles of these electronic properties together with that of the torsional potential v were obtained through SCF *ab initio* calculations of the RHF level with the standard 6-311G** basis set using the Gaussian 94 package [40]. The force gradient method with analytical gradient was used for full optimization of the structural parameters every 10° along the torsional angle α. In addition to the Hartree–Fock calculations, electronic correlation effects on the profiles of energy, chemical potential and hardness have been estimated through MP2 theory. This point is discussed in section 3.4. The optimized geometrical parameters at the HF/6-311G** level for the *gauche* stable conformations are quoted in table 1. The bond lengths of HSOH are quite close to those of its parent HOOH and HSSH molecules, and the SO distance is intermediate between the OO and SS distances. It is interesting to note that the *gauche* stable conformation of HOOH is closer to the *trans* isomer, whereas in the sulphur containing molecules it is found midway between the *trans* and *cis* isomers.

The electronic chemical potential and hardness have been calculated by applying equation (4) with ε_H and ε_L obtained from the RHF calculations on the neutral molecules. Besides electronic correlation effects, this procedure for estimating μ and η may involve small errors arising from the inadequacy of Koopmans' theorem, but it has been shown that it leads to correct qualitative results [17, 37–39]. In figure 1 we display the profiles of v, μ and η along α.

Table 1. *Ab initio* 6-311G** structural parameters (in Å and deg) and dipole moments (in debye) of the *gauche* conformation of hydrogen peroxides.

Parameter	HOOH	HSOH	HSSH
R(OH)	0.942	0.942	
R(SH)		1.333	1.331
R(OO)	1.386		
R(SO)		1.652	
R(SS)			2.078
HOO	102.7		
HOS		109.1	
HSO		98.7	
HSS			98.6
α_0	63.7	88.4	90.2
$\lvert\vec{\mu}\rvert$	1.911	1.992	1.573

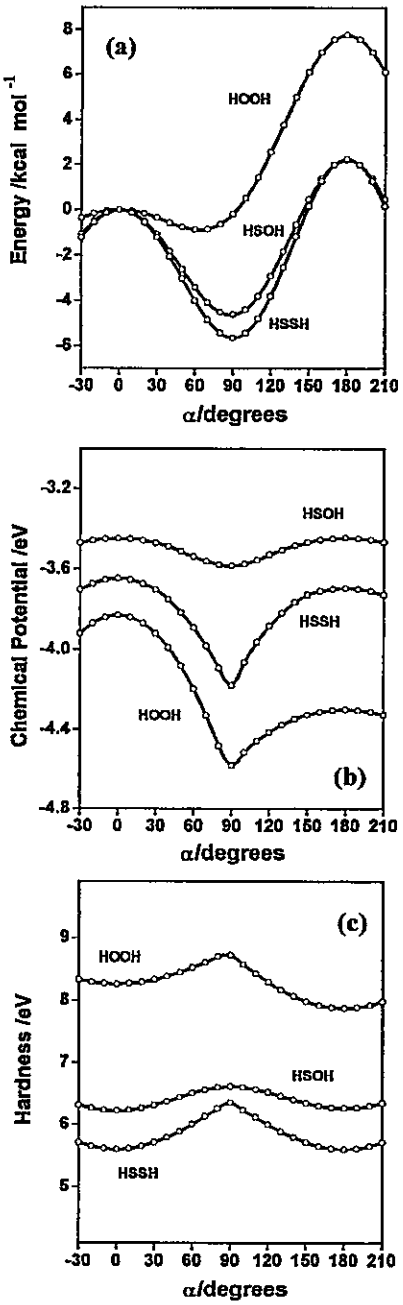

Figure 1. Profiles along the torsional angle α of (*a*) the torsional potential, (*b*) the chemical potential and (*c*) the hardness. The open circles indicate calculated values and the lines connecting them are spline interpolations.

3.1. *Characterization of the stable isomer*

We note that in figure 1(*a*) the energy profiles of HSOH and HSSH are similar to each other but they differ significantly from that of HOOH. In table 2 we

Table 2. Activation properties and parameters defining the profiles of energy, chemical potential and hardness of HOOH, HSOH and HSSH. Potential energies (v) are in kcal mol^{-1}, and μ and η are in eV.

Parameter	HOOH	HSOH	HSSH
$\Delta v^{\neq}_{trans}$	0.87	4.62	5.65
$\Delta v^{\neq}_{cis}$	8.65	6.83	7.90
Δv°	7.78	2.21	2.25
β	0.279	0.486	0.502
$v(\beta)$	− 0.87	− 4.62	− 5.65
$\mu(\beta)$	− 4.24	− 3.58	− 4.17
$\eta(\beta)$	8.56	6.62	6.35
κ_v	− 15.03	− 22.68	− 26.92
κ_μ	− 1.41	− 0.55	− 2.02
κ_η	2.00	1.48	3.01
ϱ_μ	− 0.33	− 0.67	− 0.39
ϱ_η	0.46	1.78	0.58
ϱ	− 0.71	− 0.37	− 0.67

collect the optimized activation barriers together with the relevant properties of the *gauche* conformation and the parameters needed to define the profiles of v, μ and η along the reaction coordinate. The *gauche* stable conformation was found at $\beta = 0.279$, 0.486 and 0.502 for HOOH, HSOH and HSSH, respectively with *cis* barriers higher in energy than *trans* that were found to be $\Delta v^{\neq}_{trans} = 0.87$, 4.62 and 5.65 kcal mol^{-1}. Experimental *trans* barriers are available for HOOH and HSSH: these are 1.10 kcal mol^{-1} [21] and 5.82 kcal mol^{-1} [22], in very good agreement with our computed values. It is interesting to note that the *trans* barrier of HSOH is found within the limits defined by the corresponding barriers of HOOH and HSSH.

Using the optimized $\Delta v^{\neq}_{trans}$ and Δv° values in equation (12) we have determined the κ_v parameters of the three molecules. These are κ_v(HOOH) = −15.03 kcal mol^{-1}, κ_v(HSOH) = −22.68 kcal mol^{-1} and κ_v(HSSH) = −26.92 kcal mol^{-1}. We mention here that the use of β and Δv° in equation (11) to obtain the κ_v's leads to unreliable results due to numerical instabilities that appear for values of β very close to 0.50, as is the case for HSOH and HSSH. However, we have used equation (11) to check the consistency of the potential model: the numerical values of the κ_v's are used to get an independent estimation of β, and we obtained 0.241, 0.451 and 0.458 for HOOH, HSOH and HSSH, respectively, values that are quite close to the optimized ones. In fact the difference in β entails a very small shift of about 5° in the torsional angle, and may be used to estimate the accuracy of our results. We consider that consistency has been reached within a reasonable error margin in β, and therefore further results from the model should be considered as being quite reliable.

Now, knowing the κ_v's, it is possible to have a better characterization of the *gauche* stable isomers by computing the torsional force constants through equation (16). We obtain k(HOOH) = 0.0382 mdyn Å rad^{-2}, k(HSOH) = 0.0781 mdyn Å rad^{-2} and k(HSSH) = 0.0929 mdyn Å rad^{-2}. As for the barrier heights, we note that the force constant of HSOH is found within the limits of the corresponding values of HOOH and HSSH, although it is closer to k(HSSH) as expected from inspection of the energy profiles.

The k values show that HSSH is torsionally quite a rigid molecule, followed by HSOH; by contrast HOOH presents a large amplitude librational motion around the equilibrium angle α_0. It is worth mentioning that only in the later molecule do we have a significant deviation of β_0 (equation (19)) with respect to β, we have found $\beta_0 = 0.435$, 0.488 and 0.490. The considerable difference between β and β_0 observed in HOOH is due to the relatively high value of Δv°. In the other two molecules the difference between β and β_0 is not relevant. We shall see that a maximum value of the central bond electron population in HOOH is found very close to β_0.

3.2. *The profiles of μ and η*

In figure 1(*b*,*c*) we display the profiles of chemical potential and hardness. From the optimized $\mu[\beta]$ and $\eta[\beta]$ values we have determined the parameters κ_μ and κ_η of equations (5) and (6), and these are quoted in table 2 together with κ_v and ϱ. Therefore the analytical profiles of v, μ and η are fully defined through a knowledge of the parameters involved. Although not shown here, it should be noted that these parametric profiles produce values of energy, chemical potential and hardness that are in quite close agreement with the computed points displayed in the figures. In figure 1(*b*) we note that the μ profiles of HOOH andf HSSH are qualitatively similar: in both cases μ drops down sharply from the *trans* conformation, and these two molecules present the higher variation of the chemical potential along α. Note that the minimum value of μ is found around $\alpha = 90°$ and in HOOH it is significantly apart from the energy minimum of figure 1(*a*). In HSOH, μ remains quite constant along the reaction coordinate. In figure 1(*c*) we note that all three molecules present a hardness maximum near $\alpha = 90°$. In general, it is well known that μ and η present a critical point near the position where the energy profile has a critical point. This is the case for HSOH and HSSH but, as already remarked, HOOH presents a shifting between the position of the energy minimum and the critical points of μ and η.

In hydrogen peroxide the critical points for μ and η were found at about $\beta = 0.45$, quite close to β_0, the

position for the maximum value of the torsional force constant. This indicates that the specific local interactions that ensure stability of the *gauche* conformation are not at the origin of the hardness maximum, probably due to the fact that the chemical potential does not remain constant along the reaction coordinate, as required by the PMH.

3.3. *The principle of maximum hardness*

In figure 2 we provide new illustrations of the validity of the PMH by displaying both the torsional potential and the molecular hardness along the reaction coordinate. As expected from the PMH, it can be seen that in all three cases the energy minimum is associated with a hardness maximum whereas energy maxima are connected with hardness minima. It is clear that the maximum hardness condition complements the minimum energy criterion for molecular stability.

However, it has been shown that the PMH is not the product of a simple opposite relation between energy and hardness; for example, hardness and energy profiles may present critical points that are shifted one to another giving rise to peculiar types of behaviour in the $\{\eta, v\}$ space [9]. In the present case, an analysis of the profiles of v and η shows that globally these properties have opposite trends, although there are some discrepancies that should be due to other effects or to the fact that the PMH was shown to hold under the constraints of constant μ and external potential [18]. These quantities certainly vary along the reaction coordinate, preventing the PMH from being applied free of 'external effects' as it should be. In HOOH the maximum hardness is found to be located near β_0, where the torsional force constant is a maximum, and considerably apart from β, where the energy is a minimum. In HSOH we find that the *cis* conformation is harder than the *trans*, even though the latter isomer is more stable. Although there is no requirement that the more stable isomer be the harder, since the maximum of the PMH is a local one only, our results indicate that the specific interactions governing the hardness profile are different from those characterizing the energy profile, unless the chemical potential and the external potential are constant or nearly constant along the isomerization process. In HSSH these previously mentioned external effects must cancel to give rise nicely to opposite energy and hardness profiles.

3.4. *The effect of electronic correlation on v, μ and η*

To quantify the effect of the electronic correlation on these global properties, we have performed MP2//6-311G** calculations with full geometry optimization at each point of the reaction coordinate. These calculations led to the MP2 profiles of v, μ and η. A comparison of

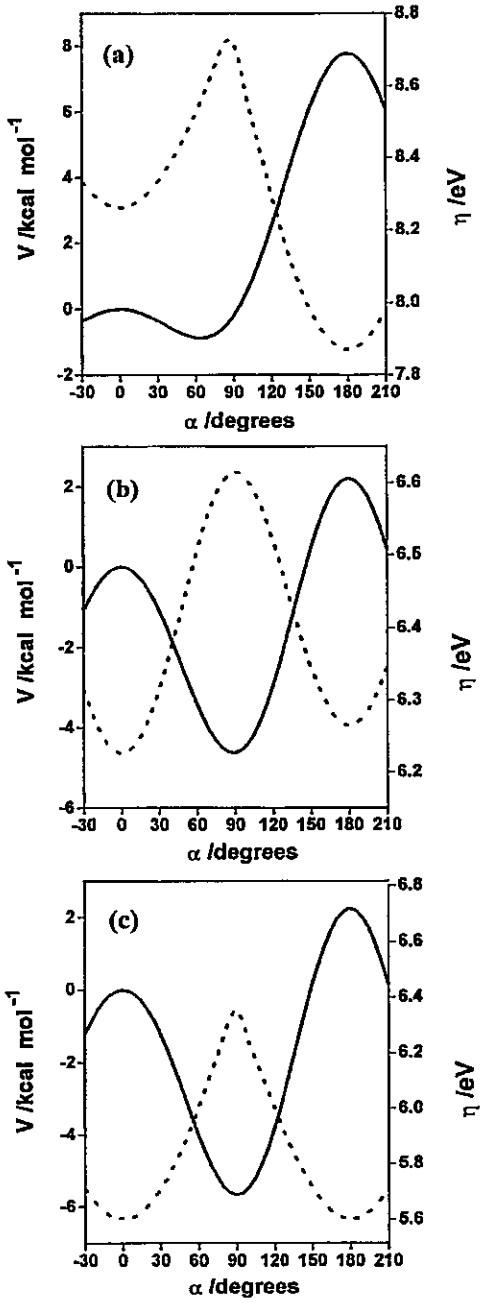

Figure 2. Energy (——) and hardness (– – –) profiles along α for (*a*) HOOH, (*b*) HSOH, and (*c*) HSSH.

the MP2 and RHF profiles is given in figure 3. In all three molecules the effect of electronic correlation on the torsional potential and hardness profiles is quite small: there is no change in the position of the critical points and only the *cis* barrier is affected by correlation. In HSOH the increment of the *cis* barrier due to correlation effects attains a maximum value of about 0.60 kcal mol^{-1}. In general we observe that correlations do not produce any change in the overall trends displayed by v and η along the reaction coordinate, and MP2 trends are

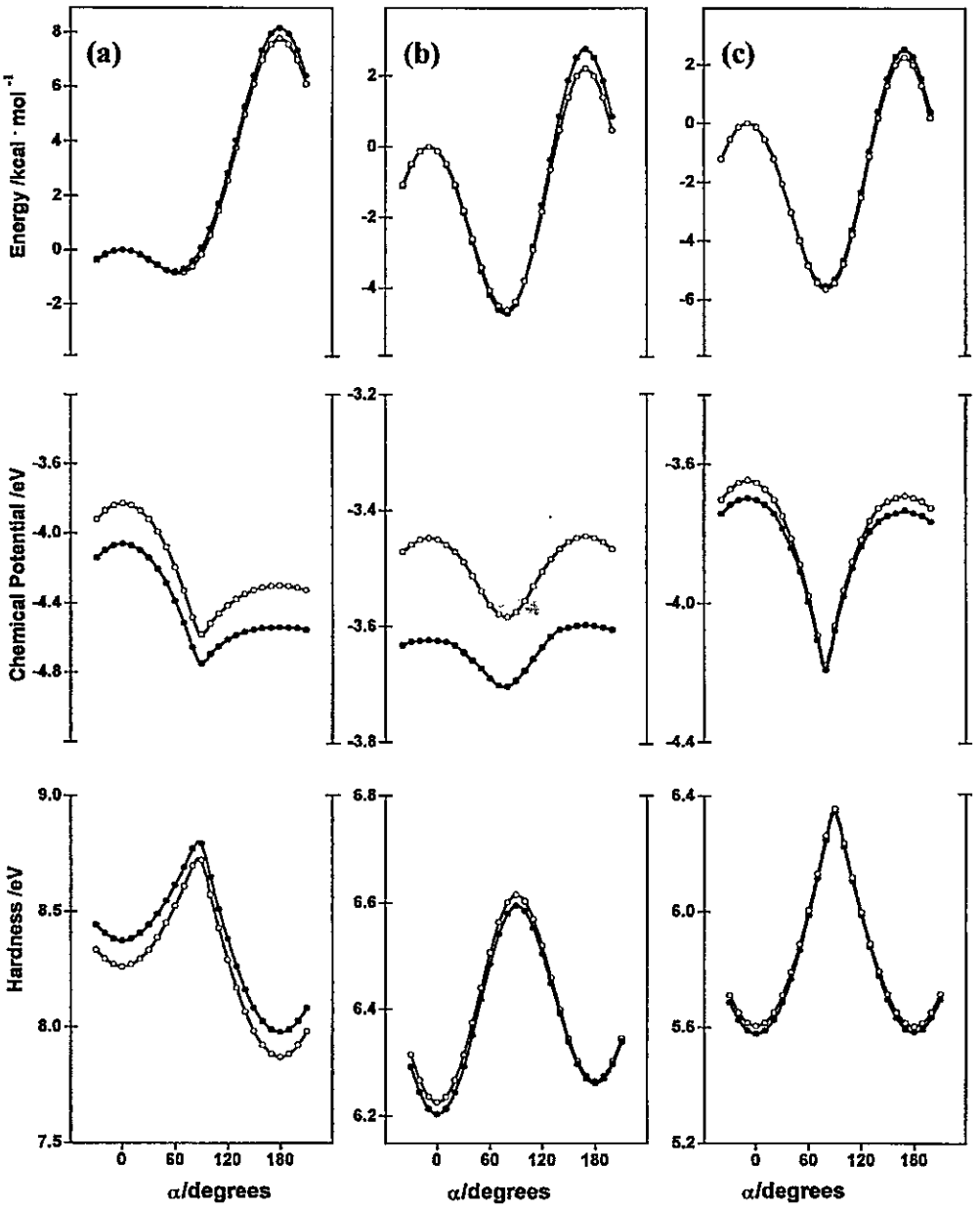

Figure 3. The effect of electronic correlation on the profiles of ν, μ and η for (*a*) HOOH, (*b*) HSOH, and (*c*) HSSH (°, RHF calculations; •, MP2 calculations).

similar to the RHF feature. In contrast to this, correlation effects are not negligible in the evaluation of μ, especially in the torsional barrier regions of HOOH and HSOH; however, as for ν and η, the overall features of the MP2 and RHF profiles are similar.

3.5. *The isomerization mechanisms*

In order to get more insights into the torsional mechanism, quantitative characterization of the charge density is necessary. However, since there is not a rigorous and unique way to do this, a population analysis may be useful for interpretive purposes. We analyse in this section the evolution along ω of the Mulliken electronic population localized on the bond regions. The total bond electronic population of the molecule is given by:

$$\rho_{\text{bond}} = \rho_{\text{XH}} + \rho_{\text{XY}} + \rho_{\text{YH}},$$

with X, Y = O, S. Figure 4(*a*) shows the evolution of ρ_{bond} and figure 4(*b*) shows the variation of the central bond population ρ_{XY}. In HOOH and HSOH ρ_{bond} decreases monotonically when going from *trans*

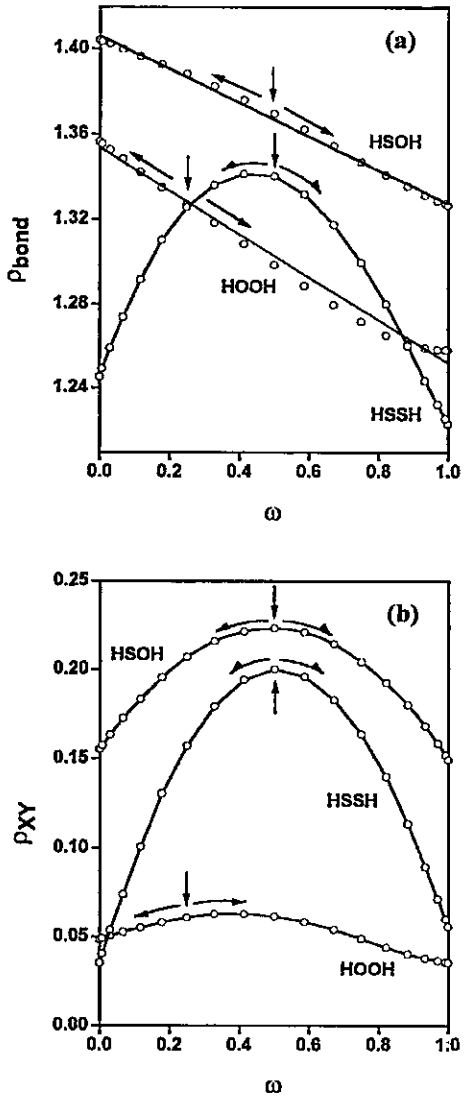

Figure 4. (*a*) Total bond electronic population and (*b*) central bond population along the reaction coordinate ω. The vertical arrow indicates the position of the stable conformation. The arrows pointing to the left indicate the *trans* path and those pointing to the right indicate the *cis* path, for the isomerization reaction. The open circles indicate calculated values and the lines connecting them are spline interpolations.

($\omega = 0.0$) to *cis* ($\omega = 1.0$), whereas in HSSH it displays parabolic behaviour with a maximum value at the *gauche* isomer. In all three molecules the local central bond populations ρ_{XY} shows parabolic behaviour with a maximum value in the *gauche* region. In connection with the torsional force constants, where we have found that $k(\text{HSSH}) > k(\text{HSOH}) > k(\text{HOOH})$, one should expect the same order for ρ_{XY}. By contrast we have found that all along the reaction coordinate $\rho_{SO} > \rho_{SS} > \rho_{OO}$. These results indicate that the stable conformations are not determined only by strong overlaps but also by specific through space interactions, and the associated forces should be characterized through the electrostatic Hellman–Feynman theorem [9]. This seems to be the case for hydrogen peroxide, where ρ_{OO} presents a maximum value not at the energy minimum but at around β_0, where the torsional force constant and the hardness display maximum values.

Figure 4(*a*) shows that in HOOH and HSOH the stable isomer is not associated with an extreme value of ρ_{bond}, which indicates that the two mechanisms for isomerization, the *trans* and *cis* paths, are different because they are accompanied by increasing and decreasing values of ρ_{bond}, respectively. Because of this feature we are going to identify qualitatively the *trans* mechanism mainly with the through bond type of interactions (increasing ρ_{bond}) whereas the *cis* mechanism will be associated with through space electrostatic interactions (decreasing ρ_{bond}). The case of HSSH is different: here any departure from the equilibrium structure involves a decrease in both ρ_{bond} and ρ_{SS}, no matter which reaction path. This indicates that local changes concentrated on the atomic centres must increase. In the above mentioned terms, we conclude that in HSSH both reaction paths are characterized mainly by through space electrostatic interactions.

3.6. *Nature of the barriers to internal rotation*

Since there is no change in the total number of electrons during the internal rotation, any change in ρ_{bond} must be accompanied by an opposite change in the atomic charges. The change in local atomic charges along the reaction coordinate must be reflected in the change of a global property like the dipole moment, and figure 5 shows the evolution of this property along ω. The simultaneous analysis of the bond electronic populations and dipole moments will help explain the nature of the two potential barriers involved in the rotational isomerization process.

In hydrogen peroxide and thioperoxide we have a *trans* barrier that can be rationalized in terms of an increasing ρ_{bond} and decreasing dipole moment, and therefore this barrier is due mainly to through bond interactions. Opposite to this is the *cis* barrier, which is associated with a decreasing ρ_{bond} and an increasing dipole moment, leading to an electrostatic through space barrier. As already mentioned, in HSSH both torsional paths are accompanied by decreasing values of ρ_{bond} and ρ_{SS}, an increasing dipole moment indicating that the *cis* barrier is associated with electrostatic through space interactions. In contrast to this, it is not possible to be certain in classifying the nature of the *trans* barrier: it must arise from a delicate balance of through bond and through space interactions.

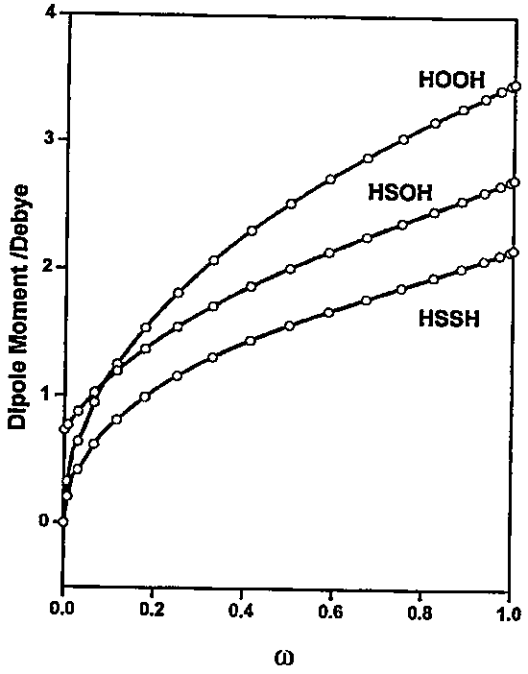

Figure 5. Dipole moments of the three dihydride molecules along the reaction coordinate ω. The open circles indicated calculated values and the lines connecting them are spline interpolations.

4. Conclusion

We have performed a theoretical study of the internal rotation of hydrogen peroxide, thioperoxide and persulphide. Calculations at the *ab initio* HF//6-311G** and MP2//6-311G** levels show that these are *gauche* molecules presenting the interesting feature of having a single well with two energy barriers. The isomerization processes have been characterized through a study of the profiles of the potential energy, chemical potential and molecular hardness. In contributing to the knowledge of oxygen and sulphur dihydride molecules, we have shown that monitoring simultaneously global properties like v, μ and η, together with local properties like electronic populations, helps rationalize energetic and mechanistic aspects of a chemical reaction.

The mechanisms for departure from the equilibrium conformation have been characterized through the change in ρ_{bond} and dipole moments. This led to a qualitative identification of the specific intramolecular interactions that are at the origin of the physical nature of the two potential barriers that are present in these molecules. An important result of this paper is that the PMH is qualitatively verified for the three molecules, even though μ varies along the reaction coordinate. Variation of μ seems to be at the origin of the shifting detected in the position of the critical points of energy and hardness.

The authors are grateful for financial support from FONDECYT through Project No. 1961021. S.G.O. acknowledges CONICYT for a graduate fellowship.

References

[1] PARR, R. G., and YANG, W., 1995, *Ann. Rev. phys. Chem.*, **46**, 701.
[2] PARR, R. G., and PEARSON, R. G., 1983, *J. Amer. chem. Soc.*, **105**, 7512.
[3] PEARSON, R. G., 1985, *J. Amer. chem. Soc.*, **107**, 6801.
[4] PEARSON, R. G., 1987, *J. chem. Educ.*, **64**, 561.
[5] PARR, R. G., and YANG, W., 1989, *Density Functional Theory of Atoms and Molecules* (Oxford University Press).
[6] DREIZLER, R. M., and GROSS, E. K. V., 1990, *Density Functional Theory* (Berlin: Springer-Verlag).
[7] CHATTARAJ, P. K., NATH, S., and SANNIGRAHI, A. B., 1994, *J. phys. Chem.*, **98**, 9143.
[8] CÁRDENAS-JIRÓN, G. I., LAHSEN, J., and TORO-LABBÉ, A., 1995, *J. phys. Chem.*, **99**, 5325.
[9] CÁRDENAS-JIRÓN, G. I., and TORO-LABBÉ, A., 1995, *J. phys. Chem.*, **99**, 12730.
[10] CÁRDENAS-JIRÓN, G. I., GUTIÉRREZ-OLIVA, S., MELIN, J., and TORO-LABBÉ, A., 1997, *J. phys. Chem.* A, **101**, 4621.
[11] CHATTARAJ, P. K., 1996, *Proc. Indian Natl. Sci. Acad.*, **62**, 513, and references therein.
[12] PEARSON, R. G., 1997, *Chemical Hardness* (New York: Wiley-VCH).
[13] DATTA, D., 1992, *J. phys. Chem.*, **96**, 2409.
[14] PEARSON, R. G., and PALKE, W. E., 1992, *J. phys. Chem.*, **96**, 3283.
[15] GÁZQUEZ, J. L., MARTÍNEZ, A., and MÉNDEZ, F., 1993, *J. phys. Chem.*, **97**, 4059.
[16] NATH, S., SANNIGRAHI, A. B., and CHATTARAJ, P. K., 1994, *J. molec. Structur. Theochem.*, **309**, 65.
[17] CÁRDENAS-JIRÓN, G. I., LETELIER, J. R., and TORO-LABBÉ, A., 1998, *J. phys. Chem.* A, in press.
[18] PARR, R. G., and CHATTARAJ, P. K., 1991, *J. Amer. chem. Soc.*, **131**, 1854; CHATTARAJ, P. K., LIU, G. H., and PARR, R. G., 1995, *Chem. Phys. Lett.*, **237**, 171.
[19] FLEMING, P. R., LI, M., and RIZZO, T. R., 1991, *J. chem. Phys.*, **95**, 865.
[20] LUO, X., FLEMING, P. R., and RIZZO, T. R., 1992, *J. chem. Phys.*, **96**, 5659.
[21] HUNT, R. H., LEACOCK, R. A., PETERS, C. W., and HECHT, K. T., 1965, *J. chem. Phys.*, **42**, 1931.
[22] PELZ, G., YAMADA, K. M. T., and WINNEWISSER, G., 1993, *J. molec. Spectrosc.*, **159**, 507.
[23] HERBST, E., and WINNEWISSER, G., 1989, *Chem. Phys. Lett.*, **155**, 572.
[24] HERBST, E., WINNEWISSER, G., YAMADA, K. M. T., DEFREES, D. J., and MCLEAN, A. D., 1989, *J. chem. Phys.*, **91**, 5905.
[25] BALUCANI, N. BENEVENTI, L., CASAVECCHIA, P., STRANGES, D., and VOLPI, G. G., 1991, *J. chem. Phys.*, **94**, 8611; BALUCANI, N., CASAVECCHIA, P., STRANGES, D., and VOLPI, G. G., 1993, *Chem. Phys. Lett.*, **211**, 469.
[26] SMARDZEWSKI, R. R., and LIN, M. C., 1997, *J. chem. Phys.*, **66**, 3197.
[27] IRAQI, M., and SCHWARZ, H., 1994, *Chem. Phys. Lett.*, **221**, 359.
[28] CHRISTEN, D., MACK, H. G., and OBERHAMMER, H., 1988, *Tetrahedron*, **44**, 7363.

[29] DOBADO, J. A., and MOLINA, J., 1994, *J. Phys. chem.*, **98**, 7819.
[30] ALLERES, D. R., COOPER, D. L., CUNNINGHAM, T. P., GERRATT, J., KARADAKOV, P. B., and RAIMONDI, M., 1995, *J. chem. Soc.*, **91**, 3357.
[31] CÁRDENAS-LAILHACAR, C., and TORO-LABBÉ, A., 1990, *Theoret. Chim. Acta*, **76**, 411.
[32] HA, T.-K., and CENCEK, W., 1991, *Chem. Phys. Lett.*, **182**, 519.
[33] CIMIRAGLIA, R., TOMASI, J., and CAMMI, R., 1989, *Chem. Phys.*, **136**, 399.
[34] CÁRDENAS-JIRÓN, G. I., and TORO-LABBÉ, A., 1997, *J. molec. Struct. Theochem*, **390**, 79.
[35] LUKE, B. T., and MCLEAN, A. D., 1985, *J. phys. Chem.*, **89**, 4592.
[36] XANTHEAS, S. S., and DUNNING JR., T. H., 1993, *J. phys. Chem.*, **97**, 18; O'HAIR, R. A. J., DEPUY, C. H., and BIERBAUM, V. M., 1993, *J. phys. Chem.*, **97**, 7955.
[37] PAL, S., VAVAL, N., and ROY, R., 1993, *J. phys. Chem.*, **97**, 4404.
[38] CHATTARAJ,. P. K., NATH, S., and SANNIGRAHI, A. B., 1993, *Chem. Phys. Lett.*, **212**, 223.
[39] NATH, S., SANNIGRAHI, A. B., and CHATTARAJ, P. K., 1994, *J. molec. Struct. Theochem.*, **306**, 87.
[40] FRISCH, M. J., TRUCKS, G. W., SCHLEGEL, H. B., GILL, P. M. W., JOHNSON, B. G., ROBB, M. A., CHEESEMAN, J. R., KEITH, T. A., PETERSON, G. A., MONTGOMERY, J. A., RAGHAVACHARI, K., AL-LAHAM, M. A., ZAKRZEWSKI, V. G., ORTIZ, J. V., FORESMAN, J. B., CIOLOWSKI, J., STEFANOV, B. B., NANAYAKKARA, A., CHALLACOMBE, M., PENG, C. Y., AYALA, P. Y., CHEN, W., WONG, M. W., ANDRES, J. L., REPLOGLE, E. S., GOMPERTS, R., MARTIN, R. L., FOX, D. J., BINKLEY, J. S., DEFREES, D. J., BAKER, J., STEWART, J. P., HEAD-GORDON, M., GONZÁLEZ, C., and POPLE, J. A., 1994, Gaussian 94 (Pittsburgh, PA: Gaussian, Inc.).

Using Sanderson's Principle to Estimate Global Electronic Properties and Bond Energies of Hydrogen-Bonded Complexes

Soledad Gutiérrez-Oliva, Pablo Jaque, and Alejandro Toro-Labbé*

Departamento de Química Física, Facultad de Química, Pontificia Universidad Católica de Chile, Casilla 306, Correo 22, Santiago, Chile

Received: February 29, 2000; In Final Form: July 11, 2000

In this paper, we use Sanderson's geometric mean equalization principle for electronegativity (χ) to derive expressions for molecular hardness (η) and its derivative (γ) that are used to estimate the electronic properties of 14 molecules and bimolecular hydrogen-bonded complexes. Beyond the determination of electronic properties, it is shown that Sanderson's scheme can be very useful as a method for rationalizing chemical reactions when both N and v change. We have found that the conditions of maximum hardness and minimum polarizability complement the minimum energy criterion for stability of molecular aggregates. Finally, we propose a new scheme for obtaining molecular properties from the isolated fragments that produces results that are in excellent agreement with those determined through Sanderson's scheme.

1. Introduction

A formation reaction results from the combination of constituent fragments. The resulting system, a molecule or an aggregate, presents properties that, in many cases, can be rationalized in terms of the properties of the isolated constituent fragments. The main problem that arises when using this approximation to estimate molecular properties is that the bonding potential and redistribution of the electron density among the fragments are not considered, and structural relaxation due to new specific through-bond and through-space interactions is not allowed within this scheme. In fact, the approach of using the properties of rigid isolated fragments to estimate the corresponding properties of a system made up of these fragments entails errors such as the completeness of the basis sets and the mixing of electronic states. The effects of such errors are not considered at all in fragment addition schemes, and therefore, the quantities determined in this way are not expected to be very accurate. However, the use of addition rules to estimate global properties of composite systems is attractive mainly because they may be useful in predicting qualitative features. In this paper, we investigate whether one can safely estimate global molecular properties from the corresponding values associated with the constituent fragments through the application of Sanderson's principle of electronegativity equalization.[1−3] Also, we explore how these electronic properties can be related to bond energies involved in molecule and aggregate formation processes.

Within the frame of density functional theory (DFT),[4−6] a complete characterization of an N-particle wave function requires knowledge of only N and the external potential $v(\vec{r})$. The response of the system to any external perturbation is measured by the electronic chemical potential (μ) and the hardness (η) when N is varied for a fixed $v(\vec{r})$. Complementary to this, the polarizability (α) can be used in understanding the behavior of the system for changing $v(\vec{r})$ at constant N.[7] In DFT, μ is the Lagrange multiplier associated with the normalization constraint that the electron density integrates to N; the association with classical structural chemistry is achieved by the identification of μ as the negative of the electronegativity (χ). Definitions of χ (or μ) and η were given by Parr et al.[8] and Parr and Pearson,[9] respectively. Chemical potential (electronegativity) and hardness are global electronic properties that are implicated in the reactivity of molecular systems, and they are well-established quantities that have evoked considerable research activity in the last years.[10−14]

The product of a chemical reaction can be seen as resulting from the combination and redistribution of atom's or fragment's electron densities, giving rise to a new electronic distribution from which the electronic properties of the new molecule or aggregate are derived. It is well-known by now that molecular electron densities exhibit local topological features that makes it possible to recognize atomic or fragment shapes within the molecule.[15−17] In this context, it is important to characterize the effect of combination and redistribution of electron densities on global electronic properties that have been defined as the response of the system to external perturbations.

To relate the molecular electronegativity to those of the constituent atoms or fragments, Sanderson proposed a geometric mean equalization principle, that defines the molecular electronegativity as the geometric mean of the electronegativities of the constituent atoms or fragments.[1−3] In recent papers, we have extended this approach to estimate molecular hardness from the corresponding property of the constituent atoms or fragments.[18,19] In this paper, we go further by estimating for the first time numerical values of γ [$\gamma \equiv (\partial\eta/\partial N)_v$] in molecules, obtaining expressions for η and γ from the geometric mean of χ (or μ), and then investigating how these properties, together with the polarizability α, might be related to the energy of conventional and hydrogen bonds.

This study concerns the formation of four molecules of the type HCX−YH from radicals HCO, HCS, OH, and SH and 10 cyclic hydrogen-bonded bimolecular complexes of the type HCX−YH···HCY−XH formed by combinations of the HCX−

* Author to whom correspondence should be addressed. E-mail: atola@puc.cl.

10.1021/jp000777e CCC: $19.00
Published on Web 09/13/2000

YH species (X, Y = O, S). Our main goal in this paper is to discuss the validity of Sanderson's addition scheme and to investigate whether this approach can be used to discuss reordering of electronic density due to the bonding process.

2. Theoretical Background

Within the framework of DFT, the chemical potential and hardness for an N-particle system with total energy E and external potential $v(\vec{r})$ are defined as follows:[4-6]

$$\mu = \left(\frac{\partial E}{\partial N}\right)_{v(\vec{r})} = -\chi \tag{1}$$

and

$$\eta = \frac{1}{2}\left(\frac{\partial^2 E}{\partial^2 N}\right)_{v(\vec{r})} = \frac{1}{2}\left(\frac{\partial \mu}{\partial N}\right)_{v(\vec{r})} \tag{2}$$

In numerical applications, μ and η are calculated through the following approximate versions of eqs 1 and 2, based upon the finite-difference approximation and Koopman's theorem:[5]

$$\mu \approx -\frac{1}{2}(I + A) \simeq \frac{1}{2}(\epsilon_L + \epsilon_H) \tag{3}$$

and

$$\eta \approx \frac{1}{2}(I - A) \simeq \frac{1}{2}(\epsilon_L - \epsilon_H) \tag{4}$$

where I is the ionization potential, A is the electron affinity, and ϵ_H and ϵ_L are the energies of the highest-occupied molecular orbital (HOMO) and the lowest-unoccupied molecular orbital (LUMO), respectively. In this paper, μ and η will be calculated using the MO energies.

The energy involved in forming a molecule or aggregate from n_f non-bonded constituent fragments is given by

$$\Delta E_{n_f} = E - E^\circ_{n_f} \tag{5}$$

where E is the energy of the fully optimized resulting molecule or aggregate and $E^\circ_{n_f} = \sum_x^{n_f} E_x$, with E_x the energy of the fragment x duly optimized. Note that, in our applications, the energy of the bimolecular complexes can be estimated from the energy of two (E°_2) and four (E°_4) fragments. It is important to point out here that both basis set superposition and the mixing of electronic states are source of errors in the estimation of ΔE_{n_f}; however, attempts to evaluate them are beyond the scope of this paper.

Sanderson's equalization principle states that the electronegativity of a molecule is given by the geometric mean of the electronegativities of the isolated atoms (or fragments)[1-3]

$$\mu^\circ_{n_f} = -\left(\prod_x^{n_f} |\mu^\circ_x|\right)^{1/n_f} \tag{6}$$

where μ°_x is the chemical potential of fragment x. Note that the larger the value of n_f, the less accurate the result because of the number of bonds and bonding potentials not being considered in the calculations of $\mu^\circ_{n_f}$.

Within this scheme, the hardness is obtained by differentiating $\mu^\circ_{n_f}$ with respect to N,[18,19] thus obtaining

$$\eta^\circ_{n_f} = \left(\frac{\partial \mu^\circ_{n_f}}{\partial N}\right)_{v(\vec{r})} = \frac{\mu^\circ_{n_f}}{n_f}\sum_x^{n_f}\frac{\eta^\circ_x}{\mu^\circ_x} \tag{7}$$

η°_x is the hardness of fragment x. The difference between the approximate values ($\mu^\circ_{n_f}$ and $\eta^\circ_{n_f}$) and the actual values obtained using eqs 3 and 4 from the ab initio calculations (μ and η) can be attributed to relaxation of the electron density after bonding. Quantification of this difference may help in developing an understanding of the reordering of the electron density as the reaction takes place.

The derivative of the hardness with respect to N at constant external potential was defined previously as the third-order property γ; it was numerically studied only in atoms and atomic ions with the result that, in most cases, it is smaller than μ and η.[20] Within the Sanderson scheme, we obtain from eq 7

$$\gamma^\circ_{n_f} = \left(\frac{\partial \eta^\circ_{n_f}}{\partial N}\right)_{v(\vec{r})} = \frac{(\eta^\circ_{n_f})^2}{\mu^\circ_{n_f}} - \frac{\mu^\circ_{n_f}}{n_f}\sum_x^{n_f}\left(\frac{\eta^\circ_x}{\mu^\circ_x}\right)^2 + \frac{\mu^\circ_{n_f}}{n_f}\sum_x^{n_f}\frac{\gamma^\circ_x}{\mu^\circ_x} \tag{8}$$

This provides an analytic expression to estimate γ from atomic (or fragment) chemical potentials and hardnesses. Notice that $\eta^\circ_{n_f}$ and $\gamma^\circ_{n_f}$ have been defined by dropping, from the original definitions, the numerical factors $^1/_2$ and $^1/_3$, respectively.

3. Computational Methods

Although restricted Hartree−Fock (RHF) calculations are not expected to give accurate hydrogen-bond energies, it has been recently shown that they are highly consistent with DFT/B3LYP results.[19] Therefore, all calculations were performed at the RHF level of theory with the standard 6-311G** basis set using the Gaussian 94 package.[21] Radical fragments were calculated using the UHF theory. The electronic chemical potential and molecular hardness have been calculated by applying eqs 3 and 4, respectively, with ϵ_H and ϵ_L obtained from the RHF/UHF calculations of the fully optimized species.

In Table 1, we display reference values of energy, chemical potential, and hardness of the initial isolated radical species HCX and XH (X = O, S). Formation of molecules HCO−OH (**M1**), HCS−OH (**M2**), HCO−SH (**M3**), and HCS−SH (**M4**) from the two constituent radicals involves a change in energy and electronic properties mainly due to formation of a covalent C−X bond (X = O, S). Thus, in comparing $\mu^\circ_{n_f}$ and $\eta^\circ_{n_f}$ with respect to the actual values of μ and η determined from ab initio calculations on the fully optimized molecule, we will obtain, as a qualitative result, the effect of the bonding potential on these specific electronic properties.

Among many possible bimolecular structures, we will review here only cyclic complexes that are estabilized by two hydrogen bonds.[19] Combinations of monomeric units of formic (HCO−OH), thione−formic (HCS−OH), thiol−formic (HCO−SH), and dithioformic (HCS−SH) acids leads to 10 cyclic bimolecular complexes, **C1**−**C10** (see Table 2). To build them, two approaches have been considered: (a) formation from two neutral molecules ($n_f = 2$) where the ab initio optimized values of E, μ, and η of each HCX−YH (X, Y = O, S) species are used to produce E°_2, μ°_2, and η°_2 (note that these quantities do not contain the hydrogen-bonds potentials); and (b) formation from four isolated radical fragments ($n_f = 4$). The latter approach leads to E°_4, μ°_4, and η°_4 values in which the effect of two covalent and two hydrogen-bond potentials are not included. In Table 2, we define the species under study and quote the values of $E^\circ_{n_f}$, together with the reaction energies ΔE_2 and ΔE_4,

TABLE 1: Energy, Chemical Potential, and Hardness for the Fully Optimized Radical Structures Determined at the Ab Initio UHF/6-311G Level[a]**

fragment	E	μ	η
CHO	−113.2802	−0.1327	0.2450
OH	−75.4107	−0.1906	0.3153
CHS	−435.9153	−0.1492	0.1852
SH	−398.0929	−0.1907	0.1864

[a] All values are in atomic units.

which should be proportional to the bond energies involved in forming the molecules and aggregates.

4. Results and Discussion

Estimating C−X Bond Energies. We note in Table 2 that all ΔE_{n_f} values are negative, indicating that formation of molecules (**M1**−**M4**) and bimolecular complexes (**C1**−**C10**) are favorable processes. Note that, in formation reactions, $E^{\circ}_{n_f}$ and E are the total energies of reactants and products, respectively. For our purposes, the most relevant feature appearing in the formation energy of **M1** and **M2** is that their ΔE_2 values can be identified with the energy of a single C−O bond, the average value determined from Table 2 being $\langle \Delta E_2 \rangle_{CO} \approx 0.12$ au. Note that the average value of the experimental C−O bond energy has been estimated to be 0.13 au,[22] in reasonable agreement with our estimate. In the formation of **M3** and **M4**, $-\Delta E_2$ is mainly attributed to formation of a single C−S bond, for which the average experimental bond energy is 0.10 au;[22] our estimation is $\langle \Delta E_2 \rangle_{CS} \approx 0.08$ au. Although the numerical values may differ to some extent, our results show that the C−O bond is correctly estimated as being stronger than the C−S bond by about 0.04 au, in qualitative agreement with the experimental data.[22]

When the complexes are formed from four isolated fragments ($n_f = 4$), the reaction energies can be related to the energies of the bonds being formed. Table 2 shows that, in **C1**, **C2**, and **C3**, the ΔE_4 values goes from −0.28 au (**C1**) up to −0.25 au (**C3**); these values correspond to the approximate contribution of the two C−O bonds being formed ($\Delta E_4 \approx 2\langle \Delta E_2 \rangle_{CO}$). In **C4**−**C7**, we find that the average value of ΔE_4 is 0.21 au, with quite a small dispersion. This can be associated with the energetic contribution due to formation of one C−O and one C−S bond ($\Delta E_4 \approx \langle \Delta E_2 \rangle_{CO} + \langle \Delta E_2 \rangle_{CS}$). In **C8**−**C10**, we find that $\Delta E_4 \approx -0.16$ au, which is the energetic contribution due to formation of two C−S bonds ($\Delta E_4 \approx 2\langle \Delta E_2 \rangle_{CS}$).

Estimating Hydrogen-Bond Energies. It is important to mention that, although Hartree−Fock calculations are not expected to be very accurate in estimating hydrogen-bond energies, our ΔE_2 values follow the correct qualitative trend and compare satisfactorily well with other theoretical estimates.[23] Recent DFT/B3LYP calculations on the complexes we are discussing here led to hydrogen-bond energies that are in very good agreement with the HF results (see Figure 8 of ref 19). Concerning the comparison with experimental data, we note that our energies quantitatively match the available experimental data. For example, $\Delta E_2 = -0.0233$ au for **C1**[24] (compared with $\Delta E_2 = -0.0231$ au from Table 2), and the energy of a single hydrogen bond in **C10** was measured to be 0.0016 au,[25] which is very close to one-half of our ΔE_2 value given in Table 2 ($\Delta E_2/2 = 0.0019$ au), where the factor $^1/_2$ is introduced for proper comparison as **C10** contains two hydrogen bonds. This latter result suggests that hydrogen-bond energies for the series of systems we are studying here might be rationalized in terms of the sum of individual H-bond energies present in the complex.

To explore this idea, we use the ΔE_2 values for the dimers **C1** and **C10**, which present only H···O or H···S bonds, as reference values defining the energy of the respective bonds: i.e., E(H···O) = ΔE_2(**C1**)/2 = −0.01155 au and E(H···S) = ΔE_2(**C10**)/2 = −0.00185 au. Using these values, we approximate the ΔE_2 values for the remaining eight complexes as $\Delta E_2^{(a)} = \sum_X E$(H···X), simply the sum of energies of H-bonds present in the system. The results are included in Table 3. We note that this estimation of ΔE_2 is rather crude, exhibiting considerable errors that go up to 70% (**C3**). Thus, the rough estimation of the H-bond energies from the reference systems **C1** and **C10** is not accurate enough to get an adequate description of the remaining ΔE_2 values.

A considerably better approach to ΔE_2 can be obtained if we consider not only the corresponding H-bonds but also the effect that the neighboring heteroatom may have, thus defining the energy of fragments X−H···Y (X, Y = O, S). To do so, we use as a reference four dimers (**C1**, **C3**, **C8**, and **C10**) that present the desired fragments: E(OH···O) = ΔE_2(**C1**)/2 = −0.01155 au; E(OH···S) = ΔE_2(**C3**)/2 = −0.00595 au; E(SH···O) = ΔE_2(**C8**)/2 = −0.00445 au; and E(SH···S) = ΔE_2(**C10**)/2 = −0.00185 au. Note that the presence of a sulfur atom adjacent to the H-bond makes the H-bond weaker than it would be in the presence of oxygen. Now we define $\Delta E_2^{(b)} = \sum_{X,Y} E$(XH···Y); the results are shown in Table 3 and compared with ΔE_2 and $\Delta E_2^{(a)}$. It can be seen that the deviations with respect to the calculated ΔE_2 values are now very small; they go up to 0.82 kcal/mol in **C6** (the larger deviation of $\Delta E_2^{(a)}$ with respect to ΔE_2 was found in **C8** and was 8.91 kcal/mol). This indicates that the effect of the heteroatom adjacent to the H-bond is very important in characterizing the different H-bond energies. In summary, we estimate the H···O bond energy to be 0.0080 ± 0.0036 au and the H···S bond energy to be 0.0039 ± 0.0021 au, the H···O bond being about twice as strong as the H···S bond.

Force Constants and Hydrogen-Bond Energies. In bimolecular systems when the energy is estimated using $n_f = 2$, the quantity $\Delta E_2 = E - E_2^{\circ}$ gives an estimate of the hydrogen-bond energies, because the larger ΔE_2 is, the stronger the pair of hydrogen bonds being formed is expected to be. Table 3 shows that the bond energy decreases with the number of electrons and that the O···H bonds are stronger than the S···H bonds. The strength of a chemical bond is usually represented by its force constant; in our case, we expect ΔE_2 to be related with the force constants k associated with the pair of hydrogen bonds of the complex. These force constant values have been determined through ab initio frequency calculations on the optimized structure of the complexes, and the results are displayed in Figure 1a, where a good linear correlation can be observed between ΔE_2 and k for the 10 complexes identified by their total number of electrons, the correlation factor being 0.980. Because there are four systems having 64 electrons (**C3**, **C5**, **C6**, and **C8**), two with 72 electrons (**C7** and **C9**), and two with 56 electrons (**C2** and **C4**), we plot the average of their ΔE_2 and k values, obtaining an enhanced correlation, as is apparent in Figure 1b ($R = 0.996$). Thus, the ab initio force constants are consistent with expectations based on the energetic results: the stronger the hydrogen bond, the higher its $|\Delta E_2|$ value.

Chemical Potential. Equation 6 has been used to obtain the chemical potential within Sanderson's scheme. The estimates for **M1**−**M4** require the ab initio data (μ_x and η_x) for the isolated radicals x = CHO, OH, CHS, and SH that are quoted in Table

TABLE 2: Total and Reaction Energies of Molecular Systems and Formation Processes[a]

system		$-E$	$-E_2^\circ$	$-E_4^\circ$	$-\Delta E_2$	$-\Delta E_4$
HCOOH	(M1)	188.8205	188.6910		0.1295	
HCSOH	(M2)	511.4454	511.3260		0.1194	
HCOSH	(M3)	511.4493	511.3731		0.0762	
HCSSH	(M4)	834.0867	834.0082		0.0785	
HCOOH···HCOOH	(C1)	377.6641	377.6410	377.3819	0.0231	0.2822
HCOOH···HCSOH	(C2)	700.2840	700.2659	700.0170	0.0181	0.2670
HCSOH···HCSOH	(C3)	1022.9027	1022.8908	1022.6520	0.0119	0.2507
HCOOH···HCOSH	(C4)	700.2847	700.2698	700.0641	0.0149	0.2206
HCOOH···HCSSH	(C5)	1022.9176	1022.9072	1022.6992	0.0104	0.2184
HCOSH···HCSOH	(C6)	1022.9068	1022.8947	1022.6992	0.0121	0.2076
HCSSH···HCSOH	(C7)	1345.5389	1345.5320	1345.3342	0.0069	0.2047
HCOSH···HCOSH	(C8)	1022.9076	1022.8987	1022.7463	0.0089	0.1613
HCSSH···HCOSH	(C9)	1345.5425	1345.5360	1345.3813	0.0065	0.1612
HCSSH···HCSSH	(C10)	1668.1770	1668.1733	1668.0164	0.0037	0.1606

[a] All values are in atomic units.

TABLE 3: Double Hydrogen-Bond Energies of Bimolecular Aggregates[a]

complex	N	$-\Delta E_2$	$-\Delta E_2^{(a)}$	$-\Delta E_2^{(b)}$
C1	48	0.0231	0.0231	0.0231
C2	56	0.0181	0.0134	0.0175
C3	64	0.0119	0.0037	0.0119
C4	56	0.0149	0.0231	0.0160
C5	64	0.0104	0.0134	0.0104
C6	64	0.0121	0.0134	0.0134
C7	72	0.0069	0.0134	0.0078
C8	64	0.0089	0.0231	0.0089
C9	72	0.0065	0.0134	0.0063
C10	80	0.0037	0.0037	0.0037

[a] All values are in atomic units.

1. The effect of relaxation and redistribution of the electronic density on the chemical potential due to formation of covalent and hydrogen bonds can be quantitatively characterized by the numerical values of $\mu_{n_f}^\circ$ with reference to the calculated chemical potential; numerical values are listed in Table 4. We note that the deviations of $\mu_{n_f}^\circ$ with respect to the reference ab initio values are reasonably small; in most cases, μ_2° approaches the reference value better than μ_4° does. As for the energy, the chemical potential seems to be quite dependent on the number of fragments used.

When two fragments are brought into contact, electrons will flow from the one of higher chemical potential to that of lower μ, the amount of flowing charge being proportional to the difference in the chemical potentials of the fragments.[8] A qualitative estimation of the charge transfer (ΔN) involved in the formation process of a two-fragment reaction can be determined through the following expression:[5,8,10,12]

$$\Delta N = \frac{1}{2}\frac{(\mu_x - \mu_y)}{(\eta_x + \eta_y)} \qquad (9)$$

with x and y representing the different fragments used in the formation of the desired product. The values of ΔN are quoted in Table 5, where it is interesting to note that reactions involving formation of covalent bonds are accompanied with high positive values of ΔN whereas, in bimolecular complex formation, we find smaller values of ΔN. According to eq 9, the amount of charge (δN_{n_f}) that is not relaxed in the formation process from the rigid fragments must be proportional to $\Delta\mu_{n_f} = (\mu - \mu_{n_f}^\circ)$. Thus, we simply define $\delta N_{n_f} \equiv \Delta\mu_{n_f}$ and quote its values in Table 5. It is interesting to note, for bimolecular complexes, that formation from four fragments in most cases implies higher values of this index than formation from two

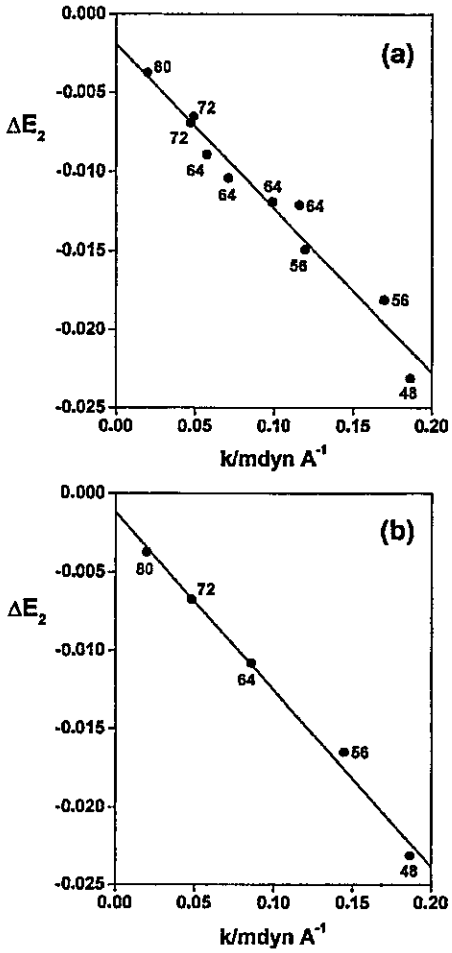

Figure 1. (a) Correlation between hydrogen-bond energies and H-bond force constants of bimolecular aggregates identified by their number of electrons. (b) Same as in panel a but using the average values of ΔE_2 and k in systems presenting the same number of electrons.

fragments, thereby implying that reordering of the electron density becomes increasingly important with the number of fragments.

Molecular Hardness. Within Sanderson's scheme, we have determined the molecular hardness using eq 7; the results that are quoted in Table 4 must be compared with the reference ab initio values also included in the table. It is interesting to note that hardness can be approached using either η_2° or η_4°, depending on the specific system, both approaches represent

TABLE 4: Calculated and Estimated Electronic Properties of Isolated Molecules and Molecular Aggregates[a]

system	μ	μ_2°	μ_4°	η	η_2°	η_4°	γ_2°	γ_4°
M1	−0.1554	−0.1590		0.3138	0.2783		0.0247	
M2	−0.1402	−0.1686		0.2206	0.2441		0.0214	
M3	−0.1391	−0.1591		0.2608	0.2246		0.0431	
M4	−0.1532	−0.1687		0.1996	0.1872		0.0062	
C1	−0.1503	−0.1554	−0.1590	0.3204	0.3138	0.2783	0.0317	0.0247
C2	−0.1411	−0.1476	−0.1638	0.2251	0.2652	0.2619	0.0303	0.0269
C3	−0.1462	−0.1402	−0.1686	0.2169	0.2206	0.2441	0.0153	0.0214
C4	−0.1402	−0.1470	−0.1590	0.2609	0.2863	0.2515	0.0281	0.0380
C5	−0.1601	−0.1543	−0.1638	0.2021	0.2563	0.2342	0.0398	0.0326
C6	−0.1320	−0.1397	−0.1638	0.2215	0.2408	0.2342	0.0231	0.0326
C7	−0.1604	−0.1466	−0.1687	0.1966	0.2108	0.2157	0.0148	0.0187
C8	−0.1331	−0.1391	−0.1591	0.2607	0.2608	0.2246	0.0240	0.0431
C9	−0.1511	−0.1460	−0.1638	0.2000	0.2319	0.2065	0.0288	0.0289
C10	−0.1576	−0.1532	−0.1687	0.1965	0.1996	0.1871	0.0084	0.0064

[a] All values are in atomic units.

TABLE 5: Estimation of Charge Transfer (ΔN) in Formation of Molecular Systems and Bimolecular Complexes

system	ΔN	δN_2	δN_4
M1	0.0516	0.0036	
M2	0.0414	0.0284	
M3	0.0672	0.0200	
M4	0.0558	0.0155	
C1	0.0	0.0051	0.0087
C2	−0.0142	0.0065	0.0227
C3	0.0	−0.0060	0.0224
C4	−0.0142	0.0068	0.0188
C5	−0.0021	−0.0058	0.0037
C6	0.0011	0.0077	0.0318
C7	−0.0155	−0.0138	0.0083
C8	0.0	0.0060	0.0260
C9	−0.0153	−0.0051	0.0127
C10	0.0	−0.0044	0.0111

TABLE 6: Comparison of Hardness Determined through Different Methods[a]

system	η^b	eq 7[c]	ref 26	ref 27
M1	0.3138	0.2783	0.2757	0.2779
M2	0.2206	0.2441	0.2333	0.2417
M3	0.2608	0.2246	0.2117	0.2137
M4	0.1996	0.1872	0.1858	0.1858
C1	0.3204	0.3138	0.3138	0.3138
C2	0.2251	0.2652	0.2591	0.2631
C3	0.2169	0.2206	0.2206	0.2206
C4	0.2609	0.2863	0.2849	0.2861
C5	0.2021	0.2563	0.2440	0.2503
C6	0.2215	0.2408	0.2390	0.2399
C7	0.1966	0.2108	0.2096	0.2098
C8	0.2607	0.2608	0.2608	0.2608
C9	0.2000	0.2319	0.2261	0.2282
C10	0.1965	0.1996	0.1996	0.1996

[a] All values are in atomic units. [b] η is the reference ab initio value. [c] Equation 7 is used with $n_f = 2$.

good approximations of the actual ab initio result. Qualitative consistency between η_2° or η_4° indicates that eq 7 is a reliable expression for estimating molecular hardness. There are a few different ways to estimate η from fragment values: the arithmetic average for softness[26] ($S = 1/\eta$) and the geometric mean principle for hardness[27] are among the most relevant treatments for determining hardnesses. In Table 6, we compare the numerical values of η calculated using eq 7 with values determined using the above-mentioned treatments. We note that the comparison is quite satisfactory, with only very small deviations among the values obtained through the different methods being observed. This result adds evidence for an important feature of hardness: it is a quite stable property. This attribute, in combination with the principle of maximum hardness (PMH),[28−30] which states that molecular systems at equilibrium tend to states of highest hardness, suggest that, for systems in which the energy is difficult to obtain, knowledge of η may open the way for obtaining energetic information.[18]

Relation Between Energy and Hardness. The connection between energy and hardness through the PMH prompted us to investigate the relation between the formation energies ΔE_2 and ΔE_4 of the bimolecular complexes and the corresponding hardnesses η_2° and η_4°, determined using eq 7. Panels a and b of Figure 2 show good linear correlations between ΔE_{n_f} and $\eta_{n_f}^\circ$ for the complexes identified by their total number of electrons. These correlations are substantially improved when we use the average value of the properties of complexes with the same number of electrons (N = 56, 64, and 72), as shown in Figure 2c,d. As dictated by the PMH, we see that the more stable the complex is, the harder it appears to be.

There have been few interesting and useful attempts to relate electronic properties to reaction energies.[14,31,32] Pearson[31] proposed an empirical method for ranking the order of Lewis acids and bases in terms of their hardness at their reaction sites. More recently, Gázquez[32] proposed an expression for the bond energy in terms of the chemical potential, the hardnesses, and the condensed Fukui functions of the isolated species. In our search for a relation between the hydrogen-bond energies and the electronic properties of the isolated species, we have tested the Gázquez expression with the result that it overestimates the H-bond energies although it indicates correctly that the main contribution to the bond energy comes from the change in the hardness of the system.

To close this discussion, it is interesting to note that the analysis of Figures 1 and 2 suggests that hardness and the H-bond force constants must be related. In Figure 3, we show the nice linear relations connecting these properties. It can be seen that the stronger the bond being formed, the harder the complex. This result confirms the fact that there is direct proportionality between hardness and force constants, as correctly pointed out recently by Arulmozhiraja and Kolandaivel.[33]

Polarizability of Hydrogen-Bonded Systems. Along with the PMH, Chattaraj et al. have proposed a minimum polarizability principle (MPP), which states that the natural direction of evolution of any system is toward a state of minimum polarizability.[34] In general, the conditions of maximum hardness and minimum polarizability complement the minimum energy criterion for molecular stability.[35] The polarizability of the isolated molecules and those of the hydrogen-bonded systems determined through the ab initio calculations are quoted in Table 7, together with the best approach to the polarizability of the hydrogen-bonded systems: the simple addition of the polariz-

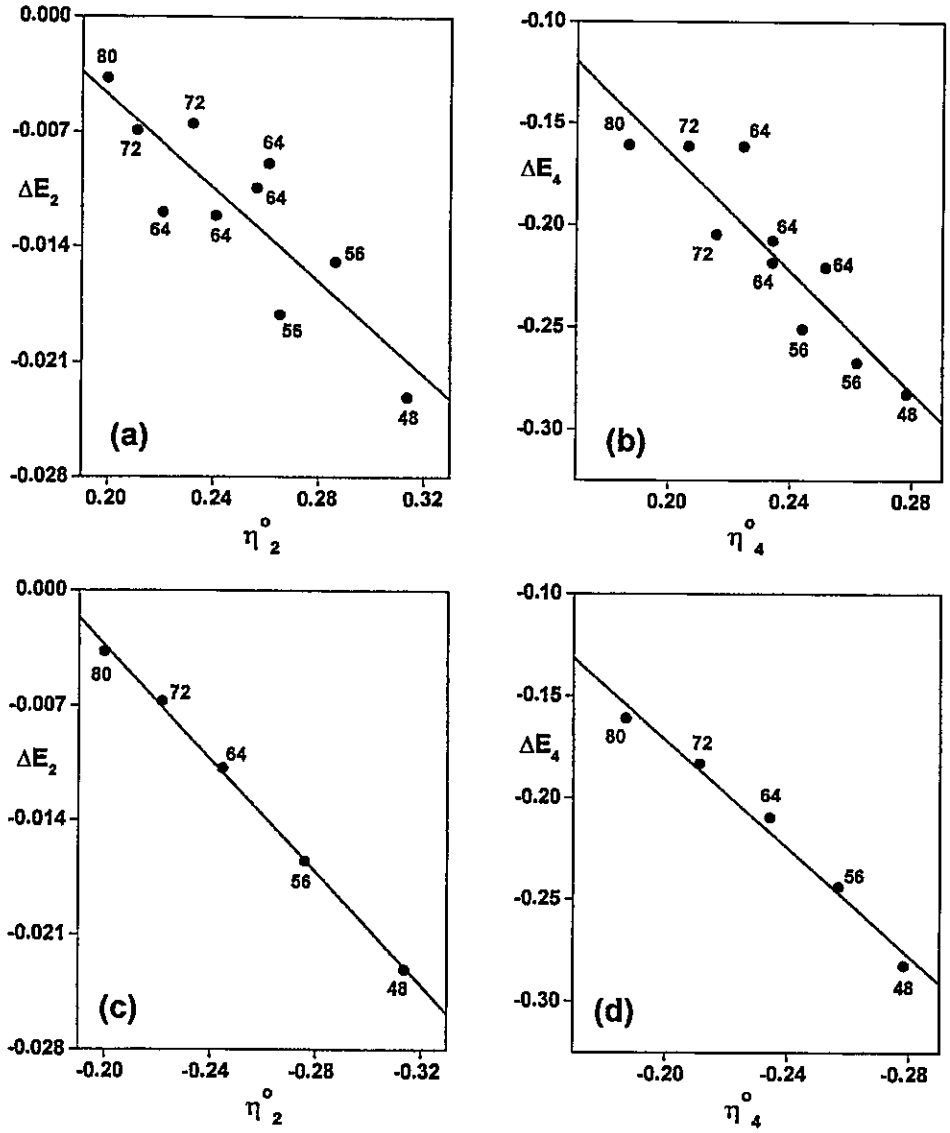

Figure 2. Correlation between bond energy and hardness of the product determined from the Sanderson approximation with (a) $n_f = 2$ and (b) $n_f = 4$. (c) and (d) Same as in panels a and b but using the average values in systems presenting the same number of electrons.

abilities of the constituent monomeric units (α_2°, the fourth column of Table 7). Figure 4a shows the excellent quality of this approach. Our results suggest that the polarizability of a composite system is given by the sum of the n_f individual polarizabilities

$$\alpha_{n_f}^\circ = \sum_x^{n_f} \alpha_x^\circ \qquad (10)$$

where α_x° stands for the polarizabilities of the monomeric units. The above expression is not an attempt to define an addition scheme for polarizabilities; it simply comes from the empirical observation of the present results.

Adding electrons to a system will increase its polarizability because α is proportional to N; our results concerning the hydrogen-bonded complexes confirm this proportionality, as shown in Figure 4b. On the other hand, we have shown recently[19] that the H-bond energy is proportional to N; therefore, one should expect ΔE_2 be related to the polarizability. However, Figure 5a shows a very scattered plot of ΔE_2 against the reaction polarizability $\Delta\alpha_2$ (fifth column in Table 7), where this latter quantity is defined as the difference between the polarizabilities of the product (the H-bonded system) and reactants (the sum of monomeric units). The expected consistency in our results is achieved when the polarizability of the reactants is defined as the arithmetic mean of the polarizabilities of the monomeric units, thus defining the reaction polarizability as $\Delta\bar{\alpha}_2 = \alpha - (\sum_x \alpha_x)/2$, which is given in Table 7. Figure 5b shows a quite good linear correlation in which it is apparent that the lower the reaction energy, the lower the reaction polarizability. This result suggests the possibility of extending the validity of the MPP to allow for comparisons of relative energies and polarizabilities. Furthermore, ΔE_2 displays a linear correlation with the polarizability of the product, as shown in Figure 5c. In summary, the more stable the product species, the harder and less polarizable it was found to be.

We have mentioned that the polarizability can be used to understand the behavior of the system when the external potential is changed at constant N.[7] Formally, the chemical potential is a function of N and a functional of the external

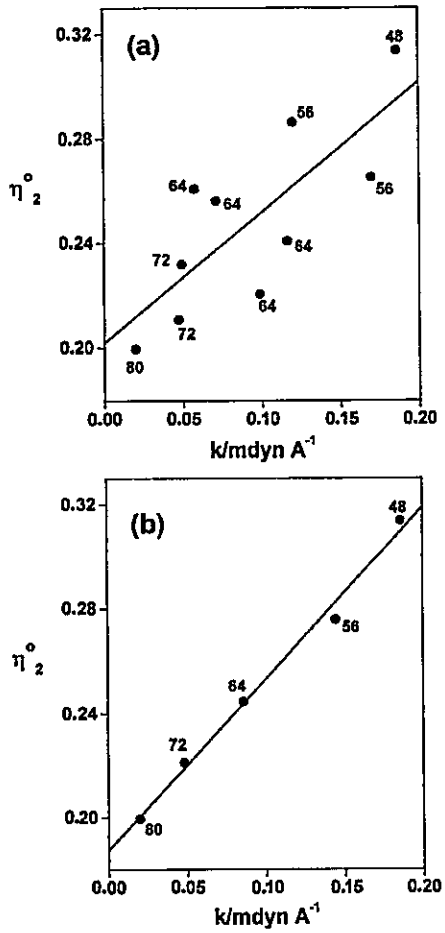

Figure 3. (a) Correlation between hardness and H-bond force constants of bimolecular aggregates. (b) Same as in panel a but using the average values in systems presenting the same number of electrons.

TABLE 7: Calculated and Estimated Polarizabilities of Isolated Molecules and Molecular Aggregates[a]

system	N	α	α°_2	$\Delta\alpha_2$	$\Delta\bar{\alpha}_2$
M1	24	15.1733			
M2	32	28.2873			
M3	32	27.7830			
M4	40	43.4183			
C1	48	30.9583	30.3466	0.6117	15.7850
C2	56	45.7427	43.4606	2.2821	24.0124
C3	64	60.5700	56.5746	3.9954	32.2827
C4	56	43.6490	42.9563	0.6927	22.1709
C5	64	60.9957	58.5916	2.4041	31.6999
C6	64	58.0750	56.0703	2.0047	30.0399
C7	72	75.0847	71.7056	3.3791	39.2319
C8	64	56.3013	55.5660	0.7353	28.5183
C9	72	72.9003	71.2013	1.6990	37.2997
C10	80	88.6140	86.8366	1.7774	45.1957

[a] All values are in atomic units.

potential $v(\vec{r})$, so we can write $\mu \equiv \mu[N,v(\vec{r})]$. To relate the change of the external potential to the reaction polarizability, we differentiate eq 6 with respect to $v(\vec{r})$, thus defining the quantity $F^\circ_{n_f}$.

$$F^\circ_{n_f} \equiv \left(\frac{\delta\mu^\circ_{n_f}}{\delta v}\right)_N \approx \frac{\mu^\circ_{n_f}}{n_f}\Delta v \sum_x^{n_f}\left(\frac{f^\circ_x}{\mu^\circ_x}\right) \qquad (11)$$

Because the formal definition of $F^\circ_{n_f}$ is analogous to the Fukui function used to quantify the reactivity of specific sites on a given molecule and because it contains information on the overall change from reactants to products through Δv, we call it the Reaction Fukui Function (RFF). It can be seen from eq 11 that $F^\circ_{n_f}$ is a global property that contains the fragment reactivities through the Fukui functions $f^\circ_x = (\delta\mu^\circ_x/\delta v)_N$. Therefore, we expect $F^\circ_{n_f}$ to be a property measuring the global reactivity of the system.

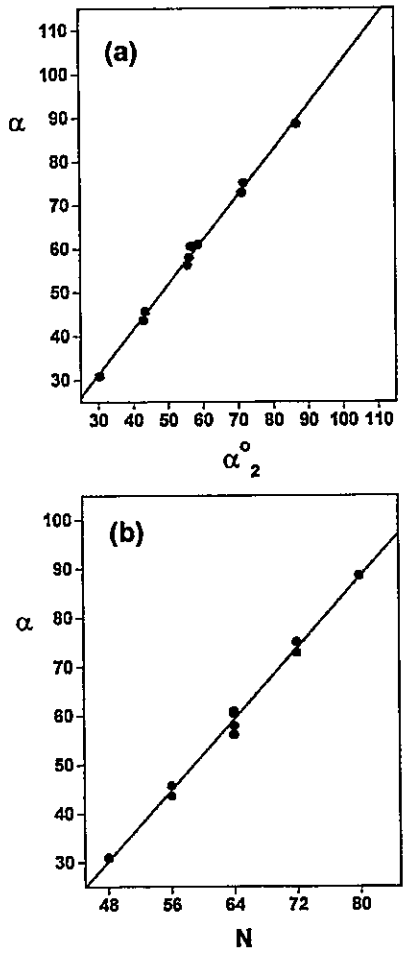

Figure 4. (a) Comparison of the calculated polarizability of the hydrogen-bonded complexes with the estimation of eq 10. (b) Characterization of the calculated polarizability with the total number of electrons of the H-bonded complexes.

We have determined numerical values of RFF approaching Δv by the electron–nuclei potential (V_{ne}) obtained from the ab initio calculations; in fact, we have used $\Delta v = [V_{ne}(\text{product}) - \sum V_{ne}(\text{reactants})]$. The f°_x values were approximated as N_x/N, with N_x being the number of electrons of fragment x and N the total number of electrons of the composite system such that $\sum_x N_x = N$. In Figure 6a, we show that the RFF is linearly related to the reaction energy, indicating that the RFF may be a measure of the exothermicity of the reaction: the lower ΔE_2, the higher the RFF value. On the other hand, Figure 6b indicates that the RFF is related to the reaction polarizability through a very good straight line. This result shows that the polarizability is the right response of the system when the external potential is changed, and it emphasizes the usefulness of determining accurate values for this property. On the other hand, it is clear that the whole procedure based upon Sanderson's scheme is a powerful tool for characterizing chemical reactions when both N and v change.

The Hardness Derivative. Hardness is now recognized as an important property for characterizing chemical processes, so

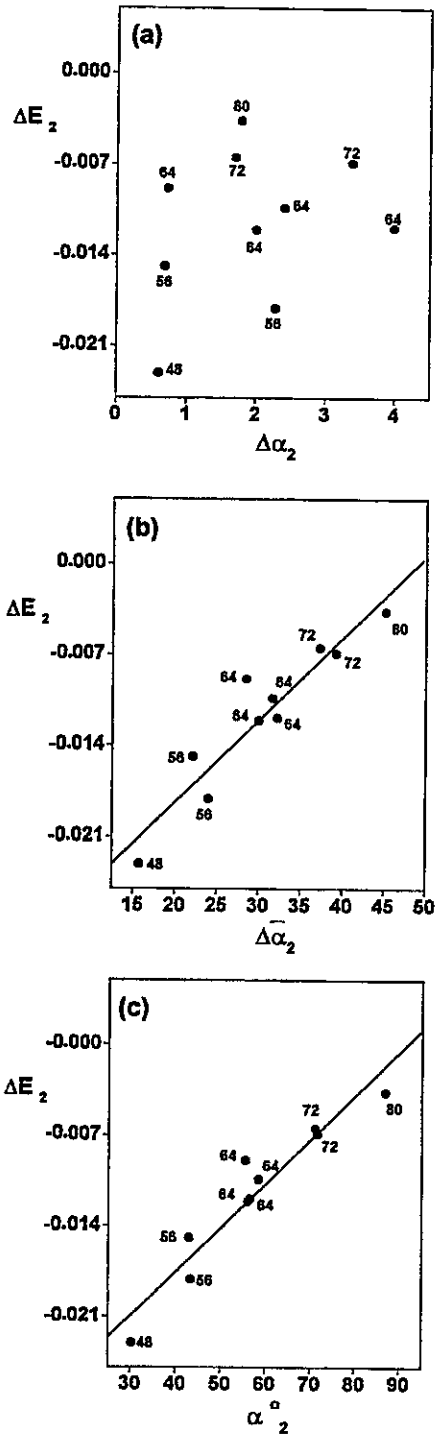

Figure 5. Representation of reaction energies ΔE_2 against (a) the reaction polarizability defined as $\Delta\alpha = \alpha(\text{product}) - \sum_x \alpha_x$, (b) the reaction polarizability defined as $\Delta\bar{\alpha} = \alpha(\text{product}) - (\sum_x \alpha_x)/n_f$, and (c) the polarizability of the bimolecular complex from eq 10. All values are in atomic units.

it is necessary to know how it changes with the number of electrons and the external potential. The quantity γ measures the change of η with N. We have used eq 8 to estimate numerical values of this property. We first note that to evaluate the third term of eq 8, we need the values of γ_x° of the isolated fragments; these were estimated from the following approximate formula proposed by Fuentealba and Parr:[20]

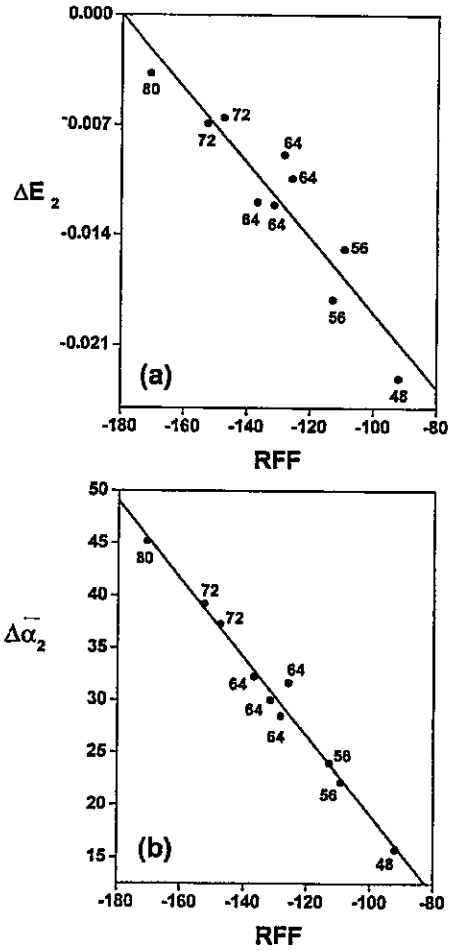

Figure 6. Characterization of the reaction Fukui function (RFF) with (a) the reaction energy and (b) the reaction polarizability. All values are in atomic units.

$$\gamma_x^\circ \approx \left[\frac{\epsilon_L}{\epsilon_L - 3\epsilon_H}\right]_x^\circ \eta_x^\circ \qquad (12)$$

Equation 8 shows a quite complex dependence of γ with respect to η that is far from being linear, as indicated by eq 12. The validity of this latter equation and its consistency with Sanderson's scheme has been tested by calculating η and γ using eqs 7 and 8 to check their possible linear relation. Values of γ_2° and γ_4° for the 14 compounds we are studying here are quoted in Table 4. We note that, in all cases, they are positive and very small. The linear dependence between γ and η could not be obtained, as is apparent in Figure 7a,b. These results are in agreement with expectations based on the very definition of γ.[20] When the atomic data of Fuentealba and Parr[20] are used to build the properties of the bimolecular complexes, thus producing η_{10}° and γ_{10}° from the 10 constituent atoms, we obtain negative values of γ and linear behavior with η, as shown in Figure 7c. It should be noted that because there are systems presenting the same atomic composition, their values of η_{10}° and γ_{10}° are the same. Thus, in Figure 7c, the systems have been ordered in terms of their total number of electrons.

A New Additivity Scheme for μ and η. In this section, we propose a new additivity scheme for the chemical potential and hardness that is based upon dimensional analysis of eq 11, which shows that it is possible to define the inverse of the chemical potential of a composite system as

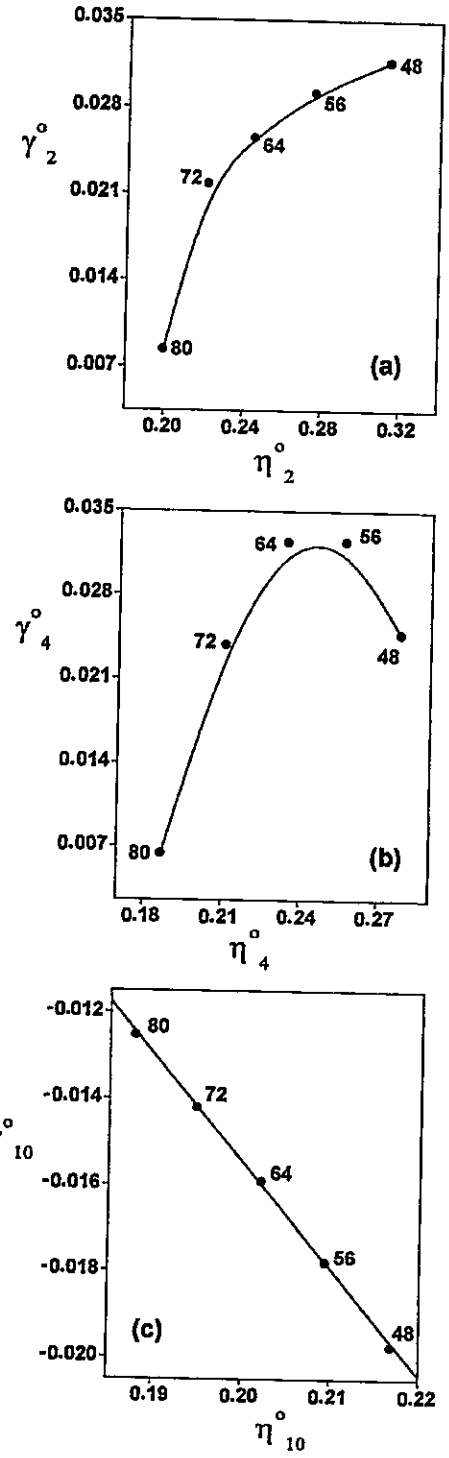

Figure 7. Relationship between $\eta^{\circ}_{n_f}$ and $\gamma^{\circ}_{n_f}$ of the H-bonded systems ordered in terms of their total number of electrons: (a) $n_f = 2$, (b) $n_f = 4$, and (c) $n_f = 10$ (from atomic data in ref 20). All values are in atomic units.

$$\frac{1}{\mu'_{n_f}} \approx \sum_x^{n_f} \left(\frac{f^{\circ}_x}{\mu^{\circ}_x}\right) \tag{13}$$

Determination of the chemical potential of a composite system from the properties of the isolated fragments by means of eq 13 produces results that are in very good agreement with those determined using eq 6. This can be verified in Figure 8, where

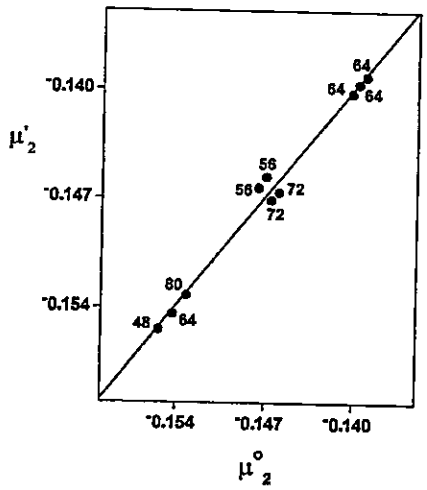

Figure 8. Comparison of chemical potentials determined through eqs 6 and 13. All values are in atomic units.

we compare both approaches for estimating the chemical potential of the 10 bimolecular complexes using $n_f = 2$. Moreover, we have verified that, in all cases studied here, μ'_{n_f} provides a better approach to the reference ab initio value than does $\mu^{\circ}_{n_f}$ determined from eq 6; this was verified for $n_f = 2$, 4, and 10. These results show that eq 13 represents a valid alternative to the original Sanderson's formulation. It is interesting to note that this new expression contains the electronic population of the isolated fragment, a local quantity, together with the chemical potential, a global property of the fragment.

Characterization of higher-order derivatives of eq 13 is straightforward. In the new framework the hardness is given by

$$\eta'_{n_f} = \left(\frac{\partial \mu'_{n_f}}{\partial N}\right)_{v(\bar{r})} = (\mu'_{n_f})^2 \sum_x^{n_f} \frac{1}{(\mu^{\circ}_x)^2} [f^{\circ}_x \eta^{\circ}_x - h^{\circ}_x \mu^{\circ}_x] \tag{14}$$

where h°_x is a measure of the fluctuation of the chemical hardness due to a change in the external potential. Alternatively, through the Maxwell relation, h°_x can be seen as the response of the Fukui function to a change in the total number of electrons.

$$h^{\circ}_x = \left(\frac{\delta \eta^{\circ}_x}{\delta v}\right)_N = \left(\frac{\partial f^{\circ}_x}{\partial N}\right)_v \tag{15}$$

Recently, Parr et al.[36] have defined the electrophilicity index as $W = \mu^2/2\eta$. In analogy with this definition, we can define a nucleophilicity index from eq 14 as

$$\frac{\eta'_{n_f}}{(\mu'_{n_f})^2} = \sum_x^{n_f} \frac{1}{(\mu^{\circ}_x)^2} [f^{\circ}_x \eta^{\circ}_x - h^{\circ}_x \mu^{\circ}_x] \tag{16}$$

which is a positive defined quantity. The above set of equations containing local and global properties opens a method for characterizing the reactivity and selectivity concepts in an unified perspective.

5. Concluding Remarks

We have used Sanderson's Principle to estimate the first, second, and third derivative of the energy with respect to the total number of electrons. The results for $\mu^{\circ}_{n_f}$ and $\eta^{\circ}_{n_f}$ show that,

in the cases treated here, Sanderson's geometric mean equalization principle is adequate for predicting these electronic properties of composite systems. Numerical values for the third-order property, γ, were found to be very small and positive, in agreement with the expected behavior.

Numerical results for bond energies at the RHF/6−311G** level were qualitatively satisfactory and quantitatively in agreement with the available bond-energy data. We have found that principles of maximum hardness and minimum polarizability are operative for rationalizing the formation of molecules and bimolecular aggregates. Sanderson's scheme has been shown to be very useful not only in determining electronic properties but also in rationalizing chemical reactions when both N and v change. Finally, we have proposed a new scheme for obtaining molecular properties from the isolated fragments with quite encouraging results for chemical potentials. In this approach, local and global properties play equivalent roles, which may lead to methods for simultaneously characterizing the reactivity and selectivity concepts in chemical processes.

Acknowledgment. This work was supported by Cátedra Presidencial en Ciencias 1998 awarded to A.T.L. and by FONDECYT through Project 1990543. P.J. is grateful to CONICYT for a graduate fellowship.

References and Notes

(1) Sanderson, R. T. *Science* **1955**, *121*, 207.
(2) Sanderson, R. T. *Chemical Bonds and Bond Energy*, 2nd ed.; Academic Press: New York, 1976.
(3) Parr, R. G.; Bartolotti, L. J. *J. Am. Chem. Soc.* **1982**, *104*, 3801.
(4) Hohenberg, P.; Kohn, W. *Phys. Rev. B* **1964**, *136*, 834.
(5) Parr, R. G.; Yang, W. *Density Functional Theory of Atoms and Molecules*; Oxford University Press: New York, 1989.
(6) Parr, R. G.; Yang, W. *Annu. Rev. Phys. Chem.* **1995**, *46*, 701. Bartolotti, L. J.; Flurchick, K. *Rev. Comput. Chem.* **1996**, *7*, 187. Ziegler, T. *Chem. Rev.* **1991**, *91*, 651.
(7) See, for exemple: Jensen, F. *Introduction to Computational Chemistry*; John Wiley and Sons: Chichester, U.K., 1999.
(8) Parr, R. G.; Donnelly, R. A.; Levy, M.; Palke, W. E. *J. Chem. Phys.* **1978**, *68*, 3801.
(9) Parr, R. G.; Pearson, R. G. *J. Am. Chem. Soc.* **1983**, *105*, 7512.
(10) Pearson, R. G.; Songstad, J. *J. Am. Chem. Soc.* **1967**, *89*, 1827. Pearson, R. G. *Inorg. Chem.* **1984**, *23*, 4675. Pearson, R. G. *J. Am. Chem. Soc.* **1985**, *107*, 6801. Pearson, R. G. *J. Chem. Educ.* **1987**, *64*, 561. Pearson, R. G., *Structure and Bonding 80, Chemical Hardness*; Sen, K. D., Ed.; Springer-Verlag: Berlin, 1993.
(11) Parr, R. G.; Chattaraj, P. K. *J. Am. Chem. Soc.* **1991**, *113*, 1854. Chattaraj, P. K.; Nath, S.; Sannigrahi, A. B. *J. Phys. Chem.* **1994**, *98*, 9143. Chattaraj, P. K.; Liu, G. H.; Parr, R. G. *Chem. Phys. Lett.* **1995**, *237*, 171. Chattaraj, P. K.; Cedillo, A.; Parr, R. G. *J. Chem. Phys.* **1995**, *103*, 10621. Datta, D. *J. Phys. Chem.* **1992**, *96*, 2409. Sengupta, D.; Chandra, A. K.; Nguyen, M. T. *J. Org. Chem.* **1997**, *62*, 6404;
(12) Gázquez, J. L. In *Chemical Hardness*; Sen, K. D., Mingos, D. M. P., Eds.; Springer: Berlin, 1993. Gázquez, J. L.; Martínez, A.; Méndez, F. *J. Phys. Chem.* **1993**, *97*, 4059. Gázquez, J. L.; Méndez, F. *J. Phys. Chem.* **1994**, *98*, 116. Gázquez, J. L.; Méndez, F. *J. Phys. Chem.* **1994**, *98*, 4591. Parr, R. G.; Gázquez, J. L. *J. Phys. Chem.* **1993**, *97*, 3939. Pérez, P.; Contreras, R.; Vela, A.; Tapia, O. *Chem. Phys. Lett.* **1997**, *269*, 419. Contreras, R.; Fuentealba, P.; Galván, M.; Pérez, P. *Chem. Phys. Lett.* **1999**, *304*, 405.
(13) Chermette, H. *J. Comput. Chem.* **1999**, *20*, 129. Geerlings, P.; De Proft, F.; Langenaeker, W. *Adv. Quantum Chem.* **1999**, *33*, 303. Momenteau, M.; Reed, C. A. *Chem. Rev.* **1994**, *94*, 659.
(14) Toro-Labbé, A. *J. Phys. Chem. A* **1999**, *103*, 4398. Gutiérrez-Oliva, S.; Letelier, J. R.; Toro-Labbé, A. *Mol. Phys.* **1999**, *96*, 61. Cárdenas-Jirón, G. I.; Lahsen, J.; Toro-Labbé, A. *J. Phys. Chem.* **1995**, *99*, 5325. Cárdenas-Jirón, G. I.; Toro-Labbé, A. *J. Phys. Chem.* **1995**, *99*, 12730. Cárdenas-Jirón, G. I.; Gutiérrez-Oliva, S.; Melin, J.; Toro-Labbé, A. *J. Phys. Chem. A* **1997**, *101*, 4621. Solà, M.; Toro-Labbé, A. *J. Phys. Chem. A* **1999**, *103*, 8847. Pérez, P.; Toro-Labbé, A. *J. Phys. Chem. A* **2000**, *104*, 1557.
(15) Bader, R. F. W. *Atoms in Molecules*; Clarendon Press: Oxford, U.K., 1990.
(16) Cioslowski, J.; Mixon, S. T. *J. Am. Chem. Soc.* **1991**, *113*, 4142.
(17) Cioslowski, J.; Stefanov, B. B. *Mol. Phys.* **1995**, *84*, 707.
(18) Cárdenas-Jirón, G. I.; Toro-Labbé, A. *J. Mol. Struct. (THEOCHEM)* **1997**, *390*, 79.
(19) Jaque, P.; Toro-Labbé, A. *J. Phys. Chem. A* **2000**, *104*, 995.
(20) Fuentealba, P.; Parr, R. G. *J. Chem. Phys.* **1991**, *94*, 5559.
(21) Frisch, M. J.; Trucks, G. W.; Schlegel, H. B.; Gill, P. M. W.; Johnson, B. G.; Robb, M. A.; Cheeseman, J. R.; Keith, T. A.; Peterson, G. A.; Montgomery, J. A.; Raghavachari, K.; Al-Laham, M. A.; Zakrzewski, V. G.; Ortiz, J. V.; Foresman, J. B.; Ciolowski, J.; Stefanov, B. B.; Nanayakkara, A.; Challacombe, M.; Peng, C. Y.; Ayala, P. Y.; Chen, W.; Wong, M. W.; Andres, J. L.; Replogle, E. S.; Gomperts, R.; Martin, R. L.; Fox, D. J.; Binkley, J. S.; Defrees, D. J.; Baker, J.; Stewart, J. P.; Head-Gordon, M.; González, C.; Pople, J. A. *Gaussian 94*; Gaussian Inc.: Pittsburgh, PA, 1995.
(22) Berry, R. S.; Rice, S. A.; Ross, J. *Physical Chemistry*; John Wiley and Sons: New York, 1980.
(23) Del Bene, J. E. *J. Phys. Chem.* **1988**, *92*, 2874. Kumpf, R. A.; Damewood, J. R. *J. Phys. Chem.* **1989**, *93*, 4478. Kim, Y. *J. Am. Chem. Soc.* **1996**, *118*, 1522. Lim, J. H.; Kim, Y. *J. Phys. Chem. A* **1997**, *101*, 2233.
(24) Clague, A. D. H.; Bernstein, H. J. *Spectrochim. Acta* **1969**, *A25*, 593. Curtiss, L. A.; Blander, M. *Chem. Rev.* **1988**, *88*, 827. Winkler, A.; Mehl, J. B.; Hess, P. *J. Chem. Phys.* **1994**, *100*, 2717. Winkler, A.; Hess, P. *J. Am. Chem. Soc.* **1994**, *116*, 9233.
(25) Allen, G.; Colclough, R. O. *J. Chem. Soc.* **1957**, *3*, 3912.
(26) Yang, W.; Lee, C.; Ghosh, S. K. *J. Phys. Chem.* **1985**, *89*, 5412.
(27) Chattaraj, P. K.; Nandi, P. K.; Sannigrahi, A. B. *Proc. Indian Acad. Sci., Chem. Sci.* **1991**, *103*, 583. Chattaraj, P. K. *Curr. Sci.* **1991**, *61*, 391.
(28) Pearson, R. G. *J. Chem. Educ.* **1987**, *64*, 1987.
(29) Pearson, R. G. *Chemical Hardness*; Wiley-VCH: Oxford, U.K., 1997.
(30) Chattaraj, P. K. *Proc. Indian Natl. Sci. Acad.* **1996**, *62*, 513.
(31) Pearson, R. G. *J. Am. Chem. Soc.* **1988**, *110*, 7684.
(32) Gázquez, J. L. *J. Phys. Chem. A* **1997**, *101*, 9464.
(33) Arulmozhiraja, S.; Kolandaivel, P. *Mol. Phys.* **1997**, *92*, 353.
(34) Chattaraj, P. K.; Sengupta, S. *J. Phys. Chem.* **1996**, *100*, 16126. Chattaraj, P. K.; Poddar, A. *J. Phys. Chem. A* **1998**, *102*, 9944. Chattaraj, P. K.; Poddar, A. *J. Phys. Chem. A* **1999**, *103*, 1274.
(35) Chattaraj, P. K.; Fuentealba, P.; Jaque, P.; Toro-Labbé, A. *J. Phys. Chem. A* **1999**, *103*, 9307.
(36) Parr, R. G.; Szentpaly, L. V.; Liu, S. *J. Am. Chem. Soc.* **1999**, *121*, 1922.

CHARACTERIZATION OF CHEMICAL REACTIONS THROUGH CLASSICAL CONCEPTS AND DFT DESCRIPTORS.

SOLEDAD GUTIÉRREZ-OLIVA, PABLO JAQUE
AND ALEJANDRO TORO-LABBÉ

Laboratorio de Química Teórica Computacional (QTC),
Facultad de Química, Pontificia Universidad Católica de Chile.
Casilla 306, Correo 22, Santiago, Chile.

In this paper we point out that classical concepts of reactivity in connection with DFT descriptors are adequate and powerful tools for characterizing chemical reactions. The conceptual classical model, in which a reaction proceeds from one energy minimum to another via an intermediate maximum, together with the principles of maximum hardness and minimum polarizability provide the necessary elements to discuss the activation and relaxation processes in terms of the activation chemical potential and hardness. Illustrative examples of representative systems undergoing internal rotations, intramolecular rearrangements and double proton transfer confirm the validity of this approach.

1 Introduction

1.1 Classical Concepts of Chemical Reactivity.

Chemical processes can be characterized through reaction profiles that illustrate the way in which the properties of the reacting systems changes as a function of the reaction coordinate (RC). These properties may be either global (energy, chemical potential, hardness, polarizability, etc.) or local (electronic populations, Fukui functions, etc.). Within the Born–Oppenheimer approximation the RC represents the nuclear reorganization that takes place as the reaction move forward, i.e. the bond lengths and bond angles that change during the chemical reaction, the RC is therefore a multidimensional coordinate[1–3]. In many cases the reaction coordinate may be a conformational variable connecting two conformations that can be viewed as the reactants and products of a chemical reaction, unfortunatelly in most chemical processes the RC is quite difficult to visualize. In this work we are concerned with elementary reactions within the framework of transition state theory in which reactants (**R**) change into products (**P**) passing by a transition state (**TS**), with all three states connected by a given RC [4].

Understanding chemical reactivity allows one to predict the reaction mechanism and to determine how the activation energy depends on specific proper-

ties of the reactants and products. In this context the identification of these properties and the characterization of the transition state becomes especially important. For the first purpose Density Functional Theory (DFT)[5–8] is well suited to describe the electronic reorganization that takes place during a chemical reaction through the definition of global and local reactivity properties. On the other hand, to characterize transition states there is a set of interesting conceptual tools that give complementary insights on their structure and properties [5]. These conceptual tools are: **(a)** the well known Hammond postulate (HP) [9] that interrelates the position of the transition structure to the exothermicity of the reaction, the HP states that if the TS is near in energy to a given adjacent stable complex, then it should be also similar in structure to the same complex; **(b)** the Leffler's postulate [10] suggests a mechanistic interpretation of the so-called Brønsted coefficient (β) [11]: it is a measure of the location of the TS along the RC, this defines β as a similarity index that can be interpreted as the degree of resemblance of the TS with respect to the product; **(c)** the Marcus equation (ME)[12] that provides a simple expression for the activation energy in terms of the reaction energy and the structural properties of reactants and products; and **(d)** the Principle of Maximum Hardness (PMH)[13–15] that asserts that molecular systems at equilibrium tend to states of high hardness, therefore TS's are expected to present a minimum value of hardness [16–18]. Although these principles are not widely applicable they provide a conceptual framework to rationalize transition states and to help characterize the reaction mechanisms. The connection between DFT and classical reactivity concepts is the subject of this chapter.

1.2 DFT Descriptors of Chemical Reactivity.

Within the conceptual frame of DFT, the ground–state energy of a chemical system is a functional of the electron density $\rho(\vec{r})$. This means that all properties of the system are determined by $\rho(\vec{r})$. Since the theorems of Hohenberg–Kohn [19,20] establishes a correspondence between the electron density and the external potential $v(\vec{r})$, a complete characterization of an N–particle wavefunction needs only N and $v(\vec{r})$ and the energy of the system may be expressed as a function of the electron number N and a functional of the external potential $v(\vec{r})$, so $E[\rho(\vec{r})] \equiv E[N, v(\vec{r})]$. The total differential of the energy is given by [5,7]:

$$dE = \mu dN + \int \rho(\vec{r}) dv(\vec{r}) d\vec{r}, \tag{1}$$

where

$$\mu = \left(\frac{\partial E}{\partial N}\right)_v \quad \text{and} \quad \rho(\vec{r}) = \left[\frac{\delta E}{\delta v(\vec{r})}\right]_N, \tag{2}$$

are the chemical potential and the ground-state electron density, respectively. The chemical potential is a global property that characterizes the escaping tendency of electrons from the equilibrium system [21], μ is a function of N and a functional of $v(\vec{r})$, ($\mu \equiv \mu[N, v(\vec{r})]$) and has the following total differential:

$$d\mu = \eta dN + \int f(\vec{r}) dv(\vec{r}) d\vec{r}, \tag{3}$$

where

$$\eta = \frac{1}{2}\left(\frac{\partial \mu}{\partial N}\right)_v \quad \text{and} \quad f(\vec{r}) = \left[\frac{\delta \mu}{\delta v(\vec{r})}\right]_N = \left(\frac{\partial \rho(\vec{r})}{\partial N}\right)_v, \tag{4}$$

are the hardness [22,23] and the Fukui function [24,25] of the system, respectively. η can be seen as a resistance to charge transfer, it is a global property of the system and depends on both N and $v(\vec{r})$. $f(\vec{r})$ is a local property of the system and it measures the reactivity of the different sites within the molecule. The total differential of $\eta[N, v(\vec{r})]$ is:

$$d\eta = \gamma dN + \int h(\vec{r}) dv(\vec{r}) d\vec{r}, \tag{5}$$

where

$$\gamma = \frac{1}{3}\left(\frac{\partial \eta}{\partial N}\right)_v \quad \text{and} \quad h(\vec{r}) = \left[\frac{\delta \eta}{\delta v(\vec{r})}\right]_N = \left(\frac{\partial f(\vec{r})}{\partial N}\right)_v. \tag{6}$$

γ is a global property measuring the change in the hardness due to the variation of the electron number [26], $h(\vec{r})$ is a local property that measures the fluctuation of the chemical hardness due to a change in the external potential, or through the Maxwell relation, it can be seen as the response of the Fukui function to a change in the total number of electrons.

When a reaction move forward along the RC, a redistribution of the ground-state electron density is occurring, the resulting change of the energy can be rationalized in terms of the response of the system when changing N and $v(\vec{r})$ and can be characterized through the above defined global and local indexes, these are used as chemical reactivity descriptors [27]. The response of the

system when N is varied for a fixed $v(\vec{r})$ is measured by μ and η while local properties, such as the Fukui function, measure the response of the system for changing the external potential at constant N. Since the Fukui functions are the specific subject of other contributions to this book, here we are going to focus our attention to the analysis of the evolution of global molecular properties during a chemical reaction. However, along the reaction coordinate the external potential certainly changes and to understand the behavior of the system for changing $v(\vec{r})$ at constant N, we will use the polarizability (α), a global property of the system. Chattaraj *et al* have proposed the principle of minimun polarizability (PMP) [28,29] which states that the natural direction of evolution of any system is toward a state of minimum polarizability. In general the conditions of minimun polarizability and maximun hardness complement the minimun energy criterion for molecular stability, and are criteria that we will use to characterize our systems.

Chemical potential, hardness and its inverse, the softness ($S = 1/2\eta$) are among the most important global properties aimed at describing chemical reactivity. In numerical applications, μ and η are calculated through the following approximate equations based upon the finite difference approximation and the Koopmans' theorem [30]:

$$\mu \approx -\frac{1}{2}(I + A) \simeq \frac{1}{2}(\varepsilon_L + \varepsilon_H) \tag{7}$$

and

$$\eta \approx \frac{1}{2}(I - A) \simeq \frac{1}{2}(\varepsilon_L - \varepsilon_H), \tag{8}$$

I is the ionization potential, A is the electron affinity, ε_H and ε_L are the energies of the highest occupied molecular orbital (HOMO) and the lowest unoccupied molecular orbital (LUMO), respectively.

1.3 Reaction Coordinates.

Within the transition state theory it is assumed that a reaction proceeds from one energy minimum to another via a reaction coordinate (RC) passing by an intermediate maximum, this classical picture is displayed in Figure 1(a) represented by an energy profile where the stationary points are connected through the RC. At the transition state the eigenvector for the imaginary frequency characterizes the RC and the whole reaction path may be determined from standar calculations that defines the intrinsic reaction

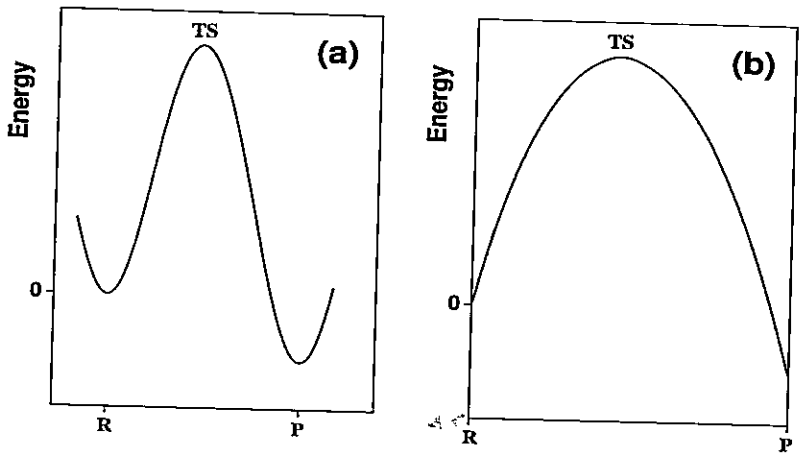

Figure 1. Generic energy profiles along the reaction coordinate (a) and the reduced reaction coordinate (b).

coordinate (IRC) [31–33]. On the other hand, it is always possible to express the RC in terms of a reduced reaction coordinate (RRC) running from 0 to 1 thus measuring the reaction progress when going from reactants to products. In Figure 1(b) we show a schematic view of the same energy profile but now along a new reduced variable called ω [34,35]. It is important to point out that the ω–representation provides a correct and straightforward characterization of the position and the energy of the transition state, this allows to handle chemical process in a quite simple and schematic way, and without losing relevant information.

This chapter is organized as follows, in section 2 we give the theoretical background for rationalizing internal rotation reactions and in section 3 we describe the theoretical tools aimed at rationalizing bond breaking and transfer reactions. Section 4 contains a subject that is a little different although it lies within the study of formation reactions, the characterization of additivity schemes aimed at determining aggregate's properties from the combination of constituent fragments' properties. In the light of the combination of classical reactivity and DFT concepts, in section 5 we briefly analyze few illustrative ex-

amples of rotational isomerization, intramolecular reordering and intermolecular proton transfer reactions. In section 6 we present the conclusions of the present work and suggest few directions for future research.

2 Rotational Isomerization Processes.

In this section we are concerned with the study of the internal rotation process from the perspective of the simultaneous evolution of the potential energy (V), the electronic chemical potential (μ) and the molecular hardness (η). Let us consider a *trans* $\rightleftharpoons$ *cis* conformational transformation occurring through the internal rotation with respect to a given bond in the molecule, in such a case the RC is the torsional angle α that is measured from the *trans* ($\alpha = 0$) to the *cis* ($\alpha = \pi$) conformations. The model potential that we use to describe internal rotations is [36]:

$$V(\alpha) = \frac{1}{4}K_V(1 - \cos^2\alpha) + \frac{1}{2}\Delta V^\circ(1 - \cos\alpha), \tag{9}$$

where the *trans* conformation is taken as the origin of the energy; K_V is the sum of the torsional force constants of the *trans* and *cis* conformations ($K_V = k_t + k_c$) and $\Delta V^\circ = (V(\pi) - V(0))$ is the energy difference between the reference isomers [34–36].

In conformational reactions the reduced reaction coordinate ω is called *conformational function* and it measures the reaction progress when going from reactants to products. The conformational function for the internal rotation is defined as:

$$\omega(\alpha) = \frac{1}{2}\left(1 - \cos\alpha\right), \tag{10}$$

and in the ω–representation the potential energy is given by:

$$V[\omega] = K_V f[\omega] + \omega\Delta V^\circ, \tag{11}$$

with $f[\omega] = \omega(1 - \omega)$. Since the only requirement on $f(\omega)$ is that it must be symmetric with respect to $\omega = 0.50$, there are many functions qualifying with this condition that can be used to express the potential energy of Eqn.(11).

Since μ and η are global properties of the system, their evolution along ω can be expressed through the same analytic form used for $V[\omega]$ [37,38]:

$$\mu[\omega] = K_\mu f[\omega] + \omega\Delta\mu^\circ, \tag{12}$$

and

$$\eta[\omega] = K_\eta f[\omega] + \omega\Delta\eta^\circ. \tag{13}$$

The parameters $(\Delta\mu^\circ, K_\mu)$ and $(\Delta\eta^\circ, K_\eta)$ have the same meaning that $(\Delta V^\circ, K_V)$ have for $V[\omega]$. To determine the numerical values of the parameters of Eqns.(11)–(13) we use a prescription we gave in previous works [36–38]. It is important to point out that since V, μ and η depend on the same function $f(\omega)$ it is possible to establish analytic relations between them although the extend of the application of this relations is still matter of research [39].

The position of the TS can be determined by differentiating Eqn.(9) and through Eqn.(10) we obtain:

$$\left(\frac{dV}{d\alpha}\right)_{\alpha=\alpha_0} = 0 \Rightarrow \cos\alpha_0 = -\frac{\Delta V^\circ}{K_V} \Rightarrow \omega(\alpha_0) \equiv \beta = \frac{1}{2} + \frac{\Delta V^\circ}{2K_V}. \tag{14}$$

β is the Brønsted coefficient and following the Leffler interpretation it measures the degree of resemblance of the TS with respect to the products. Putting β in Eqn.(11) yields to the following expression for the energy barrier hindering the internal rotation:

$$V[\beta] \equiv \Delta V^{\neq} = \frac{1}{4}K_V + \frac{1}{2}\Delta V^\circ + \frac{(\Delta V^\circ)^2}{4K_V}. \tag{15}$$

This is the Marcus equation [12], it was originally proposed to characterize electron transfer processes but later on have been shown to be useful in the interpretation of the activation energy of many chemical reactions. Note that the Marcus equation is consistent with the Leffler definition of the Brønsted coefficient as the derivative of the activation energy with respect to the reaction energy ΔV°. Indeed the Marcus equation provides the necessary framework for a quantitative analytic representation of the Hammond postulate through the Leffler interpretation of the Brønsted coefficient.

3 Bond Breaking and Transfer Reactions.

3.1 Introduction.

The above analytic results can be used to characterize the transition states of more complex chemical processes since within the transition state theory any chemical reaction can be rationalized in terms of elementary steps that links reactants, transition states and products: $\mathbf{R} \rightarrow (\mathbf{TS})^{\neq} \rightarrow \mathbf{P}$ [4]. The stationary states are connected by the intrinsic internal reaction coordinate (IRC) that comes out from standard calculations, along the IRC it is possible to define the profiles of energy, chemical potential, hardness and polarizability that allows one to characterize the reaction and the properties of the transition state. To characterize the TS we use again the Marcus equation and the Brønsted coefficient. The energy barrier $\Delta E^{\neq}$ is then given by:

$$\Delta E^{\neq} = \frac{1}{4}K + \frac{1}{2}\Delta E^{\circ} + \frac{(\Delta E^{\circ})^2}{4K}. \tag{16}$$

From the knowledge of ΔE° and $\Delta E^{\neq}$ we can obtain the parameter K that in turn we use to determine the position of the TS along the IRC, assuming the validity of the Brønsted coefficient already defined:

$$\beta = \frac{1}{2} + \frac{\Delta E^{\circ}}{2K} \tag{17}$$

It is very important to note that to characterize the position of the TS there is no need of an explicit definition of the reaction coordinate, the Marcus equation provides the necessary framework to get insight on the TS.

3.2 Activation Properties: Chemical Potential, Hardness and the ME.

For isoenergetic reactions the ME reduces to:

$$\Delta E_0^{\neq} \equiv \frac{1}{4}K \tag{18}$$

and the TS is located halfway between reactants and products ($\beta = 1/2$). The quantity $\Delta E_0^{\neq}$ is our equivalence with the so called Marcus' intrinsic activation energy. This is the barrier height for the case in which there is no energetic driving force, this quantity should be related to purely electronic properties such as chemical potential and hardness. The ME can now be rewritten as:

$$\Delta E^{\neq} = \Delta E_0^{\neq} + \frac{1}{2}\Delta E^{\circ} + \frac{(\Delta E^{\circ})^2}{16\Delta E_0^{\neq}}. \tag{19}$$

Inspection of Eqn.(19) indicates that when the reaction is exergonic ($\Delta E^{\circ} < 0$) $\Delta E^{\neq}$ is smaller than the intrinsic barrier whereas for endergonic reactions ($\Delta E^{\circ} > 0$) $\Delta E^{\neq}$ becomes larger than the intrinsic barrier. As already mentioned, the intrinsic barrier should be interpreted in terms of electronic and structural properties, in this context in a recent paper we have suggested that the Marcus' intrinsic barrier can be rationalized in terms of the electronic properties μ and η. The following expression relating $\Delta E_0^{\neq}$ as been proposed [40] :

$$\Delta E_0^{\neq} = \frac{1}{2}Q_{\eta}\Delta\mu^{\neq} + \frac{1}{2}Q_{\mu}\Delta\eta^{\neq}, \tag{20}$$

where $\Delta\mu^{\neq} \equiv [\mu(TS) - \mu(R)]$ and $\Delta\eta^{\neq} \equiv [\eta(TS) - \eta(R)]$ are the activation chemical potential and hardness, respectively. The parameters Q_{η}, Q_{μ} have been related to the amount of electronic charge transferred during the chemical reaction, they can be determined numerically through:

$$Q_{\eta} = \frac{(\Delta E^{\neq} - \Delta E^{\circ})}{(\Delta\mu^{\neq} - \Delta\mu^{\circ})}, \tag{21}$$

and

$$Q_{\mu} = \frac{(\Delta E^{\neq} - \Delta E^{\circ})}{(\Delta\eta^{\neq} - \Delta\eta^{\circ})}; \tag{22}$$

Note that the validity of the PMH leads to opposite curvature for the energy and hardness, this entails a negative value for the parameter Q_{μ}.

3.3 Reaction Mechanisms.

The concept of reaction mechanism is related to the notion of molecular structure in that any reactive process can be represented by nuclear displacements of the molecular system in going from the reactants to the products. These displacements are related with the forces acting on the system to bring reactants into products. Let assume the force acting on the system depends only on the position along the reaction coordinate, it is then defined as:

$$F(\omega) = -\frac{dE}{d\omega}, \tag{23}$$

assuming that $E(\omega)$ can be expressed as [40]:

$$E(\omega) = K\omega(1-\omega) + \omega\Delta E^{\circ}, \tag{24}$$

then,

$$F(\omega) = -(K + \Delta E^{\circ}) + (2K)\,\omega. \tag{25}$$

To have an adequate description of the whole chemical reaction it is useful to distinguish the different processes taking place along the reaction coordinate. In the reactants region an activation process is taking place with the following associated activation work:

$$W_{act} = \int_0^{\beta} F(\omega)d\omega = \Delta E^{\neq}, \tag{26}$$

in the product region we have a relaxation process, the work associated is:

$$W_{rel} = \int_{\beta}^{1} F(\omega)d\omega = \Delta E^{\circ} - \Delta E^{\neq}. \tag{27}$$

Isoenergetic reactions present the transition state at $\beta = 1/2$, in absolute values the activation work is equal to the relaxation work. In contrast to this, exoenergetic reactions are characterized by an early transition state ($\beta < 1/2$) and by an activation work smaller than the relaxation work. Finally, an endoenergetic reaction is characterized through a $\beta > 1/2$ and an activation work larger than the relaxation work.

It is important to point out that the use of Eqns. (19) and (20) together with Eqns. (26) and (27), provides the necessary elements to discuss the activation and relaxation works in terms of the activation chemical potential and hardness. This opens new ways to link classical reactivity concepts with the DFT reactivity descriptors.

Now we can identify the activation and relaxation processes as being driven by chemical potential and hardness, respectively. To do so we assume Eqn.(20) valid for all ω and define the energy profile as:

$$E(\omega) = \frac{1}{2}Q_\eta \mu(\omega) + \frac{1}{2}Q_\mu \eta(\omega). \tag{28}$$

Consequently, the force appears to be splitted into two contributions that are associated to chemical potential and hardness driving processes:

$$F(\omega) = -\frac{1}{2}Q_\eta \frac{d\mu}{d\omega} - \frac{1}{2}Q_\mu \frac{d\eta}{d\omega}. \tag{29}$$

Using straightforward definitions and considering that $Q_\mu < 0$ to comply with the PMH, $F(\omega)$ can be splitted as:

$$F(\omega) = -F_\mu(\omega) + F_\eta(\omega). \tag{30}$$

This equation permits a qualitative analysis of $F(\omega)$ in terms of the sign that it takes when moving along ω:

$$(0 \leq \omega < \beta): \qquad F(\omega) < 0 \qquad \Rightarrow \qquad F_\mu(\omega) > F_\eta(\omega) \tag{31}$$

and when going from the reactants to the transition state (the activation process), it is the chemical potential term that drives the reaction. At the transition state we have that:

$$(\omega = \beta): \qquad F(\beta) = 0 \qquad \Rightarrow \qquad F_\mu(\beta) = F_\eta(\beta) \tag{32}$$

and both driving forces are equilibrated and cancels to each other. When stepping down from the transition state to the products (the relaxation process), we have:

$$(\beta < \omega \leq 1): \qquad F(\omega) > 0 \qquad \Rightarrow \qquad F_\eta(\omega) > F_\mu(\omega) \tag{33}$$

and this part of the reaction is controlled by the hardness term as the system rearrange himself to reach a maximum hardness configuration. In summary, this simple model suggest that activation processes are basically driven by μ whereas relaxation processes are driven by η.

4 Formation Reactions: Fragment Chemistry.

If it is possible to estimate safely the molecular electronic descriptors from constituent fragments, then it would be also possible to estimate the corresponding properties of transition states from combination of known reactants structures and properties through the application of adequate additivity schemes. Within this context it is worth to explore how properties of fragment combine themselves to approach quantitatively the values measured or calculated for a given resulting molecule or aggregate. In such a situation the suitability of the combined models reviewed in this work may increase considerably.

The establishment of rigorous foundations for the concept of electronegativity and hardness allows for the introduction of combination schemes relating the properties of the constituent fragments to the properties of the resulting molecules or aggregates. Although the bonding potential and redistribution of the electron density among the fragments are not considered in these procedures, the use of combination rules is quite appealing mainly because of their predictive quality. To relate the molecular electronegativity to those of the constituent atoms or fragments Sanderson proposed a geometric mean equalization principle that defines the molecular electronegativity as the geometric mean of the electronegativities of the n_f constituent atoms or fragments [41]:

$$\mu^s_{n_f} = -\left(\prod_x^{n_f} |\mu_x|\right)^{1/n_f}, \tag{34}$$

where μ_x is the chemical potential of fragment x. From the Sanderson's formula for μ, we estimate molecular or aggregate hardnesses as [42,43]:

$$\eta^s_{n_f} = \frac{\mu^s_{n_f}}{n_f} \sum_x^{n_f} \frac{\eta_x}{\mu_x}, \tag{35}$$

η_x is the hardness of fragment x.

There are other methods for calculating μ and η, for example Ghosh *et al* [44] expresses the aggregate hardness as the reciprocal of the aggregate softness computed as the average of the softness of the constituent fragments, accordingly it is calculated as:

$$\frac{1}{\eta^g_{n_f}} = \frac{1}{n_f}\sum_x^{n_f}\frac{1}{\eta_x}, \tag{36}$$

Another aggregation scheme has been introduced by Chattaraj *et al* [45] which expresses the hardness of the aggregate molecule as the geometric mean of the respective hardness of the constituent fragments as follows:

$$\eta^d_{n_f} = \left(\prod_x^{n_f}\eta_x\right)^{1/n_f} \tag{37}$$

More recently we have proposed expressions for determining μ and η of a composite system, these are [46,47]:

$$\frac{1}{\mu^\circ_{n_f}} = \sum_x^{n_f}\left(\frac{f_x}{\mu_x}\right), \tag{38}$$

and

$$\eta^\circ_{n_f} = (\mu^\circ_{n_f})^2\sum_x^{n_f}\frac{1}{(\mu_x)^2}\left[f_x\eta_x - h_x\mu_x\right], \tag{39}$$

where h_x is a measure of the fluctuation of the chemical hardness due to a change in the external potential, or through the Maxwell relation, it can be seen as the response of the Fukui function to a change in the total number of electrons:

$$h_x = \left(\frac{\delta\eta_x}{\delta v}\right)_N = \left(\frac{\partial f_x}{\partial N}\right)_v. \tag{40}$$

Determination of the chemical potential and hardness of a composite system from the property of the isolated fragments by means of the above equations produce results that are in very good agreement with the ones determined with other schemes, as can be verified in the next section.

5 Applications.

5.1 Computational Details.

Full geometry optimization for all the species along the reaction coordinates for all the reactions considered in this paper have been performed using the Gaussian 94/98 packages [48,49]. In addition to this, frequency calculations were performed on the reference species and transition states for a complete characterization of these states.

The results for the internal rotation of HXNX (X=O,S) were obtained through DFT(B3LYP) calculations with standard 6–311G** basis sets. For the inversion of diimine, the reaction coordinate is the angle NNH along which we have performed DFT(B3LYP)/6-311G** calculations to determine the profiles of the global properties we are interested in. In this case, we had to perform extra calculations since the standard basis set was not able to give reasonable results for polarizability, to obtain reasonable values for this property, we have used the Sadlej's basis set [50] that is designed to reproduce molecular electric properties, especially polarizabilities. For double proton transfer reactions we present results at the RHF level of theory with the standard 6-311G** basis set.

5.2 Rotational Isomerization of HXNX.

In this section we will discuss results for the *trans* $\rightleftharpoons$ *cis* isomerization reaction of HXNX (X=O,S), Figure 2. Among a number of systems we have studied during the last years, we have chosen nitrous acid HO-NO and its sulfur analogue HS-NS because they are quite simple systems that can undergo rotational isomerization. Besides, compounds containing an S(O)-N bond may serve as a prototype for the S(O)-N linkage in some oximes and inorganic compounds [34,35,51] that we are interested in.

In Figure 3 we display the profiles of energy, chemical potential, hardness and polarizability along the torsional angle defined as the dihedral angle HXNX. Note that the corresponding scales are not explicit to stress the qualitative information that is interesting within the context of this article.

Figure 3 provides an illustration of the validity of the principles of maximum hardness and minimum polarizability in these rotational systems. The energy minimum is associated with a maximum of hardness and a minimum of polarizability whereas the TS is associated with a hardness minimum and a

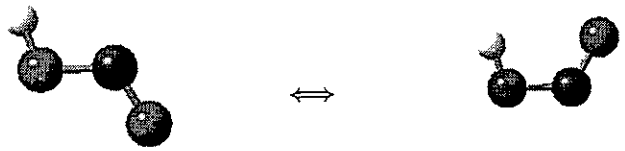

R P

Figure 2. Representation of the conformational equilibrium in the rotational isomerization reaction of HXNX (X=O,S) molecules.

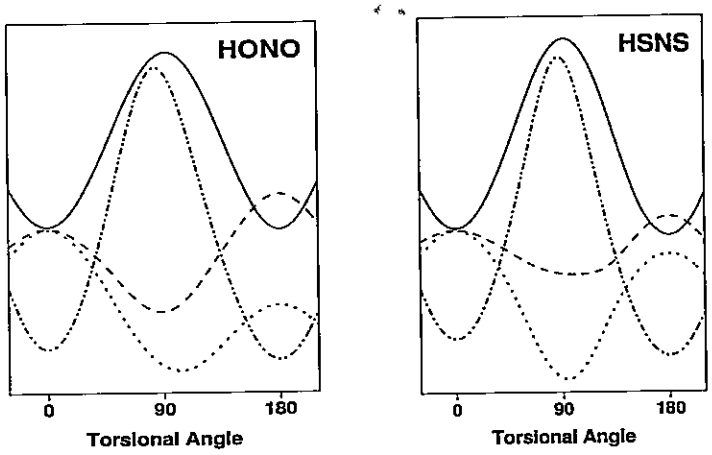

Figure 3. Profiles of energy (—), chemical potential (···), hardness (- - -) and polarizability (-·-·) along the torsional angle for the internal rotation isomerization reaction of HXNX molecules.

maximum of polarizability. In these cases the maximum hardness and minimum polarizability condition nicely complement the minimum energy criterium for molecular stability. In Table 1 (columns two and three) we quoted the characteristic values of the properties under study.

Table 1. Relevant activation and reaction properties for the processes under study (E, μ, and η in kcal/mol; α is in atomic units.)

Properties	HONO	HSNS	HNNH	$(HCOOH)_2$	$(HCSSH)_2$
ΔE°	-0.2396	-1.1207	3.3534	0.0	0.0
$\Delta E^{\neq}$	13.0050	15.3879	49.5864	17.9311	37.3895
$\Delta\mu^{\circ}$	-5.5221	-1.9453	-1.1860	0.0	0.0
$\Delta\mu^{\neq}$	-10.2284	-12.1109	22.6876	-1.7633	-1.9327
$\Delta\eta^{\circ}$	2.5100	1.1295	0.4706	0.0	0.0
$\Delta\eta^{\neq}$	-6.2123	-3.5768	-19.7258	-6.1245	-7.7497
$\Delta\alpha^{\circ}$	-0.1030	-0.4130	0.4670	0.0	0.0
$\Delta\alpha^{\neq}$	2.7100	6.8190	0.2760	1.0890	17.6313

5.3 Intramolecular Rearrangement Reactions.

We refer the reader to the different types of intramolecular rearrangement reactions that we have studied recently, keto–enol and imine–enamine tautomerisation processes have studied in the light of the ideas despicted in this chapter with very encouraging results [52,53]. A number of systems undergoing intramolecular rearrangement have also been studied emphasizing their Hammond or anti–Hammond character in relation with the PMH [54]. Among these rearrangement reactions we want to include in this review the inversion mechanism for the *trans* $\rightleftharpoons$ *cis* isomerization reaction of diimide (HN=NH) that has been for long time a challenging system for theoretical methods. Diimine or diazene is a short lived species that has been identified as one of the decomposition products of the hydrazoic acid and hydrazine reaction. Although diimine cannot be isolated under ordinary conditions, its infrared spectrum suggest that isomerization may occurs through the inversion mechanism [55].

In Figure 4 are displayed the profiles of energy, chemical potential, hardness and polarizability along the inversion coordinate.

The profiles displayed in Figure 4 exhibit the trends that are expected from the PMH and PMP, the TS has been found to be softer and more polarizable than the reference stable conformations. The correctness of the trends shown by the different properties indicate that inversion may be the right mechanism

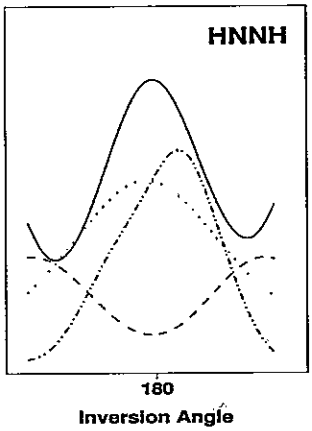

Figure 4. Profiles of energy (—), chemical potential (···), hardness (- - -) and polarizability (-·-·)along the inversion coordinate for the inversion isomerization reaction of diimine.

for isomerization of diimine, the other mechanisms that has been suggested is a rotation around the double bond but it presents a higher energy barrier [39,55].

5.4 Double Proton Transfer in $(HCXXH)_2$.

Proton transfer (PT) is one of the simplest and fundamental reactions in chemistry, it is important in oxidation–reduction reactions occurring in many chemical and biological process. Double proton transfer (2PT) in simple systems has been used to model key properties of many chemically and biologically important multiproton transfer systems.

Recently we have performed an extensive study of 2PT reactions in bimolecular complexes formed by combinations of molecules of the type CHX-YH (X,Y=O,S) We have observed an interesting feature: the energetic properties of all bimolecular complexes lie within an interval whose extrema are defined by the corresponding energetic values of $(HCOOH)_2$ and $(HCSSH)_2$. Therefore in this review we decided to focus our attention on the synchronous 2PT processes occuring in $(HCOOH)_2$ and $(HCSSH)_2$, as indicated schematically

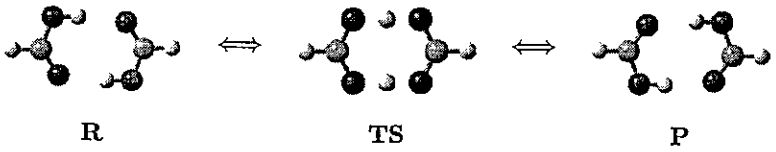

Figure 5. Schematic reaction diagram for double-proton transfer.

in Figure 5.

Characterization of various properties of the transition states of 2PT reactions allows one to identify the specific interactions stabilizing the complexes and helps determine the physical nature of the energy barrier for the simultaneous transfer of two protons. The profiles of E, μ, η and α for double proton transfer of formic acid and dithioformic acid dimers, were obtained through single points calculations of the fully optimized structures indicated by the IRC procedure, they are displayed in Figure 6. We first note that in both reactions μ presents intermediate values between E and η. As can be seen, the profiles of μ decreases to reach a quite flat region around the TS, where three critical points can be perceived. The profiles of η and α indicate the simultaneous validity of the principles of maximum hardness and minimum polarizability. Transition state structures are therefore characterized through a maximum value of energy and polarizability and a minimum value of hardness, as required by the PMH and PMP [43].

In Figure 7 we display the force profiles determined by numeric differentiation of the energy profiles given in Figure 6. Note that $F(\omega)$ is negative in the reactants region and it is positive in the products region, this allows to distinguish the different processes taking place along the reaction coordinate as shown in section 3. It is interesting to note that the force profiles present critical points around the TS, this may be defining regions where the specific interactions and electronic reordering may be of different nature than those encountered at the vicinity of reactants and products. These results suggest that determination of local properties such as electronic population and Fukui functions at the vicinity of the TS may be useful as complementary information for characterizing more specific aspects of the reaction mechanism.

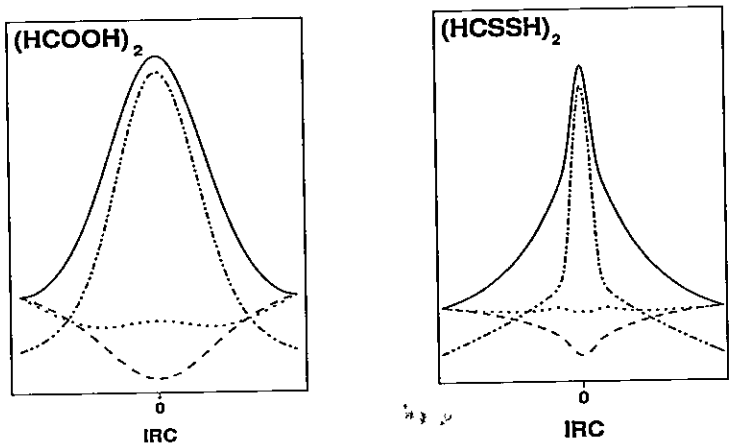

Figure 6. Profiles of E (—), μ ($\cdots$), η (- - -) and α (-·-·-) in 2PT reactions.

5.5 Formation Reactions.

To illustrate the validity of additivity schemes to determine μ and η we are going to review results that we have obtained for the formation of cyclic bimolecular structures which are estabilized by two hydrogen bonds. Combinations of monomeric units of formic (HCO–OH), thione–formic (HCS–OH), thiol–formic (HCO–SH) and dithioformic (HCS–SH) acids, leads to ten cyclic bimolecular complexes, **C1** to **C10**. For the ten resulting bimolecular complexes we have determined μ and η using the different additivity schemes discussed in section 4 with $n_f = 2$, the results are quoted in Tables 2 and 3. Second column contains the *ab initio* reference values. In Table 3 appear two values for the hardness determined from Eqn.(39), since it is no possible to obtain an explicit evaluation of h_x, we first calculated η using $h_x = 0$ (fourth column); a rough estimation of h_x from four symmetric reference dimers was enough to get a new set of hardness values from Eqn.(39), these are quoted in the fifth column of Table 3.

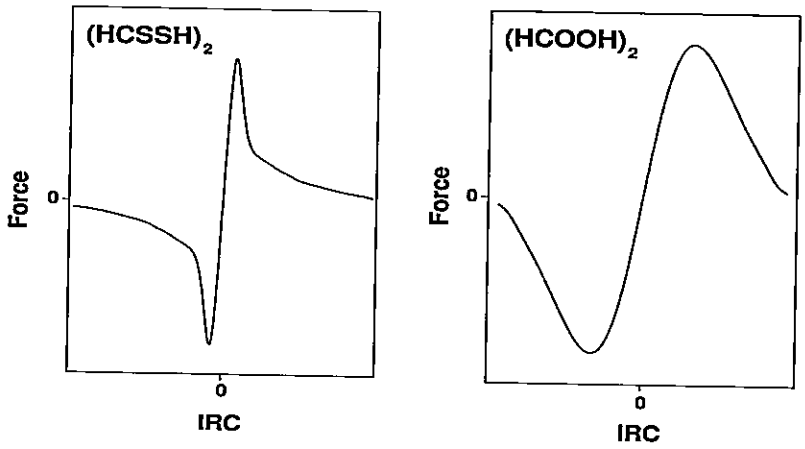

Figure 7. Profiles of the force along the IRC in 2PT reactions.

Table 2. Comparison of aggregate's chemical potential determined from different addition schemes. (All values are in atomic units.)

System	μ	Eq.(34)	Eq.(38)
HCOOH···HCOOH	-0.1503	-0.1554	-0.1554
HCOOH···HCSOH	-0.1411	-0.1476	-0.1463
HCSOH···HCSOH	-0.1462	-0.1402	-0.1402
HCOOH···HCOSH	-0.1402	-0.1470	-0.1456
HCOOH···HCSSH	-0.1601	-0.1543	-0.1540
HCOSH···HCSOH	-0.1320	-0.1397	-0.1396
HCSSH···HCSOH	-0.1604	-0.1466	-0.1471
HCOSH···HCOSH	-0.1331	-0.1391	-0.1391
HCSSH···HCOSH	-0.1511	-0.1460	-0.1466
HCSSH···HCSSH	-0.1576	-0.1532	-0.1532

It can be noticed that in most cases, Eqns. (38) and (39) gives a better approach to the reference *ab initio* value than do the other approaches. We conclude that our additivity scheme for μ and η, which incorporates the fragment condensed fukui function (which is approximated by the electronic population of the fragment), yields consistently better results compared to those obtained

Table 3. Comparison of aggregate's hardness determined from different addition schemes. (All values are in atomic units.)

System	η	Eq.(35)	Eq.(39)	Eq.(39)	Eq.(36)	Eq.(37)
HCOOH···HCOOH	0.3204	0.3138	0.3138	0.3204	0.3138	0.3138
HCOOH···HCSOH	0.2251	0.2652	0.2565	0.2575	0.2591	0.2631
HCSOH···HCSOH	0.2169	0.2206	0.2206	0.2169	0.2206	0.2206
HCOOH···HCOSH	0.2609	0.2863	0.2813	0.2842	0.2849	0.2861
HCOOH···HCSSH	0.2021	0.2563	0.2416	0.2433	0.2440	0.2503
HCOSH···HCSOH	0.2215	0.2408	0.2407	0.2388	0.2390	0.2399
HCSSH···HCSOH	0.1966	0.2108	0.2102	0.2067	0.2096	0.2098
HCOSH···HCOSH	0.2607	0.2608	0.2608	0.2607	0.2608	0.2608
HCSSH···HCOSH	0.2000	0.2319	0.2303	0.2288	0.2261	0.2282
HCSSH···HCSSH	0.1965	0.1996	0.1996	0.1965	0.1996	0.1996

following the other schemes. In fact this brings out the vital importance of the *weight* of the constituent fragments within the composite system. The consequent encouraging results open up the possibility that better approximations of the fukui function can enhance the quality of prediction of global aggregate properties from the constituent fragment properties. Characterization of TS properties using these addition schemes under the constraint imposed by the reactivity models seems to be an interesting subject to explore in the future.

6 Concluding Remarks.

In this paper we wanted to point out that classical concepts of reactivity in connection with DFT descriptors are adequate and powerful tools for characterizing chemical reactions. Within the framework of the Hammond postulate and Marcus equation we have introduced the principle of maximum hardness to check the expected consistency between energetic and electronic properties. A number of useful formulae aimed at rationalizing chemical reactions in terms of the change of relevant electronic properties along the reaction coordinate have been derived and used for understanding the qualitative behavior of processes having different values for the reaction energy. Many of the relationships that have been discussed in this review have been applied with success in the quantitative rationalization of different kind of chemical reactions.

The conceptual classical model used to represents chemical reactions provides

the necessary elements to discuss the activation and relaxation processes in terms of the activation chemical potential and hardness. An important qualitative result of our study is that in a chemical reaction the activation process is controlled by the change in the chemical potential while the relaxation process is controlled by the change in the chemical hardness. We believe that this qualitative observation, although certainly not general, may open new ways to link classical reactivity concepts with the DFT reactivity descriptors.

Acknowledgments. The authors are happy to dedicate this paper to Professor Robert G. Parr in his 80th birthday. This work was supported by Cátedra Presidencial en Ciencias awarded to A.T.L and by FONDECYT through projects No.1990543, 2000050 and 2010139. PJ wish to thank Departamento de Postgrado y Postítulo, Universidad de Chile for financial support through projects PG13/99 and PG20/2000.

7 References.

1. Polanyi, J.C.; Wong, W.H. *J. Chem. Phys.*, **1969**, 51, 1439.
2. Hodgson, B.A.; Polanyi, J.C. *J. Chem. Phys.*, **1971**, *55*, 4745.
3. Levine, R.D.; Bernstein, R.B. *Molecular Reaction Dynamics and Chemical Reactivity*, Oxford University Press: New York **1987**.
4. See for example: Pross, A., *Theoretical and Physical Principles of Organic Reactivity*, John Wiley, New York **1995**.
5. Parr, R.G.; Yang, W. *Density Functional Theory of Atoms and Mole cules*, Oxford University Press: New York **1989**.
6. Dreizler, R.M.; Gross, E.K.V. *Density Functional Theory*, Springer, Berlin **1990**.
7. Sen, K.D. (Editor), *Structure and Bonding 80: Chemical Hardness*, Springer-Verlag, Berlin **1993**.
8. Koch, W.; Holthausen, M.C. *A Chemist's Guide to Density Functional Theory*, Wiley-VCH, Weinheim **2000**.
9. Hammond, G.S. *J. Am. Chem. Soc.*, **1955**, 77, 334.
10. Leffler, J.E. *Science*, **1953**, 117, 340.
11. For a complete discussion of the significance of the Brønsted coefficient see: Pross, A.; Shaik, S.S. *New J. Chem.*, **1989**, 13, 427.
12. Marcus, R.A. *Annu. Rev. Phys. Chem.*, **1964**, *15*, 155.
13. Pearson, R.G. *Chemical Hardness: Applications from Molecules to Solids*; Wiley–VCH Verlag GMBH: Weinheim, **1997**.
14. Pearson, R.G. *J. Chem. Educ.*, **1987**, 64, 561; *Acc. Chem. Res.*, **1993**, 26, 250.
15. Parr, R.G.; Chattaraj, P.K. *J. Am. Chem. Soc.*, **1991**, 113, 1854.; Chattaraj, P.K.; Liu, G.H.; Parr, R.G. *Chem. Phys. Lett.*, **1995**, 237, 171.; Chattaraj, P.K. *Proc. Indian Natl. Sci. Acad.- Part A*, **1996**, 62, 513.
16. Datta, D. *J. Phys. Chem.*, **1992**, 96, 2409.

17. Gutiérrez-Oliva, S.; Letelier, J.R.; Toro–Labbé, A. *Mol. Phys.*, **1999**, 96, 61.

18. Parr, R.G., Chattaraj, P.K. *J. Am. Chem. Soc.*, **1991**, 113, 1854; Chattaraj, P.K.; Nath, S.; Sannigrahi, A.B. *J. Phys. Chem.*, **1994**, 98, 9143.

19. Hohenberg, P.; Kohn, W. *Phys. Rev. B*, **1964**, 136, 834.

20. Kohn, W.; Sham, L. J. *Phys. Rev.*, **1965**, 140, A1133.

21. Parr, R.G.; Donnelly, R. A.; Levy, M.; Palke, W. E. *J. Chem. Phys.*, **1978**, 68, 3801.

22. Parr, R.G.; Pearson, R.G. *J. Am. Chem. Soc.*, **1983**, 105, 7512.

23. Pearson, R.G. *Inorg. Chem.*, **1988**, 27, 734.; Pearson, R.G. *J. Am. Chem. Soc.*,**1988**, 110, 7684.

24. Parr, R.G.; Yang, W. *J. Am. Chem. Soc.*, **1984**,106, 4049.

25. Yang, W.; Parr, R.G. *Proc. Natl. Acad. Sci. USA*, **1985**, 82, 6723.

26. Fuentealba, P.; Parr, R.G. *J. Chem. Phys.*, **1991**, 94, 5559.

27. Chermette, H. *J. Comp. Chem.*, **1999**, 20, 129; De Proft, F.; Geerlings, P. *Chem. Rev.*, **2001**, 101, 1451.; Ayers, P.W.; Parr, R.G. *J. Am. Chem. Soc.*, **2000**, 122, 2010.

28. Chattaraj, P.K.; Sengupta, S., *J. Phys. Chem.*, **1996**, 100, 16126; Chattaraj, P.K.; Poddar, A. *J. Phys. Chem. A*, **1998**, 102, 9944; Chattaraj, P.K.; Poddar, A. *J. Phys. Chem. A*, **1999**, 103, 1274.

29. Chattaraj, P.K.; Fuentealba, P.; Jaque, P.; Toro–Labbé, A. *J. Phys. Chem. A.* **1999**, 103, 9307.; Torrent-Sucarrat, M.; Luis, J.M.; Duran, M.; Solà, M. *J. Am. Chem. Soc.*, **2001**, 103, 7951.

30. Parr, R.G.; Zhou, Z. *Acc. Chem. Res.*, **1993**, 26, 252.; Pearson, R.G. *J. Am. Chem. Soc.*, **1985**, 107, 6801.

31. Fukui, K. *J. Phys. Chem.*, **1970**, 74, 4161.; Fukui, K. *Acc. Chem. Res.*, **1981**, 14, 363.

32. Gonzalez, C.; Schlegel, H.B. *J. Chem. Phys.*, **1989**, 90, 2154.

33. Gonzalez, C.; Schlegel, H.B. *J. Phys. Chem.*, **1990**, 94, 5523.

34. Cárdenas-Jirón, G.I.; Letelier, J.R.; Maruani, J.; Toro-Labbé, A. *Mol. Eng.*, **1992**, 2, 17.

35. Cárdenas-Jirón, G.I.; Toro-Labbé, A.; Bock, Ch. W.; Maruani, J. *In Structure and Dynamics of Non-Rigid Molecular Systems*; Smeyers, Y.G. Ed; Kluwer Academic Publisher: Dordrecht, **1994**, 97.

36. Cárdenas-Lailhacar, C.; Toro-Labbé, A. *Theor. Chim. Acta*, **1990**, 76, 411.; Bock, Ch. W.; Toro-Labbé, A. *THEOCHEM* , **1991**, 232, 239.

37. Cárdenas-Jirón, G.I.; Lahsen, J.; Toro–Labbé, A. *J. Phys. Chem.*, **1995**, 99, 5325.

38. Cárdenas-Jirón, G.I.; Toro–Labbé, A. *J. Phys. Chem.*, **1995**, 99, 12730.

39. Cárdenas-Jirón, G.I.; Gutiérrez-Oliva, S.; Melin, J.; Toro–Labbé, A. *J. Phys. Chem. A*, **1997**, 101, 4621.

40. Toro–Labbé, A. *J. Phys. Chem. A*, **1999**, 103, 4398.

41. Sanderson, R.T. *Science*, **1955**, 121, 207.; Sanderson, R.T. *Chemical Bonds and Bond Energy*, 2nd Ed., Academic Press: New York **1976**.

42. Cárdenas-Jirón, G.I.; Toro–Labbé, A. *J. Mol. Struct. (Theochem)*, **1997**, 390, 79.

43. Jaque, P.; Toro–Labbé, A. *J. Phys. Chem. A*, **2000**, 104, 995.

44. Yang, W.; Lee, C.; Ghosh, S.K. *J. Phys. Chem.*, **1985**, 89, 5412.

45. Chattaraj, P.K.; Nandi, P.K.; Sannigrahi, A. B. *Proc.-Indian Acad. Sci. Chem.*, **1991**, 103, 583.

46. Gutiérrez-Oliva, S.; Jaque, P., Toro-Labbé, A. *J. Phys. Chem. A*, **2000**, 104, 8955.

47. Sengupta, S.; Toro-Labbé, A. *J. Phys. Chem. A*, submitted.

48. Gaussian 94, Frisch, J.M.; Trucks, G.W., Schlegel, H.B. et al. Gaussian Inc., Pittsburgh PA, **1995**.

49. Gaussian 98, Revision A-9 Frisch, J.M.; Trucks, G.W., Schlegel, H.B. et al. Gaussian Inc., Pittsburgh PA, **1998**.

50. Sadlej, A.J. *Collect. Czech. Chem. Commun.*, **1988**, 53, 1995.

51. Chattaraj, P.K.; Gutiérrez-Oliva, S.; Jaque, P., Toro-Labbé, A. to be published.

52. Pérez, P.; Toro–Labbé, A. *J. Phys. Chem. A*, **2000**, 104, 1557.

53. Pérez, P.; Toro–Labbé, A. *Theor. Chem. Acc.*, **2001**, 105, 422.

54. Solà, M.; Toro–Labbé, A. *J. Phys. Chem. A*, **1999**, 103, 8847.

55. Chattaraj, P.K.; Zevallos, Y.; Pérez, P.; Toro–Labbé, A. *J. Phys. Chem. A*, **2001**, 105, 4272.

MOLECULAR PHYSICS, 2003, VOL. 101, NO. 18, 2841–2853

Taylor & Francis
Taylor & Francis Group

Towards understanding the molecular internal rotations and vibrations and chemical reactions through the profiles of reactivity and selectivity indices: an *ab initio* SCF and DFT study

PRATIM K. CHATTARAJ[1]*, SOLEDAD GUTIÉRREZ-OLIVA[2], PABLO JAQUE[2] and ALEJANDRO TORO-LABBÉ[2]*

[1]Department of Chemistry, Indian Institute of Technology, Kharagpur, 721 302, India

[2]Laboratorio de Química Teórica Computacional (QTC), Departamento de Química Física, Facultad de Química, Pontificia Universidad Católica de Chile, Casilla 306, Correo 22, Santiago, Chile

(*Received 24 January 2003; revised version accepted 23 May 2003*)

Ab initio SCF and DFT(B3LYP) calculations are performed with 6-311G** basis sets for obtaining insights into molecular internal rotations in HXNX (X=O,S), different vibrational modes in water and double proton transfer reaction in $(HONO)_2$. While chemical reactivity is analyzed in terms of the profile of the global reactivity parameters, such as energy, chemical potential, hardness, polarizability, molecular valency and electrophilicity indices, the site selectivity is understood through the variations in local descriptors, such as the Fukui function and atomic valency. Principles of maximum hardness and molecular valency and the minimum polarizability principle are found to be valid in almost all cases. Rotational isomerization reactions can be better characterized by making use of the maximum hardness principle along with Hammond's postulate. Extremum points in electrophilicity during internal rotations, vibrations and chemical reaction can be located from those of chemical potential and hardness. The Fukui function and atomic valency show inverse behaviour in most cases.

1. Introduction

Density functional theory (DFT) [1, 2] has been quite successful in providing a theoretical basis for popular qualitative chemical concepts, such as electronegativity (χ) [3, 4] and hardness (η) [5, 6]. Pauling [3] introduced the concept of electronegativity as 'the power of an atom in a molecule to attract electrons to itself'. 'All the constituent atoms in a molecule have the same electronegativity value which is roughly equal to the geometric mean of the electronegativities of the corresponding isolated atoms', according to Sanderson's electronegativity equalization principle [7]. The idea of hardness was put forward by Pearson [5, 8] in his famous hard–soft acids and bases (HSAB) [5, 7] principle which states that 'among potential partners of equal electronegativity hard likes hard and soft likes soft'. Another hardness-related principle is the maximum hardness principle (PMH) [10, 11] whose statement is 'there seems to be a rule of nature that molecules arrange themselves so as to be as hard as possible'. Polarizability (α) was one of the most important properties on which the concepts of hardness and softness were originally developed [5, 6]: a hard species is less polarizable and a soft species is more polarizable. Based on this inverse relationship [12] between α and η, a minimum polarizability principle (MPP) [13, 14] has been proposed which states that [13] 'the natural direction of evolution of any system is toward a state of minimum polarizability'. It has also been shown [15] that 'a system is harder and less polarizable in its ground state than in any of its excited states'. Molecular valency [16, 17] (V) also often becomes maximum for the most stable configuration/conformation.

As a complement to the above-mentioned global reactivity indices, local reactivity descriptors usually condensed to an atom, such as the Fukui function ($f_k^{\pm}$), local softness (s_k), electrophilicity index (ω_k) and atomic valency (V_k), are necessary for explaining site selectivity in a molecule and identify specific interactions which characterize the reaction mechanisms [2, 8, 18].

*Authors for correspondence. e-mail: pkc@chem.iitkgp.ernet.in; atola@puc.cl

Molecular Physics ISSN 0026–8976 print/ISSN 1362–3028 online © 2003 Taylor & Francis Ltd
http://www.tandf.co.uk/journals
DOI: 10.1080/0026897032000112900

In the present work the internal rotations and resulting rotational isomerization in HXNX (X=O,S), different symmetric and asymmetric vibrational modes of water and the intermolecular double proton transfer reaction in $(HONO)_2$ are studied at the *ab initio* SCF level as well as using DFT. Profiles of reactivity indices, such as μ, η, α and V, and the relevant selectivity indices, such as $f_k^{\pm}$ and V_k for the above-mentioned processes, are characterized and discussed in the light of reactivity-selectivity principles.

In section 2, we present the theoretical background necessary to follow the forthcoming analysis, details of computations are presented in section 3 while section 4 deals with the results and discussion. Finally section 5 contains our concluding remarks.

2. Theoretical background

2.1. *Chemical reactivity*

Electronegativity (χ) and hardness (η) have been defined respectively as the following first-order and second-order derivatives for an N-electron system with total energy E,

$$\chi = -\mu = -\left(\frac{\partial E}{\partial N}\right)_{\upsilon(\mathbf{r})} \tag{1}$$

and

$$\eta = \frac{1}{2}\left(\frac{\partial^2 E}{\partial N^2}\right)_{\upsilon(\mathbf{r})}, \tag{2}$$

where $\upsilon(\mathbf{r})$ is the external potential which is produced by external charges to the system of electrons; μ is the chemical potential, that is a Lagrange multiplier associated with the normalization constraint of DFT [1, 2]. Recently Parr *et al.* [19] have provided the following definition for the electrophilicity index (ω)

$$\omega = \frac{\mu^2}{2\eta}, \tag{3}$$

which measures the energy stabilization upon electronic saturation of the system, when electrons flow from the surroundings with a higher chemical potential than that of the system. These global reactivity parameters and the associated electronic structure principles have been very helpful in understanding chemical reactivity and form the backbone of any reactivity theory [20].

2.2. *Site selectivity*

Local reactivity descriptors like the Fukui function ($f(\mathbf{r})$) and local softness ($s(\mathbf{r})$) are necessary for explaining site selectivity in a molecule. The Fukui function is defined as [18]

$$f(\mathbf{r}) = \left(\frac{\delta\mu}{\delta\upsilon(\mathbf{r})}\right)_N = \left(\frac{\partial\rho(\mathbf{r})}{\partial N}\right)_{\upsilon(\mathbf{r})}; \tag{4}$$

in the absence of orbital relaxation it becomes just the density of the frontier molecular orbital and makes a bridge between Fukui's frontier orbital theory [21] and DFT [1, 2]. Owing to the discontinuity [22] of the derivative $(\partial\rho(\mathbf{r})/\partial N)_{\upsilon(\mathbf{r})}$ at an integral value of N, three different types of $f(\mathbf{r})$ can be defined as follows:

$$\begin{aligned} f^+(\mathbf{r}) &= \left(\frac{\partial\rho(\mathbf{r})}{\partial N}\right)^+_{\upsilon(\mathbf{r})} \approx [\rho_{N+1}(\mathbf{r}) - \rho_N(\mathbf{r})] \approx \rho_L(\mathbf{r}), \\ f^-(\mathbf{r}) &= \left(\frac{\partial\rho(\mathbf{r})}{\partial N}\right)^-_{\upsilon(\mathbf{r})} \approx [\rho_N(\mathbf{r}) - \rho_{N-1}(\mathbf{r})] \approx \rho_H(\mathbf{r}), \\ f^o(\mathbf{r}) &= \frac{1}{2}[f^+(\mathbf{r}) + f^-(\mathbf{r})]; \end{aligned} \tag{5}$$

at point $\mathbf{r}$, $f^+(\mathbf{r})$ measures reactivity toward a nucleophilic attack, $f^-(\mathbf{r})$ measures reactivity toward an electrophilic attack and $f^o(\mathbf{r})$ measures reactivity toward a radical attack. Connection with the frontier orbital theory is achieved through $\rho_H(\mathbf{r})$ and $\rho_L(\mathbf{r})$, the frontier orbitals (HOMO and LUMO) densities. With all other factors remaining the same, the maximum value of the Fukui function at a given site would be preferred by a reagent because that will cause the largest change in the chemical potential as indicated in equation (4) [2, 18]. The above quantities can also be condensed to an atom k in a molecule in terms of the population on that atom [23], namely,

$$\begin{aligned} f_k^+ &= \int_k [\rho_{N+1}(\mathbf{r}) - \rho_N(\mathbf{r})]\,d\mathbf{r} = [q_k(N+1) - q_k(N)], \\ f_k^- &= \int_k [\rho_N(\mathbf{r}) - \rho_{N-1}(\mathbf{r})]\,d\mathbf{r} = [q_k(N) - q_k(N-1)], \\ f_k^o &= \frac{1}{2}[f_k^+ + f_k^-] = \frac{1}{2}[q_k(N+1) - q_k(N-1)]. \end{aligned} \tag{6}$$

Within the frozen core approximation, these quantities can also be condensed by considering only the contributions of the frontier orbitals on a given atom, thus leading to [24]:

$$\begin{aligned} f_k^+ &= \int_k \rho_L(\mathbf{r})\,d\mathbf{r} = \rho_k^L, \\ f_k^- &= \int_k \rho_H(\mathbf{r})\,d\mathbf{r} = \rho_k^H, \\ f_k^o &= \frac{1}{2}[f_k^+ + f_k^-] = \frac{1}{2}[\rho_k^L + \rho_k^H], \end{aligned} \tag{7}$$

where ρ_k^L and ρ_k^H are the electronic population on atom k associated with the frontier orbitals LUMO and

HOMO, respectively. Local softness can be defined as [25]

$$s(\mathbf{r}) = f(\mathbf{r}) \cdot S, \tag{8}$$

where the global softness (S) is given by [26]

$$S = \frac{1}{2\eta}. \tag{9}$$

Different variants of local softness and their condensed-to-atom variants can be obtained by substituting $f(\mathbf{r})$ or f_k from equations (5) and (6), respectively. A local version of the HSAB principle is also known [27, 28]. Klopman [29] has shown that the hard–hard interactions are predominantly ionic in nature and hence 'charge-controlled', whereas the soft–soft interactions are mainly covalent in nature and hence 'frontier-controlled'. These local quantities and the related structure principles are important in analyzing the preferred site of attack as well as the type of attack by a reagent [20].

On the other hand, ω, equation (3), can also be written in terms of local contributions through the softness, equation (9), which can be written as a sum of local condensed contributions centred on the different atoms in the molecule ($S = \sum s_k$):

$$\omega = \frac{\mu^2}{2\eta} = \mu^2 \cdot S = \mu^2 \cdot \sum_k s_k = \sum_k \omega_k, \tag{10}$$

with $\omega_k = \mu^2 \cdot s_k$ being the local electrophilicity power associated with centre k.

Chemical processes produce changes in the electronic distribution on different regions of the molecular topology; Fukui functions, as well as local softness and electrophilicity, are good measures for the electronic distribution at a given atomic centre within the molecule. Complementary to these site reactivity indices, the atomic valency (V_k) provides a measure of the localization of electron density at the bond regions associated with an atom; it is calculated by adding the off-diagonal elements of the first-order density matrix as [16]:

$$V_k = \sum_{\ell \neq k} \left[\sum_{a \in k} \sum_{b \in \ell} D_{ab} D_{ba} \right], \tag{11}$$

thus giving a measure of the covalent bonds borne by atom k within the molecule. The V_k values of an atom are always very close to their classical valency although they may fluctuate from molecule to molecule. Deviations from the classical valency integer value are mainly due to the ionic character of the bond formed by atoms of different electronegativities [16, 17]. Following Klopman's observation about specific local interactions [29], a reactive centre in local soft–soft interactions is expected to be associated with a minimum value of V_k (a maximum deviation from the classical valency) whereas for hard–hard interactions a maximum value of V_k (a minimum deviation from the classical valency) should be in order.

The molecular valency (V) is obtained as

$$V = \frac{1}{2} \sum_k V_k \tag{12}$$

and is a measure of the covalent bonds within the molecule; a molecule described by covalent or slightly polar covalent bonds in its minimum energy conformation is expected to present a maximum value of V [17].

It is important to know how these reactivity and selectivity parameters vary during the progress of a physico-chemical process like molecular internal rotations, molecular vibrations or chemical reactions.

2.3. *Characterization of transition states*

To characterize the energy of transition states (TS) in internal rotations and proton transfer processes we use the Marcus equation (ME) [30]:

$$\Delta E^{\neq} = \Delta E_0^{\neq} + \frac{1}{2}\Delta E^{\circ} + \frac{(\Delta E^{\circ})^2}{16 \Delta E_0^{\neq}}, \tag{13}$$

where $\Delta E_0^{\neq}$ is the intrinsic energy barrier which can be determined by solving the second-degree equation resulting from rearrangement of equation (13) and using the calculated values of $\Delta E^{\neq}$ and ΔE°, which is the reaction energy. Note that for symmetric reactions $\Delta E^{\circ} = 0$ and the energy barrier reduces to $\Delta E_0^{\neq}$ [31]. The ME has been used successfully in the rationalization of activation energies in different kinds of chemical reactions [31]. In particular, within the framework of the Hammond postulate [32], the Marcus equation can be used to determine the position of the transition state along the reaction coordinate. This can be achieved by using the Brønsted coefficient which, following the Leffler postulate [33], is defined as the derivative of the activation energy with respect to the reaction energy [31]:

$$\beta \equiv \left(\frac{\mathrm{d}\Delta E^{\neq}}{\mathrm{d}\Delta E^{\circ}} \right) = \frac{1}{2} + \frac{\Delta E^{\circ}}{8 \Delta E_0^{\neq}}. \tag{14}$$

In symmetric reactions ($\Delta E^{\circ} = 0$), the TS is located exactly midway between reactants and products ($\beta = 0.50$) whereas for exothermic reactions ($\Delta E^{\circ} < 0$) $\beta < 0.50$ indicating that the TS is closer to reactants and $\beta > 0.50$ for endothermic reactions ($\Delta E^{\circ} > 0$) indicating that the TS is closer to the products, in agreement with the Hammond postulate [20, 31, 32].

3. Details of computation

A three-point finite difference approximation to the derivatives in equations (1) and (2) gives [2, 8]

$$\mu = -\frac{1}{2}(I + A) \tag{15}$$

and

$$\eta = \frac{1}{2}(I - A), \tag{16}$$

where I and A are the ionization potential and electron affinity, respectively. Further use of Koopman's theorem provides [34]:

$$\mu = \frac{1}{2}(\varepsilon_L + \varepsilon_H) \tag{17}$$

and

$$\eta = \frac{1}{2}(\varepsilon_L - \varepsilon_H), \tag{18}$$

where ε_L and ε_H are the lowest unoccupied and highest occupied molecular orbital energies, respectively. The μ and η values are calculated using equations (17) and (18) and in certain cases equations (15) and (16) were used for comparison purposes. The electrophilicity index and the molecular valency are obtained from equations (3) and (12), respectively.

Condensed-to-atom Fukui functions are obtained using the corresponding electronic population in equations (6) and (7); atomic valencies (V_k) were calculated by adding the off-diagonal matrix elements of the bond order matrix, equation (11).

In the present work we study internal rotations in HONO and HSNS, molecular vibrations in H_2O and the double proton transfer reaction in $(HONO)_2$; these processes are illustrated in figure 1. All the calculations have been carried out at the *ab initio* SCF level with the standard 6-311G** basis set occasionally suplemented by additional diffuse functions 6-311++G**. The DFT calculations are performed with B3LYP exchange-correlation functionals [35, 36] and 6-311G** basis set. Geometry optimization and frequency calculation (mainly to check the number of imaginary frequencies) are accomplished with the Gaussian 98 program [37]. Polarizability is calculated using both Pople's and Sadlej's [38] basis set. The profiles for the chemical reactions of different global reactivity indices E, μ, η, α, V and ω are obtained through single point calculations of the fully optimized structures previously determined during the intrinsic reaction coordinate (IRC) procedure [39, 40].

4. Results and discussion

4.1. *Rotational isomerization of HXNX (X=O,S)*

4.1.1. *Chemical reactivity*

Figure 1 (*a*) illustrates the *trans* ⇔ *cis* isomerization of HXNX, X=O,S. Table 1 presents various global reactivity parameters, namely, E, μ (calculated using equations (15) and (17)), η (calculated using equations (16) and (18)), V, $\langle\alpha\rangle$, its out-of-plane component α_{zz} and the dipole moment (DM) for the reactant, transition state and products associated with the rotational isomerization of HONO and HSNS at HF/6-311G** and B3LYP/6-311G** levels. Polarizability values calculated using both Pople's and Sadlej's basis sets are reported. In all cases the reactant and product have no imaginary frequencies whereas the transition state has one imaginary frequency, as expected. At the HF and DFT levels considered here, the *trans* ⇔ *cis* rotational isomerization of HONO and HSNS are thermodynamically favourable, in both cases the *cis* conformer being slightly more stable than the *trans* isomer.

In both cases the transition state corresponds to maximum energy, minimum hardness and minimum molecular valency values vindicating the validity of the principle of maximum hardness (PMH) and the maximum molecular valency principle (MMVP). The μ and η values calculated using either the finite difference approximation (equations (15) and (16)) or the frontier orbitals energies (equations (17) and (18)) show similar trends.

For HONO $\langle\alpha\rangle$ is maximum at the TS but it is minimum at the transition state of HSNS, a case already pointed out [41] in the context of internal rotation of formamide and thioformamide. Based on the prescription of Ghanty and Ghosh [41] we also present the zz component of α calculated using Pople's as well as Sadlej's basis sets. The α_{zz} values for transition states of all the internal rotations calculated at all levels of theory are larger than the corresponding reactant and product values which can be considered to be a signature of the minimum polarizability principle (MMP). Note that the α_{zz} component refers to the out-of-plane (perpendicular) component for the reactant, the transition state and the product. In all cases (α_{zz}) using the Pople and Sadlej's basis sets provide identical trends, *trans* -HONO is more polar than *cis* -HONO but *cis* -HSNS is more polar than *trans* -HSNS.

Torsional potential energy and electronic properties were evaluated in 10° increments along the torsional angle θ within the interval $0° \leq \theta \leq 180°$. Figure 2 depicts the resulting qualitative profiles at the Hartree–Fock level of E, μ (equation (17)), η (equation (18)), V, $(\alpha_{zz})_{Sadlej}$ and ω for the internal rotations in HONO (figure 2 (*a*)) and HSNS (figure 2 (*b*)). The B3LYP/

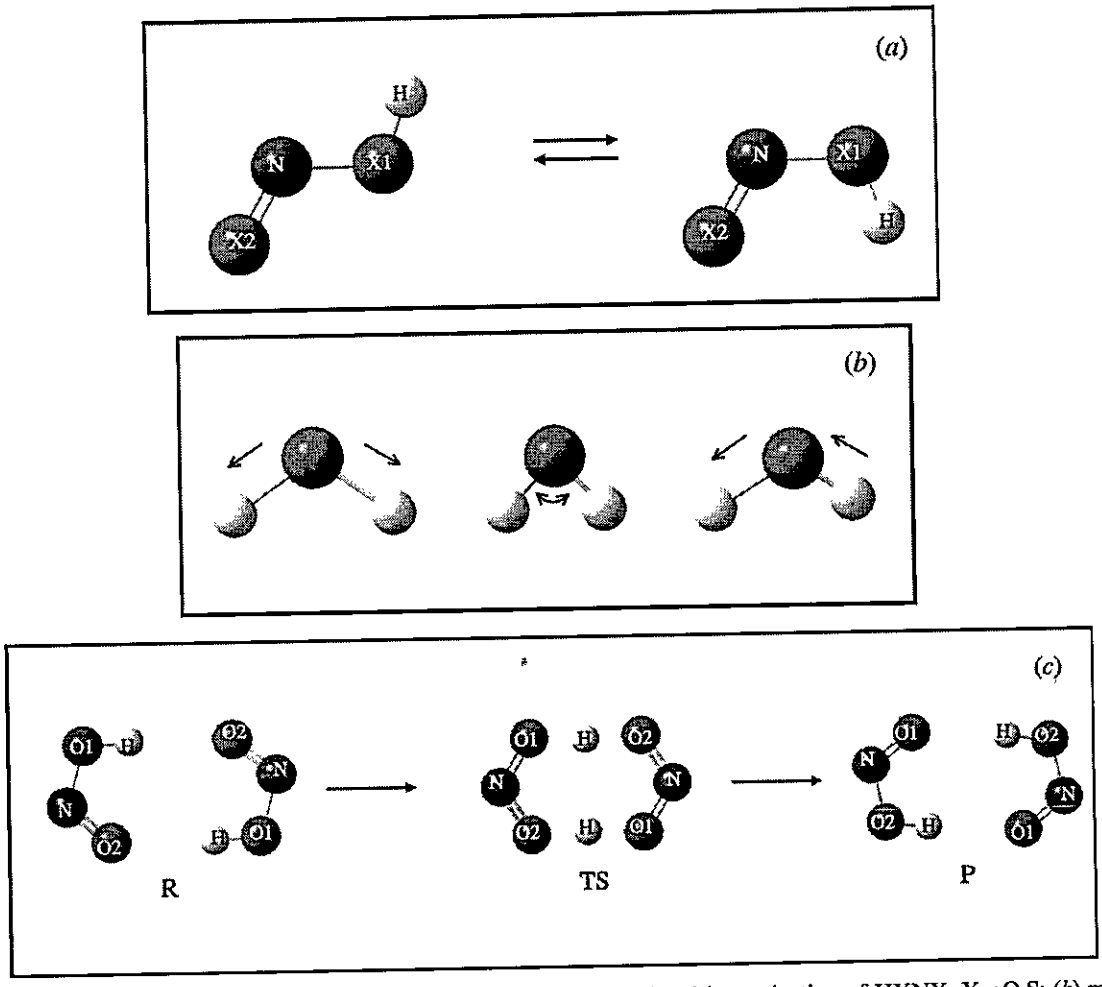

Figure 1. Illustration of the processes studied: (*a*) the *trans* ⇔ *cis* rotational isomerization of HXNX, X=O,S; (*b*) molecular vibration of the water molecule and (*c*) the double proton transfer reaction in $(HONO)_2$.

Table 1. Global properties at the stationary points for the isomerization reaction of HONO and HSNS. First entry corresponds to the HF results whereas the second entry displays the DFT results. (E, $\langle\alpha\rangle$ and α_{zz} are in au; μ and η in eV; DM is in Debye.)

	E	μ (equation 15)	μ (equation 17)	η (equation 16)	η (equation 18)	$\langle\alpha\rangle$	α_{zz}	V	DM
HONO									
trans	−204.700158	−4.3542	−4.4627	6.1825	7.7635	13.448	7.488	3.7597	2.5469
($\theta=0$)	−205.761769	−7.1580	−5.1239	8.1045	2.6803	15.352	7.806	3.9783	2.0645
TS($\theta=92.6$)	−204.682531	−6.0247	−4.8028	4.8137	7.5213	13.535	9.477	3.6886	1.8656
TS($\theta=92.5$)	−205.741044	−5.9158	−5.5675	5.6491	2.4109	15.334	10.516	3.8779	1.6155
cis	−204.701446	−4.6280	−4.7811	6.2477	7.9104	13.268	7.402	3.7497	1.5730
($\theta=180$)	−205.762150	−5.4478	−5.3634	6.2392	2.7892	15.110	7.703	3.9815	1.5151
HSNS									
trans	−850.021798	−5.0664	−4.4736	4.2301	4.8546	40.576	19.690	3.7540	1.9299
($\theta=0$)	−851.727234	−5.1876	−4.8872	3.9436	1.3062	43.653	20.249	3.9734	2.1297
TS($\theta=93.8$)	−850.001284	−4.7842	−4.7539	3.5933	4.7403	37.645	25.386	3.6253	1.7356
TS($\theta=92.7$)	−851.702711	−6.0386	−5.4124	4.1972	1.1511	42.099	27.068	3.8109	1.6378
cis	−850.022786	−5.1513	−4.5764	4.2442	4.8850	40.189	19.316	3.7627	2.2822
($\theta=180$)	−851.729019	−6.5095	−4.9716	5.2023	1.3551	43.380	19.836	3.9993	2.3820

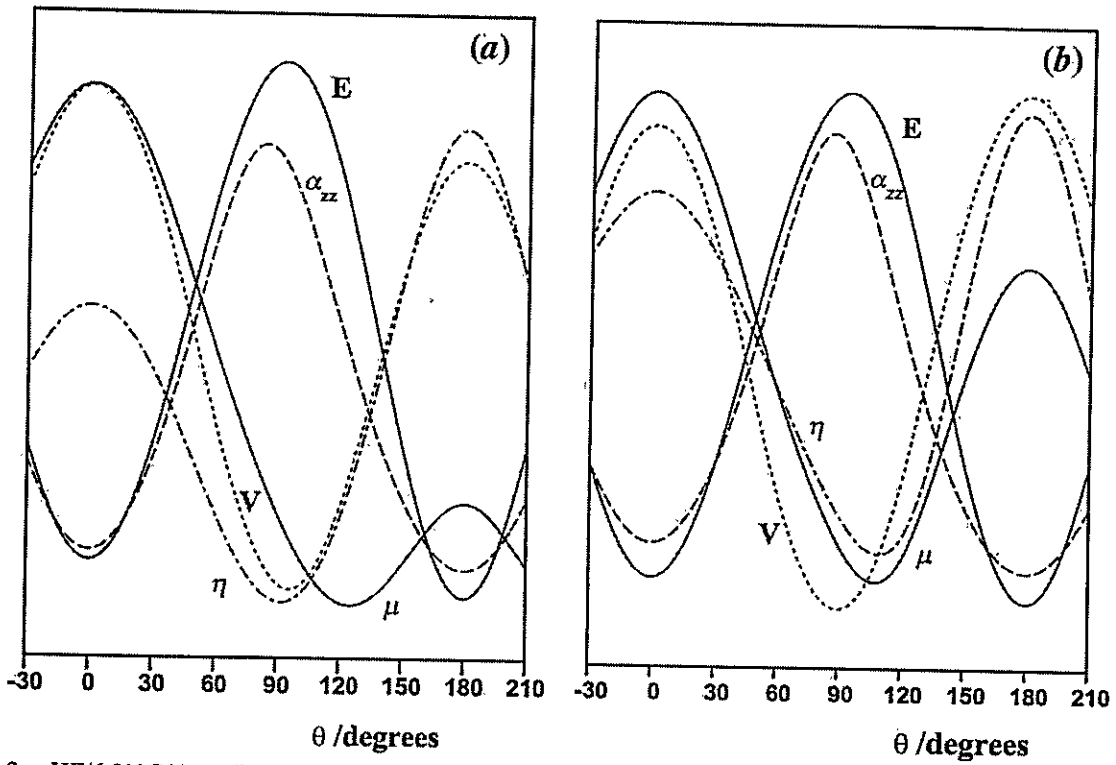

Figure 2. HF/6-311G** qualitative profiles along the torsional coordinate of global reactivity properties of (*a*) HONO and (*b*) HSNS. Representative numerical values for these properties are given in tables 1 and 2.

Table 2. Activation properties of the isomerization reaction of HONO and HSNS. All values are in kcal mol^{-1}.

	ΔE^o	$\Delta E^{\neq}$	$\Delta\mu^o$	$\Delta\mu^{\neq}$	$\Delta\eta^o$	$\Delta\eta^{\neq}$	β
HONO							
HF	−0.8082	11.0611	−7.3424	−7.8428	3.3876	−5.5852	0.4912
DFT	−0.2391	13.0051	−5.5230	−10.2296	2.5113	−6.2125	0.4977
HSNS							
HF	−0.6200	12.8728	−2.3706	−6.4638	0.7010	−2.6358	0.4941
DFT	−1.1201	15.3884	−1.9463	−12.1113	1.1277	−3.5767	0.4912

6-311G** profiles show the same trends for most properties and therefore are not included in the figure. As already mentioned, in or around the TS, E, α_{zz} and ω are maxima and μ, η and V are minima for all cases, validating PMH, MPP and MMVP. Within this frame, extremization of ω can be analyzed in terms of the same for μ and η: extremals (maximum or minimum) for μ and η correspond to an extremal in ω. Specifically the point at which both μ and η are maxima (minima), ω would be a minimum (maximum). The exact location of the extrema in ω would also be governed by the corresponding extremal locations in μ and η.

Table 2 provides relative values at HF/6-311G** and B3LYP/6-311G** levels of the energy ($\Delta E°$ and $\Delta E^{\neq}$) chemical potential ($\Delta\mu°$ and $\Delta\mu^{\neq}$) and hardness ($\Delta\eta°$ and $\Delta\eta^{\neq}$), these latter quantities being calculated using equations (17) and (18). Also included in the table is the Brønsted coefficient β (equation (14)) which indicates whether the TS is closer to the reactant or the product. As pointed out earlier by Toro-Labbé and co-workers [31], for any reaction the product is the hardest species for the Hammond-type reaction while the reactant is the harder for an anti-Hammond-type reaction. The rotational isomerizations in HONO and HSNS are of Hammond type, both reactions are exoenergetic ($\Delta E° < 0$) and $\beta < 0.5$, in agreement with the simultaneous validity of the PMH and the Hammond postulate.

It is interesting to note that at both HF and DFT levels, the torsional barriers of HONO and HSNS are quite close to each other, in both calculations HSNS

presenting a slightly higher value of $\Delta E^{\neq}$ than HONO. This is indicating that the nature of the torsional barrier is quite the same for both isomerization reactions. On the other hand, it should be mentioned that zero point energy (ZPE) corrections have no noticeable effect on the barriers given in table 2.

4.1.2. *Site selectivity*

The profiles of site selectivity indices are displayed in figure 3. Condensed Fukui functions (f_k) were determined using equations (7) which in most cases also assume their extremum values in or around the TS; the same trends are observed when using the finite difference approximation of equations (6). Atomic valencies remain quite constant along the reaction coordinate with the exception of V_{O1} in HONO and V_{S1} in HSNS which present minima at the TS. This confirms the above observation about the common nature of the torsional potential barrier of HONO and HSNS. As for the atomic valencies, Fukui functions are not strongly dependent on the torsional angle; the most remarkable changes of the Fukui function along θ are observed in the electrophilic functions of the oxygen atoms and they are nicely opposite as expected. Besides, most reactivity pattern for electrophilic or nucleophilic attacks remains quite constant along θ.

It is interesting to note that the V_{XI} profiles are inverse to those of f_{XI}^-. This fact may be explained as follows: since all V_ks are positive and the maximum value of V implies stability, a larger V_k site is supposed to be less reactive, which is the reverse of the situation if the site has larger f_k since that implies more reactivity [2, 18].

4.2. *Molecular vibrations*

4.2.1. *Chemical reactivity*

The vibrational modes of water which are studied here are illustrated in figure 1(*b*). HF/6-311G** qualitative profiles of different global reactivity indices associated with the symmetric (A_1) stretching and bending and asymmetric (B_2) stretching vibrational modes of water are presented in figure 4; the B3LYP/6-311G** profiles show exactly the same trends and therefore are not included in the figure. As already pointed out by Pearson and Palke [42], for the symmetric stretching and bending modes none of these properties except E (and η for the bending mode) attains a clear-cut extremum. For the symmetric stretching mode it can be observed that η, V, α and ω tend to unphysical extremum values when the hydrogen atoms collapse toward the oxygen atom. This behaviour is due to the strong variation of the external potential during the symmetric vibrations. More interesting results are obtained from the asymmetric stretching mode of vibration where the external potential remains constant during the nuclear motion (figure 4(*c*)). At the equilibrium geometry, E, α and ω are minima and μ, V and η are maxima confirming the validity of PMH,

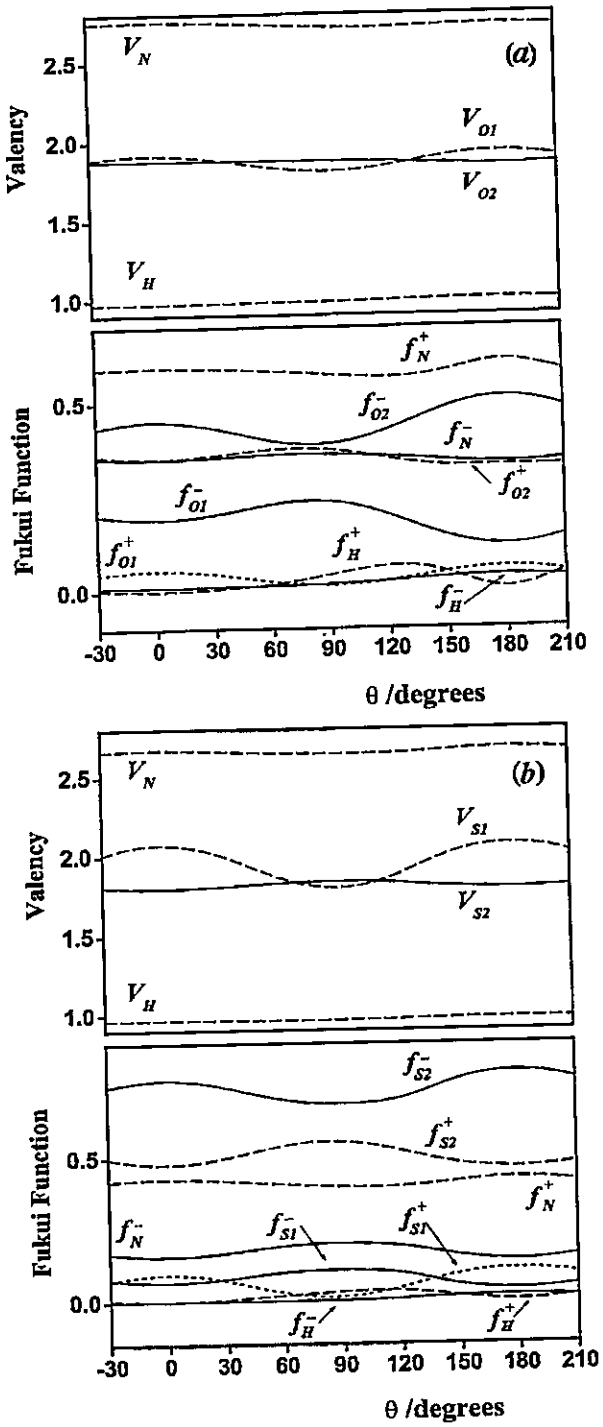

Figure 3. HF/6-311G** profiles along the torsional coordinate of local selectivity properties of (*a*) HONO and (*b*) HSNS.

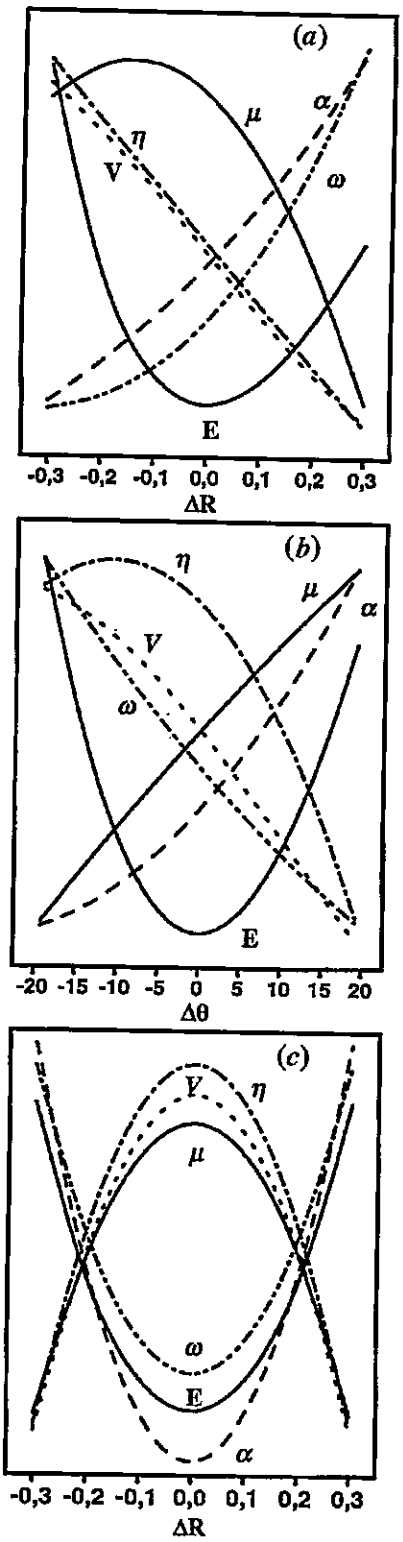

Figure 4. HF/6-311G** qualitative profiles of global reactivity properties along the vibrational modes of water: (*a*) symmetric stretching; (*b*) asymmetric bending and (*c*) asymmetric stretching.

MPP and MMVP. Since both μ and η are maxima for $\Delta R = 0$, ω attains its minimum value at the equilibrium configuration.

Figure 5 displays plots of α_{Sadlej} versus α_{Pople} and μ and η calculated with equations (15) and (16) versus those quantities calculated using equations (17) and (18) for the asymmetric stretching of H_2O at the HF/6-311G** level. The linear behaviour in all cases confirms that the use of either two possibilities to obtain the property to characterize the asymmetric molecular vibration is adequate and leads to the right description of the property during the vibrational motion.

4.2.2. *Site selectivity*

Figure 6 displays the profiles of site selectivity descriptors during the molecular vibrations at the HF level; similar trends have been found for the DFT calculations. Fukui functions have been determined using the molecular orbital approximation, equations (7), although similar trends are obtained using the finite difference approximation of equations (6). It can be observed in figures 6(*a*) and (*b*) that most local properties remain constant as the vibrational coordinate changes. In the asymmetric stretching (figure 6 (*c*)) again most local properties remain constant during the vibrational motion and we observe that f_O^+ and V_O show opposite behaviour as the bond length varies, as expected from the chemical intuition. Note that the $\{f_{H1}^+, f_{H2}^+\}$ and $\{V_{H1}, V_{H2}\}$ pairs intersect at the equilibrium geometry. It tells us that when electrophilicity at any centre goes down during oscillation it increases at some other centre and they become equal at the equilibrium position. The opposite behaviour of f_{H1}^+ and f_{H2}^+ confirms that this asymmetric stretching is the reactive mode for the dissociation of water. In all these plots HF/6-311G** and B3LYP/6-311G** calculations show identical behaviour in almost all cases. The same trends are also observed for the orbital Fukui functions.

4.3. *Double proton transfer in $(HONO)_2$*

4.3.1. *Chemical reactivity*

Figure 1(*c*) displays an illustration of the synchronic double proton transfer reaction in $(HONO)_2$; this is a symmetric reaction in which reactants are equal to products and the transition state is found exactly midway between these species. Table 3 presents numerical values of various global reactivity parameters for the reactant (product) and transition state for the double proton transfer in $(HONO)_2$ at HF/6-311G** and B3LYP/6-311G** levels. Since the protons are transferred synchronically, the profiles are symmetric and the dipole moment is zero along the reaction coordinate. Polarizability values calculated using Pople's basis

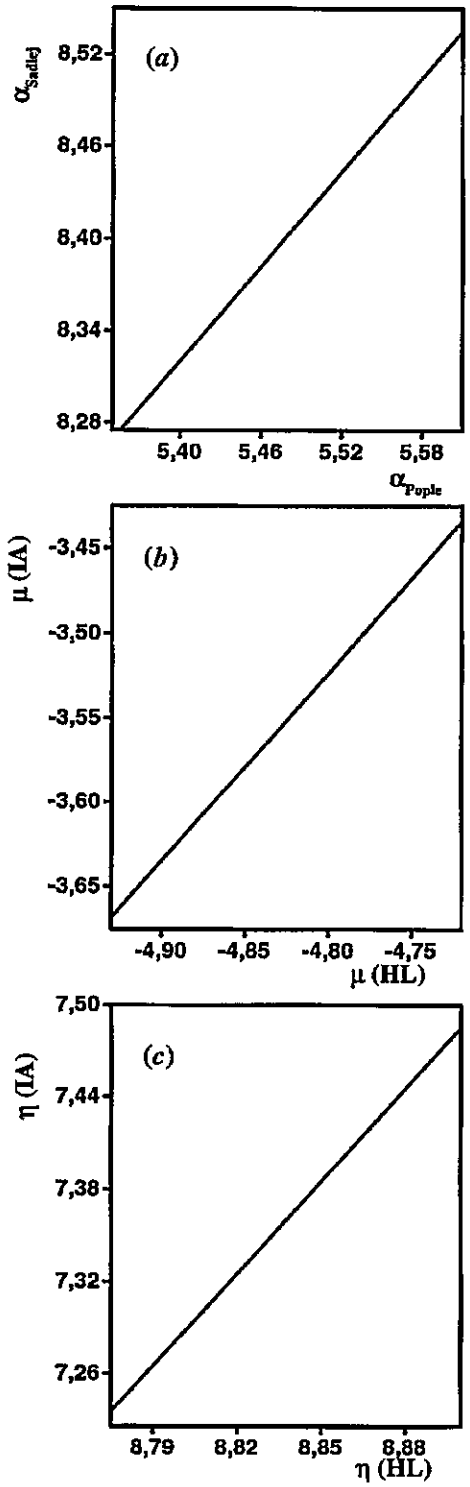

Figure 5. Characterization of the asymmetric stretching mode of water: correlation between (*a*) polarizabilities determined using different basis sets (Sadlej and Pople); (*b*) chemical potential determined using equations (15) and (17); (*c*) molecular hardness determined using equations (16) and (18).

set are also reported. In both calculations the reactant (product) has no imaginary frequencies whereas the transition state has one imaginary frequency, as expected.

Figure 7 presents the HF/6-311G** qualitative profiles of ΔE, $\Delta\mu$, $\Delta\eta$, $\langle\alpha\rangle_{Pople}$, $(\alpha_{zz})_{Pople}$, V and ω along the intrinsic reaction coordinate (IRC) of the double proton transfer reaction in $(HONO)_2$. All the profiles are symmetric owing to the symmetry of reactant and product, which happens to be the same dimer. At the TS ($IRC = 0$), all properties attain extremum values and it can be confirmed that the PMH, MPP and MMVP are valid for this reaction. It is interesting to note that μ is quite constant along the IRC and its profile attains a local maximum with two minima symmetrically positioned around the $IRC = 0$. Note that the position of these critical points coincides with the position of critical or inflection points of η, ω, α, α_{zz} and V. The critical points in μ, although hardly perceptible, may help characterize the mechanism of the reaction; the proton transfer is initiated by the displacement of the whole monomeric structures to favour the subsequent proton transfer that starts to occur within the TS region which is indicated in figure 7. This region can be defined unambiguously as the region delimited by the critical points of the force profile [14, 20, 31]. Similarly a local minimum at the TS bracketed by two local maxima is observed for the V profile. The maximum value of V at the reactants (products) together with the minimum at the TS confirms the MMVP. The profile of ω is governed by those of μ (mainly) and η; ω presents a local maximum at the TS with $\omega_{TS} \gg \omega_{Reactant(Product)}$. All the above-discussed trends were also obtained at the B3LYP/6-311G** level.

Table 4 provides relative values at HF/6-311G** and B3LYP/6-311G** levels of the activation properties such as energy ($\Delta E^{\neq}$) chemical potential ($\Delta\mu^{\neq}$) and hardness ($\Delta\eta^{\neq}$); the latter are calculated using equations (17) and (18). It is interesting to note that the B3LYP barrier is about half that of the HF barrier, with the same relation obtained for the activation hardness. The ZPE correction does not considerably change the barrier heights reported in table 4.

4.3.2. *Site selectivity*

The profiles along the intrinsic reaction coordinate of local selectivity properties are displayed in figure 8. For the double proton transfer reaction the condensed Fukui functions at the oxygen sites show reciprocal trends along the IRC when compared with those of the corresponding atomic valencies, a fact which is also observed in the cases of molecular internal rotations and vibrations. Any site with larger f_k signals high reactivity

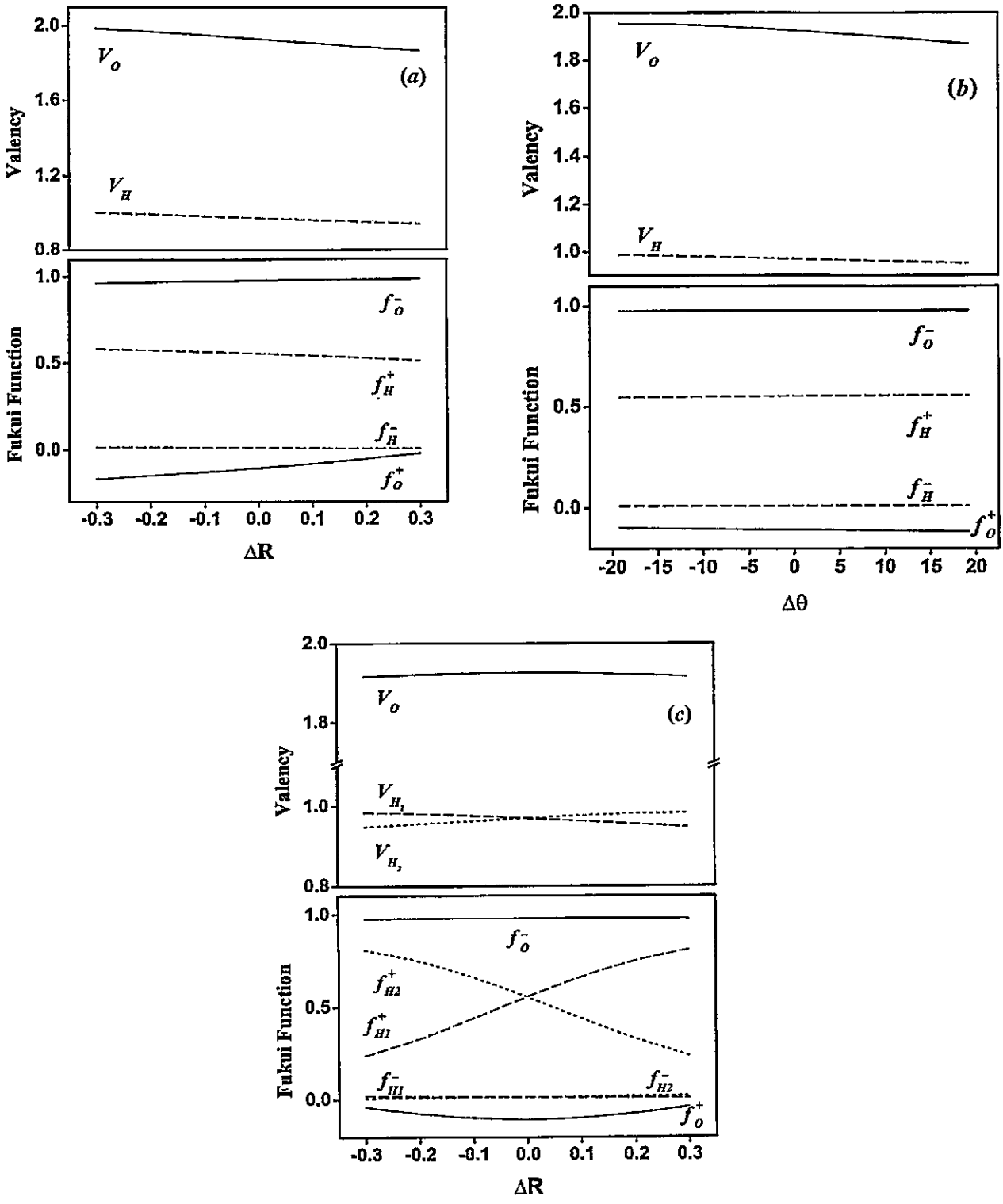

Figure 6. HF/6-311G** profiles of local selectivity properties along the vibrational modes of water: (*a*) symmetric stretching; (*b*) asymmetric bending and (*c*) asymmetric stretching.

Table 3. Reference values of global properties of reactant (product) and transition state (TS) associated with the double proton transfer in $(HONO)_2$. E, $\langle\alpha\rangle$ and α_{zz} are given in au whereas μ, η are in eV. The first entry corresponds to HF results and the second entry to B3LYP results.

	E	μ (equation 15)	μ (equation 17)	η (equation 16)	η (equation 18)	$\langle\alpha\rangle$	α_{zz}	V
R(P)	−409.411104	−4.9907	−5.0754	6.9757	7.7024	26.643	14.715	7.4699
	−411.534460	−7.8537	−5.6513	7.3094	2.5919	30.601	15.364	7.9659
TS	−409.363061	−5.1093	−5.1159	6.4796	7.0991	27.681	14.895	7.3706
	−411.509790	−5.7351	−5.6641	4.9591	2.2801	30.928	15.503	7.9545

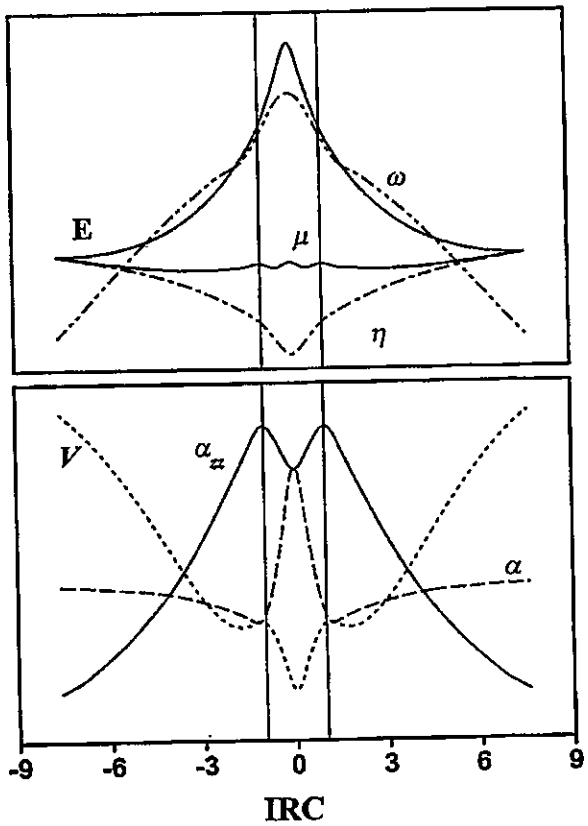

Figure 7. HF/6-311G** qualitative profiles of global reactivity properties along the internal reaction coordinate (IRC) of the synchronic double proton transfer reaction in $(HONO)_2$. The region where the transfer occurs is defined by the vertical lines around the TS.

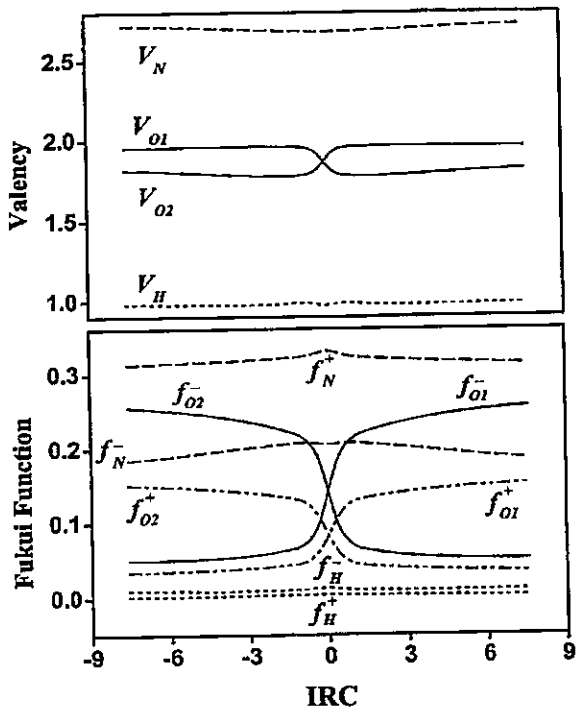

Figure 8. HF/6-311G** profiles of local selectivity properties along the internal reaction coordinate (IRC) of the double proton transfer reaction in $(HONO)_2$.

while that with high V_k implies more stability. The most pronounced changes are noticed in the profiles of $f_k^{\pm}$ for the single-bonded and double-bonded oxygen atoms. Both the single-bonded and double-bonded O centres (O1 and O2, respectively) are always more reactive towards electrophiles than nucleophiles ($f_{O2}^- > f_{O2}^+$ and $f_{O1}^- > f_{O1}^+$) although they (f^+ and f^-) exhibit similar profiles along the IRC for both O1 and O2.

Similar profiles are exhibited by $f_{O1}^{\pm}$; they start from a smaller value, increase suddenly near the TS and then level off. The profiles of f_{O1}^- and f_{O2}^- intersect at the TS as is the case with f_{O1}^+ and f_{O2}^+ which would help in locating the TS. The hydrogen profiles of Fukui functions and the valency remain more or less constant, suddenly decrease around the TS and then again remain more or less constant. The sudden change of these properties occurs exactly within the region defined in the above paragraphs and confirms the reaction mechanism in that the actual proton transfer starts at the vicinity of the transition state. On the other hand, while V_N exhibits a broad minimum along the IRC, the nucleophilic Fukui function f_N^- shows a local maximum around the TS

Table 4. Activation properties associated with the double proton transfer in $(HONO)_2$. All values are in kcal mol^{-1} but the polarizability is given in au.

Method	$\Delta E^{\neq}$	$\Delta\mu^{\neq}$ (equation 17)	$\Delta\eta^{\neq}$ (equation 18)	$\Delta\omega^{\neq}$	$\Delta\alpha^{\neq}$	$\Delta\alpha_{zz}^{\neq}$
RHF	30.1474	−0.9339	−13.9123	3.9479	1.038	0.180
B3LYP	15.4807	−0.2952	−7.1902	20.1594	0.327	0.139

indicating an increasing propensity towards an electrophilic attack.

5. Concluding remarks

Molecular internal rotations in HONO, HSNS, various symmetric and asymmetric stretching and bending vibrations in H_2O and the double proton transfer reaction in $(HONO)_2$ have been studied at the Hartree–Fock and DFT levels. Profiles of global and local reactivity and selectivity parameters have been determined.

For the internal rotations it has been found that the transition states are associated with maximum values in E, α_{zz} and ω and minimum values in μ, η and V confirming the validity of the principles of maximum hardness and molecular valency and the minimum polarizability principle. The extremal point in ω can be located by knowing the same for μ and η. Maxima (minima) in both μ and η correspond to the minimum (maximum) in ω. The Fukui function and the atomic valency at a given atomic site show an inverse relationship.

For the symmetric vibrational modes, except E, no other property attains its extremum during vibration. For the asymmetric stretching mode the equilibrium configuration is characterized by minimum E and α values and maximum μ, η and V values as would have been expected from PMH, MPP and MMVP. Since both μ and η are maxima at the equilibrium point, ω becomes a minimum. The electrophilic and nucleophilic Fukui functions in general show inverse behaviour during the vibrational coordinate variation as is the case with f_k and V_k. It implies that if a centre becomes more favourable toward an electrophilic attack for a given vibrational mode it would simultaneously become less favourable towards a nucleophilic attack.

The E, $\langle\alpha\rangle$ and α_{zz} profiles pass through maxima and the η profile passes through a minimum in the transition state of the double proton transfer reaction in $(HONO)_2$ acting as signatures of MPP and PMH. The V value for the transition state is much smaller than those of the reactant and the product which may be considered to be a consequence of MMVP. The μ value in the transition state is a local maximum in between two minima, a feature which is also reflected in the profile of other global and local properties. The V_k and f_k profiles exhibit opposite trends for this reaction and oxygen centres always prefer electrophilic attack to nucleophilic attack. The intersection points of the electrophilic (nucleophilic as well) Fukui functions for the single- and double-bonded oxygen centres may be used to locate the transition state. The N-centre becomes more prone towards electrophilic attack at the transition state.

This work was supported by FONDECYT through projects Nos 1020534, 2000050 and 2010139. PKC is grateful to the Third World Academy of Science, Italy, for financial assistance. We thank Mr B. Maiti for help in typing.

References

[1] HOHENBERG, P., and KOHN, W., 1964, *Phys. Rev.* B, **136,** 864; KOHN, W., SHAM, L. J., 1965, **140,** A1133.
[2] PARR, R. G., and YANG, W., 1989, *Density Functional Theory of Atoms and Molecules* (New York: Oxford University Press).
[3] PAULING, L., 1960, *The Nature of the Chemical Bond* (Ithaca, NY: Cornell University Press).
[4] SEN, K. D., and JORGENSEN, C. K. (eds), 1987, *Electronegativity: Structure and Bonding*, Vol. 66 (Berlin: Springer-Verlag).
[5] PEARSON, R. G., 1973, *Hard and Soft Acids and Bases (Stroudsberg*, PA: Dowden, Hutchinson and Ross); 1990, *Coord. Chem. Rev.*, **100,** 403.
[6] PARR, R. G., and PEARSON, R. G., 1983, *J. Am. chem. Soc.*, **105,** 7512.
[7] SANDERSON, R. T., 1955, *Science*, **121,** 207; 1976, *Chemical Bonds and Bond Energy*, 2nd Edn (New York: Academic Press).
[8] PEARSON, R. G., 1997, *Chemical Hardness: Applications from Molecules to Solids* (Weinheim: Wiley-VCH Verlag GMBH); PEARSON, R. G., 1993, *Chemical Hardness: Structure and Bonding*, Vol. 80, edited by K. D. Sen and D. M. P. Mingos, (Berlin: Springer-Verlag).
[9] CHATTARAJ, P. K., LEE, H., and PARR, R. G., 1991, *J. Am. chem. Soc.*, **113,** 1855; CHATTARAJ, P. K., and SCHLEYER, P. V. R., 1994, *J. Am. chem. Soc.*, **116,** 1067; CEDILLO, A., CHATTARAJ, P. K., and PARR, R. G., 2000, *Int. J. quantum Chem.*, **77,** 403; CHATTARAJ, P. K., GOMEZ, B., CHAMORRO, E., SANTOS, J., and FUENTEALBA, P., 2000, *J. phys. Chem.* A, **105,** 8815.
[10] PEARSON, R. G., 1987, *J. chem. Educ.*, **64,** 561; 1993, *Acc. Chem. Res.*, **26,** 250.

[11] PARR, R. G., and CHATTARAJ, P. K., 1991, *J. Am. chem. Soc.*, **113,** 1854; CHATTARAJ, P. K., LIU, G. H., and PARR, R. G., 1995, *Chem. Phys. Lett.*, **237,** 171; CHATTARAJ, P. K., 1996, *Proc. Ind. Natl. Sci. Acad.* A, **62,** 513; AYERS, P. W., and PARR, R. G., 2000, *J. Am. chem. Soc.*, **122,** 2010; TORRENT–SUCARRAT, M., LUIS, J. M., DURAN, M., and SOLÁ, M., 2001, *J. Am. chem. Soc.*, **103,** 7951.

[12] PEARSON, R. G., 1993, *Chemical Hardness: Structure and Bonding*, Vol. 80, edited by K. D. Sen and D. M. P. Mingos, (Berlin: Springer-Verlag); POLITZER, P., 1987, *J. chem. Phys.*, **86,** 1072; FUENTEALBA, P., and REYES, O., 1993, *J. molec. Struct. (Theochem)*, **282,** 65; GHANTY, T. K., and GHOSH, S. K., 1993, *J. phys. Chem.*, **97,** 4951; SIMÓN–MANSO, Y., and FUENTEALBA, P., 1998, *J. phys. Chem.* A, **102,** 2029.

[13] CHATTARAJ, P. K., and SENGUPTA, S., 1996, *J. phys. Chem.*, **100,** 16127; 1997, *J. phys. Chem.* A, **101,** 7893.

[14] GHANTY, T. K., and GHOSH, S. K., 1996, *J. phys. Chem.*, **100,** 12295; CHATTARAJ, P. K., FUENTEALBA, P., JAQUE, P., and TORO-LABBÉ, A., 1999, *J. phys. Chem.* A, **103,** 9307; JAQUE, P., and TORO-LABBÉ, A., 2000, *J. phys. Chem.* A, **104,** 995; GHANTY, T. K., and GHOSH, S. K., 2000, *J. phys. Chem.* A, **104,** 2975; HOHM, U., 2000, *J. phys. Chem.* A, **104,** 8418.

[15] CHATTARAJ, P. K., and PODDAR, A., 1998, *J. phys. Chem. A*, **102,** 9944; 1999, *J. phys. Chem.* A, **103,** 1274; 1999, *J. phys. Chem.* A, **103,** 8691; FUENTEALBA, P., SIMÓN-MANSO, Y., and CHATTARAJ, P. K., 2000, *J. phys. Chem.* A, **104,** 3185.

[16] SANNIGRAHI, A. B., 1992, *Adv. quantum Chem.*, **23,** 302; CHANDRA, A. K., 1994, *J. molec. Struct. (Theochem)*, **312,** 297.

[17] CHATTARAJ, P. K., NATH, S., and SANNIGRAHI, A. B., 1993, *Chem. Phys. Lett.*, **212,** 223; 1994, *J. phys. Chem.*, **98,** 9143.

[18] PARR, R. G., and YANG, W., 1984, *J. Am. chem. Soc.*, **106,** 4049.

[19] PARR, R. G., VON SZENTPÁLY, L., and LIU S., 1999, *J. Am. chem. Soc.*, **121,** 1922.

[20] CHERMETTE, H., 1999, *J. comput. Chem.*, **20,** 129; DE PROFT, F., and GEERLINGS, P., 2001, *Chem. Rev.*, **101,** 1451; GUTIÉRREZ-OLIVA, S., JAQUE, P., and TORO-LABBÉ, A., 2002, *Reviews in Modern Quantum Chemistry: A Celebration of the Contributions of Robert G. Parr*, edited by K. D. Sen (Singapore: World Scientific Press), p. 966.

[21] FUKUI, K., 1982, *Science*, **217,** 747.

[22] PERDEW, J. P., PARR, R. G., LEVY, M., and BALDUZ. J. L., JR, 1982, *Phys. Rev. Lett.*, **49,** 1691.

[23] YANG, W., and MORTIER, W., 1986, *J. Am. chem. Soc.*, **108,** 5708.

[24] ROY, R. K., PAL, S., and HIRAO, K., 1999, *J. chem. Phys.*, **110,** 8236; CONTRERAS, R. R., FUENTEALBA, P., GALVÁN, M., and PÉREZ, P., 1999, *Chem. Phys. Lett.*, **304,** 405; FUENTEALBA, P., PÉREZ, P., and CONTRERAS, R., 2000, *J. chem. Phys.*, **113,** 2544.

[25] YANG, W., and PARR, R. G., 1985, *Proc. Natl. Acad. Sci. (USA)*, **82,** 6723; YANG, W., LEE, C., and GHOSH, S. K., 1985, *J. phys. Chem.*, **89,** 5412.

[26] BERKOWITZ, M., and PARR, R. G., 1988, *J. chem. Phys.*, **88,** 2554.

[27] MENDEZ, F., and GÁZQUEZ, J. L., 1994, *J. Am. chem. Soc.*, **116,** 9298; GAŻQUEZ, J. L., and MÉNDEZ, F., 1994, *J. phys. Chem.*, **98,** 4591; LI Y., and EVANS, J. N. S., 1995, *J. Am. chem. Soc.*, **117,** 7756; NGUYEN, L. T., LEE, T. N., DE PROFT, F., CHANDRA, A. K., LANGENAEKER, W., NGUYEN, M. T., and GEERLINGS, P., 1999, *J. Am. chem. Soc.*, **121,** 5992; PAL, S., and CHANDRAKUMAR, K. R. S., 2000, *J. Am. chem. Soc.*, **122,** 4145.

[28] CHATTARAJ, P. K., 2001, *J. phys. Chem.* A, **105,** 511.

[29] KLOPMAN, G., 1968, *J. Am. chem. Soc.*, **90,** 223; KLOPMAN, G. (ed.), 1974, *Chemical Reactivity and Reaction Paths* (New York: Wiley).

[30] MARCUS, R. A., 1964, *Annu. Rev. phys. Chem.*, **15,** 155.

[31] TORO-LABBÉ, A., 1999, *J. phys. Chem.* A, **103,** 4398; GUTIÉRREZ-OLIVA, S., LETELIER, J. R., and TORO-LABBÉ, A., 1999, *Molec. Phys.*, **96,** 61; SOLÁ, M., and TORO-LABBÉ, A., 1999, *J. phys. Chem.* A, **103,** 8847; PÉREZ, P., and TORO-LABBÉ, A., 2000, *J. phys. Chem.* A, **104,** 1557; GUTIÉRREZ-OLIVA, S., JAQUE, P., and TORO-LABBÉ, A., 2000, *J. phys. Chem.* A, **104,** 8955; PÉREZ, P., and TORO-LABBÉ, A., 2001, *Theor. Chem. Acc.*, **105,** 422.

[32] HAMMOND, G. S., 1955, *J. Am. chem. Soc.*, **77,** 334; see also PROSS, A., 1995, *Theoretical and Physical Principles of Organic Reactivity* (New York: Wiley Inter Science).

[33] LEFFLER, J. E., 1953, *Science*, **117,** 340.

[34] See for example CRAMER C. J., 2002, *Essentials of Computational Chemistry. Theories and Models* (New York: Wiley).

[35] BECKE, A. D., 1992, *J. chem. Phys.*, **97,** 9173.

[36] LEE C., YANG, W., and PARR, R. G., 1988, *Phys. Rev.* B, **37,** 785.

[37] FRISCH, M. J., TRUCKS, G. W., SCHLEGEL, H. B., SCUSERIA, G. E., ROBB, M. A., CHEESEMAN, J. R., ZAKRZEWSKI, V. G., MONTGOMERY JR., J. A., STRATMANN, R. E., BURANT, J. C., DAPPRICH, S., MILLAM, J. M., DANIELS, A. D., KUDIN, K. N., STRAIN, M. C., FARKAS, O., TOMASI, J., BARONE, V., COSSI, M., CAMMI, R., MENNUCCI, B., POMELLI, C., ADAMO, C., CLIFFORD, S., OCHTERSKI, J., PETERSSON, G. A., AYALA, P. Y., CUI, Q., MOROKUMA, K., MALICK, D. K., RABUCK, A. D., RAGHAVACHARI, K., FORESMAN, J. B., CIOSLOWSKI, J., ORTIZ, J. V., BABOUL, A. G., STEFANOW, B. B., LIU, G., LIASHENKO, A., PISKORZ, P., KOMAROMI, I., GOMPERTS, R., MARTIN, R. L., FOX, D. J., KEITH, T., AL-LAHAM, M. A., PENG, C. Y., NANAYAKLARA, A., CHALLACOMBE, M., GILL, P. M. W., JOHNSON, B. G., CHEN, W., WONG, M. W., ANDRES, J. L., GONZALEZ, C., HEAD-GORDON, M., REPLOGLE, E. S., and POPLE, J. A., 1999, *Gaussian 98 (Pittsburgh*, PA: Gaussian, Inc.).

[38] SADLEJ, A. J., and URBAN, M., 1991, *J. molec. Struct. (Theochem)*, **234,** 147; SADLEJ A. J., 1988, *Collet. Czech. Chem. Commun.*, **53,** 1995.

[39] GONZALEZ, C., and SCHLEGEL, H. B., 1989, *J. chem. Phys.*, **90,** 2154.

[40] GONZALEZ, C., and SCHLEGEL, H. B., 1990, *J. phys. Chem.*, **94,** 5523.

[41] GHANTY, T. K., and GHOSH, S. K., 2000, *J. phys. Chem.* A, **104,** 2979.

[42] PEARSON, R. G., and PALKE, W. E., 1992, *J. phys. Chem.*, **96,** 3283.

Available online at www.sciencedirect.com
SCIENCE DIRECT®
Chemical Physics Letters 383 (2004) 435–440
CHEMICAL PHYSICS LETTERS
www.elsevier.com/locate/cplett

The torsional problem of oxalyl chloride: a challenge for theoretical methods

Soledad Gutiérrez-Oliva, Alejandro Toro-Labbé *

Laboratorio de Química Teórica Computacional (QTC), Facultad de Química, Pontificia Universidad Católica de Chile, Casilla 306, Correo 22, Santiago, Chile

Received 2 September 2003; in final form 27 October 2003

Abstract

The internal rotation of oxalyl chloride is investigated through ab initio Hartree–Fock and density functional theory methods. The most stable conformation is planar *trans* and a quasi-stable *gauche* isomer appearing about midway between the *trans* and *cis* isomers was also detected by the two methods. Stabilization of *trans* isomer is not only due to strong overlaps but also to *through space* interactions whereas the *gauche* conformation appears to be mainly stabilized by *through bond* interactions. In addition, the energy barrier at the *cis* conformation has been found to be mainly due to *through space* interactions.

1. Introduction

This Letter is concerned with the study of the internal rotation process of oxalyl chloride (OClC–CClO). The conformer stability of this molecule has led to considerable controversy on whether it exists in the gas phase as a single conformer or as a mixture of two or even three different stable isomers. At ambient temperature a single conformer, the *trans* form, has been observed [1]. However, infrared and Raman investigations showed that a second isomer is present in the fluid phase [2–4] and later electron diffraction studies of the gaseous phase concluded that oxalyl chloride exists as a mixture of the *trans* and *gauche* conformers [5,6]. The *trans* isomer was identified through spectroscopic and X-ray studies whereas the *gauche* isomer was characterized through electron diffraction experiments. Indeed, the *gauche* isomer was found to be less stable than the *trans* one by about 1.4 kcal/mol [5,6]. Results from Raman spectra consistently predict an energy difference between these two conformers of 0.9 kcal/mol in favor of the *trans* form [2–4].

Theoretically, the torsional potential for the internal rotation in oxalyl chloride appeared to be quite sensitive to the basis set employed in the calculations and in general it has been quite difficult for Hartree–Fock and even for post Hartree–Fock methods to characterize unequivocally the *gauche* isomer. A number calculations using a variety of basis sets were performed by different authors [7–11] with the result that most calculations failed in predicting the *gauche* stable conformation. However, many calculations showed a dip in the torsional potential suggesting that it could be due to the existence of a metastable intermediate.

The contrasting pictures provided by the experimental results and the theoretical ones motivates this theoretical study employing HF and a density functional theory method (B3LYP) that has been successfully used in various theoretical studies of compounds containing chlorine and oxygen atoms [12,13]. The aim of this Letter is to throw light on the specific intramolecular interactions that are at the origin of stabilization of the *trans* and *gauche* conformations. To do so a comparative study of Hartree–Fock and DFT methods for computing geometries and profiles of energy, electronic populations, molecular valency, dipole moments, electronic chemical potential and hardness along the internal rotation angle defined with respect to the C–C central bond has been performed.

* Corresponding author. Fax: +56-2-6864744.
E-mail address: atola@puc.cl (A. Toro-Labbé).

0009-2614/$ - see front matter © 2003 Elsevier B.V. All rights reserved.
doi:10.1016/j.cplett.2003.10.150

Chemical potential and hardness are global properties of the system and have been established as quite useful concepts which are implicated in the reactivity of chemical species. Physically, the electronic chemical potential characterizes the escaping tendency of electrons from the equilibrium system and the molecular hardness can be seen as a resistance to charge transfer [14–17]. In the present case these properties can help characterize specific isomers along the torsional angle from a different viewpoint.

2. Theoretical background and computational methods

Formal definitions of μ and η were given by Parr and Pearson [18] and a three-points finite difference approximation led them to the following working formulae of these quantities:

$$\mu = -\frac{1}{2}(\mathrm{IP} + \mathrm{EA}); \quad \eta = \frac{1}{2}(\mathrm{IP} - \mathrm{EA}). \tag{1}$$

IP and EA are the first vertical ionization potential and electron affinity of the neutral molecule, respectively. The Koopmans theorem ($\mathrm{IP} \approx -E_{\mathrm{H}}$ and $\mathrm{EA} \approx -E_{\mathrm{L}}$) allows one to write μ and η in terms of the energy of frontier HOMO (E_{H}) and LUMO (E_{L}) molecular orbitals:

$$\mu = \frac{1}{2}(E_{\mathrm{L}} + E_{\mathrm{H}}); \qquad \eta = \frac{1}{2}(E_{\mathrm{L}} - E_{\mathrm{H}}). \tag{2}$$

It is apparent from the above equations that determination of μ and η from quantum chemistry involves different kind of calculations, a ΔSCF procedure involving calculations of the system with N, $(N+1)$ and $(N-1)$ electrons should be used when applying Eq. (1), whereas only one restricted SCF calculation is needed when using Eq. (2). It has been shown that for closed shell molecules the method based on Koopmans's approximations seems to be good enough in determining μ and η [19–21]. However, in attention to the difficulties encountered in oxalyl chloride, Koopmans's based calculations were checked when necessary through extra calculations using unrestricted (UHF and UB3LYP) and restricted open shell (ROHF and ROB3LYP) methodologies.

A quite simple measure of the localization of electron density at the bond regions can be defined by the sum of electronic populations localized on bond regions of the molecule, it is given by

$$\rho_b(\alpha) = 2\rho_{co}(\alpha) + 2\rho_{cc\ell}(\alpha) + \rho_{cc}(\alpha). \tag{3}$$

Since there is no a unique way to perform a population analysis it is useful for interpretative and quantitative purposes to consider the molecular valency V_{m} that also provide a measure of the localization of the electron density at the bond regions, therefore it may be used to check consistency with the above defined ρ_b index. V_{m} is calculated by adding the off-diagonal elements of the first order density matrix and then summing over all the atoms in the molecule:

$$V_{\mathrm{m}} = \frac{1}{2}\sum_{k}\sum_{\ell \neq k}\left[\sum_{a\in k}\sum_{b\in \ell} D_{ab}D_{ba}\right], \tag{4}$$

thus giving a measure of covalent bonds in the molecule. The V_{m} value is always quite close to the total number of covalent bonds although it may fluctuate. Deviations from the total number of covalent bonds of the molecule may appear due to either the ionic character of the bond formed by atoms of different electronegativities or hyperconjugative interactions.

The profiles of global and local molecular properties were constructed by constraining the dihedral angle α to fixed values in the interval going from 0 (*trans*) to 180 (*cis*) degrees, optimizing the remaining geometrical parameters every ten degrees along α. All calculations were performed at the Hartree–Fock (HF) and DFT levels with the standard 6-311G** basis set and using the package GAUSSIAN 98 [22]. A Becke [23] three parameters nonlocal exchange functional with the nonlocal correlation functional of Lee, Yang and Parr [24], denoted by B3LYP, was used within the DFT theory. Although not discussed here, extra calculations were also performed whenever it was necessary to confirm some specific results.

3. Results and discussion

3.1. Torsional potential

In Fig. 1 are displayed the torsional potential determined through the HF and DFT methods. Note that both curves displays the same qualitative trend, in both

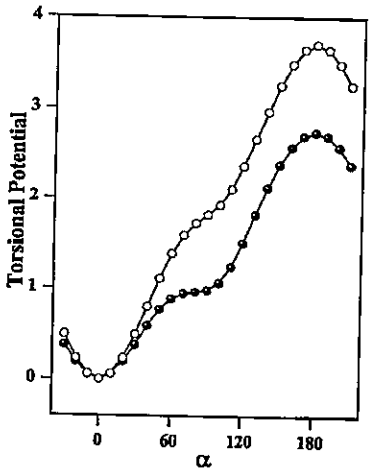

Fig. 1. HF/6-311G** (open circles) and B3LYP/6-311G** torsional potential (in kcal/mol) for the internal rotation of oxalyl chloride along the torsional angle α (in degrees).

methods the *cis* isomer corresponds to a transition state for the torsional motion, the energy barrier separating it from the stable *trans* conformation has been found to be about 2.5 kcal/mol in the DFT approach and 4.0 kcal/mol in the HF method. The HF minima is narrower than the DFT one indicating different quantitative estimations for the specific local interactions characterizing the stable conformation. Both curves present a dip at about $\alpha = 90°$, the *gauche* isomer that has been identified experimentally appears in our calculations as an intermediate metastable conformation energetically above the *trans* isomer by about 1.0–2.0 kcal/mol. Recalling the experimental evidence discussed in Section 1, it can be concluded that DFT calculations provides a better characterization of the *gauche* isomer than do the HF level. In the next paragraphs, the energetic evidence of the existence of a *gauche* metastable isomer will be checked out through monitoring different global and local properties.

3.2. Molecular structures

The favorable comparison geometries of the key isomers characterized by the torsional potential allows to assess the overall performance of the methods of calculation. Theoretical and the available experimental data [5,6] of geometrical parameters for the three relevant structures *trans*, *gauche* (with theoretical parameters determined by averaging the structures of isomers with $\alpha = 80°$, 90° and 100°) and *cis* are displayed in Fig. 2, it can be checked that the agreement of HF and DFT with the experimental data is quite satisfactory.

3.3. Electronic population analysis

A quantitative characterization of the charge density is provided by the already defined bond populations and molecular valency. We analyze in this section the evolution along α of the Mulliken electronic population localized on the bond regions [25] and the molecular valency [26,27].

Figs. 3a and b display the profiles along α of the electronic populations $\rho_b(\alpha)$ and $\rho_{cc}(\alpha)$. Both populations present minima at the *trans* and *cis* conformation and a maximum at the *gauche* one. This indicate that both planar conformations, *trans* and *cis*, are not determined only by strong overlaps but also by specific *through space* interactions by means of the associated electrostatic Hellman–Feynman forces. The maximum at the *gauche* metastable conformation indicates that this species is mainly stabilized by *through bond* interactions.

The above discussed results are confirmed by the shape exhibited by the molecular valency along α, Fig. 3c. V_m present a maximum at the gauche conformation confirming that this isomer is favored by *through bond* interactions. Indeed, it is interesting to note that both methods predict an appreciable extent of hyperconjugative interaction between π bondings of the C–O bonds and σ bondings on the C–Cl bonds, thus producing V_m values higher than the total number of covalent bonds encountered in the molecule.

Following the same line of thinking as above, it is possible to identify, at least qualitatively, the nature of the potential barrier at the *cis* conformation. We note that when going from the *gauche* isomer toward the *cis* one, ρ_b, ρ_{cc} and V_m decrease, since the total electronic population remains constant, there is a rearrangement of the bond electronic population favoring localization of the electronic population on specific atomic centers, this should lead to an important change of the dipole moment (see Fig. 4), it increases toward the *cis* isomer and decreases when going toward the *trans* isomer. The energy barrier at the *cis* conformation should be therefore of the *through space* type. In other words, at the *cis* conformation the barrier to internal rotation mostly arises owing to the electrostatic interactions among local charges centered at the oxygen and chlorine atoms.

On the other hand, the charge concentration at the bond region observed at the *gauche* isomer is accompanied by a shortening of the central CC bond distance, Fig. 3d, this result is perfectly consistent with the above described populations and valency behavior.

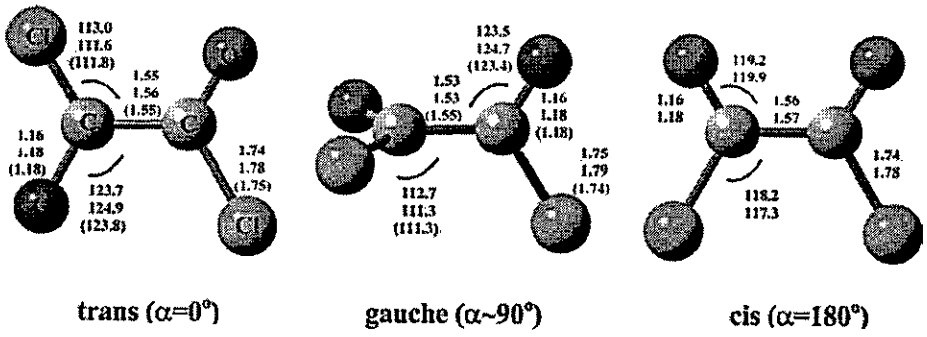

Fig. 2. HF/6-311G** (first entry) and B3LYP/6-311G** structural parameters of the key isomers along the torsional angle. Experimental values from [5,6] are given in parentheses. Bond distances are in Å; bond angles in degrees.

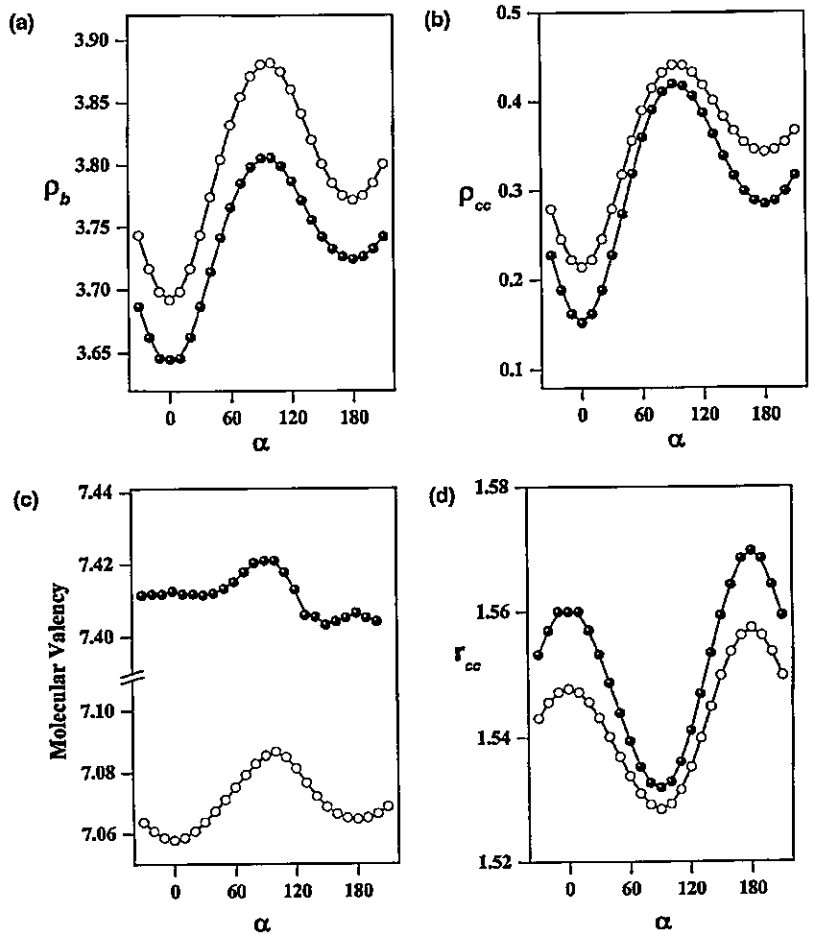

Fig. 3. HF/6-311G** (open circles) and DFT/B3LYP/6-311G** profiles of: (a) total bond population; (b) central CC bond population; (c) molecular valency and (d) CC bond distance along the torsional angle α.

3.4. Dipole moment

Since the above discussion suggests that the relative energy of the key conformations along α can be rationalized in terms of electrostatic *through space* and *through bond* interactions, it is pertinent to analyze the evolution of the dipole moment (DM) along the reaction coordinate, we expect this property to give a qualitative account of the *through space* electrostatic interactions. Fig. 4 shows that DM increases monotonically from the stable *trans* conformation to reach a maximum at the *cis* unstable isomer. A maximum value of DM together with minima of ρ_b, ρ_{cc} and V_m at the *cis* isomer confirm that the barrier is mostly due to *through space* interactions.

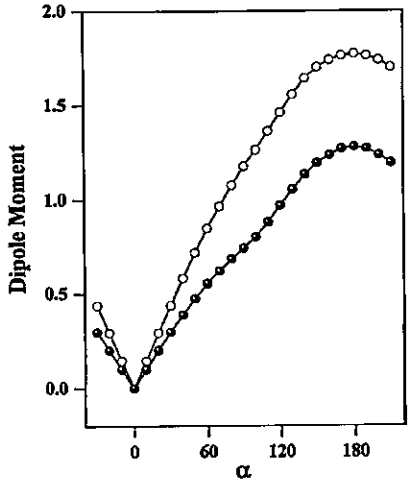

Fig. 4. HF/6-311G** (open circles) and DFT/B3LYP/6-311G** dipole moment (debye) profiles along the torsional angle α.

3.5. Chemical potential and hardness

Fig. 5a and b displays the profiles of μ and η, calculated from Eq. (2), along the torsional angle α. It is found that DFT and HF profiles are alike, chemical potential and hardness display maximum at the *gauche* conformation and minima at the *trans* and *cis* isomers. It is important to consign that the very opposite situation is observed when μ and η are estimated from the

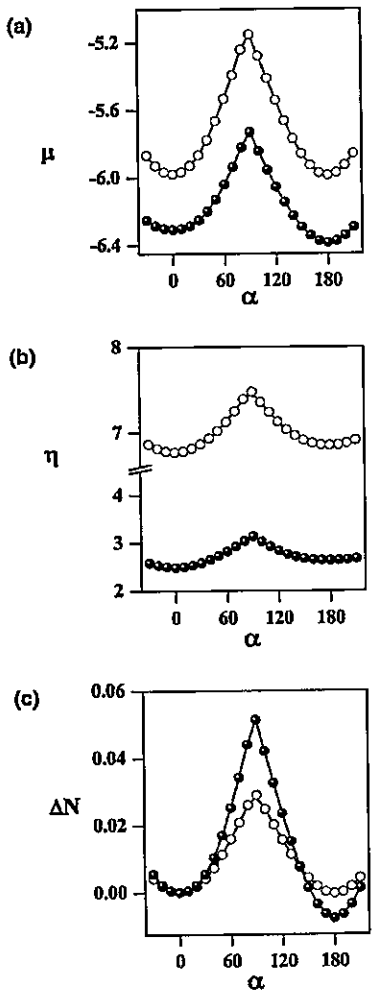

Fig. 5. HF/6-311G** (open circles) and DFT/B3LYP/6-311G** torsional profiles of: (a) chemical potential; (b) molecular hardness and (c) intramolecular charge transfer. Values of μ and η are in eV.

ΔSCF scheme (Eq. (1)) and using either unrestricted or restricted-open shell formalisms. However in all cases an abrupt change in the tendency displayed by the property is observed at the *gauche* isomer, this might be evidence of crossing of electronic quantum states.

Fig. 5a shows that chemical potential, both HF and DFT, exhibits considerable variations along the torsional angle, μ presents minima at the planar *trans* and *cis* conformations and a maximum at the *gauche* isomer. Changes in chemical potential indicate that rearrangements of the electronic density is taking place, variation of μ during the internal rotation can be explained in terms of electron transfer from conformations with high values of μ to conformations with low values of μ, in the present case the electronic flux goes from the *gauche* conformation toward the planar ones. Moreover, the amount of flowing charge ΔN along the internal rotation coordinate can be estimated by borrowing a formula for intermolecular charge transfer [18,28] in which ΔN is proportional to the difference in the chemical potential of the involved species. The intramolecular charge transfer occurring when going from a reference conformation at α_1 to α can be obtained by adapting the above mentioned expression to conformational changes, this leads to [29]:

$$\Delta N(\alpha) = \frac{1}{2}\frac{[\mu(\alpha) - \mu(\alpha_1)]}{[\eta(\alpha) + \eta(\alpha_1)]}. \quad (5)$$

This expression shows that when the system is brought out of its conformational equilibrium electronic reflushing is driven by changes in the chemical potential, at the same time the sum of hardness acts as a resistance to it.

The HF and DFT profiles of ΔN calculated using the trans conformation as reference ($\alpha_1 = 0°$) are displayed in Fig. 5c, the maximum observed at the *gauche* conformation is confirming the electronic reflushing already established through the analysis of the electronic population and dipole moments.

On the other hand, the principle of maximum hardness [30–35], quite useful in characterizing reactivity of molecular systems, states that systems in their ground state arrange themselves so as to be as hard as possible, provides a criterium to decide about the physical sound of the hardness profiles displayed in Fig. 5b. At the *trans* stable isomer a maximum hardness is expected so that in this region a unrestricted wave function might be adequate. In contrast, the *cis* unstable isomer is expected to present a minimum of hardness, therefore in this region the restricted descriptions of Fig. 5c seems to be at least qualitatively correct.

4. Concluding remarks

Hartree–Fock and DFT calculations of the torsional potential of oxalyl chloride have been presented. Planar isomer *trans* has been found to be stable whereas the *cis* isomer corresponds to a transition state for the torsional motion. Evidence from energy, electronic populations and dipole moment profiles indicates that the stability of the *trans* isomer is due to a delicate balance between *through bond* and *through space* interactions and the potential barrier at the *cis* conformation is mainly due to *through space* interactions.

Both HF and DFT calculations have indicated the probable existence of a metastable *gauche* isomer, although this was not conclusive from the energy profiles, the analysis of the profiles along the torsional angle of different global and local properties support this conclusion. Maximum electronic population at the *gauche* isomer indicate that this is specially stabilized by *through bond* interactions.

The observed change of trends occurring at the *gauche* isomer suggests that the *gauche* metastable conformation is a kind of turning point that help define two

specific regions presenting different behavior of the molecular properties studied in this Letter. The change around the *gauche* isomer is specially dramatic for chemical potential and hardness and the direction of change depends on the methodology used to determine these properties which are directly related with the frontier electronic states. This result suggest that a correct characterization of the profiles of such electronic properties might include different theoretical approaches suitable for the different regions defined along the reaction coordinate.

Acknowledgements

This work was supported by FONDECYT through Project Nos. 1020534 and 2010139.

References

[1] K.G. Kidd, G.W. King, J. Mol. Spectrosc. 16 (1968) 411.
[2] J.R. Durig, S.E. Hannum, J. Chem. Phys. 52 (1970) 6089.
[3] J.F. Davis, A. Wang, J.R. Durig, J. Mol. Struct. 293 (1993) 27.
[4] J.R. Durig, J.F. Davis, A. Wang, J. Mol. Struct. 375 (1996) 67.
[5] K. Hagen, K. Hedberg, J. Am. Chem. Soc. 95 (1973) 1003.
[6] D.D. Danielson, L. Hedberg, K. Hedberg, K. Hagen, M. Traetteberg, J. Phys. Chem. 99 (1995) 9374.
[7] J. Tyrrel, J. Am. Chem. Soc. 98 (1976) 5456.
[8] Ch.W. Bock, A. Toro–Labbé, J. Mol. Struct. (Theochem) 232 (1991) 239.
[9] D.M. Hassett, K. Hedberg, C.J. Marsden, J. Phys. Chem. 97 (1993) 4670.
[10] M.L. Senent, J. Mol. Struct. 406 (1997) 51.
[11] G. Chung, Y. Kwon, J. Mol. Struct. (Theochem) 496 (2000) 199.
[12] B.S. Jursic, J. Chem. Phys. 106 (1997) 2555.
[13] F. Bulat, A. Toro-Labbé, Chem. Phys. Lett. 354 (2002) 508.
[14] R.G. Parr, W. Yang, Density Functional Theory of Atoms and Molecules, Oxford University Press, New York, 1989.
[15] R.G. Pearson, Chemical Hardness: Applications from Molecules to Solids, Wiley–VCH, Weinheim, 1997.
[16] H. Chermette, J. Comp. Chem. 20 (1999) 129.
[17] P. Geerlings, F. De Proft, W. Langenaeker, Chem. Rev. 103 (2003) 1793.
[18] R.G. Parr, R.G. Pearson, J. Am. Chem. Soc. 105 (1983) 7512.
[19] S. Gutiérrez-Oliva, P. Jaque, A. Toro-Labbé, J. Phys. Chem. A 104 (2000) 8955.
[20] S. Gutiérrez-Oliva, P. Jaque, A. Toro-Labbé, in: K.D. Sen (Ed.), Reviews in Modern Quantum Chemistry: A Celebration of the Contributions of Robert G. Parr, World Scientific Press, Singapore, 2002, p. 966, and reference therein.
[21] P.K. Chattaraj, S. Gutiérrez-Oliva, P. Jaque, A. Toro-Labbé, At. Mol. Phys. 101 (2003) 2841.
[22] M.J. Frisch et al., GAUSSIAN 98, Gaussian Inc., Pittsburgh, PA, 1999.
[23] A.D. Becke, J. Chem. Phys. 96 (1992) 2155, 98 (1993) 5648.
[24] H. Lee, W. Yang, R.G. Parr, Phys. Rev. B 37 (1988) 785.
[25] S. Gutiérrez-Oliva, J.R. Letelier, A. Toro–Labbé, Mol. Phys. 96 (1999) 61.
[26] P.K. Chattaraj, S. Nath, A.B. Sannigrahi, Chem. Phys. Lett. 212 (1993) 223.
[27] P.K. Chattaraj, P. Pérez, J. Zevallos, A. Toro-Labbé, J. Phys. Chem. A 105 (2001) 4272.
[28] R.G. Parr, R.A. Donnelly, M. Levy, W.E. Palke, J. Chem. Phys. 68 (1978) 3801.
[29] J. Cadet, A. Grand, C. Morell, J.R. Letelier, J.L. Moncada, A. Toro-Labbé, J. Phys. Chem. A 107 (2003) 5334.
[30] R.G. Pearson, J. Chem. Educ. 64 (1987) 561.
[31] R.G. Parr, P.K. Chattaraj, J. Am. Chem. Soc. 113 (1991) 1854.
[32] P.K. Chattaraj, G.H. Liu, R.G. Parr, Chem. Phys. Lett. 237 (1995) 171.
[33] D. Datta, J. Phys. Chem. 96 (1992) 2409.
[34] P.K. Chattaraj, S. Nath, A.B. Sannigrahi, J. Phys. Chem. 98 (1994) 9143.
[35] M. Torrent-Sucarrat, J.M. Luis, M. Duran, M. Solà, J. Am. Chem. Soc. 103 (2001) 7951.

JOURNAL OF CHEMICAL PHYSICS VOLUME 121, NUMBER 10 8 SEPTEMBER 2004

Analysis of two intramolecular proton transfer processes in terms of the reaction force

Alejandro Toro-Labbé[a] and Soledad Gutiérrez-Oliva
Departamento de Quimica Fisica, Facultad de Quimica, Pontificia Universidad Catolica de Chile, Casilla 306, Correo 22, Santiago, Chile

Monica C. Concha, Jane S. Murray, and Peter Politzer[b]
Department of Chemistry, University of New Orleans, New Orleans, Louisiana 70148

(Received 11 May 2004; accepted 7 June 2004)

The negative derivative of the potential energy along an intrinsic reaction coordinate defines a force that has qualitatively a universal form for any process having an energy barrier: it passes through a negative minimum before the transition state, at which it is zero, followed by a positive maximum. We have analyzed two intramolecular proton transfer reactions in terms of several computed properties: internal charge separation, the electrostatic potentials of the atoms involved, their Fukui functions, and the local ionization energies. The variation of each of these properties along the intrinsic reaction coordinate shows a marked correlation with the characteristic features of the reaction force. We present a description of the proton transfer processes in terms of this force.
 [DOI: 10.1063/1.1777216]

I. INTRODUCTION

The course of a one-step chemical reaction, or of an individual step in a more complex process, is commonly described by the path of minimum potential energy V that links the transition state to the reactants and products. When expressed in terms of mass-weighted Cartesian coordinates, this path is known as the intrinsic reaction coordinate,[1,2] which we will denote as $\mathbf{R_C}$. An example of a $V(\mathbf{R_C})$ profile, computed at the B3LYP/6-311G** level, is shown in Fig. 1 (top) for the proton transfer

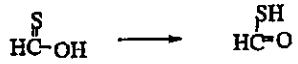

(1)

The $V(\mathbf{R_C})$ curve in Fig. 1 is typical and well known in its general appearance; the details depend of course upon the endothermicity or exothermicity of the particular reaction, the magnitude of the activation barrier and structure of the transition state, etc.

The intrinsic reaction coordinate is obtained by applying the classical equations of motion.[1,2] In this spirit, it is conceptually useful to examine the "reaction force" $\mathbf{F(R_C)}$,[3,4] given by

$$\mathbf{F(R_C)} = -\frac{\partial V(\mathbf{R_C})}{\partial \mathbf{R_C}}. \tag{2}$$

Since $V(\mathbf{R_C})$ increases before the transition state and decreases afterwards, $\mathbf{F(R_C)}$ must be, respectively, negative and positive, as can be seen in Fig. 1 (bottom). At the transition state $[\partial V(\mathbf{R_C})/\partial \mathbf{R_C}]_{TS}=0$ and hence $\mathbf{F(R_C)}_{TS}=0$. Finally, $\mathbf{F(R_C)}$ has a minimum and a maximum at the two inflection points of $V(\mathbf{R_C})$,

$$\frac{\partial^2 V(\mathbf{R_C})}{\partial \mathbf{R_C}^2} = 0 = \frac{\partial \mathbf{F(R_C)}}{\partial \mathbf{R_C}}. \tag{3}$$

The general form of $\mathbf{F(R_C)}$ follows rigorously from that of $V(\mathbf{R_C})$, and thus is universal, independent of the specific reaction, as long as it involves an energy barrier. (For the reverse reaction, $\mathbf{R_C}$ would increase in the opposite direction and the $\mathbf{F(R_C)}$ profile would be the negative of that in Fig. 1.)

Figure 1 shows that the reaction force is initially dominated by an increasingly retarding (negative) component, but is eventually reversed by a developing driving (positive) one. At the transition state, the two exactly balance. Afterwards, the driving component becomes more and more dominant, until another reversal occurs and the reaction force gradually diminishes as the products are approached. Thus the $\mathbf{F(R_C)}$ profile draws attention to the inflection points of $V(\mathbf{R_C})$ as marking transitions between different stages of a one-step process.

In order to relate this general picture to the detailed evolutions of some actual chemical reactions, we have computed $V(\mathbf{R_C})$, $\mathbf{F(R_C)}$, and several other properties for two intramolecular proton transfers, Eqs. (1) and (4),

(4)

The $V(\mathbf{R_C})$ and $\mathbf{F(R_C)}$ profiles of reaction (4) are presented in Fig. 2.

[a]Author to whom correspondence should be addressed. Electronic mail: atola@puc.cl
[b]Author to whom correspondence should be addressed. Electronic mail: ppolitze@uno.edu

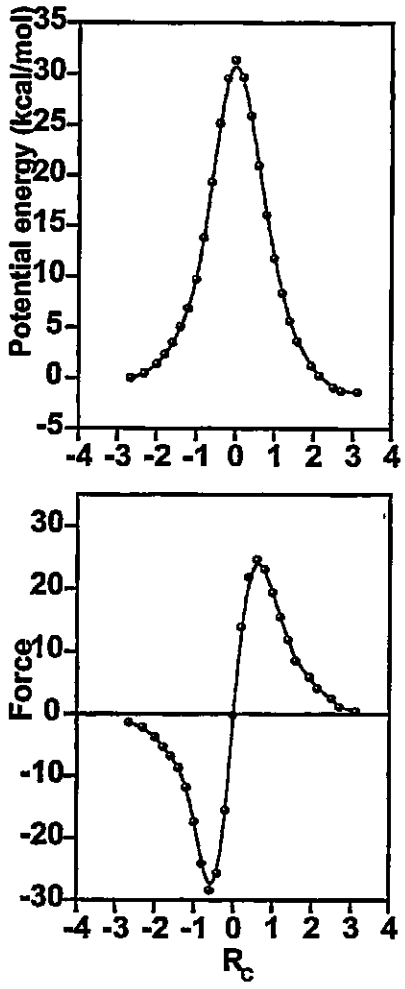

FIG. 1. Potential energy $V(\mathbf{R}_C)$ and force $\mathbf{F}(\mathbf{R}_C)$ profiles along intrinsic reaction coordinate of reaction (1).

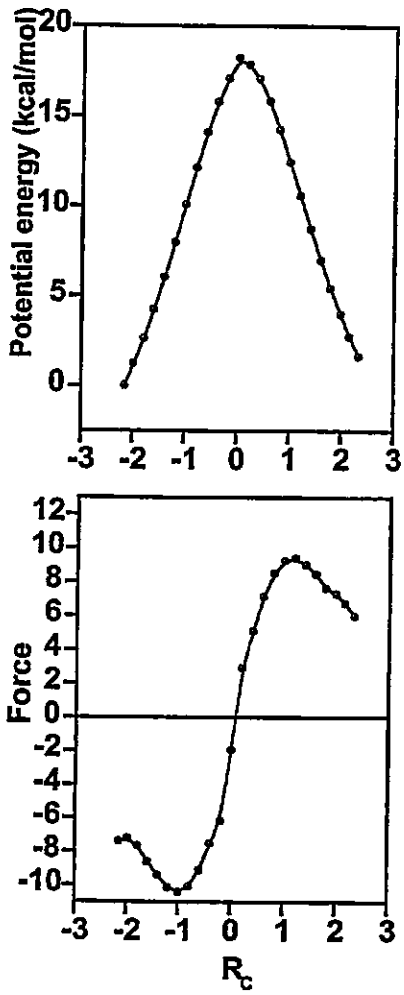

FIG. 2. Potential energy $V(\mathbf{R}_C)$ and force $\mathbf{F}(\mathbf{R}_C)$ profiles along intrinsic reaction coordinate of reaction (4).

II. PROCEDURE

We shall follow the progress of reactions (1) and (4) in terms of several computed properties. These will reflect the changes occurring in (a) the systems' charge distributions, and (b) their capacities for electron transfer.

A. Molecular electrostatic potentials and related properties

The electrostatic potential $V(\mathbf{r})$ that is created at a point $\mathbf{r}$ by the electrons and nuclei of a molecule is given by

$$V(\mathbf{r})=\sum_A \frac{Z_A}{|\mathbf{R}_A-\mathbf{r}|}-\int \frac{\rho(\mathbf{r}')d\mathbf{r}'}{|\mathbf{r}'-\mathbf{r}|} \tag{5}$$

in which Z_A is the charge on nucleus A, located at $\mathbf{R}_A$, and $\rho(\mathbf{r})$ is the molecule's electronic density. $V(\mathbf{r})$ is a physical observable, which can be determined experimentally by diffraction techniques,[5–8] as well as computationally. Its sign in any region of space depends upon whether the positive contribution of the nuclei or the negative one of the electrons is dominant there.

The molecular electrostatic potential has, for several decades, been recognized as an effective means of analyzing and interpreting molecular reactive behavior, particularly noncovalent interactions.[6,7,9–15] For these purposes, $V(\mathbf{r})$ is frequently computed on the molecular "surface," as defined in some appropriate manner; we follow Bader *et al.* in taking this to be the 0.001 a.u. (electrons/bohr^3) contour of $\rho(\mathbf{r})$,[16] which encompasses about 98% of the electronic charge.

The most negative values of the surface potential $V_S(\mathbf{r})$, i.e., the local minima, designated $V_{S,\min}$, are generally associated with the lone pairs of electronegative atoms, e.g., N, O, F, Cl, etc.; the most positive, $V_{S,\max}$, are likely to be near any hydrogens bonded to such atoms. Indeed, the magnitudes of $V_{S,\max}$ and $V_{S,\min}$ correlate with quantitative measures of hydrogen-bond-donating and -accepting tendencies.[17,18]

In recent years, it has been shown that a large number of liquid, solution, and solid phase properties that depend upon noncovalent interactions can be expressed analytically in terms of certain statistical quantities that serve to characterize the molecular surface electrostatic potential.[14,17,19–21] We shall invoke one of these, the average deviation of $V_S(\mathbf{r})$, in the present discussion; it is labeled Π, and defined by

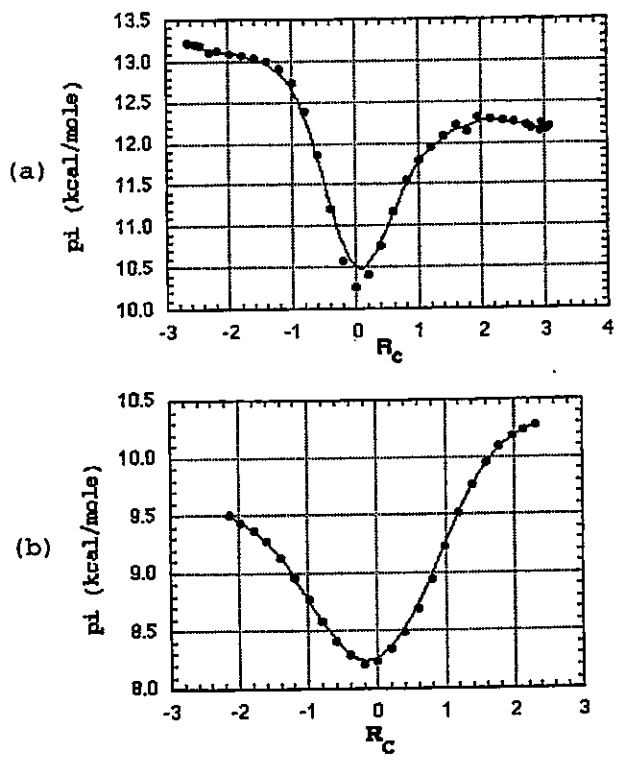

FIG. 3. Variation of Π (Pi) along intrinsic reaction coordinate of reaction (1), at top, and reaction (4), at bottom.

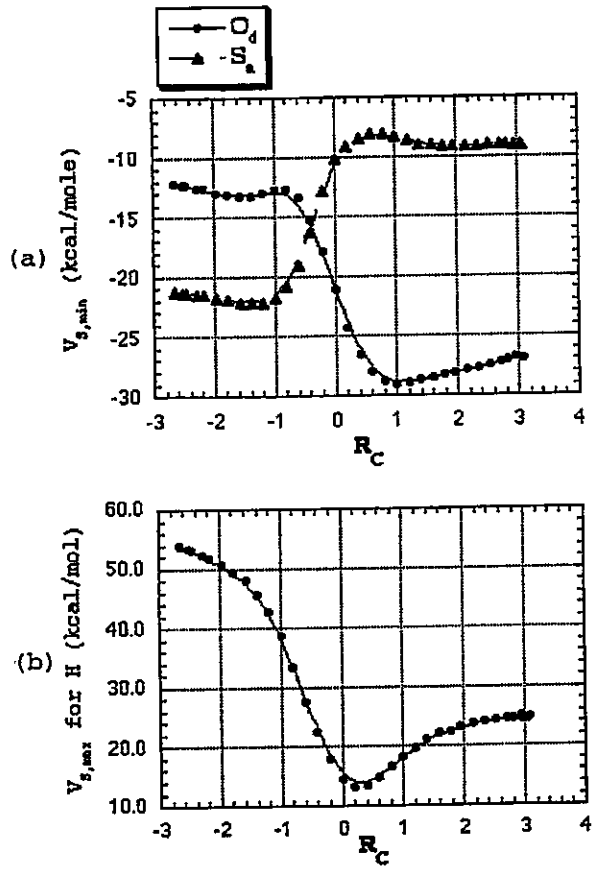

FIG. 4. (a) Variation of $V_{S,\min}$ for oxygen O_d (proton donor) and sulfur S_a (proton acceptor) along intrinsic reaction coordinate of reaction (1). (b) Variation of $V_{S,\max}$ for proton being transferred in reaction (1).

$$\Pi=\frac{1}{n}\sum_{i=1}^{n}|V_S(\mathbf{r}_i)-\bar{V}_S|. \tag{6}$$

The summation in Eq. (6) is over the point on a grid covering the molecule's surface. $\bar{V}_S$ is the average of $V_S(\mathbf{r})$,

$$\bar{V}_S=\frac{1}{n}\sum_{i=1}^{n}V_S(\mathbf{r}_i). \tag{7}$$

Π is interpreted as a measure of the internal charge separation in a molecule, which is present even when the dipole moment is zero due to symmetry, as in BF_3, CO_2, 1,3,5-trinitro-benzene, etc.; it correlates with various empirical measures of polarity.[22,23]

B. The Fukui function

Another guide to molecular reactivity that is also related directly to the overall charge distribution is the Fukui function, $f(\mathbf{r})$,[24,25]

$$f(\mathbf{r})=\left(\frac{\partial\rho(\mathbf{r})}{\partial N}\right)_{\nu(\mathbf{r})}. \tag{8}$$

In Eq. (8), N is the number of electrons and $\nu(\mathbf{r})$ is the external potential, which would normally be that due to the nuclei. Due to the discontinuous nature of the derivative in Eq. (8),[26] it can have three values at any point $N=N_0$,[24,25] each of which is viewed as an index of a type of reactivity. Our interest is in $f^-(\mathbf{r})$, which corresponds to approaching from the side $N_0-\delta$ and is taken to be a measure of reactivity toward electrophiles (such as a proton). A common approximation is[24,25]

$$f^-(\mathbf{r})=\rho_{\mathrm{HOMO}}(\mathbf{r}), \tag{9}$$

where $\rho_{\mathrm{HOMO}}(\mathbf{r})$ is the electronic density in the highest occupied molecular orbital. Equation (9) establishes a link with Fukui's frontier orbital theory of reactivity.[27] In applying $f^-(\mathbf{r})$ to analyze reactive behavior, it is often "condensed" to contributions from the individual atoms,[28,29] by partitioning $\rho_{\mathrm{HOMO}}(\mathbf{r})$ among them; this can be done by Mulliken's population analysis[30] (as in this work) or by some other procedure.[31]

C. Average local ionization energy

A somewhat different approach is in terms of the average local ionization energy $\bar{I}(\mathbf{r})$, defined originally within the framework of Hartree-Fock theory by[32]

$$\bar{I}(\mathbf{r})=\sum_i\frac{\rho_i(\mathbf{r})|\epsilon_i|}{\rho(\mathbf{r})} \tag{10}$$

in which $\rho_i(\mathbf{r})$ and ϵ_i are, respectively, the electronic density and the energy of the ith occupied atomic or molecular orbital. With the support of Koopmans' theorem,[33] which pro-

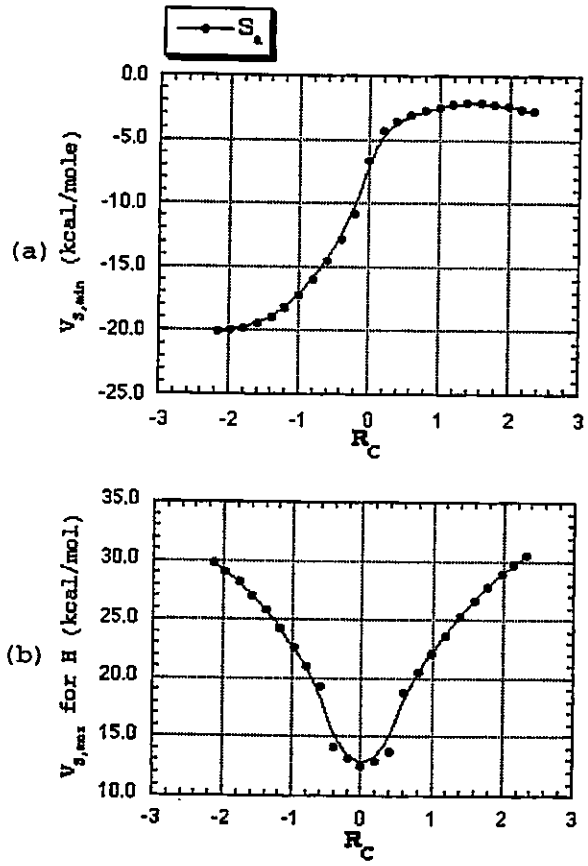

FIG. 5. (a) Variation of $V_{S,\min}$ for the sulfur that accepts the proton (S_a) in reaction (4). $V_{S,\min}$ for the donor sulfur cannot be separately identified during the latter portion of the reaction due to overlapping with $V_S(\mathbf{r})$ of the nearby oxygen. (b) Variation of $V_{S,\max}$ for proton being transferred in reaction (4).

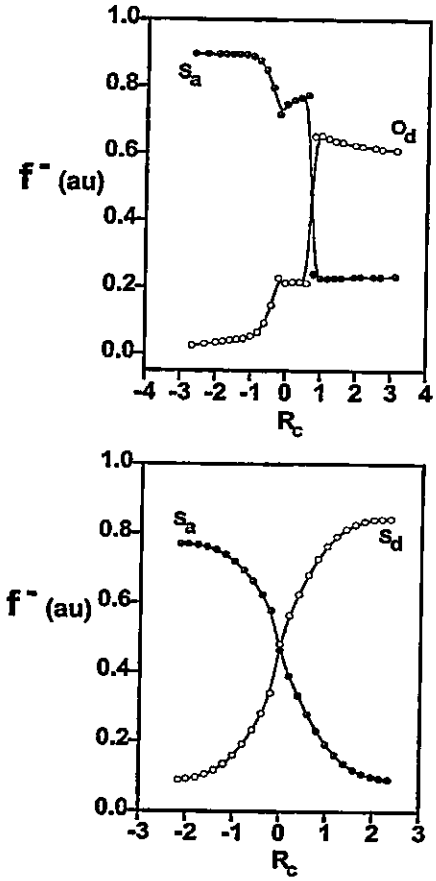

FIG. 6. Variation of Fukui functions for the proton donor and acceptor atoms, indicated by subscripts, in reactions (1), at top, and (4), at bottom.

vides some justification for treating the $|\epsilon_i|$ as the electrons' ionization potentials, we interpret $\bar{I}(\mathbf{r})$ as the average energy required to remove an electron at any point $\mathbf{r}$ in the neighborhood of an atom or molecule. $\bar{I}(\mathbf{r})$ focuses upon the point in space, not upon a specific orbital.

Earlier work has shown that $\bar{I}(\mathbf{r})$ is related to some important features of atoms and molecules, including shell structure,[34] local polarizability,[35,36] local temperature,[37] and bond strain.[38] More relevant in the present context is that $\bar{I}(\mathbf{r})$ has proven to be an effective guide to reactivity toward electrophiles. For this purpose, we compute it on the 0.001 a.u. molecular surface and look for its lowest values, $\bar{I}_{S,\min}$; these indicate the sites of the most reactive electrons, most easily transferable to an electrophile. $\bar{I}_{S,\min}$ have been successful in predicting the activating and directing effects of benzene substituents,[32,39] reactive sites on various organic molecules, including the nucleotide bases,[40,41] and pK_a and proton affinities.[41,42] It has been demonstrated that $\bar{I}_{S,\min}$ obtained by Kohn-Sham density functional calculations are as reliable as the Hartree-Fock.[39]

For processes that involve electrophilic attack and some degree of charge transfer, $V_S(\mathbf{r})$ and $\bar{I}_S(\mathbf{r})$ complement each other quite effectively: $V_S(\mathbf{r})$ shows where an approaching electrophile will initially be attracted, and $\bar{I}_S(\mathbf{r})$ indicates how available are the electrons at these and other sites. This complementarity has been discussed in detail elsewhere.[41]

D. Computational approach

The B3LYP/6-311G** procedure was used for the geometry optimizations, the potential energy and force profiles, and the Fukui functions. The electrostatic potentials and average local ionization energies on the molecular surfaces were calculated at the B3LYP/6-31G* level.

III. RESULTS

The key points along the intrinsic reaction coordinate in terms of which reactions (1) and (4) will be analyzed are the minimum and maximum of $\mathbf{F}(\mathbf{R_C})$ and the transition state, where $\mathbf{F}(\mathbf{R_C})=0$. For reaction (1), the minimum and maximum are at -0.60 and $+0.60$, respectively, on the $\mathbf{R_C}$ axis; for reaction (4), the corresponding points are -1.00 and $+1.19$. (These values reflect the near symmetry of $V(\mathbf{R_C})$ for each of these two reactions.) The transition states are at $\mathbf{R_C}=0$.

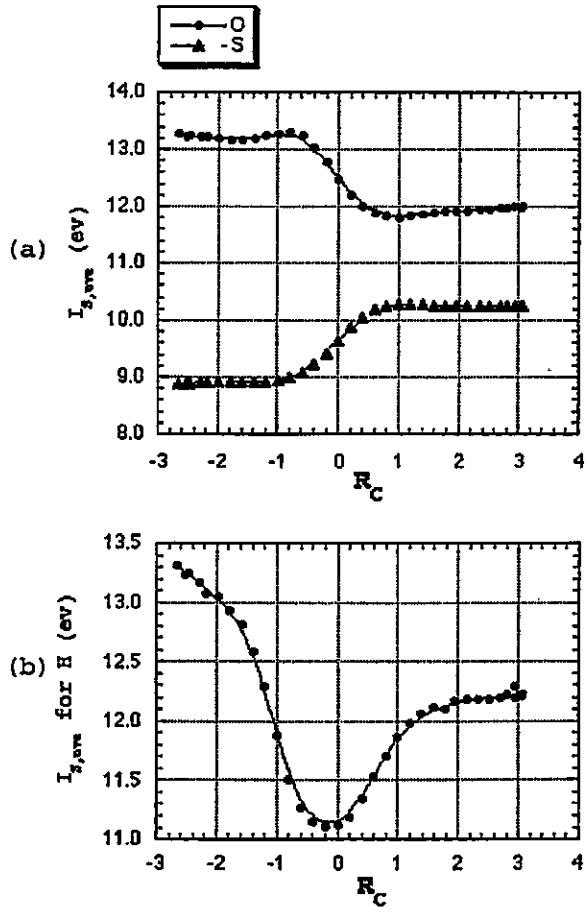

FIG. 7. (a) Variation of $\bar{I}_{S,av}$ for oxygen (proton donor) and sulfur (proton acceptor) along intrinsic reaction coordinate of reaction (1). (b) Variation of $\bar{I}_{S,av}$ for proton being transferred in reaction (1).

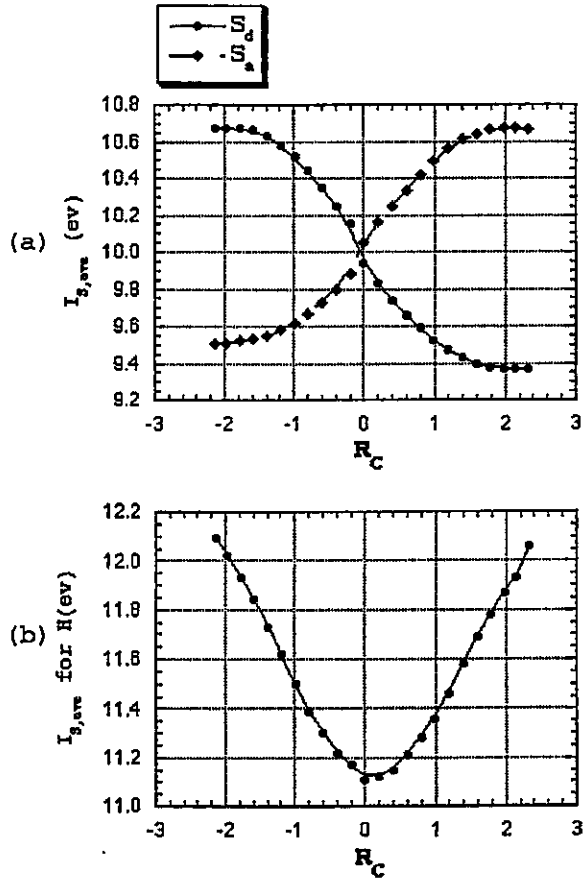

FIG. 8. (a) Variation of $\bar{I}_{S,av}$ for the sulfur that donates the proton (S_d) and the sulfur that accepts it (S_a) in reaction (4). (b) Variation of $\bar{I}_{S,av}$ for proton being transferred in reaction (4).

We look first at a property of the whole system, Π, which we interpret as indicative of internal charge separation. Its variations through the course of the two reactions are shown in Fig. 3. Particularly interesting is that each $\Pi(\mathbf{R_C})$ curve has a minimum at essentially $\mathbf{R_C}=0$. In terms of this criterion, therefore, the most balanced internal charge distributions are found in the transition states.

In order to examine this in greater detail, we consider next the molecular surface electrostatic potentials $V_S(\mathbf{r})$ associated with the key atoms involved in these proton transfers. In both reactants and both products, there are local minima, $V_{S,\min}$, near the oxygens and sulfurs, and local maxima, $V_{S,\max}$, near the labile protons. The variations of the $V_{S,\min}$ during the course of the reactions are depicted in Figs. 4(a) and 5(a). (Figure 5(a) shows $V_{S,\min}$ only for the acceptor sulfur in reaction (4); $V_S(\mathbf{r})$ of the donor blends together with that of the nearby oxygen as the transfer progresses, and the donor $V_{S,\min}$ can then no longer be identified.) In each instance, the atom losing the proton goes from less to more negative, while the one receiving it does the opposite. What is significant, however, is the general pattern of these changes: initially very slow and gradual, followed by a sudden and rapid large increase or decrease, and then again slow and gradual. Figures 4(a) and 5(a) are indeed somewhat reminiscent of titration curves in analytical chemistry! What is significant is that the transitions between the two types of changes—slow and gradual versus fast and large—occur at the values of $\mathbf{R_C}$ corresponding to the minima and maxima of $\mathbf{F}(\mathbf{R_C})$, i.e., the inflection points of $V(\mathbf{R_C})$. Meanwhile, the $V_{S,\max}$ of the protons being transferred pass through minima at or very near the transition states [Figs. 4(b) and 5(b)]. The resultant of all of these factors is fully consistent with the overall charge distribution being most balanced in the transition state. Finally, the Fukui functions f^- for the oxygen and sulfurs (Fig. 6) are essentially the mirror images of the respective $V_{S,\min}$ [Figs. 4(a) and 5(a)].

Proceeding now to the energetics of electron transfer to or from the proton, Figs. 7 and 8 show the variation of the average local ionization energies $\bar{I}_{S,av}$ on the atoms participating in the proton transfer. (The respective atoms' portions of the molecular surfaces were determined by the segmental analysis procedure of Brinck *et al.*[43]) The $\bar{I}_{S,av}$ profiles for the donor and acceptor atoms, Figs. 7(a) and 8(a), are overall analogous to those of their $V_{S,\min}$, the donors' $\bar{I}_{S,av}$ decreasing and the acceptors' increasing. These parallels between $V_{S,\min}$ and $\bar{I}_{S,av}$ can be understood by recognizing that as an atom becomes more negative, its highest-energy electron is

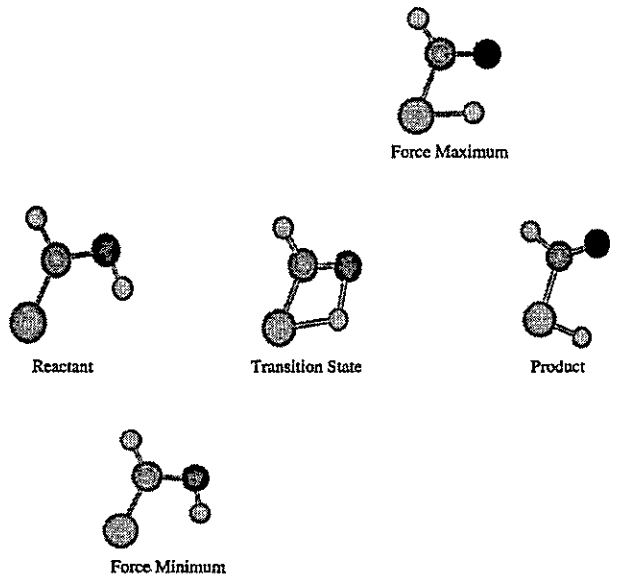

FIG. 9. Structure of system at key points along intrinsic reaction coordinate of reaction (1). The dark circle represents the oxygen O_d (proton donor). The key computed distances involving the proton, O_d and S_a (proton acceptor) are as follows: reactant, O_d-H=0.972 A; force minimum, O_d-H=0.979 A; transition state, O_d-H=1.366 A, S_a-H=1.669 A; force maximum, O_d-H =1.568 A, S_a-H=1.520 A; product, S_a-H=1.344 A.

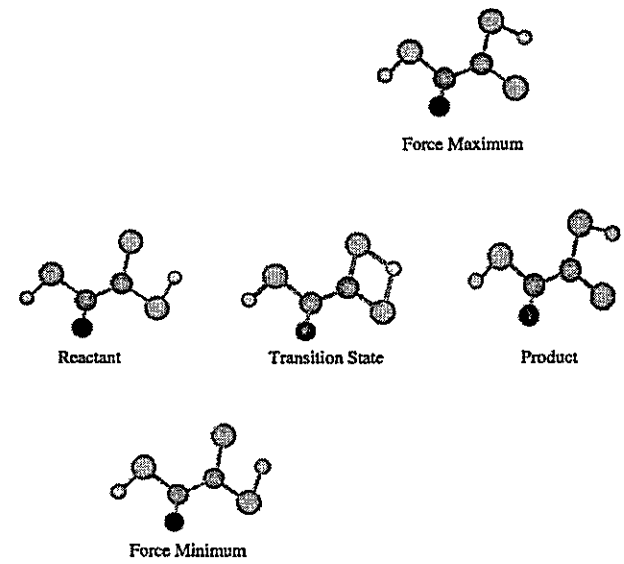

FIG. 10. Structure of system at key points along intrinsic reaction coordinate of reaction (4). The proton donor sulfur S_d is at the right. The key computed distances involving the proton, S_d and S_a (proton acceptor) are as follows: reactant, S_d-H=1.355 A; force minimum, S_d-H=1.471 A; transition state, S_d-H=1.720 A, S_a-H=1.694 A; force maximum, S_d-H =2.000 A, S_a-H=1.452 A; product, S_a-H=1.356 A.

less tightly held, and vice versa. The curves are again titrationlike, with the transitions between regions of slow, gradual, and fast, large change being at the minima and maxima of $\mathbf{F}(\mathbf{R_C})$. The hydrogen $\bar{I}_{S,\mathrm{av}}$ complete the analogy by having minima at the transition states, Figs. 7(b) and 8(b), which is where the hydrogens being transferred have the lowest $V_{S,\max}$.

IV. DISCUSSION AND SUMMARY

The manner in which these computed properties vary as the reactions progress fully complements the reaction force profiles in emphasizing the special significance of the inflection points of $V(\mathbf{R_C})$, which are the minimum and maximum of $\mathbf{F}(\mathbf{R_C})$, and the maximum of $V(\mathbf{R_C})$, which is the zero of $\mathbf{F}(\mathbf{R_C})$. Figures 9 and 10 show the structures of each system at the key points along the intrinsic reaction coordinate. The initial phase of each proton transfer is primarily a rotation of the donor-H bond toward the acceptor, coupled with a slight stretching of the former; these are opposed by an increasing retarding force. At the $\mathbf{F}(\mathbf{R_C})$ minimum, this begins to be countered by the growing attraction of the proton to the electronic charge of the acceptor. As the proton moves more into the domain of the acceptor, $V_{S,\min}$ of the latter rapidly becomes less negative, while that of the donor does the opposite. Meanwhile, $V_{S,\max}$ of the proton, which is now influenced by both the donor and the acceptor electrons, reaches its least positive value at the transition state. The $\mathbf{F}(\mathbf{R_C})$ maximum corresponds basically to a stretched and rotated acceptor-H bond; thereafter the driving force toward the equilibrium product structure decreases as the bond becomes shorter and moves to its equilibrium angle.

An interesting concept that emerges from the analysis that has been presented is that, at least in some respects, the transition state is one of maximum balance (despite being energetically the least stable). This is true in terms of both the internal charge distribution and the reaction force.

ACKNOWLEDGMENT

The authors acknowledge the financial support for this work provided by FONDECYT through project numbers 1020534 and 7020534.

[1] K. Fukui, Acc. Chem. Res. **14**, 363 (1981).
[2] C. Gonzalez and H. B. Schlegel, J. Phys. Chem. **94**, 5523 (1990).
[3] A. Toro-Labbé, J. Phys. Chem. A **103**, 4398 (1999).
[4] P. Jaque and A. Toro-Labbé, J. Phys. Chem. A **104**, 995 (2000).
[5] R. F. Stewart, J. Chem. Phys. **57**, 1664 (1972).
[6] *Chemical Applications of Atomic and Molecular Electrostatic Potentials*, edited by P. Politzer and D. G. Truhlar (Plenum, New York, 1981).
[7] G. Naray-Szabo and G. G. Ferenczy, Chem. Rev. (Washington, D.C.) **95**, 829 (1995).
[8] D. Feil, in *Molecular Electrostatic Potentials: Concepts and Applications*, edited by J. S. Murray and K. Sen (Elsevier, Amsterdam, 1996), Chap. 13.
[9] E. Scrocco and J. Tomasi, Top. Curr. Chem. **42**, 95 (1973).
[10] E. Scrocco and J. Tomasi, Adv. Quantum Chem. **11**, 115 (1978).
[11] P. Politzer and K. C. Daiker, in *The Force Concept in Chemistry*, edited by B. M. Deb (Van Nostrand Reinhold, New York, 1981), Chap. 6.
[12] P. Politzer, P. R. Laurence, and K. Jayasuriya, Environ. Health Perspect. **61**, 191 (1985).
[13] P. Politzer and J. S. Murray, in *Reviews in Computational Chemistry*, edited by K. B. Lipkowitz and D. B. Boyd (VCH, New York, 1991), Vol. 2, Chap. 7.
[14] J. S. Murray and P. Politzer, in *Molecular Orbital Calculations for Biological Systems*, edited by A.-M. Sapse (Oxford University Press, New York, 1998), Chap. 3.
[15] P. Politzer, J. S. Murray, and Z. Peralta-Inga, Int. J. Quantum Chem. **85**, 676 (2001).
[16] R. F. W. Bader, M. T. Carroll, J. R. Cheeseman, and C. Chang, J. Am. Chem. Soc. **109**, 7968 (1987).

[17] J. S. Murray and P. Politzer, in *Quantitative Treatments of Solute/Solvent Interactions*, edited by P. Politzer and J. S. Murray (Elsevier, Amsterdam, 1994), Chap. 8.
[18] H. Hagelin, T. Brinck, M. Berthelot, J. S. Murray, and P. Politzer, Can. J. Chem. **73**, 483 (1995).
[19] J. S. Murray and P. Politzer, J. Mol. Struct.: THEOCHEM **425**, 107 (1998).
[20] P. Politzer and J. S. Murray, Trends Chem. Phys. **7**, 157 (1999).
[21] P. Politzer and J. S. Murray, Fluid Phase Equilib. **185**, 129 (2001).
[22] T. Brinck, J. S. Murray, and P. Politzer, Mol. Phys. **76**, 609 (1992).
[23] J. S. Murray, T. Brinck, P. Lane, K. Paulsen, and P. Politzer, J. Mol. Struct.: THEOCHEM **307**, 55 (1994).
[24] R. G. Parr and W. Yang, J. Am. Chem. Soc. **106**, 4049 (1984).
[25] R. G. Parr and W. Yang, *Density-Functional Theory of Atoms and Molecules* (Oxford University Press, New York, 1989).
[26] J. P. Perdew, R. G. Parr, M. Levy, and J. L. Balduz, Phys. Rev. Lett. **49**, 1691 (1982).
[27] K. Fukui, Science **218**, 747 (1982).
[28] P. Fuentealba, P. Perez, and R. Contreras, J. Chem. Phys. **113**, 2544 (2000).
[29] P. K. Chattaraj, S. Gutierrez-Oliva, P. Jaque, and A. Toro-Labbé, Mol. Phys. **101**, 2841 (2003).
[30] R. S. Mulliken, J. Chem. Phys. **23**, 1833 (1955).
[31] R. K. Roy, S. Pal, and K. Hirao, J. Chem. Phys. **110**, 8236 (1999).
[32] P. Sjoberg, J. S. Murray, T. Brinck, and P. Politzer, Can. J. Chem. **68**, 1440 (1990).
[33] T. A. Koopmans, Physica (Utrecht) **1**, 104 (1933).
[34] P. Politzer, J. S. Murray, M. E. Grice, T. Brinck, and S. Ranganathan, J. Chem. Phys. **95**, 6699 (1991).
[35] P. Jin, T. Brinck, J. S. Murray, and P. Politzer, Int. J. Quantum Chem. **95**, 632 (2003).
[36] P. Jin, J. S. Murray, and P. Politzer, Int. J. Quantum Chem. **96**, 394 (2004).
[37] A. Nagy, R. G. Parr, and S. Liu, Phys. Rev. A **53**, 3117 (1996).
[38] J. S. Murray, J. M. Seminario, P. Politzer, and P. Sjoberg, Int. J. Quantum Chem., Quantum Chem. Symp. **24**, 645 (1990).
[39] P. Politzer, F. Abu-Awwad, and J. S. Murray, Int. J. Quantum Chem. **69**, 607 (1998).
[40] J. S. Murray, Z. Peralta-Inga, P. Politzer, K. Ekanayake, and P. LeBreton, Int. J. Quantum Chem. **83**, 245 (2001).
[41] P. Politzer, J. S. Murray, and M. C. Concha, Int. J. Quantum Chem. **88**, 19 (2002).
[42] T. Brinck, J. S. Murray, and P. Politzer, Int. J. Quantum Chem. **48**, 73 (1993).
[43] T. Brinck, P. Jin, Y. Ma, J. S. Murray, and P. Politzer, J. Mol. Model. [Electronic Publication] **9**, 77 (2003).